INFORMATION TO USERS

This manuscript has been reproduced from the microfilm master. UMI films the text directly from the original or copy submitted. Thus, some thesis and dissertation copies are in typewriter face, while others may be from any type of computer printer.

The quality of this reproduction is dependent upon the quality of the copy submitted. Broken or indistinct print, colored or poor quality illustrations and photographs, print bleedthrough, substandard margins, and improper alignment can adversely affect reproduction.

In the unlikely event that the author did not send UMI a complete manuscript and there are missing pages, these will be noted. Also, if unauthorized copyright material had to be removed, a note will indicate the deletion.

Oversize materials (e.g., maps, drawings, charts) are reproduced by sectioning the original, beginning at the upper left-hand corner and continuing from left to right in equal sections with small overlaps.

ProQuest Information and Learning
300 North Zeeb Road, Ann Arbor, MI 48106-1346 USA
800-521-0600

BOND DETERIORATION OF REINFORCING STEEL IN CONCRETE DUE TO CORROSION

Lamya Amleh

December 2000

Department of Civil Engineering and Applied Mechanics
McGill University
Montreal, Canada

A thesis submitted to the
Faculty of Graduate Studies and Research
in partial fulfilment of the requirements for the degree of
Doctor of Philosophy

To My Husband Bahjat And

Our Daughter Aishah

Abstract

This research program consists of laboratory studies of the corrosion phenomenon and field study of the deterioration due to corrosion of the Dickson Bridge. The laboratory studies examined the influence of increasing levels of corrosion on the progressive deterioration of bond between the steel and concrete and determined the extent to which the various cements and mix proportions influence the corrosion of the reinforcement as well as the chloride ion penetration. The corrosion resistance of the fly ash concrete is examined and compared with that of plain concrete to determine the effects of cement type, w/c ratio, cover thickness, and the use of different classes of fly ash on the durability of the concrete mix.

An accelerated electrochemical corrosion procedure was developed with the objective of "completely" corroding the bar in a period of 15-20 weeks. The influence of corrosion on the bond between the reinforcing steel and concrete was studied using two types of tests- the pullout and tension test. Eight levels of corrosion, ranging from no corrosion to complete corrosion, with over 25 percent steel bar weight loss due to corrosion, with wide longitudinal cracks. The phenomena of tension cracking and tension stiffening in tension specimens subjected to corrosion were also examined. The bond behaviour is influenced by the deterioration of the reinforcing bar ribs and by the reduced adhesion and cohesion of the reinforcing bar due to the widening of the longitudinal splitting crack resulting from corrosion. It was noted that low levels of corrosion (about 1-3% mass loss) lead to slight improvement of bond strength. However, bond strength decreases rapidly with an increase in the corrosion level, especially in the case of any severe localized corrosion. Analysis of the test results showed that a 5% mass loss resulted in a 9 percent decrease of the nominal bond stress. While with over 25 percent mass loss due to corrosion, a 90 percent loss of the nominal bond stress was noted.

The results indicate that the use of high volume fly ash (three different mixtures) was very effective in delaying the corrosion process as compared to that of the normal portland cement. However, the direct tensile strength of fly ash concrete as calculated from the response of the tension tests was noted to be weaker than that of normal portland cement concrete. Also, the bond performance of the steel bars embedded in the normal portland cement concrete mixtures with a low water-cement ratio of 0.32 was found to be superior than that with a concrete mixture with a larger water-cement ratio.

This research program was a part of a detailed strategic program to determine why the Dickson Bridge in Montreal deteriorated so prematurely and to create a data bank from many electrochemical, chemical, physical and mechanical tests on the various bridge components. This thesis includes the results of very detailed tests on four randomly selected 6 m by 5 m segments of the bridge, with some of the basic tests being undertaken on a grid of 0.25 m by 0.25 m. The field test data corroborates the results of six other investigators who undertook similar tests on different parts of the bridge and also repeated some of the tests to ensure reproduction of the results.

An evaluation of the steel bar mass loss and the chloride content at the steel-concrete interface in the field showed considerable scatter because of the leaching of the chlorides deeper into the deck. However, an analysis of this data for steel bar mass loss of less then 15% showed good correlation between the field test results and the laboratory data from the tension specimens constructed using the same concrete as the Dickson Bridge. Although more research is needed in this area, presently it is possible to determine the steel bar mass loss from measurement of the chloride contents in its vicinity.

Résumé

Les objectifs principaux de ce programme de recherche sont d'étudier l'influence des niveaux croissants de la corrosion sur la détérioration progressive de l'adhérence entre l'acier et le béton et pour déterminer le point auquel les divers ciments et proportions de mélange influence la corrosion de l'armature en fonction du phénomène de pénétration d'ions de chlorure. La résistance à la corrosion du béton de cendres volantes est examinée et comparée à celle du béton ordinaire pour déterminer les effets du type de ciment, le taux eau /ciment, épaisseur du béton d'enrobage, et l'utilisation de différentes classes de cendres volantes sur la durabilité du béton.

Une méthode d'essai électrochimique accélérée normalisée de corrosion a été développée avec l'objectif de corroder " complètement " l'armature dans une période de 15-20 semaines. L'influence de la corrosion sur l'adhérence entre l'armature d'acier et le béton est examinée en utilisant deux types d'essais- l'essai d'arrachement et de traction. Huit niveaux de corrosion, variant d'aucune corrosion, jusqu'a la corrosion totale avec 25 pour cent de perte de poids due à la corrosion. Les phénomènes de fissuration de traction et de raidissement de traction dans des spécimens en traction soumis à la corrosion ont été également examinés. Le comportement d' adhérence est influencé par la détérioration des nervures des barres d'armatures et par la réduction de l'adhérence et la cohésion des barres due à l'élargissement des fissures longitudinales résultant de la corrosion. On a noté que les niveaux bas de corrosion (perte environ 1-3% de masse) améliorent légèrement la résistance d'adhérence. Cependant, la résistance d'adhérence diminue rapidement avec une augmentation du niveau de corrosion, particulièrement dans le cas de corrosion localisée grave. On a constaté qu'avec une corrosion de 5% de perte de masse a diminué de 9 pour cent la résistance d'adhérence nominale, tandis que pour

une corrosion de niveau de 25 pour cent de perte de masse avait comme conséquence une perte de 90 pour cent de la résistance d'adhérence nominale

Les résultats indiquent que l'utilisation d'un volume élevé des cendres volantes (trois mélanges différents) est très efficace dans le retardement de la corrosion par rapport à celle du ciment normal Portland. Cependant, la résistance à la traction du béton de cendres volantes est plus faible que celle du ciment normal Portland. En outre, il s'est avéré que l'adhérence des barres en acier encastrées dans les bétons de ciment normal Portland avec un taux d'eau-ciment bas de 0,32 est supérieure que celle des bétons ayant des taux d'eau-ciment élevés.

Ce programme de recherche fait partie d'un programme de recherche stratégique détaillé pour déterminer la cause de détérioration préematurée du Pont Dickson à Montréal et pour créer une banque de données des résultats d'essais électrochimiques, chimiques, physiques et mécaniques sur les divers parties du pont. Cette thèse inclut les résultats des essais très détaillés sur quatre aléatoirement choisis segments du pont de 6m par 5 m, avec certains des essais de base étant entrepriss sur un grillage de 0,25 m par 0,25 m. Les données d'essai sur le terrain corroborent les résultats de six autres investigateurs qui ont entrepris des essais semblables sur différentes parties du pont et ont également répété certains des essais pour assurer la reproduction des résultats.

Une évaluation de la perte de masse d'acier des barres et du contenu de chlorures à l'interface acier-béton dans le champ a montré l'éparpillement considérable en raison de la pénétration profonde des chlorures dans le tablier. Cependant, une analyse de ces données pour des pertes de masse d'acier de moins de 15% a montré une bonne corrélation entre les résultats d'essai sur le terrain et les données de laboratoire des spécimens de tension construits en utilisant un béton semblable à celui du pont Dickson. Bien que plus de recherche soit nécessaire dans ce domaine, actuellement il est possible de déterminer la perte de masse d' acier des barres à partir de la mesure du contenu de chlorures dans sa proximité.

Acknowledgements

The author would like to express her sincerest appreciation and deepest gratitude to Professor M. S. Mirza, for his invaluable guidance, assistance, and advice throughout the execution of this research program. Professor Mirza taught me all about research and most importantly that I can play a part in it. He constantly kept track of my progress and discussed my experiments and other developments. I was constantly encouraged with very prompt reviews and a lot of constructive criticism in the writing of this thesis. I will always remember Professor Mirza with utmost gratefulness for the many productive hours involved in thought-provoking and stimulating scientific discussions, from which I benefited both professionally and personally.

The author would like to sincerely thank the NSERC Research Grant, under which it was possible to undertake the detailed field testing program on the Dickson Bridge and the related laboratory research activities. The contributions of the Canadian Electricity Association, Hydro-Quebec (Direction Principale Recherche et Developpement et IREQ- Dr. J. Mirza) and Natural Resources Canada/CANMET (Drs. V. M. Malhotra and M. H. Zhang) for suggesting the study of bond deterioration in fly ash concrete mixtures, and to the development of the concrete mixtures, preparation of the 192 pullout and auxiliary specimens and their shipment to McGill University are gratefully acknowledged.

The author would like to thank Professor Phil Distin of the Department of Mining and Metallurgy for his advice and several discussions related to the accelerated corrosion aspects of this program.

The author would like to acknowledge the several stimulating discussions with Dr. Zoubair Lounis of the Institute for Research in Construction/ National Research Council Canada and for the excellent French translation of the abstract.

The author would like to thank the following industrial partners involved in the Dickson Bridge Project:

- Corexco Inc. (Mr. G. Benchitrit)
- P. J. Materials Consultants (Mr. P. Jeffs)
- SIREM Inc., Montreal (Mr. Andre Bissaillon)
- SIKA Canada Inc.

The author would like to express her deep appreciation to Mr Mohammad Amleh for directing the work on Dickson Bridge field testing with great enthusiasm, and above all for his brotherly devotion and support. I would also like to extend my appreciation to Mr. Ali El-Jachi for his contributions towards the work on Dickson Bridge. The author would like to express her sincere thanks to Ms. Bahsheed Bahzedi Nejad Ahwazi for her contributions to the laboratory testing program for the past year. Special thanks are also extended to Mr. Nourredine Kadoum of COREXCO Inc., for his assistance with several basic issues and instrumentation.

The author would like to thank the Civil Engineering Department Staff and that of the Structure Laboratory (Messrs Ron Sheppard and Marek Przykorski) for their help, assistance, and good humor and pleasant memories of her association with them.

The author would like to express her heartfelt thanks to her parents who taught her that there is nothing impossible and only hard work, honesty, and persistence would result in achievement of what may otherwise seem unattainable. The author would also like to thank her brothers: Hisham, Muhammad, Mazin, Saleem, and sister: Asma for their support, and love. Special thanks go to Asma for her support and constant encouragement especially during the writing of this thesis.

Above all, the author is grateful to her companion and husband Bahjat and their daughter Aishah, because without their unconditional love, patience, invaluable encouragement, and understanding, the completion of this project would not have been possible. Therefore, the author affectionately dedicates this thesis to her husband and daughter.

Table of Contents

List of Figures

List of Tables

List of Symbols

ν	= the Poisson's ratio
ρ	= the resistivity in ohm-cm
ρ	= the density
ε_c	= the strain in the concrete
ε_{cm}	= the mean residual surface strain
ε_m	= the average strain
ε_s	= the strain in the steel
η	= the measured polarization
η_a	= the anodic overpotential
η_c	= the measured polarization
Δf_s	= the change of steel stress over unit length
Σo	= the nominal surface area of a bar of unit length
a	= the Tafel intercept
$A_{(c)s}$	= the equivalent area of the bar after corrosion
$A_{(uc)s}$	= the area of the steel bar in the specimen
A_b	= the area of bar
A_{ct}	= the area of the concrete subjected to tension
A_s	= the area steel reinforcement
b	= the Tafel slope
c	= the cover thickness
C_s	= the chloride surface concentration
C_x	= the chloride ion concentration at depth x
d_b	= the bar diameter
D_c	= the diffusion coefficient
E	= the actual potential
E_a	= the potential of the anode
E_c	= the potential of the cathode

E_{corr} = the corrosion potential (open circuit potential)

erf = the error function.

f_c = the ultimate concrete strength

f'_c = the concrete compressive strength

f_b = the bearing stress

f_t = the concrete tensile strength

f_y = the specified yield strength of steel reinforcement

HVFA = High Volume Fly Ash

I = the current density

$I_{corr.}$ = the corrosion current

ISAT = the Intial Surface Absorption Test

K = the equilibrium constant

L = the measured material path length (m)

l_b = the bar embedded length

ML = the Mass Loss

n = the valency

opc = the ordinary portland cement

P = the measured load

pfa = the pulverized fly ash

P_{max} = the applied force at failure

q = the change of bar force over unit length

R = the resistance in ohms

s = the slip

s_1, s_2 = the slip at arbitrary values of bond stress

S_m = the mean crack spacing

S_o = the minimum crack spacing

t = the exposure time

T = the measured transit time (s)

T = the steel force at the crack

$T_{(c)s}$ = the yield load of the corroded specimen

$T_{(uc)s}$ = the yield load of the uncracked control specimen.

T_c	= the tensile force
T_{cr}	= the cracking load in a specimen
u	= the bond stress
u_c	= the bond strength when the concrete cracks
u_{max}	= the maximum bond stress
u_{frict}	= the shear stress
V	= the longitudinal wave pulse velocity (m/s)
v_a	= the shear stress.
v_c,	= the shear stress, in the tangential
w/c	= the water/cement ratio

Chapter 1

Introduction

1.1 Background Information

Corrosion of reinforced concrete was first recognized early in the twentieth century, but it has become worse in recent decades with the widespread use of de-icing salts on highways and bridge decks. According to the results of a 5-year scientific study released by Environment Canada, the national environmental protection agency, in a typical year approximately 5 million tonnes of road salts are applied in Canada for de-icing, anti-icing, and dust suppression. Usually concrete provides an ideal protective environment for the reinforcing steel. However, when salts (chlorides or sulphates) penetrate the concrete and reach the steel rebars, corrosion normally commences. The corrosion products of the steel reinforcement will expand up to seven times its original size, developing pressures as high as 35 MPa (5000 psi) within the concrete, which cause cracking and spalling of the concrete cover and expose the rebar to further corrosion activity. Corrosion of reinforcing steel in concrete has caused catastrophic failures in some specific cases, resulting in injury and death, such as the collapse of the Berlin Congress Hall as shown in Fig. 1.1 [Isecke (1982)] and of a parking garage in Minnesota in Fig. 1.2 [Borgard *et al.* (1990)].

Recent studies by Battelle Columbus Laboratories and the National Institute of Standards and Technology show that the corrosion of metals costs the U.S. economy approximately $300 billion per year at the current prices. About one third of these costs (about $100 billion) could be reduced by proper application of "corrosion-resistant" materials and application of best technical practices to mitigate or minimize corrosion. In 1975, metallic corrosion damage cost the U.S. about $82 billion, which constituted

about 4.9% of its gross national product (GNP); about 60% of these costs were noted to be unavoidable. The remaining avoidable 40% of the cost ($33 billion) were attributed to the failure to use the best practices known then. A more recent study showed that compared with the 1975 costs, the 1995 costs decreased to about 4.2% of the GNP; the avoidable costs reduced by about 35%. However, these avoidable costs still amount to over $100 billion per year. The cost of rehabilitation for corrosion of reinforcing steel is estimated to be about $3 billion per year in Canada (Davis, 2000).

The cost of Canada's infrastructure is estimated between three and five trillion dollars and because of lack of funding and related political decisions leading to deferred maintenance, the current infrastructure deficit is well over $100 billion. Attempts are being made by the parties directly related to the crisis to find technical, financial and political solutions. It should be emphasized that the condition of infrastructure has a direct impact on Canada's productivity, international competitiveness, socio-economic developments and above all the quality of life of all citizens in Canada. To ensure that Canada continues to be the number one country, to live in, Canadian engineers must assume a responsible leadership role to ensure that the crisis is mitigated successfully. It should also be noted that if no corrective measures are taken now, the infrastructure will continue to deteriorate at an accelerated rate and it may cost a few hundred billion dollars and in some cases, it may have to be replaced at a much higher cost.

Chloride-induced corrosion of reinforcing steel in concrete bridge decks, parking garage slabs and marine structures has been identified as the primary cause of concrete deterioration. The distress in concrete is caused basically by several interactive factors and characterized mainly by the severe environment, unsuitable materials, inadequate construction practices and specifications in conjunction with other structural weaknesses. The cost of repairing existing Canadian concrete parking structures has been estimated to be between $6-8 billion. The Ontario Ministry of Transportation will be spending approximately $700 million on the repair and rehabilitation of its bridges. The Province of Quebec has committed to spend about $65 million over the next 5 years on the repair and rehabilitation of the Montreal area

bridges, and another $334 million on the repair of the area roads. The Federal Government has spent recently $150 million on the repair and rehabilitation of the Champlain Bridge in Montreal.

In the United States, there are more than 581,000 bridges in the national highway infrastructure system. Nearly 32% of these bridges are listed as structurally deficient or functionally obsolete (ASCE, 1998). The cost of repairing and replacing these bridges is estimated at $100 billion, and approximately 20 percent of the total estimated cost is due to the corrosion deterioration of concrete bridges. Based on the information provided by the Strategic Highway Research Program (SHRP), it is estimated that the cost of the corrosion damage in the United States transportation system now stands at over $20 billion, and it is increasing at the rate of $500 million per year. From a survey of collapsed buildings in England from 1974 to 1978, Mehta and Monteiro (1992) showed that eight concrete building structures collapsed because of the corrosion of the steel reinforcement. In 1975, the U.S. Interstate Highway System alone reported the need for US $6 billion for repair and replacement of reinforced concrete bridge decks. In addition, it was reported that at least 4800 of the 25000 bridges in the State of Pennsylvania were found to be in dire need of repair [Mehta and Monteiro (1992)]. The repair and maintenance of reinforced concrete structures is becoming increasingly important and extensive. In order to increase the reliability of the structure and to reduce maintenance costs, eliminating or at worst impeding the corrosion problem is very important. Also, to design new concrete structures and to repair existing deteriorated concrete structures requires an understanding of the various causes and mechanisms of corrosion of reinforcing and prestressing steel along with their performance in the varying aggressive environments.

The concrete cover acts as a physical barrier to the access of aggressive agents because of its strength and resistance to wear and tear, and to permeation of fluids containing harmful compounds. The high alkalinity of the concrete normally provides excellent corrosion protection to the reinforcing steel. Despite the "interest" in the

protective qualities of concrete, corrosion of steel is the most common cause of distress in concrete structures. Use of de-icing salts in cold climate countries aggravates this situation. Concrete structures subjected to seawater spray in marine structures and carbonation of concrete in industrial environments also lead to depassivation of the protective oxide layer on the reinforcing steel. These distresses have also occurred from avoidable errors in the concrete mixtures, lack of quality control in mixing, placing, consolidating and curing of the concrete resulting in permeable concrete. In addition, incorrect use of the different types of cements, supplementary cementitious materials, superplasticizers and other additives available commercially and used without a full understanding of their properties have also resulted in deterioration of concrete structures because of steel corrosion.

Embedded reinforcing steel is normally immune from corrosion because of the high alkalinity of the concrete; the pH of the pore water solution can be higher than 12.5, which protects the embedded steel against corrosion. This alkalinity of concrete causes passivation of the embedded reinforcing bars. A microscopic oxide layer, a "passive" film, forms on the steel surface due to the high pH -prevents the dissolution of iron. Furthermore, the concrete made using low water-cement ratios and good curing practices have a low permeability that minimizes the penetration of the corrosion inducing ingredients. In addition, low permeability increases the electrical resistivity of the concrete to some degree, thus helping in reducing the rate of corrosion by retarding the flow of the electrical current within the concrete that accompanies the electrochemical corrosion process. Consequently, corrosion of the embedded steel requires the breakdown of its passivity.

Concrete is relatively weak in tension, and it cracks when the tensile strength is exceeded in a reinforced member. Cracking is an important phenomenon specific to reinforced concrete, and it can have a significant influence on the durability of a concrete structure. The influence of new materials and new technologies being used presently, on the concrete tensile strength and the bond characteristics is not well established; the examples are the use of high-strength concretes, the use of fiber-reinforced plastic rebars, and the use of epoxy-coated rebars. Concrete tensile

strength and toughness are fundamental properties that ensure bond efficiency at the steel-concrete interface, as relatively low values of the bond stress-tensile strength ratio (u/f_t = 0.5 to 0.8) can exhibit a complex local stress and strain state [Gambarova and Rosati (1996)].

Bond between the reinforcing steel and the concrete is dependent on cohesion and adhesion at the steel concrete interface and the mechanical interlocking between the lugs or deformations of the reinforcing bar and the surrounding concrete. Corrosion results in an early loss of both cohesion and adhesion. As steel corrodes, the corrosion products that at first improve bond by a slight amount, however, the increasing levels of corrosion can result in longitudinal and transverse cracking which cause a release in the "hold" of the concrete on the bar and decreases the bond capacity at the steel-concrete interface.

It has been recognized by many researchers such as Malhotra and Carino (1991), and Cao *et al.* (1993) that the use of pozzolanic materials such as fly ash and silica fume in the concrete can lead to improved protection against steel corrosion, particularly against the ingress of chloride ions from external sources. However, there are still some concerns regarding the use of these and other new materials, that involve the possible side "effects" of pozzolanic reaction, including the reduction in the pH of the solution leading to reduction of steel passivation, or a reduced chloride threshold level.

An adequate thickness and impermeability of the concrete cover over the steel reinforcement provides both physical and chemical protection by providing an alkaline and electrically resistive medium in the immediate vicinity of the steel surface, besides providing a physical and chemical barrier to the ingress of moisture, oxygen, carbon dioxide, chlorides and other aggressive agents. According to RILEM (1987), the efficiency of the concrete cover in preventing corrosion is dependent on many factors, collectively referred as its "quality".

Over the past 15 years, Malhotra (1994) has undertaken detailed research on high volume fly ash (HVFA) concretes at the CANMET Laboratories, Ottawa. He noted that the HVFA concretes demonstrated excellent characteristics for resistance against freezing-thawing cycles, penetration to chloride ions, carbonation and alkali-aggregate reactivity. Despite the considerable research on HVFA concretes, their influence in inhibiting or impeding corrosion of the steel reinforcement and its effects on bond characteristics at the steel-concrete interface have not received adequate attention and need to be investigated further.

Corrosion of reinforcing steel can result in the loss of cross-sectional area and gradual deterioration of bond between the concrete and the reinforcing steel with increasing levels of corrosion. Besides being extremely costly, both phenomena can endanger structural safety and severely influence the serviceability of the structure. Over the past six decades, considerable research has been undertaken on bond, tension stiffening and crack width control to ensure system serviceability through control of crack width and deflections in structural concrete elements. However, very little research work has been undertaken to evaluate the effect of corrosion on bond characteristics at the steel-concrete interface, tension stiffening and the width and spacing of cracks. The corrosion of reinforcing steel, which impairs the overall durability, can perhaps impair structural safety more due to the deterioration of bond at the steel-concrete interface, than due to a loss in the cross-sectional area unless the bar size is too small.

Corrosion of the reinforcing steel causes a decrease in the bar diameter which affects adversely the mechanical properties of the steel bar in terms of its ultimate strength, yield strength, ductility, etc. Furthermore, when steel reinforcement corrodes, the corrosion products occupy a much larger volume than the original steel, and eventually exerts a large force on the surrounding concrete to cause formation of cracks that grow slowly as the reinforcement continues to corrode followed by the spalling of the concrete cover. Also, corrosion of the reinforcing steel causes changes in the surface conditions of the reinforcement steel, and the layer of the corrosion products causes loss of cohesion and adhesion at the steel-concrete interface. As

corrosion continues, it finally leads to changes in the profile of the bar rib. Eventually, all of the concrete around the steel bar is forced off by the pressure of the growing corrosion products, and the reinforcement loses not only any remaining protection against corrosion, but also loses a significant part of the bond resistance to transfer the force from the reinforcing steel to the surrounding concrete, and vice-versa.

Corrosion is very serious in the case of post-tensioned prestressed concrete due to the fact that the reinforcement is deliberately stressed in tension prior to any loading on the structure. In addition, the post-tensioning tendons are free to move within the ducts in the concrete over the beam length as they may be anchored only at the ends; such movements are prevented in grouted tendons. Therefore, rusting of tendons may take place without any visible sign on the concrete surface causing a sudden structural failure without any advance warning.

In summary, it should be emphasized that the reinforcing steel is provided in reinforced concrete to resist the tensile forces, and to produce controlled cracking within that zone. However, corrosion not only deteriorates the steel bar and its function of transferring the tensile forces, but also it deteriorates the concrete by spalling of the cover. Therefore, corrosion of the reinforcement has a strong influence on the bond behaviour at the interface between the steel reinforcement and the concrete. As corrosion of the reinforcing steel progresses, the bond strength between the reinforcing steel and the concrete diminishes progressively, and major repairs or replacement are needed. While considerable research has been undertaken about the problem, and numerous reports have discussed how this corrosion can be controlled, only limited data are available about its influence on the bond behaviour at the steel-concrete interface.

1.2 Research Significance

The author's research program was a significant part of a university-industry strategic research program to study the influence of corrosion of the reinforcing steel on the bond characteristics at the steel-concrete interface and on the durability of concrete bridges. While the durability of all concrete infrastructure facilities are influenced considerably by corrosion of the reinforcing steel, the strategic research program focused on the durability of transportation infrastructure, and in particular bridges. This focused objective was further strengthened by the availability of a decomissiond bridge (Dickson Bridge) in Montreal, which had deteriorated extensively, mostly due to corrosion of the reinforcing steel in the bridge deck and other members.

The stated objectives of the strategic research program were:

1. Detailed condition survey of the location and the state of the reinforcement (assessment of the extent and rate of corrosion; statistical analysis of data) to develop a data bank and use this information in the development of reliability-based design method to protect and to provide durability against corrosion of reinforcing steel.
2. To develop correlation between the field test and accelerated corrosion tests in the laboratory aimed at studying the corrosion phenomenon and its mitigation through protective strategies. This information will be used to develop practical design methods to ensure durability against corrosion of steel reinforcement and to guide engineers on related issues such as the protective strategies vis-a-vis concrete and steel reinforcement, concrete cover thickness, influence of the various parameters on deterioration of bond due to corrosion, etc., and evaluation of service life of new structures and residual service life of existing and repaired structures. The program will also include laboratory tests related to the Dickson Bridge parameters to study the corrosion of steel bars embedded in Dickson Bridge concrete and its correlation with the field data.
3. To examine the effect of selected steel priming systems on corrosion activity following restoration of reinforced concrete.

4. Development of practice-oriented design guidelines for durability against steel reinforcement corrosion and bond deterioration; assessment of the service life.

One of the possible causes of deterioration of the Dickson Bridge deck was the loss of bond resistance at the steel-concrete interface due to excessive corrosion of the reinforcing steel. Therefore, it was important to undertake a laboratory study of the loss of bond at the steel-concrete interface using specimens made from the same concrete as used for the Dickson Bridge deck and to undertake controlled tension tests to establish the loss of bond with increasing levels of corrosion. At the same time, the various modes of deterioration had to be examined in detail in the field, besides establishing reasonable correspondence with the laboratory tests. This objective was the focus of this investigation as a part of the overall strategic research program, with the detailed objectives stated in the next section.

A study of the influence of corrosion and cracking on the bond behaviour of reinforced concrete aimed at understanding how the bond stresses transferred from the corroded steel to the surrounding concrete (at the steel-concrete interface) and to study the influence of the progressive deterioration of bond with increasing levels of corrosion. The correlation between corrosion, bond strength and cracking of the reinforced concrete needs urgent attention.

It is anticipated that the findings of this field and laboratory research program will lead to an improved understanding of the corrosion problem, its seriousness and its influence on the deterioration of bond at the steel-concrete interface. The results will be used to develop appropriate analytical models and the related practice-oriented design tools, leading to improved design procedures and enhanced service life. In addition, the results of this program will help the practising engineers with the evaluation and amelioration of the existing infrastructure and with the design of new concrete infrastructure for durability against corrosion of the reinforcing steel. Embedded within this research project (by using the new non-destructive techniques of detecting corrosion reinforcement as well as the concrete quality) are several

benefits which will directly impact the construction industry, products, materials, components and systems.

1.3 Summary of Previous Research

This section, does not attempt a total review of all of the tests on corrosion of the embedded steel in the concrete, but rather the results of some tests that have an impact on corrosion of embedded steel in concrete are reviewed. Special attention is given to the research associated with the investigation of the influence of corrosion on bond behaviour.

Concrete in seawater is a topic that has been discussed for decades [Gjorv (1975)]. Some papers were presented as early as 1909 at the meetings of the International Association for Testing Materials in Copenhagen, which reported on corrosion mechanisms, procedures to reduce or prevent corrosion in the early investigations based on the results of the various experiments and observations. Information on the chloride content and the onset and progress of the corrosion process has been incorporated in the provisions of the various codes of practice presently used in construction in different parts of the world, but research is still needed to explain fully the corrosion phenomenon. The ACI Committee 222R (1989; 1994) reports the state-of-the art of the corrosion of metals in concrete. The basic information from these reports is also incorporated in the CSA Standards S6, S413 and S474.

Considerable research has been undertaken to study the bond characteristics of deformed bars in concrete. It has been reported by Abrams (1951) that the earliest published tests on bond of reinforced concrete with "iron bars" was carried out by Hyatt in 1877. The ACI Committee 408 (1966; 1991) and the CEB Task Group VI (1981) have summarized some of the major developments in the study of the bond characteristics over the last century.

Several researchers have investigated the bond characteristics of steel bars in reinforced concrete by studying the behaviour of reinforced concrete tension elements. Houde and Mirza (1979) obtained new basic information on the bond-slip characteristics of deformed bars at the various load levels using two different types of specimens i.e, anchorage and transfer type, along with the variation of the concrete strength from 20.5 MPa to 44.0 MPa (2980 psi to 6390 psi). Sixty-two concentric tensile specimens with No. 4, No. 6 and No. 8 bars, with twelve tests on specimens with internally instrumented No.8 bars, along with another six beam-end tests with similar internal instrumentation were tested. The specimens were sliced and examined after testing, and it was found that slips have resulted from gradual deterioration of the concrete keys in front of the ribs. The influence of the concrete cover in restraining the bar was also examined. They found that the slip of the reinforcing bar increases almost linearly with an increase in the steel stress.

The tensile behaviour of concrete members reinforced with a single reinforcing bar and the influence of transverse cracks and splitting cracks on tension stiffening has also been studied by several researchers such as Abrishami *et al.* (1995). Fracture mechanics techniques have been developed to model the influence of bond and cracking on the tension response of reinforced concrete members [Bazant (1992) and Ouyang and Shah (1994)]. However, little research has been undertaken to evaluate the effect of corrosion of the bar surface changes on the steel-concrete interface bond. Therefore, more research is needed in order to gain a better understanding of the nature of the corrosion influence on bond, and the parameters, which affect the failure of bond due to corrosion.

Page *et al.* (1978) conducted research on the effect of mix characteristics and steel surface conditions on the bond between the steel reinforcement and different mortars. It was found that the changes in the properties of the steel oxide film influence the bond strength.

Sakamoto and Iwasaki (1982) studied the influence of sodium chloride (NaCl) on bond between the reinforcing steel and the concrete using accelerated corrosion tests on 150x150x150 mm cubes, reinforced with a 16 mm diameter reinforcing bar, in accordance with the ASTM Standard C234. The deformed and plain reinforcing bars were galvanised in accordance with the Japanese Industrial Standard (JIS) H8641. The molten zinc was maintained at a temperature of 460°C and the immersion time was 30 seconds. The amounts of NaCl (dissolved in the mixing water - 188 kg/m^3 of the concrete) added to the concrete were 0, 0.1, 0.3, 1, 2, and 5 percent by the weight of sand (794 kg/m^3 of concrete) in an oven dry condition. The curing temperatures used were 20°C, 40°C and 50°C and the age at testing was 7 and 28 days. Two specimens were tested for each condition.

The bars removed from the specimens, which showed deterioration of the bond strength under conditions with high NaCl concentration and elevated temperature, showed corrosion products on the surface. The reinforcing bars in such specimens were affected by corrosion even in the case where rust was not evident. In case of the specimens with galvanized bars and subjected to similar conditions, the galvanized bars showed no signs of corrosion, and there was only some discoloration on the bar surface. Sakamato and Iwasaki (1982) also noted that the layer of the corrosion products becomes dense in its structure because of the constraint of the surrounding concrete. This decreases the rate of consumption of zinc and preserves the bond strength over a longer period, because the layer of corrosion products is prevented from penetrating in to the zinc surface. They concluded that zinc coating is an effective means to protect the reinforcing steel from the attack if chlorides are present in the concrete.

Al-Sulaimani *et al.* (1990) studied the influence of reinforcing bar corrosion and the associated longitudinal cracking on the steel-concrete interface bond behaviour using the standard pullout and beam tests. They used pullout tests to simulate severe local corrosion conditions, and the beam tests to simulate relatively uniform corrosion conditions along the bar length. The pullout specimens, 150-mm side cubes, were reinforced with 10, 14 and 20-mm diameter bars cast centrally to

give cover-diameter ratios of 7.50, 5.36 and 3.75, respectively. The effective embedment length-diameter ratio provided was 4.0, with the concrete and the steel strengths being 30 MPa (water/cement = 0.55) and 450 MPa, respectively. Polypropylene fibres were added (0.2 percent by volume) to the concrete for the second test series. The beams, 150 x 150 x 1000-mm in size, were reinforced with two 10 mm diameter top bars; one 12 mm diameter bottom bar isolated from the 6 mm diameter closed stirrups at 50 mm centres. The embedment lengths provided were 144 mm in one series and 300 mm in the second series, the latter being required by the ACI 318-95. The bond behaviour at the steel-concrete interface was examined at four different stages of corrosion: i) no corrosion stage, ii) precracking stage, iii) cracking stage, and iv) postcracking stage.

These stages of corrosion were achieved by impressing a direct current with a density of 2 mA/cm^2 for increasing periods on the reinforcing bar embedded in the pullout, or the beam specimens located in water. The circuitry was so arranged that the steel bar served as the anode, while a stainless steel plate situated in the water acted as the cathode.

Analysis of the test data showed that the bond strength increased with corrosion up to a certain level (about 1% loss of bar weight) because of the increased bar surface roughness with the growth of a firm layer of corrosion products on the bar surface that enhanced the bond strength at the steel-concrete interface. However, with a progressive increase in the level of corrosion, the bond strength decreased rapidly for the pullout test, but at a much lower rate than for the beams. Al-Sulaimani *et al.* (1990) noted that for the pullout tests, the bond strength becomes negligible at corrosion level of 7.5 percent weight loss for the 14-mm diameter bar. They noted that the calculated average bond stress was 1.5 times the permissible bond stress calculated using the provisions of ACI 318-95 even after a corrosion level with 5 percent loss of bar weight for the beam tests. This bond deterioration was attributed to the loss of the bar lugs or deformations, because of the severe localized corrosion in the pullout specimens, which generated flaky products of corrosion on the bar

surface, which along with the widening of the longitudinal crack resulting from corrosion, seriously deteriorated the bond strength at the steel-concrete interface.

Al-Sulaimani *et al.* (1990) observed that introduction of 0.2 percent polypropylene fibres by volume into the concrete improved the bond strength at the steel-concrete interface, particularly during the postcracking stage. This was basically due to the lower level of damage at the bar surface and the contribution of the fibres in improving the confinement and holding capacity of the concrete surrounding the bar.

Cabrera and Ghoddoussi (1992) undertook a laboratory investigation on the influence of reinforcement corrosion on bond strength of deformed bars, using beam and pullout specimens made with ordinary portland cement (OPC), and pulverised fly ash and cured in a simulated hot dry environments (35°C and 45 percent relative humidity). To achieve the different levels of corrosion, a voltage of 3 volts versus saturated calomel electrode was impressed to accelerate the corrosion process. The experimental results were used to determine the relationships between the bond strength and the corrosion rate. Similarly the ultimate bond stress was related to the crack width. They discussed the influence of the cement type on the rate of corrosion and their effect on the bond strength. The concrete with the fly ash exhibited better resistance to corrosion damage than OPC concrete basically because of its higher electrical resistivity.

Realizing that durability and service life of large-scale concrete structures exposed to aggressive environments is severely influenced by corrosion of the reinforcing steel, Oh *et.al.* (1999) developed an accelerated corrosion test, similar to that of Amleh (1996). The test specimen after 28 days of wet-curing was immersed in a five percent sodium chloride solution along with an applied voltage of 20 volts D.C. The pullout test specimens, 100 mm diameter by 200 mm high and reinforced symmetrically with a single steel reinforcing bar, were made from normal portland cement concrete mixture with different water-cement ratio to obtain different strengths ranging from the normal to high strengths. They also studied the influence

of mineral admixtures, such as silica fume, and granulated blast furnace slags and their combinations and noted the improvement in the rebar bond response as compared with the normal portland cement concrete mixtures. Also, the high-strength concrete mixtures showed higher bond resistance than the normal-strength concretes. Using the Faraday's law, they attempted to estimate the endurance life of the concrete structure by equating the total current from the accelerated corrosion test to the total current from the natural condition.

1.3.1 Strength and Durability of Fly Ash Concrete

Klemm (1989), noted that the first documented approach to develop a new cement that would provide mortar of better durability was made by John Smeaton in 1756, when he was engaged in a project to rebuild the Eddystone Lighthouse off the coast of Cornwall. "Smeaton realized that, for a durable masonry construction, the ordinary lime mortars of the day would not resist the damaging effects of the sea. He then undertook an investigation of the various kinds of limestones, which he could obtain and the performance of the limes they produced. In the end, Smeaton stated, "I did not doubt but to make a cement that would equal the best merchantable portland stone in solidity and durability." This comparison to Portland stone was the origin of the name Portland cement. Smeaton's structure stood for 123 years before being replaced.

Malhotra and Ramezanianpour (1994) studied the performance of concrete mixes with ground, blast-furnace-slag, fly ash and condensed silica fume under four different curing regimes. The water-to-cementitous materials ratio was 0.5 for all mixtures, excepting for the high-volume fly ash mixture for which this ratio was 0.35. The concrete specimens were moist-cured at room temperature, cured at room temperature after two days of moist curing, and also cured at 38°C and 65% relative humidity. The compressive strength of the concrete was determined at various ages, and the resistance to chloride-ion penetration was measured using the ASTM C 1202 test at different ages up to 180 days. Mercury intrusion porosimetry tests were performed on the 28-day old mortar specimens for comparison purposes.

A reduction in the moist-curing period resulted in lower strengths, higher porosity and more permeable concretes. The strength of concretes with fly ash or slag was more sensitive to poor curing than the control concrete, with the sensitivity increasing with the amounts of fly ash or slag in the concrete. Incorporation of slag or silica fume, or high volumes of fly ash in the concrete mixture increased its resistance to the penetration of chloride ions, and produced concrete with very low permeability.

Malhotra (1994) reported development of high-volume, low-calcium fly ash concretes (HVFA) with slumps in excess of 150 mm, obtained by the use of large dosages of superplasticizers. Typical cement contents were about 150 kg/m^3; the water to -cementitious materials ratio was about 0.3; the fly ash content was between 56 and 60 percent of the total cementitious material. The properties of fresh concrete in terms of setting time, bleeding, entrainment of air in fresh concrete and its density, and the dosage requirements of superplasticizers were reviewed.

Malhotra (1994) noted that because of the low cement content, the temperature rise in the HVFA concretes during the first few days after casting was very low, making it ideally suited for massive concrete structures such as dams. The HVFA concrete exhibited adequate strength development at both early and later ages, with values comparable to the normal portland cement concrete. Similar results were observed for cores drilled from the in-situ concrete that were comparable or greater than the strength of the cores obtained from the control concrete blocks. The modulus of elasticity and shrinkage and creep characteristics of HVFA concretes were comparable to those of the normal concretes. Test for water permeability, using the uniaxial flow apparatus developed at CANMET, showed that the HVFA concretes had very low permeability, although no numerical values were assigned (Bisaillon and Malhotra, 1988).

The HVFA concrete demonstrated excellent characteristics for resistance against freezing and thawing cycles, penetration to chloride ions, de-icing salts, carbonation and alkali-aggregate reactivity. A few cases of successful application of

HVFA concretes in a communication satellite block, a hotel/office complex, wharf development and stabilization of rock outcrop slopes on a highway were also reported. The excellent strength, permeability and durability characteristics of HVFA concrete can be useful in systems such as bridge decks and parking structures that are exposed to de-icing salts during the winter, and structures in seawater environment. This led to the present investigation aimed at studying the influence of the different Canadian fly ashes in inhibiting or impeding the corrosion of steel reinforcement, and its effect on the bond at the steel-concrete interface.

Gu *et al.* (1999) studied the corrosion performance of steel reinforcement in normal portland cement and high-volume fly ash (HVFA) concretes exposed to a chloride solution. They used 833 x 600 x 153 mm concrete slabs, cast from six air-entrained concrete mixtures-four with normal portland cement concrete with water-cement ratios ranging from 0.32 to 0.76 and the other two HVFA concretes with water-cementitious materials ratio of 0.32. The cover thickness to the steel bar ranged from 13 to 76mm. The concrete prisms were ponded with a 3.4 percent NaCl solution for six months and the progress of the steel rebar corrosion was monitored using the half-cell potential, linear polarization and AC impedance tests.

The performance of steel rebar in HVFA concretes after six months was found to be excellent, with no significant corrosion even with a 13 mm thick concrete cover. This performance matched that of steel bars in the normal portland cement concrete with a water-cement ratio of 0.32, and was better than that of the concrete with a water-cement ratio of 0.43. The steel corrosion was more significant with a water-cement ratio of 0.76, even with a concrete cover of 51mm over the steel rebar.

1.3.2 Previous Research at McGill University

Two detailed investigations dealing with the development of accelerated electrochemical corrosion of reinforced concrete have been completed at McGill University [Palumbo (1991), Farah (1993)]. They developed the test set-up and a

detailed procedure for accelerated corrosion testing using lollipop specimens, with the period to complete corrosion in most specimens not exceeding 45 days. The effects of the clear concrete cover thickness, deformed steel bars with and without an epoxy coating, and the effectiveness of the surface sealants were studied.

Fazio (1996) undertook a similar study of the flexural behaviour of reinforced concrete beams subjected to an identical similar accelerated corrosion regime as Amleh (1996). He tested seven beams, with different levels of corrosion.

In a preliminary series of tests (Amleh 1996), studied the influence of level of corrosion on bond strength through consideration of both the transverse and the longitudinal cracks, and the relative bond effectiveness of the corroded bars was determined from the crack spacing. Different stages of the steel reinforcement corrosion were established to study their relative bond behaviour, ranging from no corrosion at all to "complete" corrosion at the steel-concrete interface. The chloride content was obtained for each tension specimen by chemical analysis, using the Volhard Method [British Standard (1988), Part 124]. The bond strength decreased rapidly with an increase in the corrosion level, especially in the case of any severe localized (pitting) corrosion. It was found that the first level of corrosion, which represented approximately 4 percent weight loss due to corrosion, resulted in a 9 percent decrease of the nominal bond strength, while the sixth level of corrosion with an approximate 17.5 percent weight loss (the case of very heavy corrosion) due to corrosion, resulted in a 92 percent loss of the nominal bond strength. The bond behaviour was influenced by the deterioration of the reinforcing bar ribs, and by the reduced adhesion, cohesion and loss of mechanical resistance of the reinforcing bar due to the widening of the longitudinal splitting crack(s) resulting from corrosion.

1.4 Scope and Objectives of Investigation

As mentioned earlier this research program was undertaken as a part of the overall strategic research program. The Canadian Electricity Association, Hydro-Quebec and

Natural Resources Canada/CANMET were studying simultaneously the use of high-volume fly ash in grout and shotcrete for applications in hydraulic structures. The first part of the study dealt with preparation of shotcrete panels, and evaluation of the materials used, mixture proportions, mixing and shotcreting operations, and the various properties of the fresh and hardened polypropylene fibre-reinforced shotcrete incorporating silica fume and high volumes of fly ash. The workability of the fresh concrete was improved by the incorporation of fly ash and silica fume, resulting in lower operating pressures for the shotcreting. The shotcrete with silica fume had a negligible rebound compared with the one without silica fume. The polypropylene fibre-reinforced shotcrete demonstrated satisfactory workability, mechanical properties and resistance to freezing and thawing. Use of 0.5 percent polypropylene fibre by volume did not significantly improve the shotcrete compressive strength.

The second part of the detailed study by Canadian Electricity Association, Hydro-Quebec and Natural Resources Canada/CANMET examined the effects of carbonation on HVFA concretes, and compared these with a similar effect on the normal portland cement concretes with water-cement ratio of 0.32 and 0.42 as used in this research program. The HVFA concretes incorporated 58 percent of fly ash from three Canadian sources and the carbonation of the concrete was evaluated using an accelerated testing method with the specimens subjected to two different curing regimes being exposed to 3 percent CO_2 at 23°C and 65 percent relative humidity. Increasing the moist-curing period from 7 days to 28 days decreased the carbonation depth, however any further curing until 91 days did not have a significant effect on the carbonation depth. The depth of carbonation of all concretes cured in a standard moist curing room for 28 days, followed by drying for one-day in the laboratory air was less than 16mm after 140 days of exposure to 3 percent CO_2 at 23°C and 65 percent relative humidity. The carbonation depth ranged from 0 to 2.5mm for normal portland cement control concretes, and 12 to 15.5mm for HVFA concretes.

This research program has been designed to include both field and laboratory testing. The basic objectives of this research program are to study the influence of

increasing levels of corrosion on the progressive deterioration of bond between the steel and the concrete; to study the effects on the long-term durability of reinforced concrete made using new materials, and to establish relationships between the long-term data and accelerated durability testing in the laboratory. The relationship between the rebar corrosion, deteriorating bond characteristics at the steel-concrete interface and cracking of reinforced concrete need to be studied urgently:

1. to enable assessment of concrete structures damaged due to the corrosion of the reinforcing steel,
2. to develop procedures for reliability-based design of new concrete structures for durability against corrosion of the reinforcement,
3. for the repair and rehabilitation of existing corrosion-damaged concrete structures,
4. to develop a reliability-based method for design for durability against corrosion,
5. for service life prediction of new and existing concrete structures.

There has been an increased emphasis on the use of supplementary cementing materials in concrete with the objective of making concrete structures more durable. This research has specific significance to the corrosion-resistance characteristics of concrete mixtures in which different classes of fly ash and high alumina cement are used. The corrosion protection of the fly ash concrete to the reinforcing steel will be studied compared with that of plain concrete.

The objectives are to determine the effects of cement type, water-cement ratio concrete cover thickness, the use of different classes of fly ash on the related durability characteristics of the concrete. The main objective is to determine as to what extent the various cements and mix proportions influence the corrosion of the reinforcement as a function of the chloride-ion penetration phenomenon.

In addition, there are no data available on the deterioration of bond between the concrete and the reinforcing steel with the level of corrosion of the bar. Using the test data obtained in the previous investigations at McGill University, and some new tests, it is proposed to establish a standardized accelerated electrochemical corrosion testing

procedure with the objective of "completely" corroding the bar over a period of 20-25 weeks. The primary objectives of this research program are:

1. To simulate the prevalent conditions under severe local corrosion that cause significant changes on the surface conditions of the steel reinforcing bar.
2. To study the effect of varying levels of corrosion on the response of a standard tension specimen with a single reinforcing steel bar and the effectiveness of bond between the reinforcing steel and the concrete.
3. To study the bond characteristics of corroded reinforcing bars using pullout and tension specimens.
4. To evaluate the condition of the corroded steel bars from four randomly selected segments of the bridge deck, measuring approximately 6m by 5m, over a grid of 0.25m by 0.25m and to correlate this corrosion data with the results of the investigations of five other researchers who also tested the bridge.
5. To establish the correspondence between the corrosion of the reinforcing steel in the bridge deck and the corresponding corrosion characteristics obtained at different levels of corrosion from the laboratory tension tests.
6. To establish the remaining bond resistance of the reinforcing steel in the Dickson Bridge deck and other components for use in a nonlinear finite element analysis of the behaviour of the corrosion-deteriorated deck in another investigation.

The investigations of the influence of corrosion on the bond behaviour between the reinforcing steel and the concrete reported here were carried out under two series of tests, pullout and direct tension testing relative to three stages of corrosion: no corrosion, corrosion corresponding to precracking, and postcracking levels. In total, eight levels of corrosion were produced, ranging from no corrosion, (uncorroded) to complete corrosion, over 20 percent weight loss due to corrosion, with wide longitudinal cracks caused by the pressure due to the volumetric expansion of the corrosion products. Corrosion was measured as the loss of metal of the reinforcing steel bar relative to the original reinforcing steel bar weight.

1.5 Outline of Thesis

Chapter 1 addresses the goals of this research program within an overall strategic research program, besides presenting an overview of the research undertaken in the general area of bond of corroded bars in reinforced concrete where they have been the subject of study and research during the recent years. Chapter 2 presents some of the latest literature review of the mechanisms of reinforcement corrosion and the main causes of the breakdown of the protective mechanisms, which have been the subject of intensive research over the past few decades. It discusses the characteristics of the concrete that are relevant to reinforcement corrosion, and how the concrete environment protects the embedded steel. In addition, it presents several practical methods of reducing the level of corrosion in the embedded reinforcing steel, which must be taken into account to ensure a reasonable long service life. Chapter 3 reviews the basic mechanics of bond transfer between the concrete and the steel reinforcement and the associated slip of the deformed bars in the concrete, which causes cracking. The possible influence of the bond between steel and concrete is examined and the stresses and deformations in the concrete, caused by the bonding forces are also presented. This chapter also summarizes the program planned to study the parameters that are influenced by corrosion, to evaluate the bond characteristics in the corroded reinforcement in the tension specimens used in this study. The parameters studied are: i) Load-deflection response; ii) Stress-strain relationship; and iii) Crack spacing and crack width

Chapter 4 briefly describes the several techniques used to assess the concrete condition and the level of corrosion activity that were used in the field and laboratory testing, along with their advantages and limitations. These evaluations provide the cause and extent of the corrosion of the steel reinforcement. Chapter 5 presents the field studies on the abandoned Dickson Bridge undertaken as part of this investigation. It summarizes the results of several field and laboratory tests, undertaken over a grid of 0.25m by 0.25m, on four randomly selected 5 by 6m deck patches, aimed at determining why the Dickson Bridge deteriorated so rapidly.

Chapter 6 describes the experimental program of the accelerated corrosion testing to simulate the corrosion conditions in the pullout and tension specimens that underwent the accelerated testing. In addition, the experimental program of the pullout and direct tension testing of the specimens that was performed after achieving the required corrosion conditions is also presented in Chapter 6. Chapter 7 reports the discussion and analysis of the results obtained from the accelerated corrosion monitoring programs. Chapter 8 presents the discussion and analysis of the results that were obtained from the pullout-tests. Chapter 9 presents the discussion and analysis of the results that were obtained from the tension test programs, and details some of the results for the tension specimens, constructed using the Dickson Bridge concrete, which will be useful in the nonlinear finite element analysis studies of the deteriorated bridge deck. An overall discussion of the analytical investigation of the experimental results then follows in Chapter 10, its relationship to the field conditions, in addition to the discussion of the aspects of the design of reinforced concrete structures subjected to corrosion of the reinforcement. A brief summary of the experimental and analytical work as well as the conclusions are presented in Chapter 11, and recommendations for further research and development of the influence of corrosion on bond behaviour at the steel-concrete interface are included.

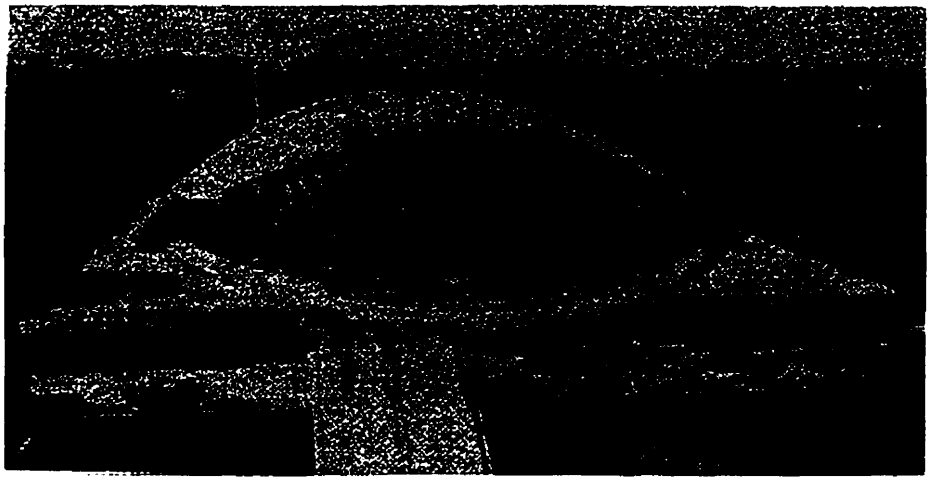

Fig. 1.1: Collapse of the Berlin Congress Hall, [Isecke (1982)].

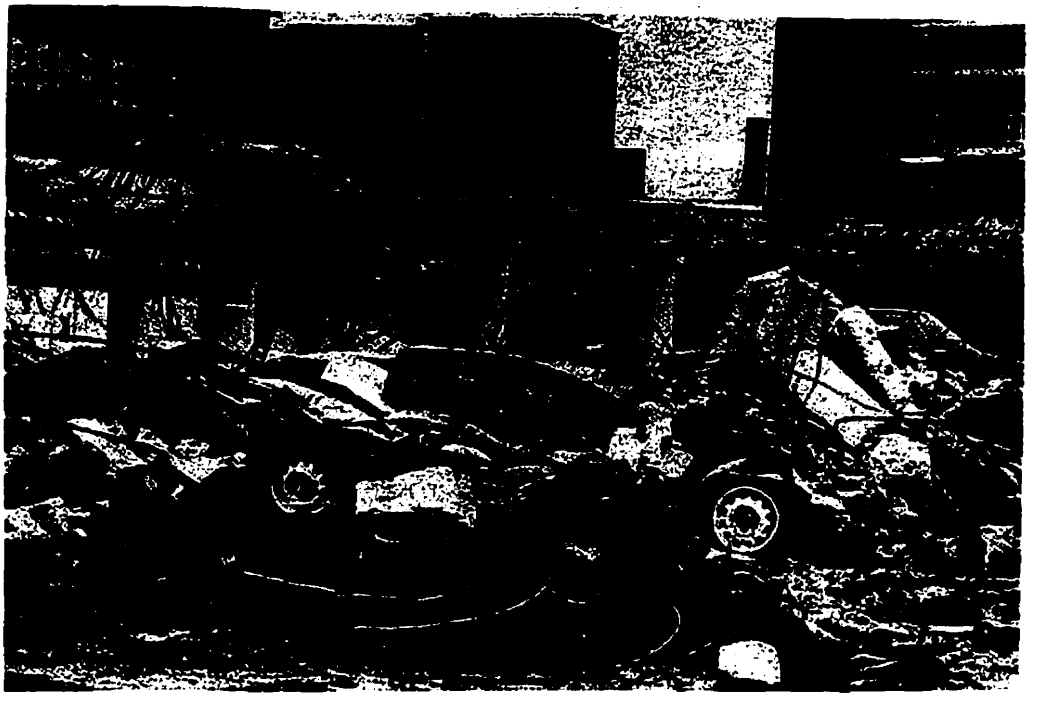

Fig. 1.2: Collapse of a salt-damaged parking garage,
[Engineering News Record (1984)].

Chapter 2

Corrosion of Steel in Concrete and its Mitigation

2.1 Introduction

Steel in concrete is normally immune from corrosion because of the high alkalinity of the concrete; the pH of the pore water solution can be about 12.5 or higher, which protects the embedded steel against corrosion. This alkalinity of concrete causes passivation of the embedded reinforcing bars. A microscopic oxide layer, which is the 'passive' film, forms on the steel surface due to the high pH that prevents the dissolution of iron. Furthermore, the concrete made using low watert o cement ratio and good curing practice, has low permeability that minimizes the penetration of the corrosion inducing agents. In addition, low permeability is believed to increase the electrical resistivity of the concrete to some degree which helps in reducing the rate of corrosion by retarding the flow of electrical currents within the concrete that accompany the electrochemical corrosion. Consequently, corrosion of the embedded steel requires the breakdown of its passivity.

The steel reinforcement in a majority of concrete structures or concrete elements does not corrode because of these inherent protective characteristics, as long as there is a suitable quality of concrete and proper design of the structure for the

intended environmental exposure that does not change during the life of the structure. However, corrosion of the steel in the concrete may result when the conditions mentioned above are not met in reinforced or prestressed concrete. In places of very severe exposure, such as pilings in sea water or bridge decks exposed to deicing salts, the use of other protective measures, i.e. corrosion inhibitors, coatings on steel or sealing of the concrete surface, or cathodic protection may be required.

2.2 Concrete as an Electrolyte

An understanding of some of the elements of the concrete structure is essential for discussing the factors influencing corrosion. Concrete consists of cement paste and coarse and fine aggregates, and the aggregates usually do not play a significant role in the corrosion process. Basically, the hydrated cement paste phase of the concrete acts as the electrolyte for the transportation of ions and the ionic current.

The Dictionary of Word Origins (Ayto, 1990) defines the **concrete** as something that has 'grown together.' The word comes, via Old French concret, from Latin concretus, the past participle of concrescere 'grow together,' hence 'harden.' This was a compound verb formed from the prefix com- 'together' and crescere 'grow' (source also of English crescent, increase and accrue). Its original application in English was fairly general - referring to that which is solid or material; its use for the building material did not emerge until the early 19th century.

Concrete is a composite material, that consists primarily of a binding medium with aggregates embedded in it. The term "binding medium" refers to a mixture of hydraulic cement and water. **Cement** is a fine gray powder obtained by burning clay and limestone at very high temperatures. In origin Latin caementa meant 'stone chips used for making mortar'; etymologically, the notion behind it was originally caedmenta, a derivative of caedere 'cut' (from which English gets concise and decide). In due course, the signification of the Latin word passed from 'small broken stones' to 'powdered stone (used for mortar),' and it was in this sense that it passed

via Old French ciment into English. The most common hydraulic cement is portland cement. The ASTM C 150 defines portland cement as a hydraulic cement produced by pulverizing clinkers consisting essentially of hydraulic calcium silicates, usually containing one or more of the forms of calcium sulfate as an interground addition. Portland cement primarily consists of hydraulic calcium silicates which constitute about 80% of the mass, the remaining 20% comprising aluminates, ferrites and other compounds. The term aggregate refers to a granular material, such as sand, gravel, or crushed stone. The aggregate grading varies from fine aggregates smaller than 5mm to coarse aggregates with size usually in the range of 20 to 40 mm. The aggregates are generally considered as inert fillers.

Mehta and Monteiro (1992) and others have described the composition of the hydrated cement paste, which consists of two phases - the hydrated minerals and the pore solution (liquid phase). The basic parameters that control steel corrosion, are:

(1) The volume and composition of the pore solution.

(2) The size and distribution of pores.

(3) The presence of $Ca(OH)_2$ in the hardened paste.

Hardened concrete consists of solid phases and voids (Mehta, 1993). Solid phases include hydrated cement paste (hcp), aggregate, and the transition zone, a very thin layer between the aggregate and cement paste. This transition zone is about 20 to 50μm thick and is characterized by a higher void content than the bulk paste. Basically, the cement paste phase of the concrete acts as the electrolyte for the transportation of ions and the ionic current as aggregates usually do not play a significant role in the corrosion process. To a very large extent, the chemistry and particularly the physical structure of the cement paste determines the durability of the concrete and the nature of any deterioration (Lea, 1970). In general, the aggregates of concrete do not play a significant role in the protection or corrosion of reinforcing steel as there are no leachable ions. Also, the aggregates are usually less permeable than hydrated cement paste, however, its inclusion in the concrete creates low-density transition zones and makes concrete more permeable.

2.2.1 Transition Zone

Among the solid constituents of concrete, it is the transition zone that has the greatest influence on the concrete strength, its elastic modulus, and permeability. Maso found that in freshly compacted concrete, water films form around the large aggregate particles, where it would account for a higher water/cement (w/c) closer to the larger aggregate than away from it. Also, ettringite and calcium hydroxide form in the transition zone making this layer weak and porous. If mineral admixtures are incorporated into the concrete, calcium hydroxide reacts further with the supplementary cementing materials and forms calcium silicate hydrate (C-S-H), which reduces the zone thickness, making it denser, and less permeable. In fact, the main cementing reaction of Portland cement is the hydration of the calcium silicates to form C-S-H.

2.2.2 Pore Solution

The pore solution composition has a great influence on whether the steel embedded in the concrete will remain passivated, or it will commence to corrode. Recent research has shown that ingress of soluble sodium and potassium compounds can lead to pH values of greater than 13 in the pore solution in ordinary portland cements, however, the pH of the pore solution of blended cement concretes has been observed to be lower. Considerable research has also been undertaken to determine the influence of the cement composition on the degree of binding of the chloride ions, because it is the free chloride ions in the pore solution that are available for attacking the steel and initiating corrosion.

2.2.3 Water in Concrete

Water is the principal agent of destruction of materials. Water exists in the hydrated cement paste in many forms; it can accumulate in the concrete pores and capillaries and the amount of water depends on the pore size distribution and environmental humidity. This water, or rather the pore water solution, can be classified into

different types depending on how difficult it is to remove it from the concrete. For the water in the hardened cement paste, it can exist in the following forms:

1. Capillary Water: It refers to the water existing in the capillaries which are 5 nm in diameter or larger. The water will be held by capillary tension if the capillary size is smaller than 50 nm. For large capillaries, with diameter greater than 50 nm, water is considered as free water because its removal will not have any effect on the concrete volume.
2. Adsorbed water: This type of water exists close to the solid surface and is held in place by attractive forces. Adsorbed water is lost when the paste is dried to about 30% relative humidity. Depending on the surface energy of the solid, water adsorption is not limited to a mono-layer, but follows a model of multi-layer adsorption.
3. Interlayer water: This is a monomolecular water layer that is held between the layers of C-S-H (C-S-H is one of the solid phases in the hydrated cement paste). This water is lost only on very strong drying, below 11% relative humidity.
4. Chemically combined water: This water exists in the cement hydration products in the form of hydrates and is not lost on drying.

2.2.4 Calcium Hydroxide

The volume of solids in the hydrated cement paste consists of 20 to 25 percent of calcium hydroxide, $Ca(OH)_2$, crystals. Detailed studies of the hydrated cement paste have shown limited solubility of $Ca(OH)_2$ in aqueous solutions and it remains as a solid substance distributed in the hydrated cement paste. While tricalcium silicate, C_3S, and dicalcium silicate, C_2S, have been known to contribute to the strength of the hydrated cement paste, the contribution of the large calcium hydroxide, $Ca(OH)_2$ crystals, because of its considerably lower surface area-volume ratio, is much lower. However, $Ca(OH)_2$ helps maintain a high pH level in the hydrated cement paste and provides a useful pH buffer for the pore solution. In addition, $Ca(OH)_2$ tends to form large crystals with a distinctive hexagonal-prism morphology, where it precipitates as

a coating over the steel surface, the pore walls, the mold walls, which provide physical protection to the steel bars. This explains why the various reinforcement corrosion tests cannot be extrapolated to the behaviour of the steel embedded in the concrete in "real" structures. It should also be noted that the higher the concentration of $Ca(OH)_2$ in the hydrated cement paste, the longer will be the time for the carbonation front to penetrate the concrete cover thickness and reach the steel surface.

2.2.5 Transport Processes in Concrete

Typical transport processes convey water into the concrete interior either due to a hydrostatic pressure head or wetting forces (capillary suction) and by the migration of ions, either due to diffusion under a concentration gradient, or due to transport by moving water. The important factor for both of these processes is the connectivity of the pores in the concrete.

2.2.5.1 Distribution of Pores

Concrete is a porous material, whose properties depend on the pore space. Concrete has many different kinds of pores ranging from the air voids that are entrapped in the mixing process, which can be quite large, up to a few millimetres in diameter, to the capillary pores, which are essentially the space occupied by the leftover water from mixing, down to the nanometer-scale pores that exist in some of the hydration products produced by cement-water chemical reaction (Garboczi and Bentz, 1996).

The voids in the cement paste makes concrete permeable to liquids and gases. The void system in the hydrated cement paste can be divided into entrapped air voids (1000 - 5000μm), entrained air voids (50 - 1000μm), capillary voids (0.01 - 1μm), and interparticle spaces (0.001 - 0.003μm). The size and continuity of the capillary porosity, the hydrated gel pore system and the air voids control the coefficient of permeability of the hydrated cement paste. In other words, the porosity of the hydrated cement paste, or rather the pore size distribution, determines the rate of

penetration of deleterious substances such as carbon dioxide and chlorides. Pore size distribution depends primarily on the w/c ratio and on the degree of cement hydration. The water content determines the pore size and the space after either cement hydration reactions or evaporation consumes the water. The permeability of concrete is significantly reduced with low w/c ratios, as the capillary pores become discontinuous. However, ordinary concrete can never be completely impermeable because of the gel porosity and the transition zone between the hydrated cement paste and the aggregates. It is generally known those small pores, less than 50nm, influence drying shrinkage and creep. Large pores, greater than 50nm, develop with increasing w/c ratio, and in turn, these reduce the concrete strength and increase its permeability. It has been shown that for well-cured laboratory specimens, the permeability of concrete increases exponentially for mixtures with w/c ratios greater than 0.5 (Powers, 1960). For w/c > 0.7, the pore system in concrete remains continuous regardless of the degree of hydration, and for w/c = 0.6, the pores become segmented after six months of curing.

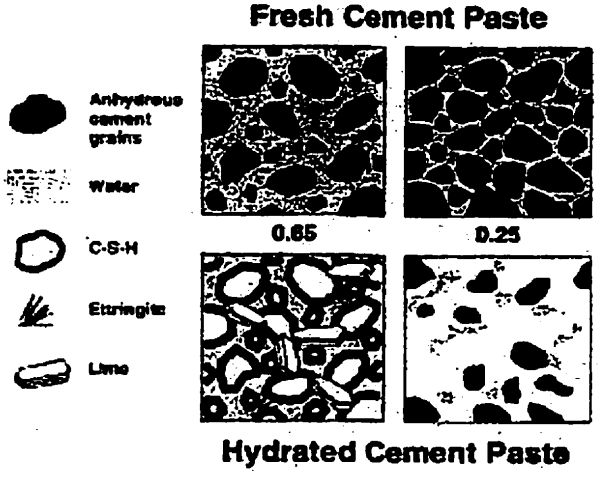

Figure 2.1: Differences in the microstructure of HCP and usual concrete

2.2.5.2 Permeability

The concrete pore system filled with air and pore water solution provides an excellent path for deleterious substances and an electrolyte. Cracking and the hydrated cement paste properties control the movement of water in mature concrete. Furthermore, the movement of water in the hydrated cement paste depends on the changes in the pore structure due to continued hydration, as cement hydrates. The capillary porosity is consumed while gel porosity increases, and the permeability drops by approximately 10-12 orders of magnitude (Mindess and Young, 1981). Many researchers have studied the mechanisms of mass transfer in concrete including adsorption, surface diffusion, vapour diffusion, ionic diffusion, and bulk flow (Powers, 1959, Barrer, 1967 and Klieger et al 1994). The analysis, even when only one mechanism is being considered, is very complicated because of the complexity of the concrete pore structure, variation in the mixture proportioning and curing, or continued hydration (Klieger et al 1994). Garboczi (1990) has discussed and compared the different methods and theories dealing with water transport in concrete. The permeability of concrete may be defined as the ease with which a fluid will pass through a porous medium under the action of a pressure differential, and therefore, it plays an important role in durability. The continuity and diameter of the pores determine the permeability of the system. Powers et al (1954 and 1958), showed that the permeability in neat pastes is influenced by the overall volume of capillary porosity. Also, Goto and Roy (1981) showed that the pore shape, volume, distribution and connectivity control the fluid flow through the microstructure.

The quality of concrete is one of the most important factors that influence the concrete cover (protector). It is important to note that the same parameters affect concrete quality, and its permeability. Wallevik (1970) stated that since the degree of impermeability of concrete plays an important part in prohibiting corrosion of the embedded steel, it is evident that various permeability numbers can be used as an index for quality.

To last, a surface exposed to the environment must be able to resist the ingress of external agents such as carbon dioxide, chloride ions dissolved in water, and water itself in excess quantities (Mirza 1995). While many of these parameters are not in themselves harmful to the concrete, they cause problems of corrosion if they can penetrate to the reinforcing steel present under the surface. If the concrete cover remains highly alkaline and impermeable, the durability of the structure is improved. Consequently, the ability of the concrete to protect the steel is important in determining its durability. The permeability of concrete can then be seen as a key factor in determining the overall durability of reinforced concrete and measuring it in situ may ensure a significant saving in repair and maintenance of structures (Mirza, 1995).

Chemical reactions occur between the different phases at the interphase surfaces while the transport processes transmit the reactants to the surface and withdraw the reaction products. These transport processes and the ingress of moisture or aggressive fluids and air, which result in chemical reactions and the consequent concrete deterioration, are controlled by the permeability of the concrete. Neville (1987) defined the permeability of a medium as a "flow property", which characterizes the ease with which a fluid will pass through the medium under a pressure differential, and therefore it represents the relative ease with which concrete can become saturated with water. In addition, the external medium in contact with the concrete, the microclimate is of considerable significance in this respect.

2.2.5.2.1 Permeability Tests

In addition to the weight gain (sorptivity) experiments, different tests have been developed to assess the absorption characteristics of the concrete for in-situ usage. These include the initial surface absorption test (ISAT) which is detailed in BS 1881:Part 5, the modified Figg hypodermic test (Figg, 1973), and the covercrete absorption test (CAT) (Dhir et al 1987). Also, the methods for assessment of

permeability of near-surface concretes, such as the AUTOCLAM, which measures the air and water permeability in addition to its sorptivity.

There are some practical difficulties with the use of ISAT on site. The Figg method is growing in popularity, however, the reported field experience is limited. This study will focus on the site measurements of concrete water permeability using the 'Autoclam' method (Basheer, 1991), which is similar in principle to the ISAT, but which uses a hydrostatic pressure of 0.5 bar to measure the in-situ water permeability. In all cases, the emphasis must be on comparative rather than quantitative application, and the results only relate only to the surface-zone properties. It must be recognized, however, that this is the critical region as far as durability performance is concerned.

Permeability measurements follow Darcy's law, which states that the coefficient of permeability is proportional to the flow rate per unit area and unit pressure gradient. Water is the most commonly used fluid to study the permeability of cement-based materials. The disadvantage of testing concrete permeability with pressure-induced gas flow (Klieger *et al* 1994), is that the moisture condition of the sample must be known and carefully controlled. Also, the moisture level must be constant throughout the tested material. Klinkenberg, (1941) and Bamforth, (1987) studied the relationships between gas and water permeability. Klinkenberg, (1941) found that the gas permeability for low porosity concrete was always greater than the water permeability. Also, it is well known that the air permeability measurements are highly dependent on the moisture content of the concrete. It has been reported that the effect of moisture content is significant to produce low permeability from high permeability concrete. Klieger *et al* (1994) found that the water-vapour diffusion, absorption and the rate of absorption, water penetration, or saturated flow tests could test water permeability. However, water will react with any unhydrated cement grains, thus changing the pore structure during the test, and reaching equilibrium flow can take several weeks.

Permeability and sorptivity measurements based on the weight gain and other tests mentioned above are useful in determining the quantity of water absorbed. However, these tests do not provide any information on the path of the advancing water, or the depth of water penetration, both of which are important when considering the durability of reinforced concrete. Therefore, the usual methods to measure transport properties in cement-based materials, especially, the hydraulic permeability and ionic diffusivity, are often time-consuming and inconsistent due to the fluid-tight seal required between the apparatus and the concrete surface, besides being quite expensive. Unfortunately, the usefulness of these methods is somewhat limited.

New techniques to measure or predict the transport properties in cement-based materials have been developed recently to provide fundamental microstructure /transport-property relationships, such as nuclear magnetic resonance, impedance spectroscopy, and microstructure-based modeling.

2.2.5.3 Chloride Migration

Chloride ions may penetrate into the concrete by absorption and capillary forces, diffusion through saturated or nearly saturated concrete, and through cracks. Capillary movement is a fast method of transport in the case of structures subjected to de-icing salts. The snow-ice melt carrying the chlorides will be absorbed into the concrete by capillary suction. However, Cady and Weyers (1983) noted that it is unlikely for water to penetrate that way, because mature concrete has a discontinuous pore system, and the concrete holds water in the capillaries, which impedes the driving potential. When chloride penetration rates are tested or modeled, both mechanisms of absorption and diffusion should be taken into account. Generally, only the diffusion mechanism is considered, and very few models consider both mechanisms. Therefore, the primary modes of transport of chloride ions into the concrete are through diffusion due to a concentration gradient in uncracked concrete and through cracks in the cracked concrete (Cady and Weyers, 1983).

Cracking provides an easy pathway for chloride ions to penetrate the concrete cover and reach the reinforcing steel. Structural cracks, however, are aligned perpendicularly to the main reinforcement and therefore, the access of chlorides to the steel bars is limited. Only subsidence cracking is dangerous with respect to chloride induced corrosion. These cracks are positioned parallel and directly above the bars, and their development depends on the concrete cover, bar diameter, and the slump of the concrete (Dakhil *et al* 1975 and Weyers *et al*, 1982).

Chloride ion migration into the concrete is an ionic diffusion process following Fick's second law (Page, 1981, Cady, 1983), which represents non-steady state diffusion and is expressed in a form of the partial differential equation:

$$\frac{\partial C}{\partial t} = D_c \frac{\partial^2 C}{\partial x^2} \qquad \textbf{(2.1)}$$

where: C = chloride ion concentration,

D_c = diffusion coefficient,

t = time, and

x = depth.

Equation 2.1 has many solutions depending on the boundary conditions. The most usual solutions used is by applying the following boundary conditions in the analysis of chloride distribution in concrete being the ones with a surface chloride concentration, C_s, being either constant:

$$C_x = 0, \qquad x \geq 0, \qquad t = 0$$

$$C_x = C_s, \qquad x = 0, \qquad t > 0$$

$$\frac{C_x}{C_s} = 1 - erf \frac{x}{2\sqrt{D_c t}} \qquad \textbf{(2.2)}$$

where: C_x = chloride ion concentration at depth x after time t,

C_s = chloride surface concentration,

erf = error function.

Whiting (1984) developed the rapid chloride permeability test to determine some measure of the chloride diffusivity. This method involves placing two disk-shaped cells on top of a concrete disc, one of which is a reservoir, the other a sink. This is shown schematically in Fig.2.2. A salt solution is used in the cathodic compartment so that the chloride is the diffusing specie, while the anodic compartment is filled with distilled water. A d.c. potential difference of 60 volts is maintained across the cathode and the anode for a 6-hour test period. The increase in the chloride concentration in the sink compartment is monitored with time by collecting a sample of 20 ml each hour and then testing it in the lab. The temperature of both compartments and the current readings are recorded with time.

The current passing through the sample results in a temperature increase from Joule heating, which is a considerable concern in permeable samples that pass large amounts of current, because a rise in temperature can have a profound effect on the diffusion coefficient. Feldman et al (1994) have investigated the Rapid Chloride Permeability Test and concluded that the test induced changes in the pore structure and the resistivity of the concrete specimens. Shane *et al.* (1997) have demonstrated that high fields affect the microstructure. Therefore, it is impossible to know if a representative specimen is being tested because of the changes in the microstructure.

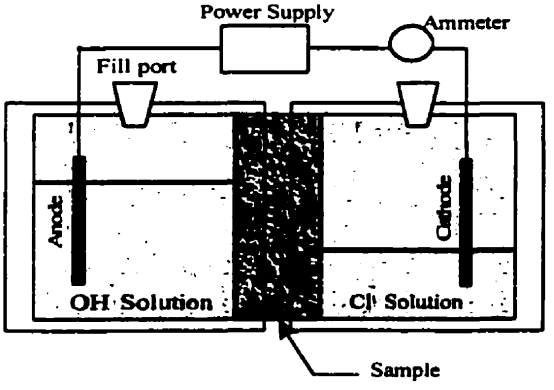

Figure 2.2: The divided diffusion cell

2.3 Principles of Corrosion

2.3.1 Why Metals Corrode?

Metals corrode because they "want" to corrode. Corrosion is the process of the transformation of a metal to its "native" form, which is the natural ore state, mostly as oxides, chlorides or sulphates. This process of transformation is known as corrosion. The principle of thermodynamics states that all spontaneous changes occur with a release of free energy from the system to the surroundings at a constant temperature and pressure. In the process of making steel, a tremendous amount of energy is put into the steel in the form of heat to separate the iron from its associated oxygen (Fig. 2.3). Nature always minimizes energy for a more stable thermodynamic condition. When corrosion occurs in nature, it is a spontaneous process and therefore occurs with the release of energy.

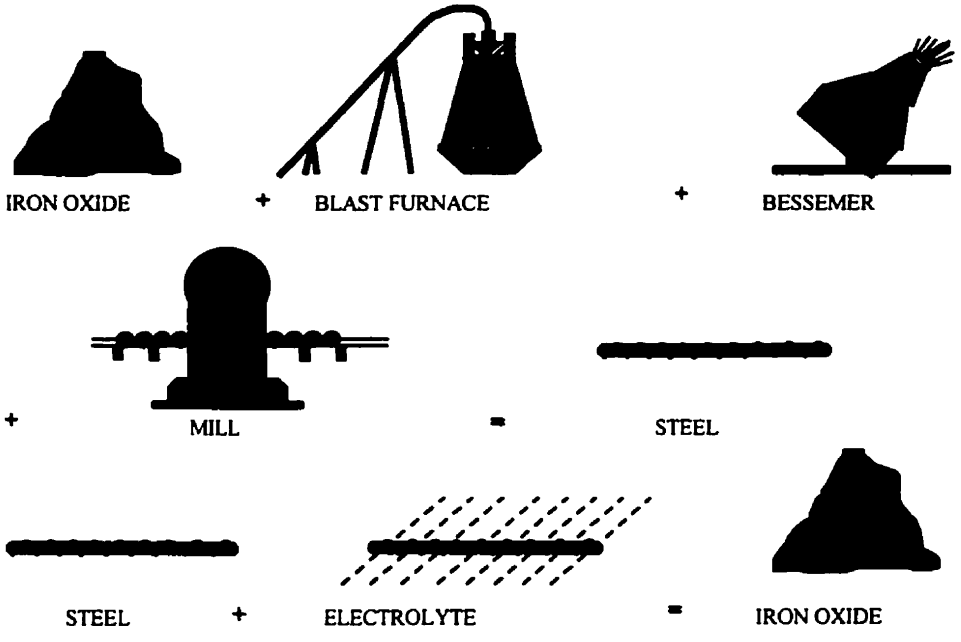

Figure 2.3: Manufacture of steel and its corrosion

Figure 2.4 demonstrates the energy profile within a spontaneous reaction to describe the free energy changes. This energy can be thought of as sphere that is held at an elevated position. The sphere at position 1 is unstable and possesses potential

energy. Some of this energy will be used up as the ball moves to position 2, a point of lower potential energy. This is the spontaneous movement direction for this particular system. Movement from position 2 to position 1 cannot be spontaneous in nature because there is an increase in the free energy, therefore, energy must be supplied from an external source for such a transition to occur.

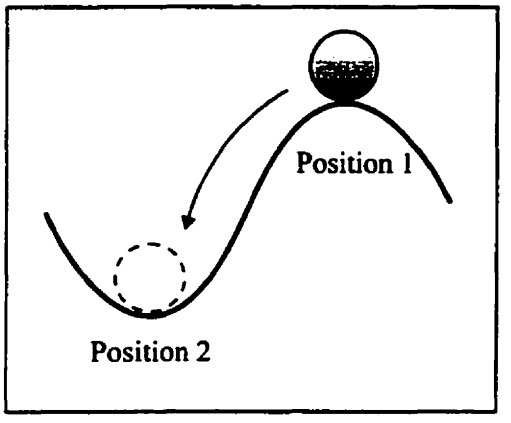

Figure 2.4: Stable and unstable positions

The corrosion of iron may occur by several mechanisms. Corrosion may initiate by bacterial action, certain bacteria (desulphovibrio desulphuricans) [Berkely and Pathmanaban (1990)], by direct oxidation (burning), or by acid attack, and by chemical attacks. Such corrosion is of little concern for steel embedded in the concrete. Indirect oxidation (electrochemical corrosion) as a result of dissimilar or non-uniform metals or dissimilar environments is of paramount importance in the deterioration of most concrete structures. Also, corrosion of the reinforcing steel in concrete by electrolysis due to "stray electrical currents" and hydrogen embrittlement, and "stress corrosion" are also relevant.

Corrosion may be defined as the destructive attack of a metal by chemical or electrochemical reactions with its environment. The electrochemical reaction refers to the chemical reaction that is associated with the electrical phenomena. Hence, corrosion of a metal can be defined as a chemical reaction of a metal with its environment as a result of which electrical current flows.

2.1.2 Electrochemical Process

The corrosion process is similar to the action that takes place in a flash light battery. Figure 2.5 shows a flash light battery which consists of an anode (zinc can), a cathode (graphite rod), an electrical conductor (wire connecting the cathode to the anode) and an electrolyte (moist paste).

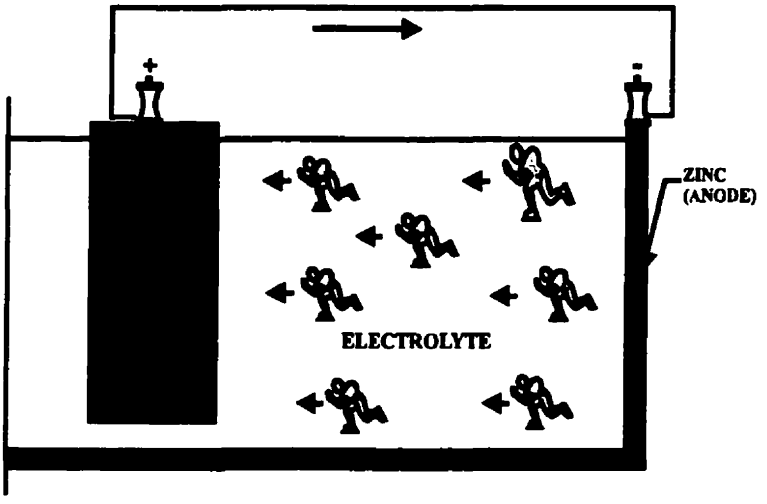

Figure 2.5: Reactions in a flashlight battery

Zinc has a higher tendency to corrode because it has more stored energy than graphite. The current will flow from the zinc surface through the electrolyte to the graphite (cathode) and back when the external terminals are connected with a wire. Ions are released from the zinc as it corrodes into the electrolyte, and they travel across the cell to the cathode where they become discharged. The passage of ions constitutes an electrical current, and as the zinc corrodes, the current continues to flow until all the zinc has been used up, or until corrosion makes a hole in it and the cell leaks. However, when the wire connecting the external terminals is disconnected, the current is interrupted and the ions released at the zinc surface have nowhere to go to be consumed, and will accumulate in such numbers that corrosion is virtually stopped. Hence, for corrosion to take place there must be a complete electrical circuit.

In summary, the chemical reaction of a corroding metal occurring at the metal-liquid interface can be written in the form of anodic and cathodic reactions (Fontana, 1986). When a metal undergoes a corrosion reaction, it is converted into an ion by a reaction with a species present in the environment. The anodic reaction, termed oxidation, occurs at the anode where corrosion of metal takes place and produces electrons. The cathodic reaction, called reduction, consumes electrons and occurs at the cathode. Reaction 2.1 represents the most general form of a corrosion reaction.

Anodic Reaction: $M \rightarrow M^{n+} + ne^-$ *(2.1)*

where M represents a metal, n is the valency and e is the electron. Reaction 2.1 does not represent a complete process as a positive ion has been generated but not a negative one. Also, free electrons generated from the anodic site must be consumed. Hence, the equation is referred to as a half-reaction because of its incompleteness. For corrosion to proceed both oxidation and reduction must occur simultaneously and at the same rate. The reduction equations are as follows:

Cathodic Reaction: $2H^+ + 2e^- \rightarrow H_2$ *for pH < 7* *(2.2)*

$O_2 + 2H_2O + 4e^- \rightarrow 4OH$ *for pH > 7* *(2.3)*

Also, the electrolyte must allow for movement of cations from the anodic sites to the cathodic ones and anions in the opposite direction. Finally, the anode and cathode must be electrically connected to allow the current flow.

The product from reaction (2.2) is the hydrogen gas, which can often cause problems such as hydrogen blistering, or hydrogen embrittlement, while the product from reaction (2.3) refers to the dissolved oxygen present in the water. The complete corrosion equation is obtained by combining the equation of the oxidation of metal M with one of the above reduction equations. In an *acidic environment*, the complete reaction becomes:

$$M + 2H^{+} \rightarrow M^{2+} + H_2(g) \qquad (2.4)$$

$$1/2\,O_2 + H_2O + M \rightarrow M^{2+} + 2\,OH^{-} \qquad (2.5)$$

Note that equation (2.5) is a combination of equations (2.1) and (2.3) and it represents the reactions in aerated water. Furthermore, the products of the above reaction often combine to form a precipitate:

$$M^{2+} + 2\,OH^{-} \rightarrow M(OH)_2 \qquad (2.6)$$

If the metal *M* represents iron *(Fe)*, then $Fe(OH)_2$, or rust is precipitated when oxygen is the corrodent.

2.3.1 Reinforcing Steel Corrosion

As mentiond earlier the embedded reinforcing steel is normally immune from corrosion because of the high alkalinity of the concrete. The two major causes of the breakdown of passivity on the embedded steel in concrete and the consequent initiation of active corrosion are:

1. The presence of chloride ions in the concrete
2. The decrease in the pH value of the aqueous solution in the concrete pores because of the reaction of the cement paste with the atmospheric CO_2.

The chemical half-cell reactions occurring at the anodic and the cathodic areas are as follows (Mehta, 1993):

At the anode: $Fe \rightarrow 2e^{-} + Fe^{2+}$ *(2.7)*

At the cathode: $\frac{1}{2}\,O_2 + H_2O + 2e^{-} \rightarrow 2(OH)^{-}$ *(2.8)*

The hydroxyl ions, OH^{-} arriving at the anodic area electrically neutralize the Fe^{2+} ions dissolved in pore water and form a solution of ferrous hydroxide at the anode (Bazant, 1979):

$$Fe^{2+} + 2OH^- \rightarrow Fe(OH)_2 \qquad (2.9)$$

This compound $Fe(OH)_2$ reacts further with additional hydroxide and available oxygen, to form the water insoluble red rust:

$$4Fe(OH)_2 + O_2 + 2H_2O \rightarrow 4Fe(OH)_3 \qquad (2.10)$$

Red rust is not the only product of corrosion of steel in concrete. Compounds such as black rust, Fe_3O_4 , green rust, $FeCl_2$, and other ferric and ferrous oxides, hydroxides, chlorides, and hydrates are also formed. Their composition depends on the availability of the pore water, its pH and composition, and oxygen supply. Figure 2.6 shows the relative increase in the volumes of the various oxides and hydroxides of iron, which increases considerably when water molecules combine with them. These large volume increases lead to large pressures (similar to bursting pressures in pipes) and cause cracking of the concrete and its delamination. The basic cycle of microcracking and cracking of the concrete, the influence of the various environmental factors, resulting in the corrosion of the embedded steel and further cracking and repetition of the cycle until the steel corrodes extensively and/or the concrete gets deteriorated or delaminated significantly is shown in Fig 2.7.

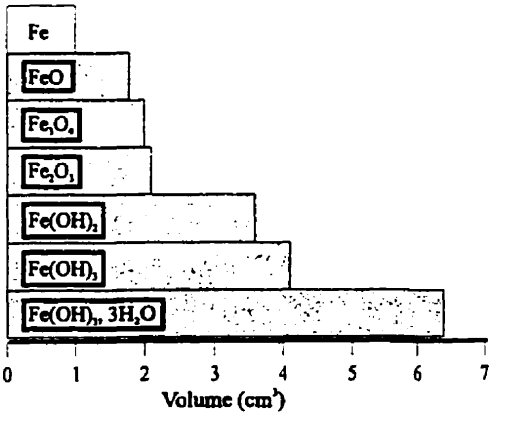

Figure 2.6: The relative volumes of iron and its corrosion reaction products, [Nielsen (1985)]

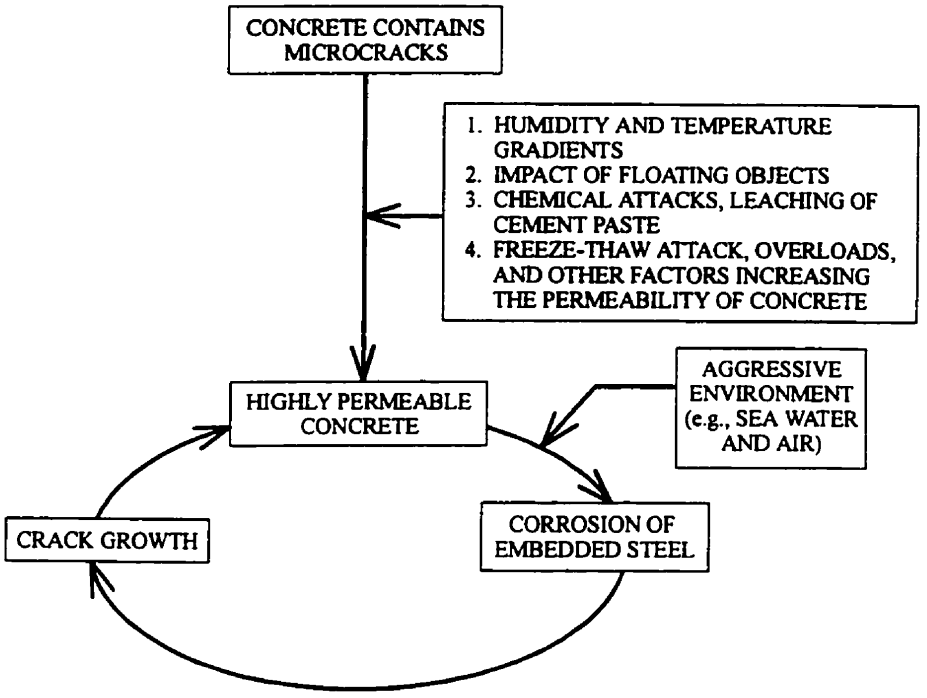

Figure 2.7: Diagrammatic representation of the cracking-corrosion-cracking cycle in reinforced concrete [Mehta (1993)]

2.3.2 Concept of Electrochemical Potential

Anodic and cathodic sites form on the surface of the metal where they are of different electrochemical potential due to the existence of heterogeneities in the corroding system. These heterogeneities in the same metal occur due to metallurgical segregation, different grain orientation or due to the local differences in the electrolyte. This can also occur when two different metals are connected and immersed in the same electrolyte, where one will act as an anode and the other as a cathode, depending on the nobility of the metals involved.

The driving force for the reactions is the difference in the electrochemical potential between the anode and the cathode. These potentials may be defined as a measure of the ease of transfer across the steel-concrete interface and the ease of ionization of the dissolved oxygen, respectively. It is not possible to determine the

absolute value of an electrochemical potential. Therefore, the potential difference between the anode (or cathode) and a reference electrode is taken as a measure of the actual potential. It is quoted in volts relative to the particular reference electrode used. A fixed difference in potential is always established between a metal and a solution containing its ions at an activity level of unity. This potential difference is arbitrarily taken to be zero for the hydrogen electrode which is used as a reference for all metal potentials.

The difference (E_c - E_a), between the potentials of the cathode, E_c, and the anode, E_a, can be very small if the anode and the cathode are quite close to each other, and the electrolyte conductivity is high and can attain a voltage of several hundreds of millivolts when the resistance of the medium is high. It should be noted that the potential of the local anode is always less than that of the cathode in the corrosion pair. When the solution in contact with the metal does not contain its ions, or if their activity is not unity, the Nernst equation allows the actual potential, E, to be determined as :

$$E = E^o - (RT/nF)\ln K \qquad \textbf{(2.11)}$$

where R is the gas constant (8.314 J/deg mole), n the valence, and K the equilibrium constant for the ions present in the solution. E^o is the standard potentials, F is Faraday's constant (96500 C/eq), and T is absolute temperature (K). Therefore, the actual potential of a corroding iron piece (known as its open circuit potential, rest potential, or corrosion potential, E_{corr}) is dependent on a variety of factors. These factors include the equilibrium potentials of the anodic and cathodic half-cell reaction, the composition of the surrounding electrolyte, the temperature, the polarization of the half-cells, and the existence of passivity.

2.3.3 Pourbaix Diagrams

The electrical potential versus pH diagrams, more commonly known as Pourbaix diagrams, are named after the originator of the concept, who devised a compact summary of the thermodynamic data for metals in aqueous environment in the form of these diagrams [Pourbaix (1974)]. Figure 2.8 shows a simplified Pourbaix diagram for iron. Based on equilibrium thermodynamics, these diagrams showing potential-pH plots define three main regions:

1. Immunity, where the metal is thermodynamically stable and is immune to corrosion.

2. Corrosion, where the ions of the metal are thermodynamically stable, and corrosion occurs at a rate which cannot be predicted thermodynamically.

3. Passivity, where the compounds of the metal are thermodynamically stable, and may protect the substrate from further reactions with the environment.

The dotted lines of Fig. 2.8 represents the thermodynamically stable region of oxygen, which is above line a, of water between lines a and b, and of hydrogen which is below line b. The iron is in the passive state at a pH in the range of 8-13 as illustrated in Fig 2.8, however, it also shows that corrosion may begin if the pH is more than 13, where a soluble ferrite, $HFeO_2^-$, forms. However, the occurrence of this phenomenon in the concrete has not been confirmed [ACI 222R (1994)].

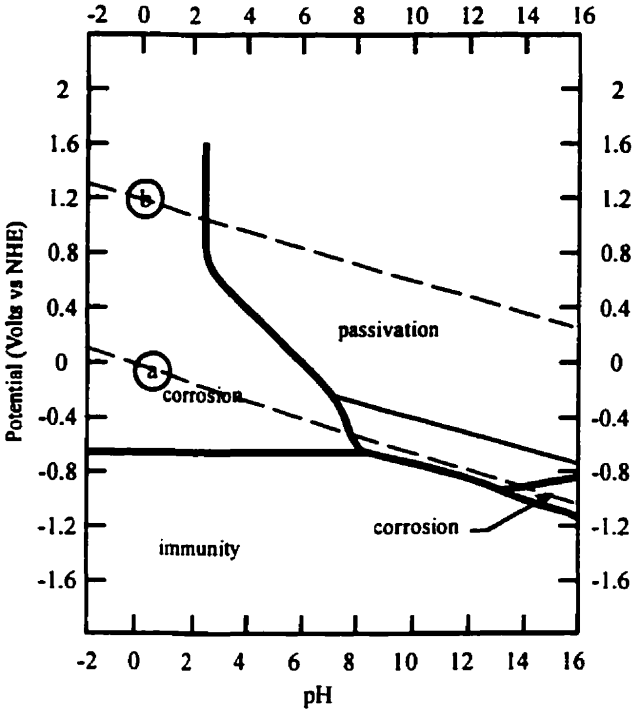

Figure 2.8: Pourbaix diagram for iron in water

2.3.4 Polarization of Half Cells

Polarization is the shift of the measured potential away from the reversible potential when a current flows through the half-cell. This polarization represents an overpotential defined as [Rosenberg *et al.* (1991)]:

$$\eta_a = E_{corr} - E_a \qquad \textbf{(2.12a)}$$

$$\eta_c = E_c - E_{corr} \qquad \textbf{(2.12b)}$$

where η_a, η_c are the overpotentials, E_a, E_c are the equilibrium potentials for the anode and the cathode, respectively and E_{corr} is the corrosion potential.

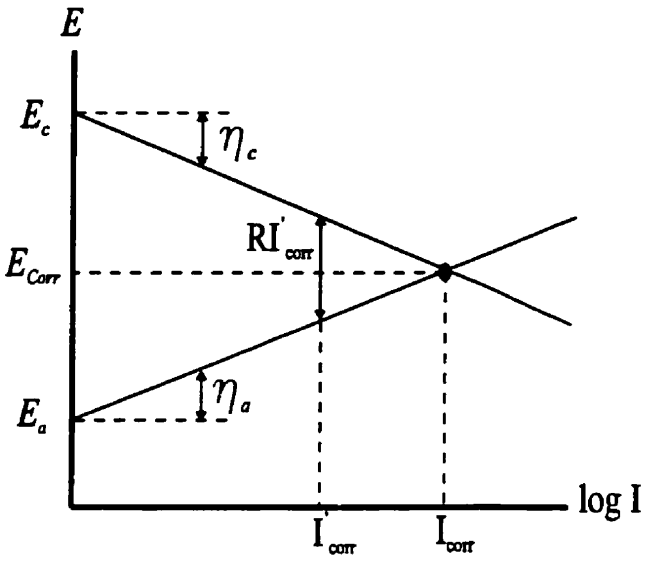

Figure 2.9: Schematic Evans diagram

Evans (1960) introduced a simplified graphic method of representing the relationship between the current, *I*, and the potential, *E*, which is known as the "polarization curve". The simplest example of an Evans diagram is illustrated Figure 2.9. The abscissa may represent the total current or its logarithm. The intersection of two curves represents the conditions at which the anodic and cathodic currents are equal and no net external current flows and, thus, defines the corrosion potential, E_{corr}, and corrosion current, I_{corr}.

The polarization process will influence the shapes of the anodic and cathodic branches of the polarization curve. There are three kinds of polarization where they may act separately or simultaneously:

1. Concentration polarization, which occurs when the concentration of the electrolyte changes in the vicinity of the electrode, such as depletion of oxygen at the cathode.

2. Ohmic polarization occurs because of the ohmic resistance of the electrolyte and of any films on the electrode surface. This produces an ohmic potential drop in accordance with the Ohm's law.

3. Activation polarization occurs due to kinetic hindrance of the rate-controlling step of the electrode reaction. Tafel (1905) showed experimentally that the measured polarization is directly proportional to the logarithm of the current density, i, for large currents in the absence of concentration and ohmic polarization:

$$\eta = a + b \log i \tag{2.13}$$

where a is constant parameter known as the Tafel intercept, and b is constant parameter known as the Tafel slope. These parameters can be obtained empirically by plotting η versus i on semilogarithmic scales. The parameter a is related to the exchange current i_o, and is a measure of the reversibility of the reaction, while parameter b gives an insight into the mechanism of the electrode reaction.

2.3.5 Morphology of Corrosion Process

The morphology of the corrosion process depends on the distribution of anodes and cathodes on the steel bar surface and on their relative areas. If the anodes and cathodes are irregularly distributed on the steel surface and change their position during the corrosion process, the attack will be more or less uniform. However, if the anodes are located at fixed points and the anodes/cathode area ratio is very small, localized attack will develop.

The corrosion rate is considered to be cathodically controlled when the cathodic process is slower. Figure 2.10 represents the logarithm of the absolute current, I, versus the potential, E, by polarizing each half-cell and demonstrates the cathodic control as the cathode has larger polarization. The corrosion rate is considered to be anodically controlled when the anodic process is slower and is shown in Fig. 2.11. There are two types of corrosion-rate controlling mechanisms [ACI Committee 222 Report, (1994)]:

1. The cathodic diffusion, where the rate of oxygen diffusion through the concrete determines the rate of corrosion.
2. The development of a high resistance path, when there is a large distance between the anodic and cathodic areas such as several feet apart, and hence, the resistance of the concrete may be of great importance.

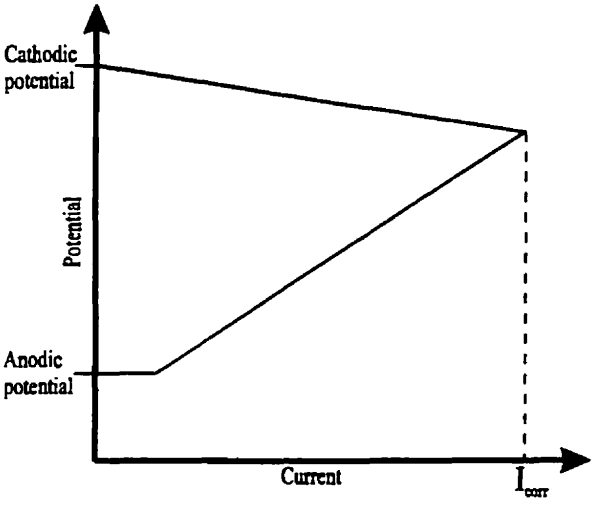

Figure 2.10: Potential vs current plots for systems under cathodic control

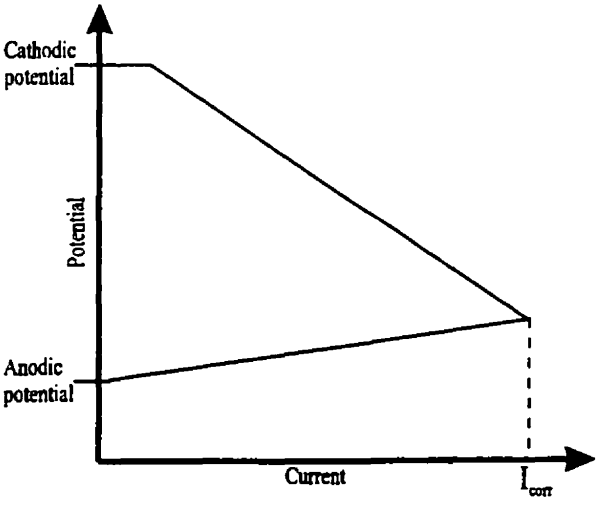

Figure 2.11: Potential vs current plots for systems under anodic control

The corrosion rate is much slower in the general corrosion when compared to pitting corrosion because of the lower cathode to anode area ratio. Another classification is based on the relative position of the anodic and cathodic sites. This relative position depends on a potential difference between the anodic and the cathodic sites. The larger the potential difference, the farther apart will be the anode and the cathode. If the two sites are in close proximity to each other, microcell corrosion occurs. Macrocell corrosion occurs when the anode and cathode sites are farther apart and a large potential difference exists between the anode and cathode. Slater (1975) suggested that accelerated corrosion of bare steel reinforcement in the decks with a bottom mat of coated steel is a result of macrocell corrosion. In most cases, however, since macrocell corrosion requires larger potential difference than the microcell corrosion does, it is more likely for the microcell corrosion to be a dominant type.

2.3.6 Passive Layer on Reinforcing Steel

The term "passivity" predates modern understanding of the protective film crystalline structures in solids. Passivity is provided by an insoluble layer formed on the metal surface which protects the metal against corrosion. It is made of chemical combinations of oxygen, though the exact composition has been difficult to determine. Cornet *et al.* (1968) by using the Pourbaix diagrams, explained how concrete with a pH of approximately 12.8 protects steel from corrosion.

The alkaline nature of the pore solution, and the oxygen within it, result in the formation of insoluble and adhering corrosion product which forms an extremely thin microfilm on the reinforcing steel bar surface. The environmental condition in the paste pore solution at the bar surface promotes the stability of this passive oxide film. It should be noted that at this stage, the corrosion does not stop, however, it is severely slowed down by the ohmic resistance of the film. Rosenberg, and Andrade (1978) and Hansson (1984) refer to their earlier works, and suggest that the passive corrosion rate of the steel embedded in the concrete is basically equivalent to the

oxidation of approximately 0.1 μm per year from the steel surface. This is negligibly small when compared with the anticipated service life of the concrete structure.

A relatively high pH and the presence of oxygen and moisture are essential for the maintenance of the passivity of the reinforcing steel embedded in the concrete. Ingress of chloride ions, or carbon dioxide into the concrete causes a reduction in pH which in turn would lead to active corrosion. While the elimination of moisture inhibits or stops the corrosion process, the effect of elimination of oxygen is not straightforward. If oxygen is absent in the pore solution at the steel-concrete interface and if its pH is greater than 9, the corrosion process will continue, however, it will result in the evolution of hydrogen, instead of the reduction of oxygen at the cathode [Rosenberg *et al.* (1989)]:

$$2H_2O + 2e^- \rightarrow H_2 + 2OH^- \qquad (2.14)$$

The corrosion rate under these conditions is an order higher (about 1 μm per year at the steel surface) than for the passive conditions with the reduction of oxygen, however, these values are still extremely low and acceptable for most concrete structures. However, the evolution of hydrogen can lead to the embrittlement of the prestressing steel in both pretensioned and post-tensioned structures and result in their sudden and catastrophic failures. When passivity is lost, the corrosion rate of the steel reinforcement is inversely proportional to the resistivity of the concrete [Gjorv (1982) and Gonzalez and Andrade (1982)].

2.3.7 Availability of Oxygen

As mentioned earlier, the presence of oxygen is an essential factor for the corrosion of iron in concrete with the addition of chlorides and a reduced alkalinity. Also, the effect of elimination of oxygen is not straightforward. In the case of concrete saturated with water, the diffusion of oxygen is strongly effected by the degree of saturation. This effect is best demonstrated in the work of Griffin and Henry (1963) as shown in Fig. 2.12. The level of corrosion increases as the sodium chloride

concentration increases until a maximum concentration is reached, beyond which the rate of corrosion decreases despite the increased chloride concentration. This is due to the reduced solubility and hence the availability of oxygen to sustain the corrosion process. Also, investigations by Shalon and Raphael (1959) indicate that the rate of steel corrosion is very slow even though chlorides are present if the concrete is continuously water-saturated.

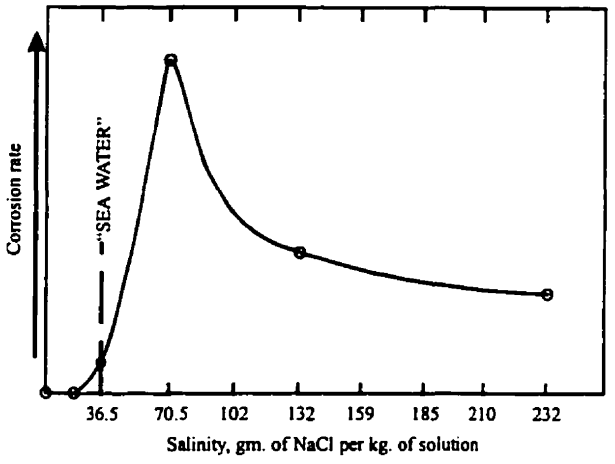

Figure 2.12: Effect of concentration of sodium chloride on corrosion rate [Griffin and Henry (1963)]

2.3.8 Corrosion Initiation

The presence of chloride ions either in the concrete mix or due to ingress from the immediate environment, and a decrease of the hydrated cement paste pore solution pH because of the concrete carbonation are two known major causes of the breakdown of the passive layer on the surface of the steel bar embedded in the concrete. These two effects can often be present simultaneously and have a stronger degrading effect on the reinforcing steel passivity. The consequences of the steel corrosion are manifested as a decrease in the bar diameter, deterioration of the mechanical properties of the reinforcing steel (e.g., the change from the normal ductile response of low carbon steel bars to a relatively brittle response in bars damaged by pitting corrosion), cracking and spalling of the concrete by the expansive

iron oxides and hydroxides, and a noticeable decrease in the bond at the steel-concrete interface.

2.3.8.1 Penetration of Chlorides

Stratful *et al.* (1975), Brown (1980) and several other researchers have shown that the presence of chloride ions in the concrete can lead to corrosion of the reinforcing steel provided that the corrosion reaction can be sustained by an adequate supply of oxygen and moisture. Chloride ions have been known to be introduced in the concrete through the use of calcium chloride as an accelerating agent for the hydration of portland cements in several countries. Some water-reducing admixtures contain small amounts of calcium chloride to offset their set retarding properties. Use of seawater, or water containing chlorides for concrete mixing and the use of aggregate exposed to seawater can introduce considerable quantities of chlorides in the concrete mix. In addition, porous aggregates are more harmful as they can retain a significant amount of chlorides as compared with the non-porous aggregates.

The most important source of chlorides in the concrete in cold climate countries is basically from the use of deicing salts on pavements and bridge decks during the winter. The ice melt-salt mixture readily penetrates more or less dry concrete by diffusion through totally or partially water-filled pores to the interior of the concrete, or in most cases by rapid capillary suction, which can cause penetration to the extent of a few millimeters in a few hours. This salt penetration occurs more slowly in wet or highly moist concrete by diffusion of the chloride ions through the pore solution in the hydrated cement paste hydrated cement paste, which results from the gradient of the chloride ion concentration at the concrete surface, and that inside the concrete. The penetration rate depends on the chloride concentration gradient. Page *et al.* (1981) estimated the typical diffusion rates in fully saturated hydrated cement paste to be about 10^{-12} meter^2 per second, which is so small that it would require several months for the chloride ions to penetrate a 10 mm thick hydrated cement paste layer, showing the importance of a concrete cover of appropriate

thickness and quality. Thus, permeability, water penetration depth and the concrete cover thickness are of great importance to the rate of penetration of chlorides.

The rate of corrosion is strongly influenced by the rate at which the chloride ions reach a critical concentration at the steel surface and the degree of binding of the chloride in the concrete [Rosenberg *et al.* (1989)], which influences the rate at which the chlorides reach the steel surface. It should be noted that not all the chlorides can attack the steel; only the freely dissolved chlorides in the cement pore solution can be involved in the corrosion process. It is generally believed that some chloride ions can react chemically with the calcium aluminate minerals in the cement gel to form "Friedel's salt" and therefore, these will not be available to attack the steel. Therefore, the tricalcium aluminate (C_3A) content of the cement has a strong influence on the amount of free chlorides remaining in the hydrated cement paste pore solution and readily available for the corrosion process. Recent research (Byfors *et al.*, 1986) has shown that additional factors influencing the degree of chloride binding include the proportion of cement in the concrete, water-cement ratio, pore solution pH, presence of sulphate ions (Holden *et al.*, 1986) and the specific surface of the cement gel. Figure 2.13 shows that the amount of chlorides required for corrosion initiation increases as the pH at the iron-liquid interface increases (Erlin and Verbeck, 1978). Figure 2.14 shows the gradient of the total chloride concentration, which depends on whether the chemical reaction occurs with the cement (Verbeck, 1975).

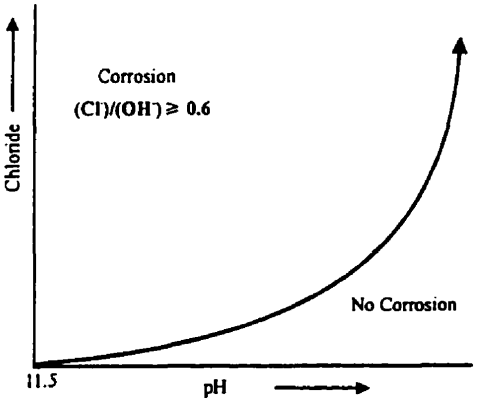

Figure 2.13: Chloride content vs pH, [Verbeck (1975)]

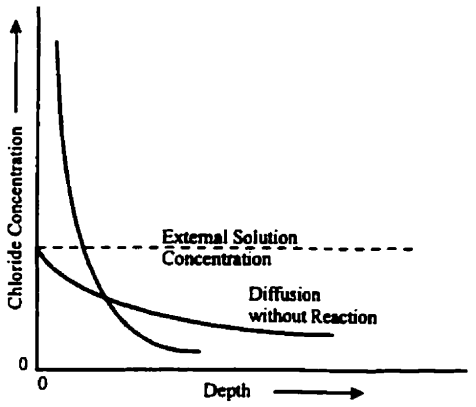

Figure 2.14: Chloride concentration vs depth of cover,
[Erlin and Verbeck (1978)]

2.3.8.1.1 Mechanism of Chloride attack

The structure of the passive film on the steel bar surface and the mechanism of its breakdown are not fully understood and considerable research on this subject is under way presently. It is agreed that in general the chloride ions replace some of the oxygen in the passive film, thereby increasing both its conductivity and solubility. This results in the loss of the protective character of the film. Also, the "initial" high potential difference across the film cannot be maintained any more and this potential at the steel surfaces decreases considerably to the value for an iron electrode.

Research and field experience has shown that chloride ions are rarely distributed uniformly over the steel surface. Similarly, the imperfections in the passive film which permit easy incorporation of the chloride ions are also nonuniformaly distributed, resulting in local breakdowns of the film and creation of macrogalvanic cells (Fig.2.15). These local active areas act as anodes where iron dissolves quite readily at a relatively low potential, while the remaining passive areas act as cathodes, where oxygen reduction takes place at a considerably higher potential (Rosenberg *et al.*, 1989). In addition to the chloride ion concentration and the availability of oxygen, the rate of iron dissolution in the galvanic cells is dependent

on the ratio of the cathode-anode areas and the electrical resistivity of the concrete between the cells.

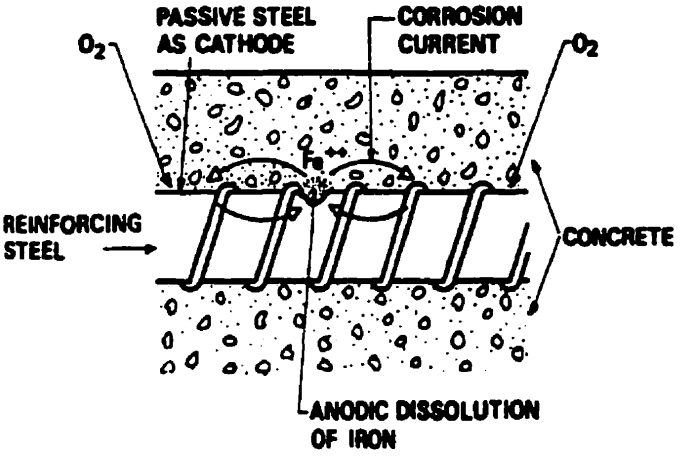

Figure 2.15: The schematic representation of the corrosion of steel in concrete, [Rosenberg *et al.*, (1989)]

The pattern of corrosion of the reinforcing steel is influenced strongly by the separation of the anodic and cathodic areas, resulting from the localized nature of the chloride attack. The concentration of positive iron ions increases in the vicinity of the anodic area along with a drop in pH at the anode, while negative hydroxyl ions are produced in the cathodic region and its vicinity. The pH decrease results in the soluble chlorides at the anode diffusing away from the anode, which results in the continuation of corrosion. At some distance from the anode, both the pH and the concentration of dissolved oxygen are higher than their values at the anode. This causes the iron chloride to breakdown and to form iron hydroxide with the release of the chloride ions, which are free to react further with the iron ions at the anode. This process continues as the iron ions migrate further from the steel and combine with the oxygen to form higher oxides, or hydroxides. As a result, the corrosion process focuses at the local anodic area instead of spreading along the bar and this results in the formation of deep pits and substantial local loss of cross sectional area. As this

process continues, eventually the bar breaks down completely leading to its severance.

The threshold chloride content below which there is a low probability of corrosion is dependent on several factors [Rosenberg *et al.* (1989)]:

1. The concrete mix details.
2. Type of cement and its specific surface area.
3. The water-cement ratio.
4. The sulphate content.
5. The curing condition, age and environmental history of the concrete.
6. Carbonation of the concrete.
7. The concrete environment (temperature and relative humidity).
8. The roughness and cleanliness of the reinforcing steel bar.

The CEB (1985) has reviewed the influence of some of these factors on the threshold chloride level which are presented in Fig. 2.16. It can be noted that when the relative humidity level in the concrete is about 50% (relatively dry concrete), the concrete ceases to act as an effective electrolyte and the transport of ions within the concrete surrounding the steel is impeded. This would slow the corrosion of the reinforcing steel considerably. By contrast, when the concrete is nearly or fully saturated, diffusion of oxygen is either considerably impeded or it ceases, again leading to a considerable reduction in the corrosion process. The risk of corrosion is the highest in the region with intermediate relative humidity (80-85%), where the concrete acts effectively as an electrolyte and sufficient oxygen is available, with the combination representing a considerably high risk of corrosion. Depending on the local experience, different threshold limits have been adapted by the different national standards. The CEB and RILEM have considered the value of 0.4 percent by the weight of cement to be appropriate. The Federal Highway Administration of the U.S.A. considers a chloride ion limit of 0.15 percent by the weight of cement to be tolerable, while a limit of 0.3 percent is considered to be dangerous.

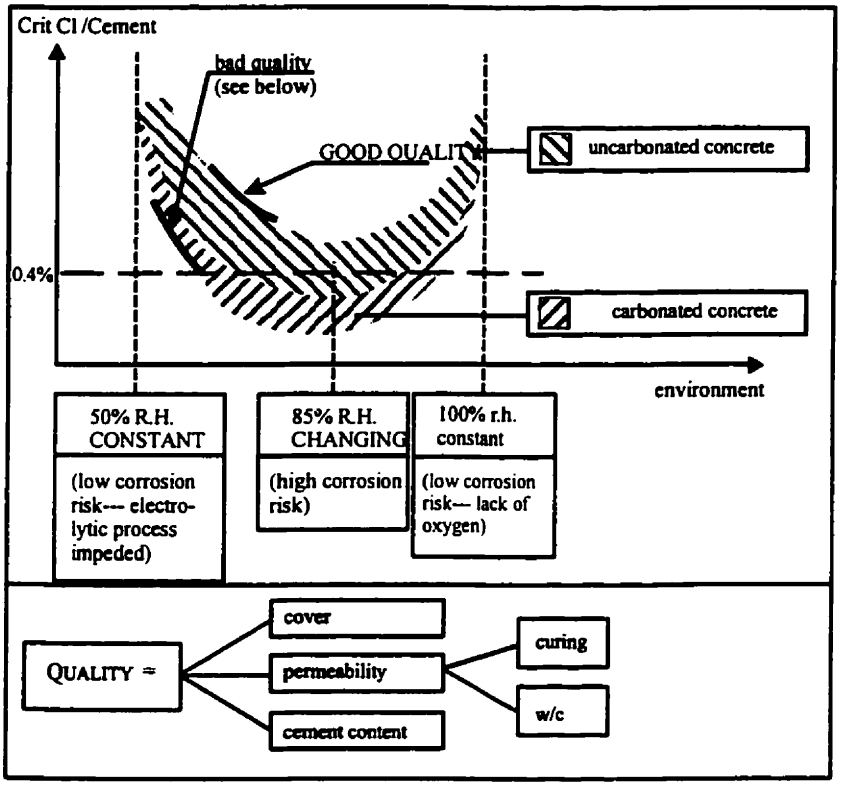

Figure 2.16: The critical chloride content according to CEB recommendations [CEB Recommendations (1985)]

Also, chloride salts are damaging through a variety of mechanisms but the most important are as follows:

1. Chlorides act as catalysts to promote corrosion. They help the depassivation of normal alkaline protection provided by the concrete cover.
2. Reduction of localized alkalinity even though there is no significant, generalized drop in pH and a shift towards a more acidic environment, in corrosion "pits" in the steel. This tends to shift the steel from the pH range where immunity to corrosion is normally imparted into a region where corrosion can occur.
3. Chloride ions are capable of migration in the concrete causing differential concentration cells.

4. Chloride ions have an adverse effect on the rate of polymerisation of the calcium silicates thus hindering the long term strength improvement and impermeability of the concrete.
5. The sulphate resistance of sulphate resisting cements is impaired by the presence of chloride salts.

The mechanism of the action of the chloride ions is not entirely understood. The general opinion is that the chloride ions act as a catalyst in the corrosion reactions (Jones, 1992). When the ion concentration becomes large, ferrous corrosion products form an acidic solution with the chlorides which neutralizes the alkaline concrete environment and further enhances corrosion. Ferrous chlorides being more soluble than the oxides move away from the reinforcing steel and expose new areas to the corrosive environment.

2.3.8.2.2 Corrosion Threshold Concentration

The value of the threshold concentration is of primary importance, and it varies for different concrete types. The results of previous studies on threshold chloride-ion concentration determination are presented in Table 2.1 (Funahashi, 1990). A level of 0.71 to 0.89 kg/m^3 is usually considered a threshold level for bare steel in regular reinforced concrete bridge decks. According to AASHTO, chloride-ion concentration less than 1.42 kg/m^3 are acceptable for bridge decks, however, deck replacement should occur when the level of chlorides reaches 2.8 kg/m^3 (Miller *et al.*,).

A second theory states that the threshold should not be based on the chloride ions only, but rather on a ratio of the chloride to the hydroxyl ions. According to Hausmann (1967), ratios above 0.6 indicate high probability of active corrosion, while ratios below 0.6 do not. It can easily be deduced that not only an increase in the chloride ion concentration will cause the ratio to increase, but a decrease in the hydroxyl ion concentration, as well. However, accurate determination of the hydroxyl ion concentration is difficult, especially at high concrete pH levels.

Table 2.1: Threshold Chloride-Ion Concentration.

Researcher(s)	Year	kg/m^3 of concrete
Lewis	1962	0.7
Hausmann	1967	0.2 - 2.8
Berman	1972	0.77
Clear and Hay	1973	0.6 - 0.9
Clear	1974	0.66
Stratfull, Jaukovich, and Spellman	1975	0.66
Cady	1978	0.6 - 1.3
Browne	1982	1.33
Pfeifer, Landgren, and Zoob	1986	0.5 - 0.9

2.3.8.3 Carbonation of Concrete

Carbonation of concrete occurs when concrete reacts with the atmospheric carbon dioxide (and sulphur dioxide) to cause gradual neutralisation of the alkalinity from the concrete surface inwards. The carbon dioxide, CO_2, in the air can penetrate slowly from the surface of the concrete through the pores of the concrete to the interior. This carbon dioxide can react with the hydration products in the hydrated cement paste, especially with $Ca(OH)_2$ which is the cause of high pH in the concrete, and with other ions in the pore solution as follows :

$$Ca(OH)_2 + CO_2 \rightarrow CaCO_3 + H_2O \qquad \textit{(2.15a)}$$

$$2NaOH + CO_2 \rightarrow Na_2CO_3 + H_2O \qquad \textit{(2.15b)}$$

The $CaCO_3$ and Na_2CO_3 precipitate in the pore of the hydrated cement past, thereby decreasing its permeability and also reducing pH of the pore solution. This reaction continues until the pore solution is neutralized. If carbonation continues beyond this stage, then carbon dioxide reacts with the other hydration products resulting in the formation of amorphous SiO_2, $Al_2(OH)_3$, $CaSO_4$, $CaCO_3$, and water.

It should be noted that the change in the value of pH due to carbonation is very sudden and it appears as a narrow zone or carbonation front separating the two zones - one towards the concrete surface with pH values less than 8, and the other into the concrete core with pH values larger than 12. The carbonation rate is dependent on the cement type, w/c ratio, cement proportion in the concrete mix, and others- basically constituting the concrete cover quality, or the cover permeability. In most cases, the rate of carbonation or the depth of carbonation from the concrete surface, x, is proportional to the square root of exposure time, t, i.e.

$$x = k\sqrt{t} \tag{2.16}$$

The permeability of the concrete plays an important role with respect to the rate of diffusion of CO_2 as it can travel through the air-filled pores in the concrete, and hence a totally saturated concrete will not carbonate. The water saturation level of the pores in the hydrated cement paste also influence the carbonation rate, because CO_2 can permeate into the concrete rapidly in the gaseous phase, however, the carbonation reaction takes place in the liquid phase (Rosenberg *et al.* 1989). Carbon dioxide cannot react with $Ca(OH)_2$ in a completely dry concrete, because of the absence of water in the pores. By contrast, in a completely water saturated concrete, carbon dioxide must first dissolve in the solution and then diffuse through the pores to reach the alkaline substance before the carbonation reaction can occur. However, it should be emphasized that at intermediate humidity levels when pores have moisture on the walls but are not completely saturated with relative humidity levels of 50 to 80 percent, carbon dioxide can rapidly reach the pore walls and have enough water present for the carbonation reaction to proceed. Recent research suggests that the square root relationship holds only at about 50% RH.

The carbonation front advances with time through the concrete cover and it reaches the level of the reinforcement. The passive film becomes unstable and active corrosion commences. This corrosion is generalized and homogeneous, and it will result in a reduction in the steel rebar cross-sectional area and formation of a

considerable amount of oxides which can either crack the concrete cover, or it may diffuse to the concrete surface through the pores. Occurrence of alternate semi-dry and wet cycles constitutes the most aggressive environment related to the neutralization of the concrete. The carbonation front advances through the semidry period, while the steel corrodes during the wet periods.If the carbonation front reaches the steel in a permanently dry environment, the steel will get depassivated, however, no significant corrosion will occur. By contrast, no carbonation will occur in a permanently wet condition and the steel will remain passive provided that no other depassivating agent, such as chloride ions, is present. However, it must be noted that in good quality low w/c concrete, carbonation is normally not an issue.

Field examinations have shown that the progress of the carbonation front is slow in sound and dense concrete, and the expected service life gets reduced because of the cover being too thin and the existence of cracks. However, carbonation often occurs rather fast, in practice either because the concrete is highly permeable, or due to microcracking in the concrete bypassing the normal diffusion processes. Excessive permeability can result from high water/cement ratios, but it can also result from poor curing of the cover concrete. Most modern specifications fail to recognise the importance of curing on the concrete quality. Table 3.4 of BS 8110, emphasizes the importance of curing on concrete in practice, which is often less than perfect. With crack widths larger than 0.4 mm, no correlation has been observed between the crack width and the amount of corrosion. The risk of corrosion is a function of the cover quality (thickness and impermeability) and of the cover/bar diameter ratio. In general, a corrosion risk is always present, however, for crack widths less than 0.4 mm, the risk is independent of the crack width.

Accumulated corrosion products, which occupy more volume than the reactants, cause cracking of the protective concrete cover. This allows for intrusion of chlorides and oxygen at a much faster rate, thus accelerating the corrosion process. Depending on the bar size, bar spacing, and cover depth, cracking can be in the form of either delamination cracking, or inclined cracking. Delamination

cracking is characterized by horizontal cracks extending from one bar to another. Inclined cracking are those that propagate to the surface at an angle of about 45°, and result in section loss and potholes, often seen in bridge decks.

2.4 Prevention of Corrosion

Since corrosion of the reinforcing steel causes early deterioration of concrete bridges, highways, parking garages, and buildings and it is a very costly problem, not only in terms of its financial implications but also for its structural safety; it is necessary to develop methods, which can extend the service life of theses bridges. The best method of corrosion prevention is proper concrete design, placing, and curing. With the use of high quality concrete with a low w/c ratio, which makes concrete more dense and less permeable, and a thicker concrete cover depth, of at least 75 mm, will prolong the time to corrosion initiation; the distance for deleterious substances to reach the reinforcing steel will be larger. The ACI Committee 201 recommends low water-cement ratios (w/c) and good concrete cover to be employed when chloride exposure conditions are moderate and severe. Tougher and even more crack resistant concrete can be made by addition of stainless steel, glass, and polypropylene fibers (Pritchard, 1986). In recent years, there has been a rapid development of the various materials and methods, which can be used for increasing the service life of concrete structures subjected to chloride attack. They include mineral admixtures, corrosion resistant reinforcement, corrosion inhibitors, cathodic protection, and surface treatments. This study concentrates on concrete with mineral admixtures by the use of high-volume fly ash in concrete.

2.4.1. Pozzolans

Pozzolan is a natural or artificial material containing silica in a reactive form (Neville 1973). The ASTM C 595-75 defines pozzolan as "a siliceous or siliceous and aluminous material which in itself possesses little or no cementitious value but which will, in finely divided form and in the presence of moisture, chemically react with

calcium hydroxide at ordinary temperature to form compounds possessing cementitious properties."

Pozzolanic activity is indicative of the lime-pozzolan reaction and it is not well understood. The pozzolanic activity consists mostly of the reaction between the reactive silica from the pozzolan and calcium hydroxide producing calcium-silicate-hydrate. Pozzolans contain high quantities of silicon dioxide and may also contain significant amounts of aluminum oxide and iron oxide. Hydration of a pozzolan, when compared with hydration of silicates in portland cement, is a slow reaction and is characterized by the low heat of hydration and slow strength gain. Hydration of silicates in portland cement results in the formation of C-S-H and calcium hydroxide (CH). In pozzolanic reactions, pozzolan reacts with CH from the portland cement hydration products and water, and forms C-S-H. The C-S-H produced in the pozzolanic reaction has lower density than that from the portland cement hydration. However, since the reaction is much slower, the products of the pozzolanic reaction fill the already existent capillary spaces in the cement paste. It improves the strength properties and reduces the permeability. Bentz and Garboczi (1991) stressed that the pozzolanic mineral admixtures do not eliminate the capillary porosity, but reduce it by significantly lowering the volume fraction of CH and at the same time increasing the total amount of C-S-H. Mineral admixtures with very fine particle sizes are known to increase the water requirement in almost direct proportion to their amount present, therefore, if the normal consistency of the mixture is desired at an unchanged w/c ratio, a water reducing admixture may be required (Mehta, 1984).

Pozzolans used in concrete include both natural and by-product materials. Natural materials include volcanic ash-the original pozzolan-pumicite and tuffs, opaline shales and cherts, calcined diatomaceous earth and burnt clays. Natural pozzolans require processing such as crushing, grinding, and size separation. The process may also involve thermal activation. The major sources of by-products are power plants and metallurgical furnaces producing cast iron, ferrosilicon alloys and

silicon metal. One of the major benefits of using industrial by-products is that they may not require any processing before being used in concrete.

The perceived benefits with the use of the by-product pozzolans in concrete are some or all of the following (Johnston 1994):

1. Improved concrete performance in terms of thermal cracking due to the low heat of hydration, durability with respect to retarded alkali-aggregate reaction, reduced freezing and thawing effects and water erosion, increased sulphate resistance, reduced permeability, resistance to chloride-ion penetration that causes corrosion of reinforcement and short and long-term strength development.
2. Utilization of a waste material that represents an environmental disposal problem.
3. Reduction in the total cost of cementitious material per unit volume of concrete.
4. Reduction in CO_2 emissions, because of reduced amount of cement.

2.4.1.2 Fly Ash

Several investigators have published reviews of the state- of- the- art of the knowledge of fly ash, however, the most comprehensive review was undertaken by Malhotra and Ramezanianpour (1994) to present the information about the most current use of fly ash in concrete. The information in the following sections has been adapted from the above state-of-the-art report and is presented here for completeness.

Combustion of pulverized coal in thermal power station produces fly ash as a by-product. Fly ash is removed from the combustion gases as a particulate residue by a dust collection system before they are discharged into the air. Fly ash particles are normally spherical and glassy, with sizes ranging from less than 1 μm up to about 150 μm. This size range is normally determined by the source of fly ash and the nature of the dust collection equipment (Malhotra and Ramezanianpour, 1994). Some larger

fly ash particles are irregular or angular in shape. Examinations of scanning electron microscope (SEM) micrographs show that the appearance of some of the particles is solid, while some larger particles appear to be portions of this, hollow spheres containing many smaller particles. For example, the fly ash from boilers at some older plants using mechanical collectors is coarser than the ones using electrostatic precipitators.

Fly ashes are pozzolans and exhibit pozzolanic activity. As mentioned earlier the metastable alumino-silicates react with calcium ions in the presence of moisture to form calcium silicate hydrates (C-S-H). Romans were the first to realize about 2000 years ago that certain volcanic ashes, when combined with lime, produced effective cements. The recent realization that fly ash is a pozzolan has resulted in its increasing use as a component of portland cement concretes.

The chemical composition of fly ash is determined by the type and amount of incombustible matter in the coal used to produce power. More than approximately 85% of most fly ashes consist of chemical compounds and glasses formed from the elements silicon, aluminum, iron, calcium and magnesium. The amount of carbon from unbound coal depends on the rate of combustion, the air/fuel rates, and the degree of polymerization of the coal. The fly ash from subbituminous coal contains very small quantities of unbound carbon, while intermittently operational plants using bituminous coals produce the largest proportion of unburnt carbon (Malhotra and Ramezanianpour, 1994).

Inclusion of fly ash in concrete mixture influences all aspects of both freshly mixed and hardened concrete. In the latter, fly ash acts both as a fine aggregate and as a cementitious constituent, and it influences the strength, finish, porosity and durability of the hardened mass as well as the cost and energy consumption. Inclusion of the fly ash has a significant effect on the rheological properties of the freshly mixed concrete.

The Canadian Standard Association (CSA, 1997) and the ASTM recognize two general classes of fly ash:

- Class C fly ash, normally produced from lignite or sub-bituminous coals; and
- Class F fly ash, normally produced from bituminous coals.

The class C fly ashes have a distinct property of self-hardening capacity in the absence of cement and possesses higher levels of calcium as compared with the class F fly ashes. They are also termed high calcium and low calcium ashes, respectively.

2.4.1.1 Structural Properties:

The use of low-calcium fly ash has shown extremely slow rates of strength development, leading to a generalized view that "fly ash reduces strength at all ages" (Lamond, 1983). This also led to considerable efforts aimed at understanding the factors, which influence the rate of strength gain in fly ash concrete. The compressive strength development of low-calcium fly ash concrete was noted to be more susceptible to curing temperatures than high calcium fly ashes.

The results of studies on influence of particle size showed that the result, were contradictory. Crow and Dunstan (1981) concluded from a detailed study on 38 concrete mixtures that ash fineness could be correlated loosely with pozolanic activity, i.e. finer ashes reacted more readily with Portland cement. Also, fineness was more critical for low-calcium ashes than for the high-calcium ones.

2.4.1.2 Durability of Fly Ash Concrete:

Permeability of concrete: Permeability of concrete is directly related to the quantity of the hydrated cementitous material at any given time. After 28 days of curing when little pozzolonic activity takes place, the fly ash concretes are more permeable than the control concretes (without the fly ash). After six months, this trend is reversed, because of the considerable imperviousness as a result of the pozzolanic reaction of fly ash.

Carbonation: The atmospheric carbon dioxide reacts with calcium hydroxide and to a smaller extent with calcium silicates and aluminates in moist conditions to form calcium carbonate. This process of carbonation occurs in all portland cement concretes. The concrete permeability along with its degree of saturation and the amount of calcium hydroxide available for reaction determines its rate of carbonation. Concrete with a low w/c, well compacted and cured, are sufficiently impermeable to limit the advance of carbonation to a few millimeters. The deleterious consequences of carbonation in a mass of concrete are shrinkage of the concrete and reduction in the corrosion resistance of steel in the immediate vicinity of carbonated concrete.

Good quality fly ash concrete is comparable to portland cement concrete in its resistance to carbonation. If a concrete mixture is placed using a low cement concrete, insufficient curing due to lack of moisture or cold temperatures, it will not be resistant to all forms of chemical and physical aggressive actions, including carbonation (Hobbs, 1988).

Repeated Cycles of Freezing and Thawing: The current practice is based on the proven fact that air entrainment makes concrete frost resistant. While the air content has the greatest effect on the freezing-thawing resistance of concrete, addition of fly ash does not have any considerable effect on the frost resistance of concrete if the strength and air content are kept constant. Malhotra and Ramezanianpour (1994) have reviewed the research results from several investigators.

Elevated Temperatures: Incorporation of fly ash in concrete does not influence the behaviour of concrete at elevated temperatures. The loss of strength and changes in other structural properties of the fly ash and portland cement concretes occur at approximately the same temperatures.

Chemical Attack: The main causes of deterioration of concrete due to chemical action are leaching of calcium hydroxide, acidic dissolution of cementitious

hydrates, atmospheric action and dissolved carbon dioxide, and the reactivity of cement content to ions in solution. The use of fly ash increases the impermeability of concrete at later ages, therefore, introduction of fly ash will improve resistance of concrete to chemical attack at later ages, however, at earlier ages, fly ash concrete can be vulnerable.

Sulphate Attack: The influence of fly ash on the sulphate resistance of concrete is not well understood and much more research is needed to establish approximate guidelines. Mather (1982) noted that a pozzlan of high fineness, high silica content and high amorphous silica is the most effective pozzolan to reduce expansion due to sulphate attack on mortars made with non- sulphate resisting cements. He also observed that the pozzolans that resulted in poor performance were fly ashes produced by the combustion of lignite.

Alkali- Aggregate Reactions (AAR): Just after discovering alkali-aggregate reactivity (AAR) causing expansion and damage in some concretes, Stanton (1942) reported that these damaging effects can be reduced by adding finely ground reactive materials to the concrete mixtures. Later on, a variety of natural and artificial pozzolan and mineral admixtures, including fly ash were noted to be effective in reducing the damage caused by AAR. The effectiveness of fly ash and other mineral admixtures in reducing expansion due to AAR appears to be limited to reaction involving siliceous aggregates.

Corrosion Reinforcing Steel: Provision of fly ash can influence both permeability and alkalinity of the concrete- both of which are significant factors in the corrosion phenomenon. When fly ash concrete is adequately cured, it is less permeable at later ages than the corresponding Portland cement concrete. The danger exists in premature exposure of fly ash concrete to aggressive agents, as a consequence of inadequate proportioning, and incomplete curing, or the quality of the fly ash. However, at later ages, the performance of fly ash concrete vis-à-vis

corrosion of the reinforcing steel can be expected to be better than that of the plain Portland cement concrete.

2.4.1.2 Silica Fume

Silica fume is a highly pozzolanic mineral admixture, it is also knows as microsilica, volatilized silica, or condensed silica fume. It is a by-product from silicon metal and ferrosilicon alloy production. The material is a very fine powder with spherical particles about 100 times smaller in size than the portland cement, or fly ash. The diameters range from 0.02 to 0.5 μm with an average of 0.1 μm. Silica fume contains 85 to 95% noncrystalline silicon dioxide.

2.4.1.3 Ground, Granulated Blast-Furnace Slag (GGBFS)

Blast-furnace slag is a by-product from the production of steel. During production, liquid slag is rapidly quenched from a high temperature by immersion in water. The slag is a glassy, granular, non-metallic product that consists essentially of silicates and aluminosilicates of calcium and other bases. It is also known as blast-furnace slag (GBFS). Slag, in addition to pozzolanic properties, and unlike Class F fly ash and silica fume, also has cementitious properties. With regard to strength, there are three grades of slag: Grade 80, Grade 100, and Grade 120. Each number corresponds to a minimum 28-day compressive strength ratio of a mortar cube made with only portland cement and a mortar cube made with 50% portland cement and 50% slag. Because of cementitious properties, particles smaller than 10 μm contribute to early strength, while particles larger than 10 μm and smaller than 45 μm contribute to later strength. Since particles greater than 45 μm are difficult to hydrate, slag is mostly pulverized to particles with diameter less than 45 μm.

Ground, granulated blast furnace slag is also known for improved workability and lower water requirements. Slag hydration is significantly influenced by temperature: hydration is accelerated at higher temperatures and retarded at lower

ones, when compared to portland cement hydration. This may lead to differences between the strength of concrete in the field and in the laboratory specimens.

2.4.2 Corrosion Inhibitors

Corrosion inhibitors are chemical substances added to cement which when properly used, are effective in retarding the corrosion of reinforcing steel in concrete. The theory of mutual dependence of anodic and cathodic reactions was carefully examined when developing corrosion inhibitors. The theory states that corrosion rate can be reduced by reducing the rate of only one of the half-cell reactions. Fontana (1986) defined a corrosion inhibitor as a substance that when added in small amounts to a corrosive environment reduces its corrosivity. Corrosion inhibitors function by forming an impervious film on the metal surface or by interfering with either the anodic or cathodic reactions, or both (Fontana, 1986). Some inhibitors such as sodium and potassium salts of chromates and benzoates have been shown to reduce the corrosion rate of the steel rebar, however, they significantly decrease the compressive strengths of the mortars to which they were added (Craig and Wood, 1970).

The general types of inhibitors are anodic, cathodic, and mixed. The anodic inhibitors react with the corrosion products of the reinforcement and form a protective film on the surface, and gradually all of the steel surface is covered, and the corrosion process ceases. With anodic inhibitors, sufficient quantities must be present to provide effective inhibition; they are dangerous when used in very small quantities, as they may cause the corrosion rate to increase. According to Trethewey and Chamberlain (1988) two types of anodic corrosion inhibitors are important for steel, one type includes oxidizing agents such as nitrates, nitrites, and chromates, and the other type includes silicates, phosphates, molybedates, and borates. These materials require dissolved oxygen to be effective.

Cathodic inhibitors affect the cathodic reaction by reacting with the hydroxyl ions to precipitate insoluble compounds on the cathodic site and prevent access to oxygen, such as salts of zinc and magnesium, or calcium. Materials such as arsenic, bismuth, antimony and some organic compounds also affect the cathodic reaction by forming a layer of adsorbed hydrogen on the cathode surface. Cathodic inhibitors are considered to be safe because the active cathode area is reduced regardless of the amount of inhibitor used. The corrosion inhibiting reaction is influenced by many factors, such as solubility, precipitation, dispersion, chloride to inhibitor ratio (anodic inhibitors only), chemical composition of cement, curing conditions, molecular structure, temperature, and pH of the pore solution. From the two corrosion inhibitor groups, anodic inhibitors were found to be more efficient than cathodic corrosion inhibitors. Presently, mixed corrosion inhibitors, chromate/polyphosphate/zinc, are being used to provide the best corrosion protection. Inhibitors can also be grouped as barrier layer formers, neutralizers, scavengers, and others.

2.4.3 Dual Systems: Reduction of Diffusion Rate and Corrosion Inhibition

Dual systems include reduced concrete permeability and corrosion inhibitors. An example is a mineral admixture, which provides reduced permeability of the cover concrete, while the corrosion inhibitor elevates the corrosion threshold level. Inhibitors are most effective when used with high-quality, low porosity concrete, which hinders the ingress of harmful chloride ions to the steel. The net result is that corrosive elements not only arrive at the steel bar depth at a later stage, but also must be present at higher concentrations for corrosion to start.

Chapter 3

Bond Behaviour

The behaviour of a reinforced concrete member is influenced to a considerable degree by the bond between the concrete and the reinforcing steel, and the associated cracking. This chapter presents some basic information on bond between the concrete and the reinforcing steel, and the associated slip and cracking phenomena in reinforced concrete. The mechanics of slip of deformed bars versus plain bars in concrete is discussed. The stress redistribution and deformations in concrete associated with bond are reviewed. A summary of the program planned to study the parameters, which are influenced by corrosion, is also presented.

3.1 Introduction

The Webster Dictionary defines bond as "a uniting or binding element or force, such as bonds of friendship, or tie". Another definition suggests: "A bond is a contract to carry out specific duties or actions. A penalty must be paid if the duties are not carried out satisfactorily". The latter definition will apply to any contractual relationship where a civil engineering works contractor is required to post a bond for satisfactory completion of the infrastructure. In the case of structural concrete, "bond stress, is the name assigned to the shear stress at the steel bar-concrete interface which, by transferring load between the bar and the surrounding concrete, modifies the steel stresses" (Park and Paulay, 1975).

Bond failure at the steel-concrete interface will not enable the tensile force to be developed in the steel reinforcing bar or prestressing strand, thus influencing the

resistance of the structural element. In the worst case, this bond failure can result in a catastrophic failure of the element and the structure, which could possibly have serious consequences, such as fatalities, injuries and loss of property. Who is responsible for such an event? Finally, the society has to bear the loss, irrespective of who is responsible for it. In some cases, the structure may not fail, however, its capacity can be influenced significantly by this bond distress, and the system will require major rehabilitation to restore its original strength and function. Again, who would be responsible for it? Again, the society bears the loss, irrespective of whoever is responsible for the bond failure-contractors, engineers, materials suppliers, etc. It is the responsibility of the engineer to ensure that bond performance is satisfactory.

The external load is very seldom applied directly to the reinforcing steel, which receives its share of the load through the surrounding concrete. Thus, an effective reinforced concrete member must have a positive interaction between the steel bar and the surrounding concrete in order to obtain a force transfer between the two materials. This phenomenon is fundamental because it influences many aspects of the behaviour of reinforced concrete such as cracking, deformability, instability and others. The transfer of the load between the steel and the concrete is affected by the phenomenon of bond at the steel-concrete interface, which ensures secure gripping of the reinforcement, and the working of the reinforcing steel in conjunction with the concrete, to form a reliable structural element capable of withstanding both tensile and compressive forces.

The bond is affected by many factors such as change in temperature, variation in the loading of a member, creep in the concrete, corrosion, etc, however, the bond must be capable of adjusting to any alteration of the above influencing phenomena. As control of crack width and deflection is one of the most important requirements for serviceability and the quality of structures, considerable research and development has been undertaken on bond, tension stiffening and crack width control. However, little research work has been undertaken to evaluate the effect of corrosion on the bond behaviour and tension stiffening. Corrosion of steel reinforcement in concrete

reduces the durability of concrete structures. The consequence of corrosion is probably more serious for the deterioration of bond between the concrete and the reinforcing steel due to corrosion than the consequence of the reduction of the load carrying capacity of the steel bars due to a decrease in the cross-sectional area, unless the steel bars are very small.

As concrete is relatively weak and brittle in tension, cracking is expected when significant tensile stress is induced in a reinforced member. Cracking is an important phenomenon specific to reinforced concrete, and it can have a considerable influence on the durability of a structure. The cracking phenomenon is accentuated further in most new materials, and new technologies are now being used in the construction field. For example, the use of high-strength concretes (characterized by relatively low tensile strength and toughness), the use of fiber reinforced plastic rebars (relatively low modulus of elasticity and high Poisson's ratio); the use of epoxy-coated rebars (limited chemical adhesion and friction). The concrete tensile strength and toughness are fundamental properties, which ensure efficient and effective bond at the steel-concrete interface, since relatively low values of bond stress (u/f_t = 0.5 to 0.8) can exhibit a local complex stress and strain state (Gambarova and Rosati, (1996)). The load carried by the concrete prior to cracking is transferred to the reinforcement crossing the crack, and the load carried across the crack by the reinforcement is gradually transferred by bond to the concrete on each side of the crack. Thus, the original specimen transforms into blocks of varying lengths separated by tension cracks, and linked by the reinforcement. Figure 3.1 illustrates the formation of the cracks, and the load sharing between the reinforcement and the concrete.

3.2 Fundamentals of Bond

3.2.1 Basic Definition

As defined earlier, "bond stress" is the shear stress at the steel bar-concrete interface which modifies the steel stress along the length of the bar by transferring the load

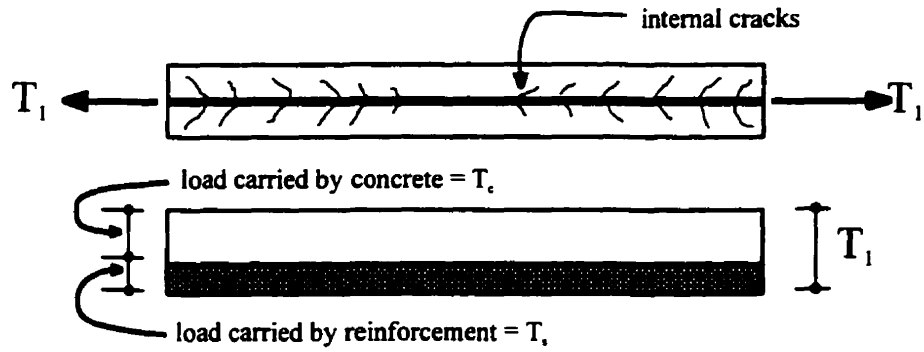

(a) Just prior to first cracking $T_1 \approx T_{cr}$

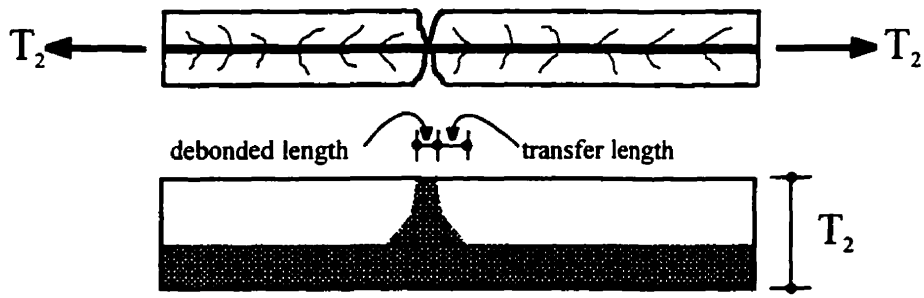

(b) Just after first cracking $T_2 \approx T_1$

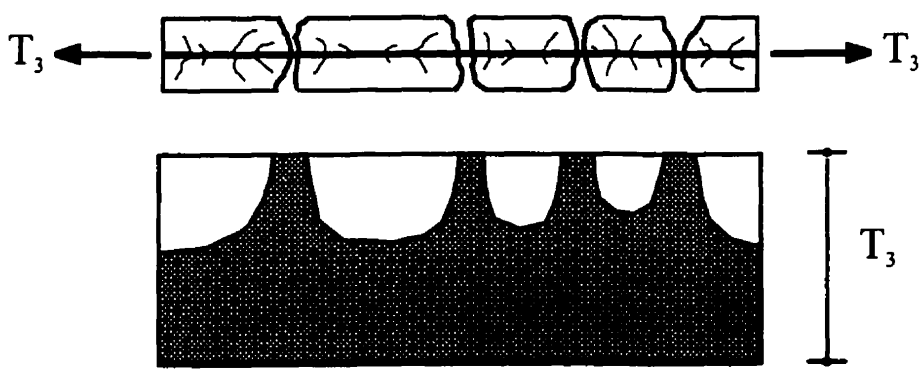

(c) Cracks fully developed $T_3 > T_2$

Figure 3.1: Load sharing between concrete and reinforcement, adapted from Collins and Mitchell (1991)

between bar and the surrounding concrete [ACI Committee 408 (1966)]. Bond stress is calculated as the nominal shear force per unit area of the bar surface. There are two important aspects to the development of bond stresses, which are the anchorage or development type, and the change of bar force along its length due to a change in the bending moment along the member (flexural bond in flexural members). Actually, the bond forces are measured by the rate of change in the force of reinforcing bars.

3.2.2 Bond Mechanisms

Based on the work of Lutz and Gergely (1967), the identified mechanisms of the bond between steel and concrete by which force is transferred from the reinforcement to the concrete and visa versa are the mechanical interlocking, adhesion and friction.

3.2.2.1 Mechanical interlock

The surface profile of a steel bar will dictate the amount of mechanical bond that can be generated between the steel bar and the concrete. The mechanical interlocking of the deformed steel bar is enhanced by the geometry of the ribs along the length of the steel bar. By contrast, prestressing steel wire tends to have a smooth surface and there is limited mechanical bond between the wire and the concrete.

For deformed steel bars, bearing against the lugs is considered to be the most significant transfer mechanism at higher load levels. The force transfer mechanism is due to the mechanical interlocking between the ribs and the concrete keys. As the ultimate bond strength is reached, shear cracks begin to form in the concrete between the ribs as the interlocking forces induce large bearing stresses around the ribs, and slip occurs. Therefore, the bar ribs restrain the slip movement by bearing against the concrete keys. The slip of a deformed bar may occur in two ways, either through pushing the concrete away from the bar by the ribs, i.e. wedging action, or through crushing of the concrete by the ribs.

3.2.2.2 Adhesion

Adhesion is the chemical bond, which is created at the interface between the reinforcement and the concrete. For relatively small loads, the basic resisting mechanism is the chemical adhesion, however, as the load is increased the chemical adhesion along the bar surface is lost quickly. Actually, it has been assumed that adhesion can break down due to the action of the service loads, or due to shrinkage of the concrete. Hence, with increasing displacement, the adhesion bond strength component is lost.

The ACI Committee 408 (1991) suggested that the bond strength due to adhesion is between 0.48-1.03 MPa. Treece and Jirsa (1989) have examined the adhesion mechanism with both uncoated and epoxy coated steel reinforcing bars, and found that the uncoated bars did adhere to the concrete while there was no evidence of adhesion between the epoxy coated and the concrete. Similarly, Cairns and Abdullah (1994) compared the bond characteristics at the interface of a steel rebar with mill-scale, and the concrete with that of a fusion-bonded epoxy-concrete interface. Specimens were cast in which the concrete was sandwiched between two plates of steel and two plates of steel with epoxy coating. A normal stress of 9 MPa was applied to the specimen prior to loading it in shear until slipping failure occurred. Minimal adhesion was observed in the case of the coated plate, and the coated plates were noted to be clean after failure, while the uncoated steel plates were covered with a layer of crushed mortar.

3.2.2.3 Friction

Similar to the mechanical interlock, the frictional bond is very dependent on the surface characteristics of the reinforcing bar. After the chemical adhesion is destroyed, some frictional slip occurs before the full bearing capacity at the ribs is mobilized. Based on the work of Treece and Jirsa (1989), the ACI Committee 408 (1994) suggested that friction can contribute up to 35% of the ultimate strength governed by the splitting of the concrete cover.

3.2.3 Bond Resistance

Bond of plain bars depends on the steel surface-to-concrete bond, which consists of chemical adhesion and friction between the mortar and the bar surface. The resisting mechanism for small loads and stresses is the chemical adhesion, however, even low stresses will cause a slip capable of breaking the adhesion between the concrete and the reinforcing steel. Bond is also developed through friction and by mechanical interlocking due to the roughness of the bar surface. Bond failure with plain bars is commonly due to the bar simply being pulled out of the concrete with little associated distress.

However, bond capacity increases significantly with the use of deformed bars basically due to the interlocking of the ribs with the surrounding concrete. The transfer of the force from the bar to the surrounding concrete occurs by the mechanical interaction between the two materials, which is the primary bond mechanism. There are three mechanisms for the development of bond at the steel-concrete interface. The bond strength developed between two ribs of a deformed bar, as shown in Figure 3.2, is a combination of the following stresses:

1. Shear stress, v_a, due to adhesion around the surface of the bar.
2. Shear stress, v_c, in the tangential direction resulting from the radial compressive stresses due to bearing of the lugs which is acting on the cylindrical concrete surface between the adjacent ribs.
3. Bearing stresses, f_b, against the face of the rib.

3.2.4 Bond Failure Modes

Principally, two types of failure can occur under monotonically increasing loads (Rehm (1961) and Lutz and Gregely (1967)): slip of the deformed bars can occur because of: (i) crushing of the concrete in front of the ribs, and (ii) splitting of the concrete by wedging action. The first mode is a direct pullout of the bar, although, in tension tests where adequate embedment length with an adequate concrete cover and standard deformed bars are provided, it is not possible to produce a bond pullout

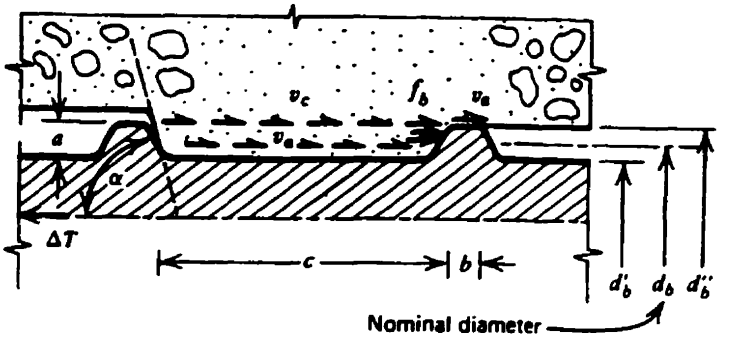

Fig.3.2: The stresses between two ribs of a deformed bar [Park and Paulay (1975)].

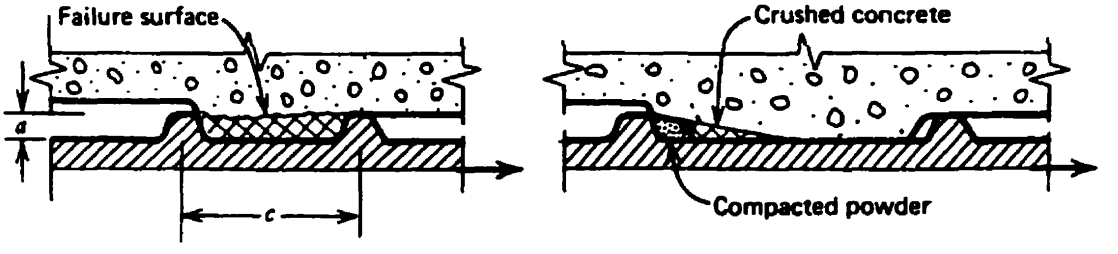

Fig.3.3: Failure mechanisms at the ribs of deformed bars [Park and Paulay (1975)].

failure, rather the bar will fracture at its loaded end. In a pullout failure, the surrounding concrete fails due to the shearing between the ribs, thus this failure depends mainly on the concrete strength and the profile and geometry of the ribs. The second mode of failure is a splitting of the concrete cover when the surrounding concrete cannot sustain the circumferential tensile stresses. The actions at the bar lugs consist of compressive forces normal to the deformation surfaces, which in turn cause tensile forces on the concrete whose radial components are similar to the bursting pressures in pipes which cause longitudinal tensile splitting of the concrete cover and the component parallel to the bar axis assists with the transfer of force between the concrete and the reinforcing steel.

Tepfers (1973) studied theoretically the circumferential stress distribution over the thickness of the concrete cylinder confining the reinforcing bars. These circumferential tensile stresses are caused by the outward radial stresses from the action of the deformed bars on the concrete cylinder as shown in Figure 3.4. He assumed three stages in the bond response of the concrete cylinder: the uncracked stage, partially cracked stage, and the plastic stage. The analyses of the cracked and partially cracked stages were based on the elastic theory. In the plastic stage, a uniform tensile stress distribution was assumed over the thickness of the concrete cylinder.

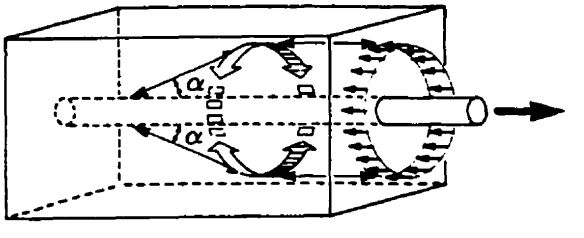

Figure 3.4: Tensile stress ring [Tepfers, 1973]

Assuming short anchorage lengths, Tepfers (1975) derived equations for the three stages, and found good agreement between the measured values of the short

anchorage tests with the partly cracked theory. If partially cracked elastic behaviour is assumed, then the bond strength, u_c, at the cracking of the concrete cover, is given by:

$$u_c = 0.6(0.5 + c/d_b) f_t \qquad (3.1)$$

For larger concrete cover thickness, the assumption of a plastic behaviour at the steel-concrete interface, gives:

$$u_c = 2(c/d_b) f_t \qquad (3.2)$$

where u_c = bond strength when the concrete cracks
c = minimum concrete cover thickness
d_b = diameter of the steel reinforcing bar
f_t = concrete tensile strength

The splitting tensile strength, f_t, (Pillai and Kirk 1988) for normal density concrete varies between 0.5 to 0.58 times $(f'_c)^{1/2}$ and as an average taken as:

$$f_t = 0.56\sqrt{f'_c} \quad MPa \qquad (3.3)$$

The experimental results (Tepfers, 1973) lie between the bond stress values obtained from the elastic and plastic theories. Tepfers considered that the deviation from the elastic theory is due to the fact that there is some plastic deformation at the steel-concrete interface. For normal-strength concrete, use of the elastic assumption (equation (3.1)) is found to be the more appropriate (Tepfers 1979). If the c/d_b value is high, failure occurs by shearing of the concrete between the ribs. The critical value of c/d_b at which the failure mechanism changes from cover splitting to concrete shearing at the steel-concrete interface has been evaluated as 2.5 by Orangun *et al* (1977), Jirsa *et al.* (1979), and by Reynolds (1982).

3.2.5 Cracking Behaviour

Cracking occurs in the concrete when the tensile stress at a given location exceeds its tensile strength and it is manifested by a separation of the concrete at this location. In plain bars, this separation between steel and concrete leads to complete loss of bond in the vicinity of the crack. Mathey and Watstein (1959) found that the crack width at the bar is nearly the same as the width at the surface of the concrete. However, in the case of deformed reinforcing bars, separation does not produce complete unloading and bond forces are transmitted solely by the rib bearing in the vicinity of a main crack, as demonstrated in Fig. 3.5, on the study of the nature of cracking around a deformed bar Goto (1971). In referring to Goto's study (1971), Beeby (1979) suggested that in the development of a crack, crack forms with a minimal width at the bar surface initially. Further loading causes loss of adhesion adjacent to the crack, transferring the load to the ribs of the bar and internal cracks form close to the main crack. Further loading causes more internal cracks to form at successively greater distances from the main crack. Steel stresses will reach a local peak at the crack, but between the cracks, the steel stress is lower due to the concrete contribution. The transfer of forces produces bond stresses.

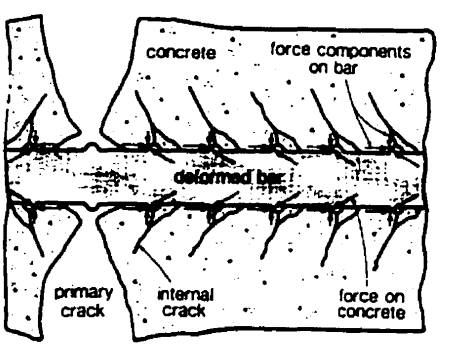

Figure 3.5: Formation of internal cracks [Goto, 1971]

3.2.5.1 Crack Spacing

The stress in the concrete at the crack location immediately after it is formed is zero. The stresses in the concrete increase with an increasing distance from the crack until the redistribution of the stresses is complete at some distance equal to the transfer length, S_o, where the stress distribution is not influenced by the crack. Within the distance $\pm S_o$ of the crack, the concrete stress is reduced below the tensile strength of the concrete, thus the next crack must form outside this region. Thus, the minimum crack spacing is S_o, and the maximum spacing would be twice that distance. Therefore, the mean crack spacing, S_m, is normally in the range:

$$S_o \leq S_m \leq 2 S_o \qquad (3.4)$$

3.2.5.2 Crack Width

The elongation of the concrete after cracking is due to the widening of the crack and the formation of new cracks. Hence, the mean crack, w_m, width is given by the mean crack spacing multiplied by the mean strain, ε_m, minus the mean residual surface strain, ε_{cm}, in the concrete between cracks:

$$w_m = S_m (\varepsilon_m - \varepsilon_{cm}) \qquad (3.5)$$

The small elastic strain in the concrete between the cracks, ε_{cm}, is usually ignored. Therefore, the relationship of the crack width and the strain of the member results in:

$$w_m = S_m \varepsilon_m \qquad (3.6)$$

Base *et al.* (1966) have stated that bond failure or slip will cause a further reduction in stress, increasing the value of S_o. Thus, the mean crack width increases as the mean spacing increases. Goto (1971) showed that the effect of the loss of adhesion and the formation of internal cracks is to reduce the rate at which force is transferred from the reinforcement to the surrounding concrete, and hence it increases

the distance from the crack over which the concrete stresses are reduced. Therefore, the spacing S_o is very much influenced by the internal failure of the surrounding concrete, and therefore it influences the mean crack width.

3.2.6 Measurement of Bond

Many different types of tests have been used to investigate the bond characteristics of the steel reinforcement in the concrete. These include the pullout tests (both the concentric and the eccentric), variety of bond beam tests (the National Bureau of Standards beam, the university of Texas beam), semibeam specimen test, and the standard tension specimen. A good overview of these tests can be found in the literature (Hsu, 1969), [Park and Paulay, (1975), Ferguson (1981), and MacGregor (1997)]. A review of the tests used in this investigation follows.

Many experimental research programs have been undertaken using the tension specimen, for example, by Broms and Raab (1961), Houde and Mirza (1972), Goto and Otsuka (1979) and others. It should be noted that cracks form in a tension specimen with increasing tensile stresses; this action will be reflected realistically in concrete beams, except for the conditions at the beam end, where the force in the bar is transferred to the concrete as in the pullout tests. In a pullout test, the concrete stress at the unloaded end is zero, and the concrete is in compression at the loaded end, while the steel is in tension, which eliminates the transverse tension cracking. In the case of pure tension tests, both the concrete and the reinforcing steel are in tension, and thus the pure tension specimen represents a simplified model of the tension zone of a reinforced concrete beam.

3.2.6.1 Pullout Tests

Most of the earlier knowledge of bond behaviour of embedded steel in concrete comes from pullout tests because of the simplicity of the test. However, this method is not intended for establishing bond strength values for structural design purposes, because pullout tests do not directly represent the stress state in the concrete beams.

In spite of these limitations, this type of test is most useful when relative rather than absolute bond resistance is acceptable, as in comparing the slip resistance of various lug sizes and patterns. Hence, this test would be adequate for studying the effect of different parameters on bond strength such as comparing the slip resistance of the various concrete mixes, some with supplementary cementing materials, and the various corrosion levels in this investigation

A bar is embedded in the centre of a concrete cylinder or prism. The cylinder is then secured and the force required to pull it out or make it slip excessively is measured, as illustrated in Fig. 3.6. The slip of the bar relative to the concrete is measured at the loaded end (bottom) and the free end (top).

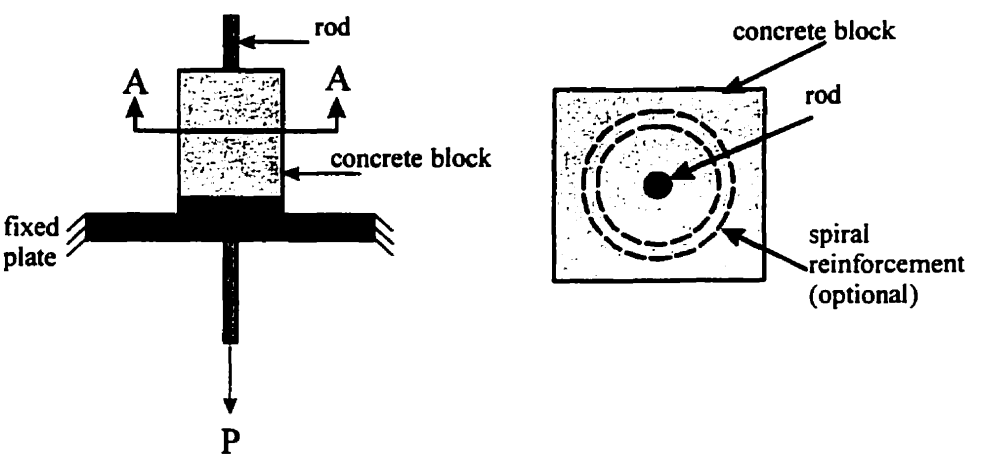

Figure 3.6: Schematic diagram of a pullout test

Figure 3.7 shows that the initial small load causes some slip and develops a high bond stress near the loaded end, leaving the upper part of the bar totally unstressed. As the applied load is increased, the slip at the loaded end also increases, and hence, both the high bond stress and slip extend deeper into the concrete specimen. The maximum bond resistance will be achieved when the slip first reaches the unloaded end. Failure occurs by (i) bar rupture if the embedment is long enough

(bond strength is higher than tensile strength of bar), or (ii) bar pullout, if the bar is very short, or light weight aggregates were used (bond strength is less than the tensile strength of the bar), or (iii) longitudinal splitting of the concrete (failure is initiated due to the concrete cracking).

The bond stresses, u_{max}, is calculated by assuming that the bond stress is uniformly distributed along the embedded length of the bar:

$$u_{\max} = \frac{P_{\max}}{\pi \cdot d_b \cdot \ell_b} \tag{3.7}$$

where u_{max} = bond stress

P_{max} = applied force at failure

d_b = bar diameter

l_d = bar embedded length

Here, the product, $\pi.d_b.\ l_d$, represents the surface area over which the bond shear stress acts. However, the calculated bond stresses vary according to the embedment length of the bar, it is argued that there cannot be a uniform stress along the section and there must be a non-linear distribution. Several researchers have proposed variations of the standard pullout tests to try to generate a more or less uniform bond stress through a test specimen.

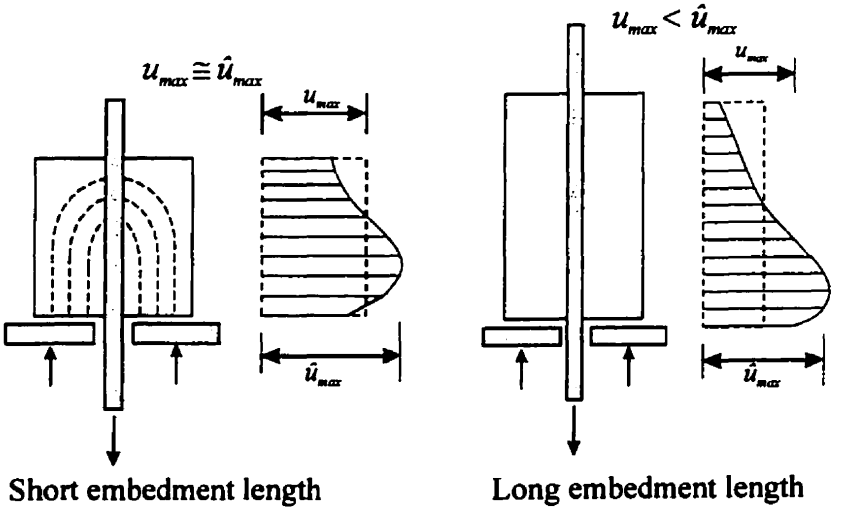

Figure 3.7: Effect of embedment length on the distribution of bond (After Leonhardt, 1964)

Leonhardt (1964) showed that with longer embedment lengths, the maximum value of bond stress, τ_{max}, becomes less representative of the average maximum stress, τ_{max}, over a section. Hence, to reflect a localized segment of bond, a small embedment length should be used as demonstrated in Fig. 3.7. Some researchers have instrumented the embedded bar internally with strain gauges such as Mirza and Jackman (1972), Houde and Mirza (1979). Knowledge of the local bond behaviour can then be extrapolated to deduce the bond stress distribution along any length of the specimen.

The important problem of concrete splitting has not been handled realistically so far. In some cases, it is necessary to provide additional spiral reinforcement in the concrete to prevent the concrete splitting during testing.

3.2.6.2 Tension Tests

In a number of modern codes, such as the CEB-MC90 (1990), the crack width is controlled by defining an effective tension area. In addition, the bond stress is important in the response of the concrete tension specimens. The present research has focussed on investigation of pure tension in reinforced concrete structures, to study the bond and the interaction between the reinforcement and the concrete under tension.

Tension tests have been used to study the mechanics of bond between steel and concrete. Goto (1971) carried out a test of this type to clarify the propagation of different types of cracks around the tensile reinforcing bars.

The response of a tension specimen, consisting of a steel bar embedded symmetrically in a cylindrical concrete specimen, and subjected to applied loads at its ends is shown in Fig. 3.8. As the applied forces on the steel bar at the specimen ends are increased, the bond stresses at the steel-concrete interface increase gradually; this causes the force transmitted to the concrete to increase until at some cross-section, it

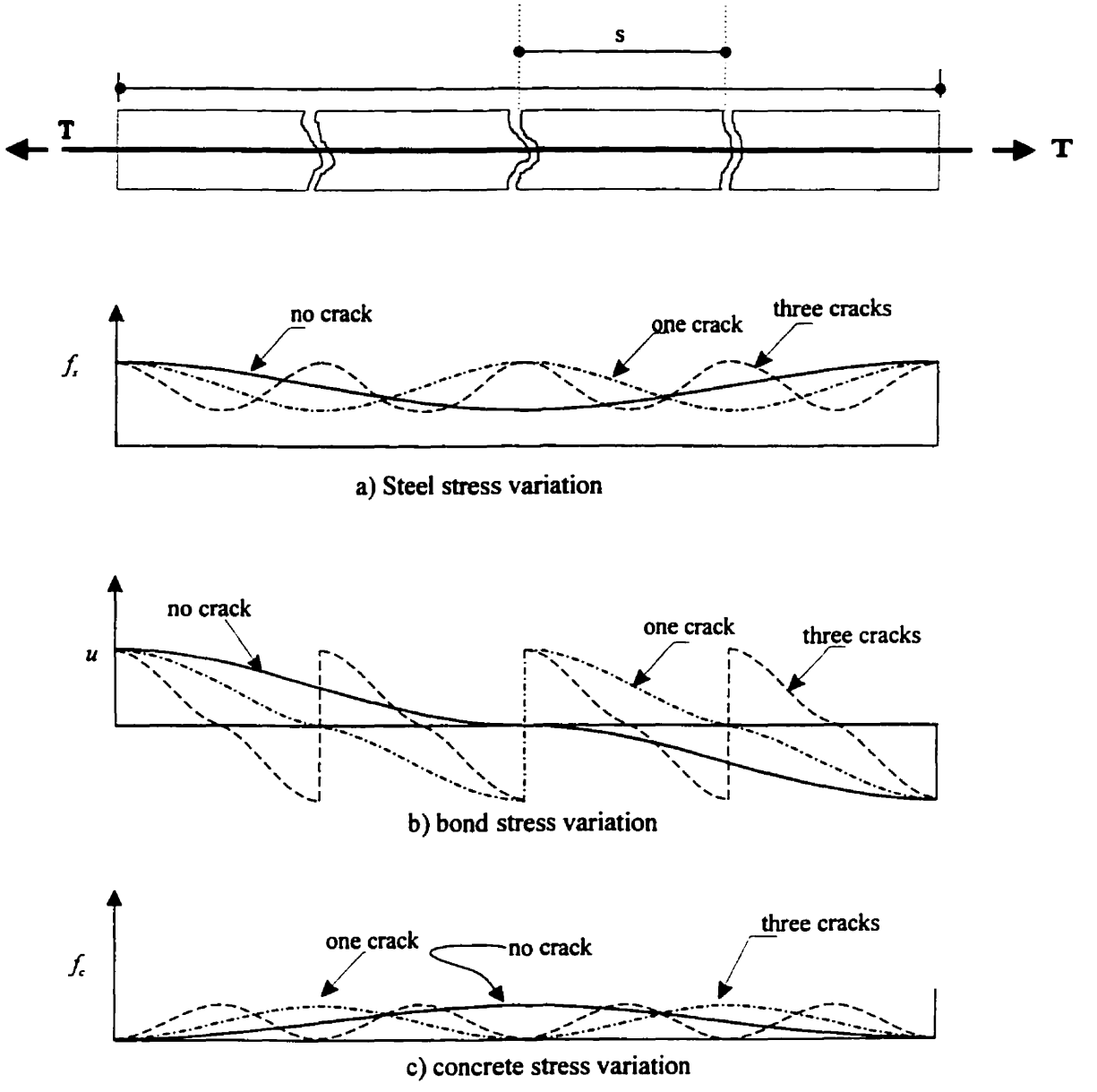

Figure 3.8: Variation of steel, bond and concrete stresses in a tension specimen

reaches a value $T_c = f_t.A_{ct}$, where f_t is the tensile strength of the concrete and A_{ct} is the area of the concrete subjected to tension. Note that just before the crack forms, the adhesion between the steel rebar and the concrete is exhausted and the concrete bears on the lugs to transfer the force from the steel to the rebar and vice-versa. In the process, there is relative slip in the rebar and the concrete, which is manifested in the opening of the crack just formed. At this stage, this concrete section with the tensile force T_c, which is equal to the tensile capacity of the section cracks, which leads to redistribution of the stresses in the steel and the concrete, and the bond stresses.

The steel force at the crack is now equal to T, the force applied at the specimen end and the resultant concrete force is zero. The redistribution of the various stresses are shown in Fig. 3.8. It the cracks are widely spaced, this redistribution can lead to development of a tensile force T_c in the concrete somewhere between the crack and the free end. As explained earlier, this section will crack and the steel, concrete and the bond stresses will be redistributed as shown in Fig. 3.8. The free body diagram of the steel bar for the condition of no, one and three cracks is shown in Fig 3.9 (a), 3.9 (b) and 3.9 (c), respectively. Note that this process will be repeated as long as the steel can transfer enough force to the concrete (T_c) to cause it to crack again. Otherwise, the cracking process will stabilize, i.e., no further cracking will occur in the specimen. It also follows that the maximum force that can be transferred from the steel to the concrete and vice-versa between two cracks is T_c. If this force becomes equal to T_c, the specimen will crack again.

Once the cracks have stabilized, any further increase in the load applied to the tension specimen will normally not result in any additional cracks, unless the concrete is weak at some location and the distance between the cracks is sufficient to cause an adequate force transfer to cause this weak section to crack. Any further increase in load will cause an increase in the steel force and therefore, the stress in the steel bar section at the crack, until finally the bar yields. However, there is no significant change in the bond stresses between the cracks and the force transferred within the cracks remains almost constant at the cracking load, T_c. It, therefore, follows that any

deterioration of bond at the steel-concrete interface due to corrosion will result in an increase in the crack spacing, because the force T_c required to crack the section will now be developed over a longer length of the bar.

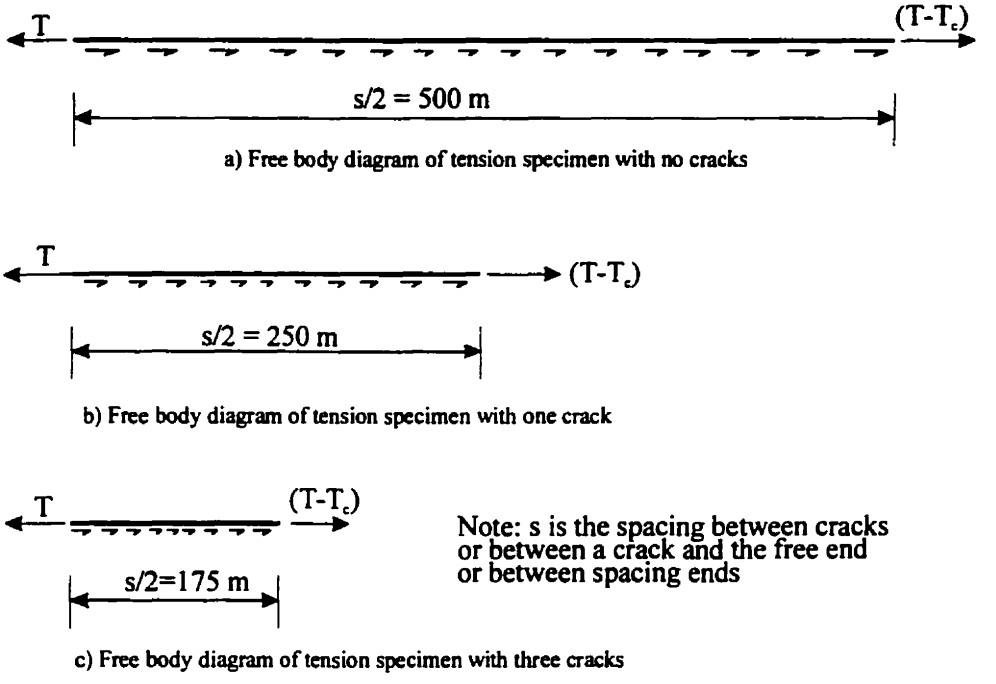

Figure 3.9: Free body diagrams showing forces on the steel bar in a tension specimen with no, one and three cracks

3.3 Cracking and Bond Stresses in Uncorroded and Corroded Specimens

Consider two identical tension specimens, which have been tested to the ultimate load an uncorroded (control) specimen with a crack spacing, s_{un}, and a corroded specimen with a crack spacing, s_c. The maximum resultant force transferred by bond from the steel to the concrete is T_c. Assume that the bond stress distribution is parabolic then the resultant bond force over a length equal to half the crack spacing is

$$(2/3)\ (u_{max})\ (s/2) = 1/3\ u_{max}\ s \qquad \textbf{(3.8)}$$

Applying this information to the uncorroded and the corroded specimens, the resultant force transferred by bond between steel and concrete is

$$T_c = 1/3\ u_{un}\ s_{un} = 1/3\ u_c\ s_c \qquad \textbf{(3.9)}$$

It should be noted that the "actual" distribution of the bond stresses at the steel-concrete interface does not remain relevant anymore because it is the resultant of the bond stresses which can have a maximum value of T_c. It does not matter whether the bond stresses are distributed parabolically, sinusoidally or uniformly; in each case the resultant of bond stresses at the steel-concrete interface over half the crack spacing will not exceed T_c. Only the coefficient (1/3) in (Equation 3.9) will change. Equation (3.9) leads to the equation:

$$u_{un} \cdot s_{un} = u_c \cdot s_c \qquad \textbf{(3.10)}$$

where u_{un} and u_c are the maximum bond stresses in the uncorroded and the corroded specimens, respectively with parabolic bond stress distributions. Note that u_{un} and u_c also represent the average bond stresses in the uncorroded and corroded specimens if the bond stresses are assumed to be distributed uniformly along the length of bar equal to half the crack spacing.

In summary, the adhesive resistance between the concrete and the steel are depleted in the early stages of loading, and further resistance arises from the frictional resistance to sliding and the bearing of the concrete on the bar lugs. If the concrete cover is quite thick, then bearing of the concrete on the lugs can lead to the crushing of the concrete at later loading stages, or the shearing on a cylindrical surface bounded by the outer edges of the bar lugs, stripping the concrete between the keys from the cylindrical surface.

3.4 Bond Stress and Development Length

To develop the yield strength, a reinforcing bar must extend a distance, l_d, within the concrete, and this distance, l_d, is required to transmit the steel bar force to the concrete by bond. Assuming that the average bond stress, u, is uniformly distributed over the distance, l_d, then equilibrium and compatibility conditions must be satisfied. Consider a reinforced concrete element of length d_x in Fig. 3.10 (a), which is located a distance x from the end of the specimen. For equilibrium, the force on the left hand side of the element, $A_c * \sigma_c + A_s * \sigma_s$, must equal the forces on the right hand side of the element, $A_c * (\sigma_c + d\sigma_c) + A_s * (\sigma_s + d\sigma_s)$, where A is the area of the material under consideration, σ_c and σ_s are the stresses in the concrete and the steel, respectively and $d\sigma_c$ and $d\sigma_s$ are the changes in the concrete and steel stresses, respectively.

$$A_c * \sigma_c + A_s * \sigma_s = A_c * (\sigma_c + d\sigma_c) + A_s * (\sigma_s + d\sigma_s) \qquad \textbf{(3.11)}$$

Therefore,

$$A_c\, d\sigma_c + A_s\, d\sigma_s = 0 \qquad \textbf{(3.12)}$$

Since the bond stress acts over the embedded perimeter of the steel bar (Fig. 3.8(b)), then

$$T = A_b f_s = u\, \Sigma o\, l_d \qquad \textbf{(3.13)}$$

where Σo is the perimeter of the steel rebar.

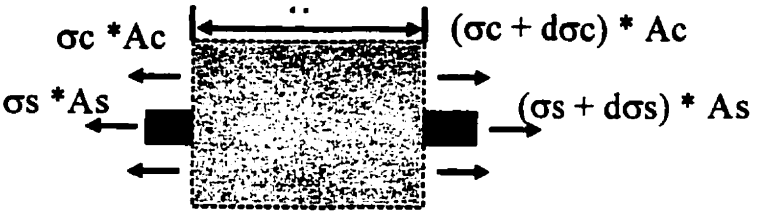

a) Element length dx with steel and concrete stresses

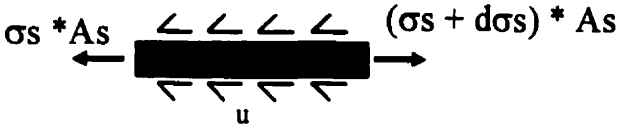

b) Free-body diagram of the steel bar of length length dx

Figure 3.10: Stresses in an element

Therefore, the development length is

$$l_d = \frac{d_b}{4u} f_s \qquad \textbf{(3.14)}$$

As mentioned earlier, to form a reliable structural element that is capable of withstanding both tensile forces, which are provided by the reinforcement, and compressive forces, which are provided by the concrete, there must be a force transfer, or bond, between the two materials. Furthermore, bond stress exists to satisfy equilibrium and conditions. If this equilibrium condition is lost than the steel bar pulls out of the concrete and the tensile force drops to zero, causing the concrete element to fail.

Bond stress must exist whenever the stress or force in the reinforcing bar changes along the length of the steel bar. Also, bond stresses do not exist if there is no change of stresses between any two sections within the steel bar. Bond force is measured by the rate of change in the force of the reinforcing bar, and the bond stress u, defined as a shear force per unit area of bar surface (Park and Paulay, 1975).

$$u = \frac{q}{\sum o} = \frac{\Delta f_s \, A_b}{\sum o} = \frac{d_b}{4} \Delta f_s \qquad (3.15)$$

where q = change of bar force over unit length

Σo = nominal surface area of a bar of unit length

d_b = nominal diameter of the bar

Δf_s = change of steel stress over unit length

A_b = area of bar

3.3 Factors Affecting Bond Strength

There are many factors that influence the bond strength between the steel and the concrete. Concrete and steel strengths, bar diameter, concrete cover thickness, embedment length, rib geometry, spacing of bars, stirrups, temperature, and corrosion are but a few of these factors. A useful review of the factors affecting bond strength is presented in the State-of-the-Art Report by ACI Committee 408 (1992). A brief discussion of the different affecting variables used to study the bond at the steel-concrete interface in this investigation is presented in the following sections.

3.3.1 Influence of Concrete Strength and Composition

Bond characteristics are not influenced only by the strength but also by the composition and consistency (i.e. cement content, water content, etc.) of the concrete mix.

3.3.1.1 Influence of concrete strength

There is a general agreement that the concrete strength has a significant influence on the bond behaviour. Perry and Thompson (1966) studied the influence of the concrete strength on the bond stress distribution over the anchorage length. They found that in eccentric pullout specimens, the location of the maximum bond stress

for the same force in the bars moved closer to the loaded end as the concrete strength was increased. This indicates a lower slip with the higher strength concretes.

Compressive strength is considered to be a key parameter in bond behaviour, because the force is transferred by bearing and bond, and failure can occur by tensile splitting and shearing of the concrete (Orangun, Jirsa and Breen, 1977). Tepfers (1973) showed that with a higher concrete strength, the slope of the bond stress distribution varies considerably over the splice length when compared to that with lower concrete strengths.

The properties of the concrete, both in tension and compression, contribute to the development of bond stresses, micro-cracking is controlled by the tensile resistance, while bearing stresses induce high compressive stresses in front of the ribs. Concrete compressive strength (f_c'), with f_c' less than 69 MPa (10,000 psi), showed strong relationship with the tensile and shear strength of the concrete (Carino and Lew, 1982).

Based on the pullout test results with concrete strengths ranging from 16 to 50 MPa, Martin (1982) observed that for a slip range of 0.01 to 1 mm, the bond stress is proportional to the concrete compressive strength. However, for very small slips less than 0.01 mm, and for high slips larger than 1 mm, the influence of the concrete compressive strength is less important and proportional to the 2/3 power of the concrete strength. Kimura and Jirsa (1992) observed that the bond stresses are proportional to the square root of the concrete strength, based on pullout tests results up to 0.25 mm slip with concrete strengths of 40, 80, and 120 MPa.

The studies of bond behaviour in the case of the more brittle, high strength concrete are limited, and there does not seem to be a general consensus about its influence on the bond capacity between the steel and the concrete. More experimental research is needed to evaluate its influence on the bond characteristics.

3.3.1.2 Influence of concrete composition

Martin (1982) studied the influence of the cement content, aggregate grading, water-cement ratios and the concrete consistencies. He concluded that the water-cement ratio is eliminated as the bond stress is related to the concrete strength. Although high water-cement ratios can lead to bleeding under the bars, especially the top bars and result in lower bond strength. He also observed that the bond properties are highly influenced by the grading of the aggregates and consistency of the fresh concrete mix. The coarser is the aggregate; the better is the bond capacity of the steel reinforcing bar. In addition, he observed that the stiffer is the mix consistency, the higher is the bond capacity; the variation of the concrete consistency has been achieved by varying the cement content by about 30%.

Gjorv *et al.* (1990) studied the effect of silica fume on the mechanical behaviour of the steel-concrete bond by using pullout tests on concrete of varying compressive strength and varying contents of silica fume (0, 8, and 16% by weight of the cement). They observed that increasing the silica fume up to 16% by weight of the cement had an improving effect on the pullout strength, especially in the high compressive strength range of the concrete. They also observed that the presence of silica fume affected the morphology and microstructure of the steel-concrete transition zone.

Hwang *et al* (1994) studied the effect of silica fume on the splice strength of deformed steel bars in high performance concrete. They reported that if a splitting failure occurred, the bond strength, normalized by the square root of the compressive strength of the beam, with replacement of 10 percent cement by silica fume, is approximately 85% of that of a similar specimen without any silica fume.

Again, there is very limited research on the influence of the concrete composition on bond behaviour. In an overview of the published literature, there is not a general agreement about the influence of the concrete composition on the bond

capacity between the steel and the concrete, which, shows that there is a need for appropriate experimental work in this area.

3.3.2 Effect of concrete cover

Bond strength increases with an increasing cover thickness. Tepfers (1973), Orangun *et al.*, (1977), and Eligehausen (1979) observed that the concrete cover and the reinforcement spacing significantly influence the type of bond failure. Splitting tensile failure occurs with small concrete covers and the bond capacity in pullout will be higher for the larger cover thickness.

3.3.3 Bar Profile

Due to the importance of the mechanical interlocking for superior bond characteristics, the geometry of the lugs or the bar rib is of a great importance to the wedging action of these ribs. Based on Rehm's research work (1968), Park and Paulay (1975) have shown that the best performance of a bar embedded in concrete over a short length `*c*' which is the rib spacing, occurs for a value of the ratio of the bearing area to the shearing area, *a/c*, where *a* is the rib height (see Fig. 3.2), equal to 0.065. Figure 3.3 illustrates the two types of failure mechanisms, associated with the geometric shape and size of the ribs. The deformation requirements of ASTM A 615-72 (1972), give the following range of values for the *a/c* ratio:

$$0.057 < a/c < 0.072. \qquad \textbf{(3.16)}$$

With reference to the steep face angle in Fig. 3.3, Lutz and Gergely (1967), stated that the bond of deformed bars is developed mainly by the bearing pressure of the bar ribs against the concrete. Pullout tests by Rehm (1957) and Lutz (1966) showed that for bars with steep rib face angle α (larger than about 40 degrees with the bar axis) slip occurs only by the compression of the concrete in front of the bar rib, while in bars with flat ribs, i.e., the angle α is small, slip occurs with the ribs sliding relative to the concrete as the rib tends to push the concrete away from the bar. This wedging action

can be a major cause of longitudinal splitting along the bar. For $45° < \alpha < 70°$, the deformations must reverse in direction on each side of the bar, [ASTM A 615-72 (1972)].

3.3.4 Influence of Corrosion on Bond

As the steel bar corrodes, the increased volume of the corrosion products results in a "bursting" pressure, which causes longitudinal splitting cracks in the specimens, with the crack width increasing with the corrosion level. This results in the breakdown of adhesion and friction at the steel-concrete interface, excepting at low corrosion levels, when there is no longitudinal cracking, and the corrosion products have a beneficial effect of improving the bond characteristics at the steel-concrete interface. At higher corrosion levels, the steel bars display localized pitting and loss of some of the ribs over the bar length, thereby weakening the rib-concrete mechanical interlocking force transfer mechanism. An examination of the number and spacing of the transverse cracks shows that as the level of corrosion increases, the transverse crack spacing also increases, reflecting the deterioration of bond characteristics at the steel-concrete interface (Amleh and Mirza, 1999).

3.4 Program Basis

In order to study the effect of corrosion on bond behaviour, the basic responses of the specimens with uncorroded and corroded bars in pullout and tension specimens are compared. The purpose of this investigation is to study the influence of various stages of corrosion on the pullout response, tension stiffening and cracking, and the influence of the pre-existing splitting due to corrosion. This kind of longitudinal splitting in uncorroded reinforced concrete is critical as it promotes bond failure, unless an adequate confinement is provided. Both longitudinal splitting cracks and transverse tensile cracks are studied.

The complete response of this series of tests is obtained by studying the following:

1. Pullout-slip response (pullout specimens)
2. Load-deformation response (tension specimens)
3. Stress-strain relationship (tension specimens)
4. Cracking behaviour (tension specimens)

3.4.1 Pullout-Slip Response

In design practice, the average bond resistance u is usually calculated assuming that it is uniformly distributed along the embedded bar length using the maximum bond stress. However, the bond stresses vary along the embedded length of the bar and a knowledge of this distribution is essential. The distribution of the bond stress is dependent on the assumed relationship between the bond stress and slip.

The Comité Euro-International du Béton (CEB) (1990) Model Code equations were developed for the bond stress-slip relationship to describe both the ascending and descending branches as in Fig. 3.11. The formulation consists of four parts:

1. $s \leq s_1$	$u = u_m (s/s_1)^{\alpha}$	$0 \leq \alpha \leq 1$	**(3.17)**
2. $s_1 < s \leq s_2$	$u = u_m$		**(3.18)**
3. $s_2 < s \leq s_3$	$u = u_m - (u_m - u_f)\,[(s - s_2)/(s_3 - s_2)]$		**(3.19)**
4. $s_3 < s$	$u = u_f = \eta\, u_f$	$0 \leq \eta \leq 1$	**(3.20)**

The CEB Model Code states that the ascending branch refers to the stage where the ribs on the reinforcement bear against the mortar matrix characterized by the local crushing and micro-cracking of the concrete. Hence, in the ascending branch, the bond stress increases according to a non-linear function up to the point where s is equal to s_1 (Equation 3.17). The horizontal line between s_1 and s_2 refers to the advanced concrete crushing and shearing off between the ribs and is believed to occur only for the confined concrete. During this stage, the bond stress is a constant maximum (Equation 3.18). The descending branch refers to the reduction of bond

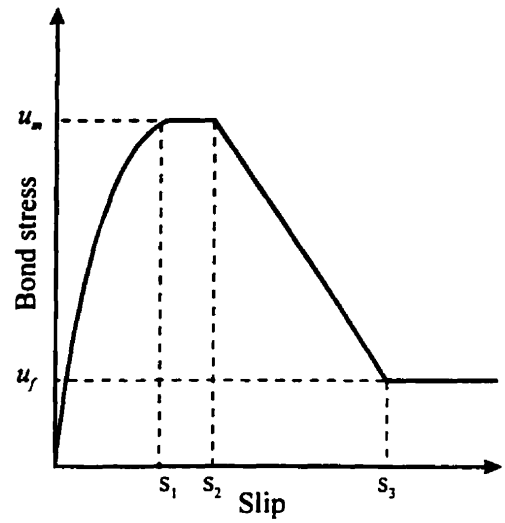

Figure 3.11: CEB bond model (Comité Euro-International du Béton, 1991)

resistance due to the occurrence of splitting cracks along the steel bar (Equation 3.19). In the final stage, the horizontal part represents a residual bond capacity, which is maintained by the presence of transverse reinforcement (Equation 3.20).

3.4.2 Load-Deflection Responses

The bond behaviour between the concrete and the reinforcing steel in a reinforced concrete member can be predicted, if the load-deformation relationship of that element is known.

Unlike plain concrete, reinforced concrete can still resist some tensile stresses after a full crack is formed. The development of the stresses in the concrete between the cracks is dependent on the bond characteristics between the reinforcing steel and the concrete. The phenomenon of concrete contribution between the cracks to the net stiffness of a member is called "tension stiffening" and plays a significant role in reducing the postcracking deformation in reinforced concrete structures. Figures 3.12 and 3.13 illustrate the tension stiffening through the presence of tensile stresses in the concrete that reduces the average axial member deformation, by considering the relationship between the load and the average strain in the concrete both before and

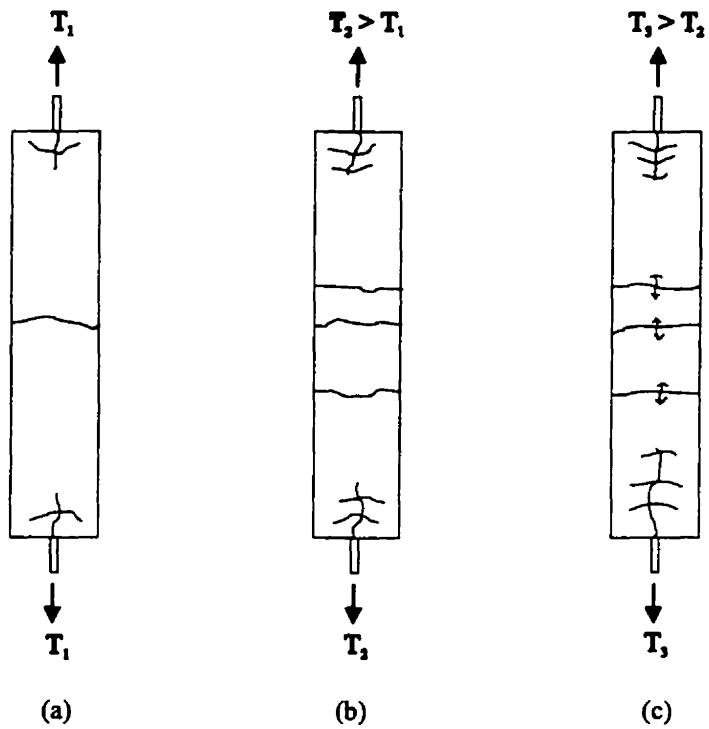

Figure 3.12: Splitting and transverse crack propagation in a tension specimen

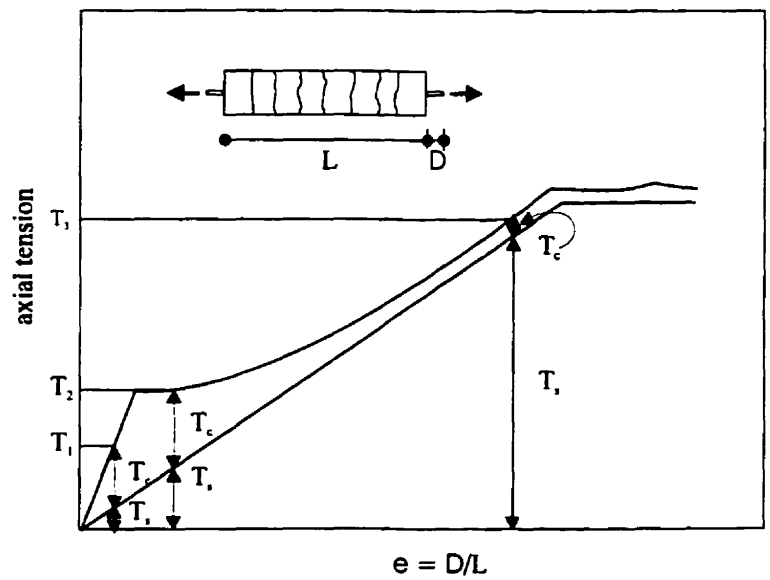

Figure 3.13: Influence of tension in concrete on load-deformation response, [Collins and Mitchell (1991)]

after cracking. The ascending part 1 represents the uncracked stage, the horizontal part 2 represents the crack formation stage, and the ascending part 3 represents the stabilized cracking stage.

3.4.3 Modified Steel Stress-Strain Relationship

To help understand and interpret the results of the load-deflection responses, and to formulate the tension stiffening effect, it is necessary to develop a modified stress-strain relationship for the specimen.

A brief review of the change in the bar size and its cross-sectional area due to corrosion is presented here. The equivalent cross-sectional area was determined using mass loss results for each specimen using the following equation:

$$\Delta A = \Delta V/L \tag{3.21}$$

giving:

$$A_{ms} = A_s - \Delta A \tag{3.22}$$

where ΔA = change in cross-sectional area.
A_s = original reinforcing steel cross-sectional area
A_{ms} = equivalent cross-sectional area
ΔV = change in volume
L = length of the corroded specimen

where the subscript *'ms'* relates to the mass loss of the corroded specimen and the subscript 's' stands for the uncorroded specimen.

After obtaining the new (equivalent) cross-sectional area of the corroded steel, the stress-strain relationships are obtained for the corroded rebars for each level of corrosion. Also, a control specimen is included in each stress-strain curve for comparison purposes. The difference in the elongation between the bare bar and the

"real" intermediate behaviour represents the "real" contribution of the concrete in tension.

3.4.4 Cracking Behaviour

There are normal variations in the spacing of the cracks, mainly due to the bond characteristics of the reinforcing bar, the difference in the tensile strength of the concrete, and the proximity of previous primary cracks, where the local tensile stress tends to decrease. The ACI Committee 224.2R-3 (1994) report suggests that for the normal range of concrete cover thicknesses, 30 to 75 mm, the average crack spacing will not reach the limiting value of twice the cover thickness until the steel stress reaches a value of 138 to 200 MPa. Because of the variability in the concrete tensile strength along the length of a tension member, cracks do not all form at the same stress level. Also, the bar ribs tend to control the crack width by limiting the slip between the concrete and the steel. The maximum crack width versus the steel stress relationship at the crack location for each specimen is obtained and compared with the control specimen, along with the crack spacing.

The results of the pullout-slip, load-deflection, stress-strain relationship and the cracking behaviour are presented later.

Chapter 4

Condition Survey of Bridge Deck

This Chapter presents detailed condition survey that was performed on four randomly selected 5m by 6m segments of the Bridge deck to determine the extent and the possible cause of deterioration. It is extremely important to correlate the in-situ data from the various tests with each other, and also with the tests on the cores obtained from the bridge deck concrete, that are commonly performed in most appraisal programs. Some of these tests results are compared with the results of the accelerated corrosion tests on tension specimens constructed using the "original" Dickson Bridge concrete mixture to compare their corrosion responses, the deterioration of bond at the steel-concrete interface and the mechanical properties of the corroded bars.

4.1 Introduction

The corrosion of steel in concrete is a fundamental problem in all concrete structures. It is now known to be the major cause of concrete deterioration. Some researchers compare corrosion to "cancer" in humans, due to the fact that corrosion has many similar cancerous properties such as "once it starts it's hard to stop" and "it is best to catch it at an early stage" (Mirza 1997).

The available techniques used to conduct any condition survey are explained briefly in the following sections, along with their advantages and limitations. These evaluations provide the cause and extent of the corrosion of steel reinforcement.

4.2 Visual Survey

The first step of any condition survey is the visual examination, which characterizes the nature of the problem and provides guidance for planning a detailed survey. The visual inspection gives an indication of what is wrong with the structure and the extent of the damage such as spalling of concrete, and it identifies the areas, which require a more detailed examination. Cracks, spalls, scales and discoloration, and any type of defect is recorded as well as photographed.

A visual investigation is a simple act of identifying typical deterioration problems and documenting their quantities. This investigation should include plans of the concrete structure, crack survey, and a general review of all of the concrete components to identify suspect areas for possible further review. The condition and functionality of all drains should be reviewed. A crack survey can be a very tedious task to perform. The proper interpretation of cracks requires the expertise of a structural engineer. For the purpose of this investigation, it is sufficient to identify only cracks which are wider than 0.5 mm (structural cracks), and non-structural cracks which are actively leaking. Cracking may be in the form of delamination cracking (not visible) or inclined cracking. Delamination cracking can easily be detected by sounding methods (Fig. 4.1).

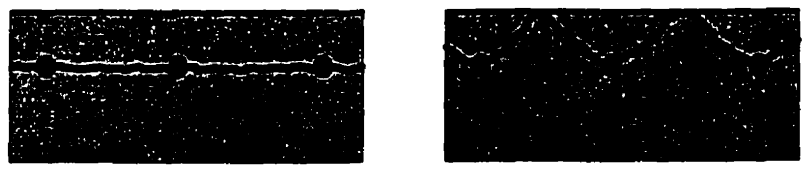

Delamination Cracking **Inclined Cracking**

Figure 4.1: Corrosion Related Cracking in Concrete.

4.2.1 Interpretation and Limitations

Interpretation of the condition survey information is based on the knowledge and experience of the engineer conducting the survey. Interpretations are according to the types of defects, for example, there are different causes for different types of cracks. The Strategic Highway Research Program (SHRP) produced guides to the different types of defects in concrete structures through an expert system, HWYCON (Kaezel *et al.*, 1994).

4.3 Delamination

In the corrosion process, the iron is changed to oxides of iron by a different number of complex reactions; the volume of the reaction products is several times the volume of the corroding iron. This builds up tensile stresses around the reinforcing steel resulting in a bursting pressure that causes fracture of the concrete at the rebar level. This can be detected at the surface of the concrete structure by different means of the delamination survey. Dragging one end of the chain across the top surface of a slab or deck usually performs the delamination survey. The areas of delamination have a distinct "hollow sound" which is easily identified. There are other sophisticated techniques used presently, such as radar, infrared, sonic and ultrasonic techniques.

4.3.1 Interpretation and Limitations

Again, the interpretation is based on the knowledge and experience of the engineer conducting the survey. Deep delamination and trapped water cause problems for accurate measurements with hammer techniques as well as for radar and infrared thermography.

4.4 Covermeter

A covermeter survey is performed to locate the position of embedded steel bars in the concrete and to measure the depth of the concrete cover to the rebar. Adequate cover

to the steel reinforcement in a structure is important to ensure that the steel is maintained at a sufficient depth into the concrete. Low concrete cover will increase the deterioration rate due to rapid access of the aggressive elements to the reinforcing steel, such as the effects of carbonation, or from aggressive chemicals. However, excessively deep cover has its own problems; the crack widths will increase with the cover thickness.

All covermeters are electromagnetic in operation. An alternating magnetic field is used to detect the presence of magnetic materials such as steel rebars. Electric currents in a coil winding in the search head generate a magnetic field, which propagates through the concrete and will interact with any buried metal present, such as the reinforcing steel. The interaction will be due to either or both of two physical properties of the steel: its magnetic permeability and /or its electrical conductivity. The interaction causes a secondary magnetic field to propagate back to the head, where it is detected by a second coil, or in some instruments by some modification of the primary field.

The assessment of the concrete cover can be implemented by means of correlation and interpretation of the maximum deflection readings. Depending on the type of the electromagnetic device, it is possible to assess the bar size by making certain assumptions about the bar and the instrument can be calibrated to convert the signal strength to distance, and to indicate the cover depth. With increasing bar size, the strength of the signal received will increase, and it will decrease with increasing bar distance (cover depth).

4.4.1 Interpretation and Limitations

Careful mapping of the position and orientation of the steel is always necessary, and to verify by removing some steel, if necessary, to ensure that accurate results are obtained. For site conditions, an average accuracy of plus or minus 5 mm, or 15 percent is suggested by the British Standard 1881 Part 204: 1988. The Standard also

lists a number of extraneous factors, which are potential sources of error. Care must always be taken when dealing with multiple bars [Aldred (1993)]. Also, the magnetic field can be influenced by iron bearing aggregates, which can give misleading results.

4.5 Half Cell Potential Measurements

The standard test method for Half-Cell Potentials of Uncoated Reinforcing Steel in Concrete and the principle of the Copper/Copper Sulphate electrode measurement technique is described in the ASTM Standard C876-91. The Half-Cell test estimates the electrical half-cell potential of uncoated reinforcing steel, for assessing the probable extent of corrosion activity of the reinforcing steel. Most corrosion failures in concrete structures are accompanied by increased potential.

Free corrosion potentials are usually measured using a suitable reference electrode, either placed in contact with the surface of the structure, or embedded within it. Potential mapping is an extension of this technique and uses sets of corrosion potential readings taken on a defined grid, plotted as iso-potential contours, to locate areas of possible corrosion activity.

4.5.1 Equipment and Test Method

The half cell is a simple device, a piece of metal (electrode) immersed in its own ion solution, such as copper in copper sulphate, silver in silver chloride, etc. When this half-cell is connected to another metal that is immersed in its own ion solution, such as iron in ferrous hydroxide (reinforcing steel), a potential difference between the two 'half cells' is noted. Figure 4.2 shows a schematic diagram of the 'half cell' potential equipment. A tube that holds a copper electrode immersed in saturated copper sulphate solution constitutes the electrode which passes through a seal at one end of the cell and is then connected to a voltmeter by a flexible wire. The other end of the cell is closed with a porous disk, which is in contact with a damp sponge to provide the electrical contact with the concrete surface.

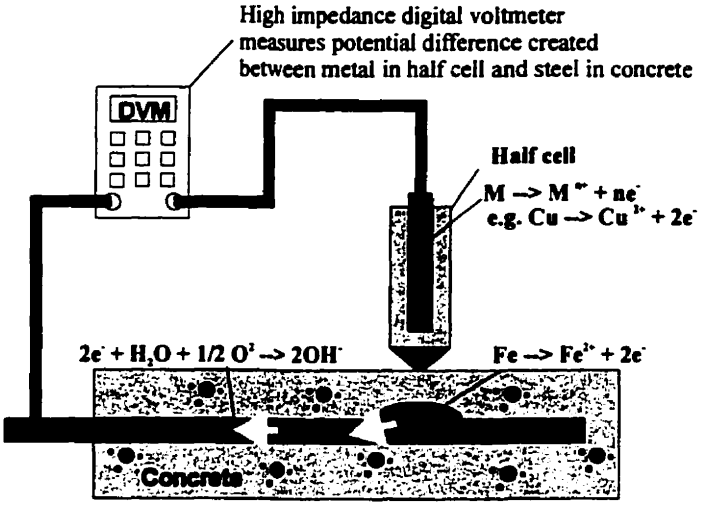

Figure 4.2: Half-cell measurement corrosion potential

Before conducting any half-cell survey, a check of the electrical continuity between the reinforcing steel bars should be performed. Repeating a small number of readings with the half-cell connected at two different points is useful as a check of the electrical continuity.

4.5.2 Method

A reinforcing bar is located near the surface, and a short length is exposed for an electrical connection. The lead from this connection is attached to the positive terminal of the voltmeter, while the negative terminal is connected to the half-cell. This standard half-cell is then moved along the concrete surface, and measurements are taken by pressing the sponge against the surface of the concrete and noting the meter readings. Two readings are taken at each location to provide protection against false results. All locations are prewetted using a fine spray of weak detergent mixture to ensure that sufficient electrolyte is present at the surface.

The potential of the reinforcing steel changes as the electrochemical reaction takes place. The voltmeter measures the difference in the electrical potential between

the electrode and the reinforcing steel. The significance of the potential readings and their relationship to the corrosion of the reinforcing steel in the concrete is well documented. According to the standard test method ASTM C 876, Standard Test Method for Half Cell Potentials of Reinforcing Steel in Concrete, the more negative the voltmeter reading, the greater the probability of active corrosion. Table 4.1 presents the guidelines for the interpretation of the potential readings for the bare reinforcing steel in concrete.

Table 4.1. Interpretation of Potential Readings.

Corrosion Potential	Corrosion Condition
> -200 mV	5% probability of no corrosion
-200 to -350 mV	Corrosion activity is uncertain
< -350 mV	95% probability of active corrosion

By convention, potentials are considered negative when measuring the potential between steel with respect to copper. A copper/copper sulphate half cell potential measurement between zero and -200 mV indicates that the reinforcing steel is passive, there is a 90% probability that corrosion is not active. An increase in the half-cell potential to -350 mV shows a higher probability that the passive layer is failing and an increasing amount of steel is dissolving. However, it is not possible to predict the level of corrosion activity with any confidence. Readings more negative than -350 mV indicate that the reinforcing steel is actively corroding, and there is a 90% probability that corrosion is active. Present criteria indicate that the potential of the copper sulphate 'half cell' as referred to a hydrogen electrode is -316mV at 22^0 C and the temperature correction is -0.9mV per degree C.

For the purpose of this survey, the test results have been presented in a tabular form using the data as recorded on the site and as an equipotential contour map which provides a graphical indication of the areas where corrosion is most likely.

4.5.3 Factors affecting the potential field

Half-cell potentials do not measure the corrosion rate; they measure the thermodynamics of the corrosion process. The interpretation of the corrosion potentials can be misleading as they are based on empirical observations rather than accurate scientific theory. Potentials are not purely a function of the corrosion condition but also other factors. There are several factors that significantly influence the measured potentials due to the concrete cover. The ohmic potential drop in the concrete therefore affects the potentials measured.

1.Concrete Cover Depth

The potential values at the concrete surface over actively corroding and passive steel become similar with an increasing concrete cover thickness. Thus the location of small corroding steel areas becomes increasingly difficult.

2.Concrete Resistivity

The concrete humidity and the presence of ions in the pore solution affect the concrete electrical resistivity. The local moisture and salt content vary across the structure and with time, and thus the concrete resistivity can change, thus causing an error of plus or minus 50 mV in the measured potentials

3.High Resistive Surface Layers

The macrocell currents tend to avoid highly resistive concrete. The measured potentials at the surface become more positive and the corroding areas may remain undetected.

4.Polarisation Effects

Very negative potential can be found in steel in concrete structures immersed in water or in the earth due to the restricted oxygen access to form a passive layer. Also, in the splash zone or above ground (transition region of the structure), negative potentials can be measured due to galvanic coupling with the immersed rebars. These negative potentials are not related to the corrosion of the reinforcement, because if there is no oxygen to sustain the passive layer for compensating cathodic reaction, there can be

no corrosion. Vassie (1991) provided a detailed description of the half-cell and its use.

5. Carbonation

The anodes and cathodes are quite close together within the carbonated concrete, hence a 'mixed potential' is measured which is an average of the anode and cathode potentials. In addition, the resistivity of the carbonated concrete is significantly affected, due to the fact that the carbonated concrete pores are partly blocked by the calcium carbonate deposits and therefore the concrete wets and dries more quickly.

4.5.4 Results and Interpretation

The patterns formed by the contours can often be a better guide in these cases. In any case, the technique should never be used in isolation, but it should be coupled with measurement of the chloride content of the concrete and its variation with depth and also the cover to the steel and the depth of carbonation. In addition, areas of rebar which show highly negative and low potentials should be exposed and examined to correlate corrosion condition with the readings.

4.6 Depth of Carbonation

Carbonation of concrete occurs when concrete reacts with the atmospheric carbon dioxide (and sulphur dioxide) to cause gradual neutralisation of the alkalinity from the surface inward. In a normal, good quality reinforced concrete, the alkaline nature of the concrete protects the steel reinforcement from corrosion, by the formation of a passive oxide layer around the steel reinforcement. The rate at which carbonation occurs is a function of the concrete quality, mainly its permeability, water/cement (w/c) ratio and the compaction. As mentioned earlier, the rate of the carbonation reaction is inversely proportional to the square root of the age of the structure. If the depth of carbonation is taken in mm. and the age of the structure in years, the constant of proportionality is approximately unity. Therefore,

for K (proportionality constant) = 1

and the rate of carbonation (mm/yr) = 1 (Age in years)$^{0.5}$
(The rate applies only at the particular age chosen. The rate cannot be used for other ages)

This gives the depth of carbonation (mm) = (Age in years)$^{0.5}$

Carbonation is slow in saturated concrete because the pores are blocked with water, hence at higher humidities the power function drops off, so that above 90% RH the depth of carbonation is likely to be (Age in years)$^{0.3}$ and continues to fall at higher humidity levels. Also, in a very dry concrete, the carbonation is slow because there is little pore fluid for reaction with carbon dioxide. Recent research suggests that the square root relationship holds only at about 50% relative humidity (RH).

Carbonation often occurs rather fast in practice, either because the concrete is permeable, or due to microcracking in the concrete bypassing the normal diffusion processes. Excessive permeability can result from a high water/cement ratio, but it can also result from poor curing of the cover concrete. Most modern specifications fail to recognise the importance of curing on the concrete quality; similarly, construction practices do not place adequate emphasis on the curing of the concrete and its enforcement by those supervising a project.

4.6.1 Test Methods

Carbonation depth is easily measured on a freshly exposed section of the concrete, by spraying the concrete with a chemical indicator, which changes colour according to the alkalinity of the concrete, such as the phenolphthalein spray. This phenophthaline turns to a strong pink colour when the concrete is alkaline (above pH 9.2) but remains colourless where the concrete is carbonated. It should be noted that the pH at which the colour of phenolphthalein changes is lower than that at which the passivity is lost (which occurs progressively below about the value of pH = 11). The test is described

in a BRE Information Sheet IP6/8, "Carbonation of Concrete Made with Dense Natural Aggregates". It should also be noted that carbonation along diffusion paths in poorly compacted concrete and along microcracks, may not be readily revealed by the phenolphthalein spray method, and the use of petrographic methods are recommended to reveal carbonation of this kind.

4.7 Chloride Determination

As mentioned earlier, the concrete provides a protective alkaline environment within a normal, uncontaminated reinforced concrete structure, which chemically protects the steel reinforcement from corrosion. However, when chlorides reach the steel surface, the chemical protection normally imparted is eliminated and the steel may then corrode, provided a sufficient supply of moisture and oxygen is available.

The chloride content of the concrete is critical to the life of the reinforcement, because small amounts of chloride can disrupt the passive layer that protects the steel from corrosion. Therefore, to assess the condition of the deteriorating concrete, it is essential to determine the chloride content in the concrete. To determine the chloride content of the concrete samples are obtained, either from the crushed concrete or more often from dust drillings undertaken using a hammer drill. To assess the penetration of the chlorides into a structure from an external source, samples of the dust from successive depths are collected and tested for the chloride content by the acid extraction from the crushed concrete, followed by a chemical determination of the chloride content by titration against silver nitrate, so that a chloride profile can be obtained. The method is described in BS1881:Part 124:1988. Chloride ion meters and rapid field test methods are also available. Like the carbonation tests, the chloride profile must be related to the cover depth so that the extent to which the rebars are exposed to high chlorides can be determined.

Chloride testing will verify the likelihood of corrosion of steel reinforcement caused by the ingress of chloride salts and the amount of chlorides which varies with the level of salt present as follows:

- Corrosion due to chloride salts is unlikely when the chloride content is less than 0.2 percent by the weight of cement.
- Corrosion of steel in interior conditions is unlikely but possible in the presence of sufficient moisture, or in exterior conditions when chloride content is between 0.2 and 1.0 percent by the weight of the cement in the concrete.
- A high risk of corrosion exists, when chloride content is above 1.0 percent by the weight of cement, irrespective of whether the concrete is in a protected environment or not.

The threshold values will vary slightly if chlorides were added during construction. A further complication occurrs due to the release of chemically bound chlorides due to carbonation of the concrete behind the steel reinforcement. Carbonation breaks down the chloroaluminates, thus freeing chlorides from their bound condition to participate in the corrosion process.

4.7.1 Test Method

Concrete cores are collected from selected spots. The cores were sliced into depths of 5 to 10 mm, 10 to 20 mm, 20 to 35 mm (or rebar level), and 35 mm to the rebar level and the first 5 mm are discarded. The concrete core slices are pulverized and kept into marked plastic bags. A chloride ion meter is used. The reagents for determining chloride content are as follows:

1. Digestive solution (prepared by mixing 60 g of glacial acetic acid, 50 g of isopropyl alcohol, and 940 g of distilled water).
2. Stabilization solution: (3.75 ppm of chloride ions in distilled water).

3. Calibration solutions (3, 9, 90, 180, and 374 ppm of chloride ions in distilled water).

The ASTM Standard C 1152-90 and SHRP-S-328, and the probe/voltmeter combination manuals (Phoenix Model CL01502 and Gilson Model HH-344) procedure was used:

The chloride probe was calibrated against five standard chloride solutions. The daily calibration data was regressed linearly to obtain the slope and the intercept of the millivolt readings versus the log of chloride concentration (Cl^- ppm):

$$log_{10}(Cl\ ppm) = a.(mV) + b \qquad \textbf{(4.1)}$$

where a = slope
b = intercept
mV = millivolt readings(mV)

Procedure: Three grams of the powdered sample are dissolved in 20 ml of the digestive solution and 80 ml of the stabilization solution. Very low concentration of chlorides in the stabilization solution, 3.75 ppm is used, which becomes 3 ppm after mixing with the digestive solution to ensure that chloride concentration is above the minimum threshold of the probe. These values are corrected to provide the net chloride content in the sample. The chloride percentage in the concrete is obtained using the following logarithmic inverse of the calibration equation:

$$Cl = (10^{(a.mV + b)} - 3)x(0.0033) \qquad \textbf{(4.2)}$$

where, the term-3 is the correction for the three ppm of chlorides in the stabilization solution and the 0.0033 is the conversion from chloride ppm to chloride percentage by the weight of concrete as follows:

1 (ppm) = 1 (mg/l) = 1/1000 (g/l) = 1/10000 (g/100 ml of sample) = 1/10000 (g/3g of concrete) = 0.0033 % by the weight of Cl in concrete.

The profile of chloride percentage is found by linear regression of the square root of Cl percentage calculated above vs the depth of the sample (Poulsen, 1990), as follows:

$$y = d.x + c \qquad \textbf{(4.3)}$$

where, c = intercept of linear regression line of chloride profile
d = slope of linear regression line of chloride profile (cm^{-1})
y = square root of chloride content (Cl) at depth x
x = depth of chloride content (cm)

- Apparent Chloride Diffusion Coefficient *(CD_a)*: The intercept (c) and the slope (d) of the profile linear regression line found above, are used in Poulsen's simplified solution of Fick's 2nd law (Poulsen, 1990) to calculate the apparent chloride diffusion coefficient *(CD_a)* as follows:

$$DC_a = (c/d)^2/12t \qquad \textbf{(4.4)}$$

where, DC_a = chloride apparent diffusion coefficient ($cm^2.s^{-1}$)
t = chloride exposure period (s), taken as 35 years for Dickson bridge.
c = intercept of linear regression line of chloride profile
d = slope of linear regression line of chloride profile (cm^{-1})
y = square root of chloride content at depth x

4.8 Resistivity Measurement

The measurement of the resistivity of the concrete gives an indication of the risk of significant reinforcement corrosion. Due to the electrochemical nature of the

corrosion process, the electrical resistivity of the concrete influences the corrosion rate of the reinforcing steel, as the ionic current must pass from the anode to the cathode for corrosion to occur.

The electrical resistivity is an indication of the amount of moisture within the concrete pores, the size and tortuosity of the pore system. Thus, it is significantly affected by the concrete quality. Also, the concrete resistivity is affected by the chlorides as they promote the retention of moisture in the concrete. The rate of corrosion then becomes increasingly related to both the resistivity of the concrete and the rate at which the oxygen can reach the steel.

In general, the lower is the electrical resistivity, the greater is the risk of corrosion, and the value of the half cell potential indicates that corrosion is occurring. This may be stated empirically as follows:

- Values greater than 12000 ohm-cm indicate that a significant rate of corrosion is unlikely.
- Values between 5000 and 12000 ohm-cm are normally related to a significant rate of corrosion.

4.8.1 Equipment Used

Figure 4.3 shows the details of the equipment, the four-probe resistivity meter or the Wenner probe, which was developed initially for measuring soil resistivity. Basically, it consists of four 6mm diameter steel probes, which are pressed onto the surface of the concrete using colloidal graphite as a contact medium. Each probe is provided with a terminal connection from which wires lead to an earth resistance meter. A current is passed between the two outer probes and the potential difference between the two inner probes is measured by the meter, which calculates and displays the resistance directly.

Millard (1991) described some of the commercially available equipments for measuring resistivity of the concrete cover. Broomfield *et al.* (1993, 1994), Newman (1966), Feliu *et al.*, (1988) have explained and shown some alternative approaches to measure the electrical resistivity of the concrete cover by a two electrode method using the reinforcing network as one electrode and a surface probe as the other.

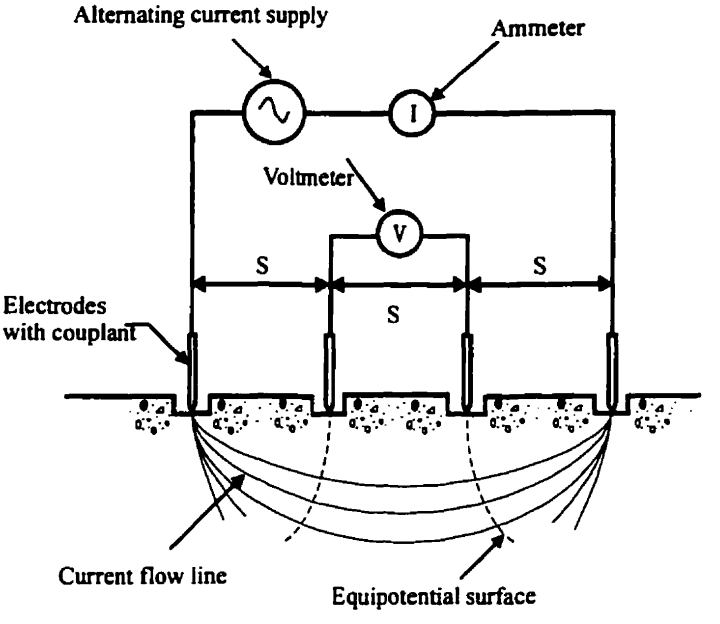

Figure 4.3: Four probe resistivity test

4.8.2 Method of Test

The test procedure is adapted from the Wenner Method for the measurement of the resistivity of soils. The areas to be considered are selected to suit the appropriate criteria A check is made using a cover meter to ensure that no reinforcement is in the immediate vicinity (nearer than about 20mm to the surface). The four 6mm diameter steel pins are then coated with colloidal graphite, pressed onto the surface and connected to the earth resistance meter. The resistance readings are read directly from the instrument.

The resistivity of the concrete (ρ) is related to the measured resistance (R) by the equation:

$$\rho = 2 R \pi a \qquad (4.5)$$

where ρ is the resistivity in ohm-cm,
R is resistance in ohms and
a is the separation of electrodes in cm.

4.9 Permeability

Permeability can be defined as the ease with which a fluid (gas or liquid), which may contain aggressive chemicals, can diffuse through a solid, and therefore, it plays an important role in the durability of concrete structures. Mechanisms of rebar corrosion, which dominate concrete deterioration in the Canadian environment, are quite permeability-related. Permeability of the concrete plays an important role in durability because it controls the movement and the rate of entry of water. However, evaluation of concrete permeability in the field has met with little success.

Deterioration and damage in any concrete system can be evaluated and predicted by the permeability of the concrete or its capacity to transport aggressive media into the concrete. The transport channels are normally formed by the pore system and the microcracks and other fissures, which vary widely in their shapes, sizes or dimensions, and other characteristics, and are normally distinguished by an extensive inner surface. Heterogeneous chemical reactions between solid liquid, and gaseous phases take place on the surface of phase separation and on the outer and the considerably larger inner surface of the pores within the concrete. These transport process and the chemical reactions are basically responsible for some of the

deterioration process and their rate controls the kinetics of the various heterogeneous reactions and therefore that of the overall deterioration of the concrete due to any chemical causes.

A commercially available non-destructive test, the Autoclam test, developed at the Queen's University of Belfast [Basheer (1991)], was used to measure the permeability of the concrete deck. The test is carried out by clamping the Autoclam to a 50 mm metal ring that is glued to the concrete surface. The Autoclam uses a hydrostatic pressure of 0.5 bar to measure the in-situ water permeability. The equipment can alternatively be used to measure a low-pressure, 0.01 bar water sorptivity. In addition, a measure of air permeability through decay of the air pressure applied to the concrete surface, can also be obtained. In all cases, emphasis must be on comparative rather than a quantitative application, and the results relate only to surface-zone properties. It must be recognized, however, that this is the critical region as far as durability performance is concerned.

After preparing the site for the test, a hollow cylinder, 160 mm in diameter and 50 mm in depth, is glued to the concrete with silicon, then filled with water for 48 hours, for a 100 % saturation of the site spot locally. The test is then carried out by clamping the Autoclam to a 50 mm metal ring, which is glued to the concrete surface with a quick setting adhesive material. The test chamber is then primed with water until bleeding occurs from the other end. Next, the pressure in the test area is increased to 0.5 bar at which point the recording of the pressure and flow commences. Readings are taken every 1 minute for the next 15 minutes. The volume of water penetrating into the concrete at a constant pressure of 0.5 bar is recorded for the evaluation of the water permeability.

Figure 4.4 shows the schematic drawing of the air permeability and the water permeability test set-up within the Autoclam apparatus.

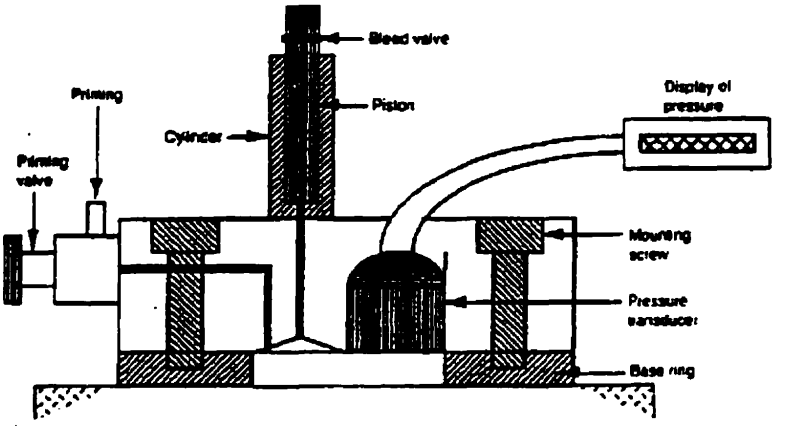

(a) Air permeability test setup

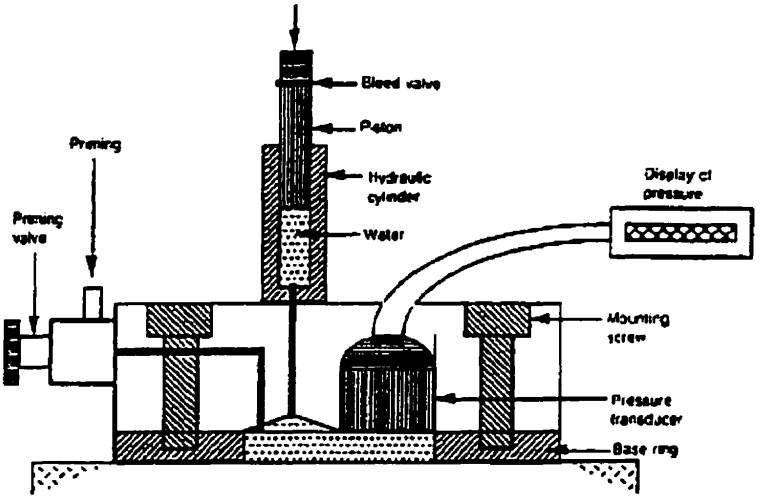

(b) Water permeability test setup

Figure 4.4: Autoclam apparatus for permeability tests

Nine permeability tests were conducted on each of the four selected sites. A plot of the quantity of water flow in m^3 (volume) between the 5^{th} and 15^{th} minutes on the Y-axis and square root of the corresponding time in minutes on the X-axis was

produced for each test. The slope of this straight line is reported as the water permeability index.

4.10 Corrosion Rates

Since corrosion occurs as the result of electrochemical reactions, electrochemical techniques are ideal for the study of the corrosion processes. Steel in good concrete will normally be passivated, attaining a high free corrosion potential which is the half cell potential (above -200 mV against Ag/AgCl reference electrode), corroding at a very low rate - often less than 1 μm/year. Actively corroding steel will typically have a free corrosion potential of below -450 mV and will corrode at a rate of up to 1 mm/year. Electrochemical techniques used to investigate corrosion problems extract mechanistic information, and predict long term corrosion rates from an array of experiments.

Corrosion potential measurements show the areas at risk of reinforcement corrosion, but such surveys cannot provide information about the "actual" rate of the corrosion attack. Also, knowledge of the corrosion rate is useful in situations where the free corrosion potential measurements fall in the band between passivity and active corrosion. Electrochemical measurement of corrosion rate is possible using a number of techniques.

(i) Linear polarization resistance measurement.
(ii) Galvanostatic transient pulse response measurement.
(iii) AC impedance analysis.
(iv) AC harmonic analysis.
(v) Electrochemical noise.

Linear polarisation resistance method (LPR) measurement is considered to be the simplest method to implement in practice and has gained widespread use. It measures the direct current (DC) through the metal/concrete interface when the electrodes are

polarised by a small electrical potential (when the potential of a metal sample in solution is forced away from its free corrosion potential, it is termed: "polarizing the sample"). The technique relies on the observation that in the region near the free corrosion potential, the overpotential to the current response of a corroding electrode is approximately linear and that the slope of this response (linear polarisation resistance) is inversely proportional to the rate of the corrosion process. Also, this current is related to the corrosion current which in turn is directly proportional to the corrosion rate, the method provides an instantaneous measurement of the corrosion rate (Fig. 4.5).

4.10.1 Measurement Techniques

LPR measurements of steel reinforcement in concrete are usually made using a potentiostat, which is an electronic device that controls the voltage difference between a working electrode (rebar) and a reference electrode (Ag/AgCl). Both electrodes are contained in an electrochemical cell. The potentiostat implements this control by injecting current into the cell through an auxiliary electrode (inert stainless steel, or similar element). The potentiostat measures the current flow between the working and the auxiliary electrodes. The controlled variable in a potentiostat is the cell potential and the cell current is the measured variable. The potential of the test electrode is measured with respect to the reference electrode and the test electrode is then polarised by a current from an external source, the potentiostat via the auxiliary electrode. The amount, polarity and time variation of the polarisation vary between the different implementations of the technique in an attempt to overcome the various non-linearities and time responses of the actual electrochemical interface (corroding rebar surface).

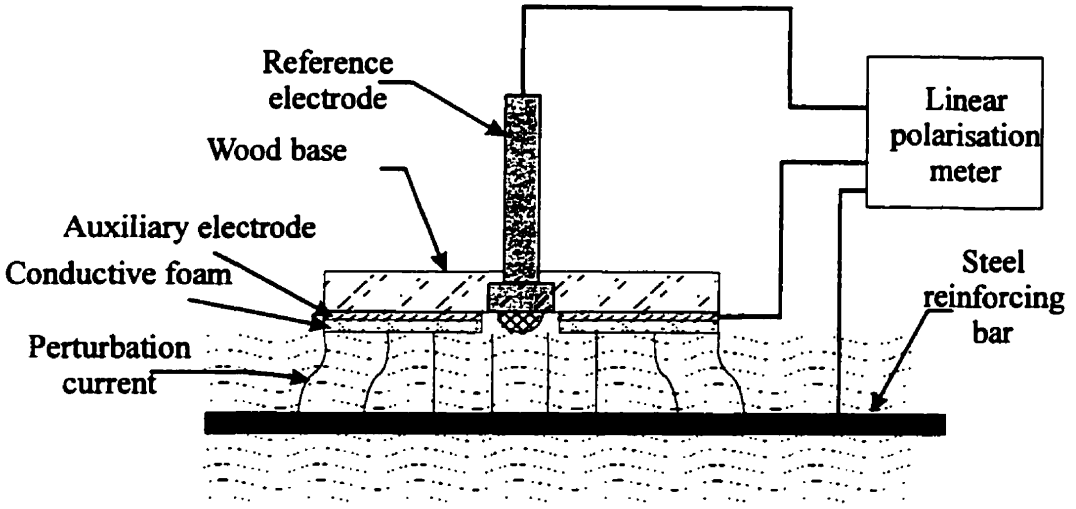

Figure 4.5: Linear polarization resistance measurement

The other laboratory electrochemical techniques for measurement of corrosion are rarely offset by the greater cost and the complexity required of their implementations. Measurements made by these techniques also tend to be more time-consuming and the results are usually more difficult to interpret. These include Potentiostatic, Galvanostatic, Potentiodynamic, Galvanodynamic and AC Impedance Spectroscopy. These have not translated effectively for field use as continuous monitors, but some of them are useful as powerful tools for problem solving.

Electrochemical Noise (ECN) is a passive electrochemical technique that requires no polarising current, but measures the naturally occurring electrochemical potential and current disturbances due to the corrosion activity. Electrochemical noise measures fluctuations of the free corrosion potential with time. Certain types of localised corrosion processes (e.g. pitting) give distinctive noise signatures, making it possible to detect and monitor these types of attacks. It is also capable of providing accurate indications of general corrosion, pitting and stress cracking when properly applied. ECN is a relatively new technique, which is gaining credibility as more field experience is gained and some large installations come on line.

Electrochemical Impedance Spectroscopy (EIS) uses a measurement of the impedance of the corroding interface to provide detailed information on the kinetics of the corrosion process. Contributions from elements such as the concrete resistivity, the actual corrosion reaction, any diffusion related processes and others may be isolated by careful analysis of the variations of the electrode impedance with the applied frequency.

The harmonic analysis effectively measures the non-linearity of the voltage-current response of the test electrode near the free corrosion potential, from which the corrosion current, and hence the corrosion rate may be computed.

4.10.2 Sources of Error

Although the LPR measurement technique is simple in principle, it is important to be aware of its limitations and possible pitfalls.

Perhaps the most important source of error is the uncertainty of the knowledge of the test electrode area. This is usually not a problem when embedded test probes, isolated from the main reinforcement are used, since their surface area can be measured accurately, but it can become significant when measurements are made with respect to the main reinforcement of the structure. The error in the area estimate tends to be the greatest when hand-held surface mounting probes are employed and it varies depending on the exact placement and geometry of the probe.

Surface mounted probes sometimes incorporate a guard ring arrangement to better define the rebar length being polarised. Essentially this uses a second auxiliary electrode, usually concentric with the main, and often driven by a separate circuitry, to confine the current flow from the main auxiliary electrode to a known area.

The resistivity of the concrete also introduces an error in the measurement. Ideally, when using a three electrode arrangement, the active tip of the reference

electrode should be placed as close as possible to the surface of the test electrode. This is usually not practical when measurements of corrosion of reinforcement in concrete are made and the actual geometry of the rebar - reference electrode - auxiliary electrode arrangement becomes a possible source of error. The resistance of the concrete between the reference electrode and the rebar or the test electrode surface effectively appears in series with the actual polarisation resistance of the corroding interface, giving an apparently lower corrosion rate reading.

It is possible to use electronic techniques to compensate for the concrete resistance, or alternatively, it is possible to measure it directly using fairly standard techniques such as the A.C. measurement or current interruption.

Conversion of the polarisation current to an "actual" penetration rate can also introduce an additional uncertainty in the results. The conversion factor (the Stern-Geary constant) depends on the chemical conditions at the test sample - electrolyte interface (rebar surface - concrete interface) and on the nature of the reactions taking place at this interface. It is important to realise that it is the conditions at the actual rebar surface that matter; these may often be different from those of the bulk concrete.

Drift of the free corrosion potential can also lead to errors in the LPR measurement. Localised corrosion, such as pitting attack, often results in large fluctuations of the free corrosion potential. Monitoring of these fluctuations may in fact be used to detect localised corrosion, as in the electrochemical noise technique. Since the LPR technique uses the free corrosion potential as a datum against which the polarisation is applied, any drift will be manifested as changes in the polarisation current. This phenomenon affects all perturbative electrochemical techniques, and not only the LPR.

The electrochemical interface between the steel and the concrete also does not respond as a simple resistance. Additional effects of double layer capacitance and

diffusion impedance cause the polarisation current to increase slowly to a steady state value following the application of the polarisation step. The time required to reach a steady state can be as long as several hours. Any reading of the polarisation current prior to a steady state condition will tend to underestimate the corrosion rate. In practice, this is often observed in situations where the rebar is passive. In these cases, the corrosion rate tends to be very low and accurate corrosion rate measurements are usually unnecessary.

The linear region of the overpotential to current response is often limited in extent. Ideally, measurements should be made in both the cathodic and the anodic directions from the free corrosion potential, slowly stepping or sweeping the applied overpotential over a range of about ±100 mV. Mathematical regression techniques can then be used to find the exact slope at the corrosion potential. In practice, the simplicity of a single polarity polarisation and the advantage of a rapid measurement tend to outweigh any likely gain in accuracy.

In summary, in practice, it is usually possible to determine the corrosion rate to at least an order of magnitude - far less than the difference between passive and active corrosion - and corrosion rate variations with time at any specific measurement location can be usually be followed to a much better accuracy. The practical trade-off is that of the measurement speed, instrument complexity and the cost against the required accuracy. In practice, it is usually preferable to obtain moderately accurate readings at a larger number of measurement points rather than more precise data from a limited number of locations.

4.11 Petrographic Examination

Petrography involves identification, systematic description and geological classification of rocks. Petrographic examination of concrete provides a much more detailed assessment of its quality than can be obtained by any other method. The ASTM Standard 856-83 provides guidance on petrographic examination of the

concrete. It involves preparing both thin sections and polished plates from samples, obtained from the concrete cores from the site. These techniques can be similarly used to provide valuable information concerning the characteristic minerals and structures existing within the concrete. Microscopical analysis of the polished plates permits observations of the thermal properties of the aggregate, water/cement ratio, cement type, cement content, carbonation, cracking, and also porosity and permeability. Power and Hammersley (1978) and French (1991) have described these microscopic methods.

Concrete can suffer from a variety of problems that can lead to its deteriorated condition for which petrography can be usefully employed in diagnosis e.g. shrinkable aggregates, alkali-aggregate reactivity, frost susceptible aggregates, sulphate attack, reinforcement corrosion, drying shrinkage, leaching, etc. In addition, petrography can yield information about the presence of deleterious materials such as dolomite, salts, organic matter etc.

4.11.1 Test Method and Equipment

Cores are obtained from the site using a rotary drill, and a plate is cut from each sample, typically about 20 mm thick. Then the plate is polished to a high quality surface to be examined under the petrographic microscope. This polished surface is used to assess the coarse and fine aggregate size, shape and distribution, the cement paste coherence, colour, and porosity, the voids distribution, size, shape, and content, the composition of the concrete in terms of the volumetric proportions of the coarse aggregate, fine aggregate, paste and void, and the distribution of cracks and microcracks. The surface is stained with a penetrating dye, so that these cracks can be seen easily. The relative abundance of rock types in the coarse aggregate is assessed.

For the thin sections, a section is cut at right angles to the external surface of the concrete from each sample, approximately of an area 24.5 cm^2, then dried at 30° C for several hours, followed by vacuum impregnation with colored epoxy resin

containing a yellow fluorescent dye which penetrates into cracks, microcracks and capillary pores in the section. Again, a plate of 10 mm thickness is cut from the sample. The concrete slice is then glued to the etched surface of a glass slide and reduced to a thickness of 30 microns by grinding and polishing, and finally sealed with a cover slip. The thin sections are subsequently examined under a combination of plain and cross polarised light using a petrographic microscope for any products of processes of deterioration of either the cement paste or the aggregate which can be recognized.

The majority of rocks are so finely crystalline that a microscope is necessary to allow precise identification of the constituent minerals. The extreme thinness of the section enables the various minerals to be distinguished according to their response in the transmitted light. Polarizing filters within the petrographic microscope produce crossed polarised light, which is affected by the crystals to produce characteristic interference colours. This feature together with the other properties such as refractive index, crystal shape and texture enable almost all of the minerals and rock types to be identified.

4.12 Compressive Strength

The strength tests are helpful to indicate whether the concrete is likely to be resistant to the penetration of chlorides and carbon dioxide, because usually the high strength concrete has low permeability. Yet it is possible to have high strength concrete which is high in permeability such as well compacted low cement content and low water/cement ratio concrete. Thus, physical testing complements the data obtained from the chemical and the microscopic tests, providing important information regarding the physical properties of the member under examination. Most commonly sought property is the strength, which enables the engineer to assess the load resistance capabilities of a structural element. This is usually supplemented with data on the reinforcement configuration, type and size, from a covermeter survey and local breakouts to verify the size and location of the reinforcement.

A variety of physical tests can be carried out on samples taken from a structure. Cores may be drilled from a structure to assess one or more of the following. For a new structure the quality of the concrete provided to the construction can be verified. For an existing structure, the quality of the concrete in the structure can provide the in-situ strength at a specific location or locations, affected and unaffected by deterioration, to establish the extent of deterioration. Also, coupled with an appropriate analysis, one can evaluate the capacity of a structure and therefore the factor of safety to carry the given loading system, or the response of a projected system for a new use. Assessment of the deterioration in the structure due to overloading, fatigue, chemical reaction, fire or explosion and weathering can also be assessed from an examination of the cores.

Depending on the location of the core sample in the structure, higher strengths can be found near to the base of a column, for example, whereas, lower strengths are likely to be found near the column top, owing to the settlement effects. The ASTM Standard C 684-81 covers the planning and interpretation of core testing

4.12.1 Preparation of the Cores

The test is carried out normally on 75mm diameter cores. The cores are usually described visually, and photographed, concentrating especially on compaction, distribution of aggregates, presence of steel etc. Various methods are available to ensure accuracy of the ends of the core, e.g., grinding to a perpendicular flat surface, capping with high alumina cement mortar and capping with a hot sulphur compound. The capped core is then crushed in a calibrated compression testing machine.

4.13 Pulse Velocity

The Ultrasonic Pulse Velocity Test is an in-situ non-destructive test carried out to determine the concrete quality and its composition. It is primarily used to assess the

conformity of concrete, i.e. detecting the presence of cracks, voids, and weak layers in concrete elements and structures. It makes use of the relationship between the measured velocities of the ultrasonic waves propagated through a medium and the physical properties of that medium, which in this case is concrete. This test method was first used in the early 1950's. The ultrasonic pulse velocity test is one of the most widely used in-situ non-destructive methods for assessing the quality of concrete. The test can be used with considerable ease in the field, and for obtaining the information about the quality of the concrete at considerable depths below the surface. The basic theory involves determining the pulse velocity of the longitudinal waves propagated in the concrete. The pulse velocity can be calculated from the following equation:

$$V = \frac{L}{T} \tag{4.6}$$

where V= longitudinal wave pulse velocity (m/s)

L= measured material path length (m)

T= measured transit time (s)

The velocity of ultrasonic pulses travelling in a solid material depends on the density and the elastic properties of that material, hence it is possible to assess the elastic properties of the material when the density and wave propagation characteristics are known. The wave velocity of a homogeneous, isotropic elastic medium is given by the equation:

$$V = \sqrt{\frac{E}{\rho}\frac{(1-\upsilon)}{(1+\upsilon)(1-2\upsilon)}} \tag{4.7}$$

where E = the dynamic elastic modulus

ρ = the density

ν = the dynamic Poisson's ratio

4.13.1 Methodology

In most cases, a simple pulser-receiver with an internal timing circuit is used with a pair of piezoelectric transducers and the time required for the wave to traverse a given path length is measured through the transmission mode. In through transmission mode, the wave is sent by one transducer and received by another, receiving and amplifying the pulse, usually on the opposite side of the material. The pulse velocity is then obtained (see Fig. 4.6).

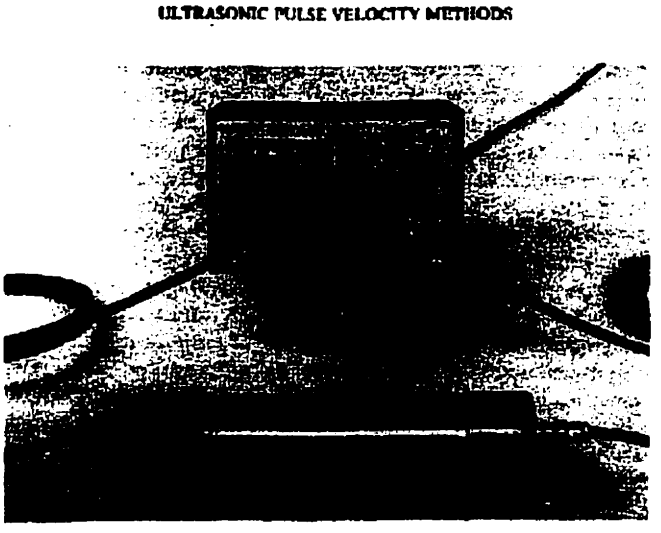

Figure 4.6: PUNDIT apparatus (C.N.S. Instruments Ltd).

The standard methods of conducting pulse velocity surveys are given in the ASTM C597 83 (ASTM 1987 c), or the BS 1881: Part 203 (BSI, 1876c) BS 1881: The BS 188: Part 203 describes three basic types of generated waves for on-site test methods, depending on accessibility within the structure. The slowest type of waves are the surface ones having an elliptical particle displacement, whereas transverse or shear waves with particle displacement at right angles to the direction of travel are faster. The fastest type of waves are the compression waves, which are longitudinal waves with particle displacement in the direction of travel being the most important as they generally provide more useful information.

The embedded reinforcing steel has a significant effect on the ultrasonic pulse velocity through a structural member. The steel should ideally be avoided by ensuring that the pulse path is located outside its zone of influence. It is suggested that a covermeter survey be conducted prior to the pulse velocity testing to avoid the reinforcement. Test results show that the zone of influence of the transverse bars is significantly less than that for comparable longitudinal bars. If the influence of steel cannot be avoided, uncertainties and loss of accuracy will inevitably be introduced when assessing the pulse velocity of the concrete. In this case reliable correlation factors are required to be used.

The Portable Ultrasonic Non-destructive Digital Indicating Tester (PUNDIT) equipment was used to obtain the pulse velocity readings in this field study using a 54 kHz transducer.

Chapter 5

Field Studies: Detailed Evaluation of Four Sites (6m by 5m) from the Deteriorated Dickson Bridge

This Chapter summarizes the results of several field and laboratory tests, undertaken over a grid of 0.25m by 0.25m, on four randomly selected 5m by 6m deck sites, as a part of a detailed research program, aimed at determining why the Montreal Dickson Bridge deteriorated so rapidly. In addition, the various field test data from the normal field rate of corrosion will be correlated with the various laboratory test results. In addition, the field test data will be used for detailed nonlinear finite element analysis of the bridge in an as constructed (new) condition with the deteriorated condition as measured in the field. The two responses (new and deteriorated conditions) will be compared and a projection will be made for the remaining service life.

5.1 Introduction

For the past few decades, concrete bridge decks, parking structures and other infrastructure in North America have been suffering from chloride-induced corrosion of the reinforcing steel, causing considerable concrete deterioration. This situation is aggravated further by the freezing and thawing cycles and by the cracking caused by the shrinkage of concrete and loading, and high thermal and humidity gradients in the extremely aggressive environment. The deterioration of structural concrete normally occurs over a period of time, depending on the environment, and the quality of

design, construction and maintenance of the infrastructure. The known parameters affecting the reinforcement corrosion in the bridge decks were the severity of the environmental and physical exposure and its duration, concrete quality in terms of workmanship, permeability, concrete cover thickness, carbonation, chloride content, and the electrical resistivity.

5.1.1 Prediction of Deterioration Behaviour Response of a System at Any Time

It would be useful to be able to predict the response of a bridge or parking garage deck at any time over its entire service life when subjected to an aggressive environment and to gradually increasing traffic loads, especially the trucks. While considerable efforts have been made successfully to determine the wheel loads of the modern day truck, even in overloaded conditions by monitoring of bridges with the traffic in motion, the efforts to model the aggressive environment and its ingress into the concrete elements is still in a stage of infancy. The Comité Europeen de Béton has made significant strides in this direction by categorising the different types of aggressive environments encountered in practice. The immediate need to be fulfilled involves the quantification of these environments and development of numerical models for their ingress into the concrete elements and the various types of damages inflicted on them.

The present investigation, using the accelerated corrosion techniques, is a useful step in understanding the behaviour of the reinforcing steel, the responses at the steel-concrete interface and the deterioration of the concrete in the immediate vicinity. However, it must be emphasised that much experimental and numerical modelling work will be needed to forecast the response of any type of infrastructure, especially the bridge and parking garage decks at different stages of their service lives and to extrapolate these to widely varying microclimates acting in the field and the performance of the system. There is a need to develop models for the various microclimates which can act on different parts of the structural element, the transport

processes which are responsible for the ingress of the various aggressive elements and the resulting degradation and loss of structural integrity, performance and service life of these elements.

The present strategic research investigation (1997-2000) on the post- mortem of the Dickson Bridge, constructed in 1959 and decommissioned in 1993, consisted of six different studies into the performance responses of the bridge deck and other elements of the bridge using electrochemical, chemical, physical, electrical and mechanical tests. Two investigators from the Queen's University of Belfast evaluated the air and water permeability and the in-sites chloride migration using specially developed tests and apparatus. Another detailed study examined the underside (soffit) of the bridge deck, beams and girders and column piers. Some of the electrochemical tests were repeated on the deck top to ensure their repeatability.

5.2 Objectives of Dickson Bridge Investigation

The objectives of this investigation undertaken by the author on the Dickson Bridge are:

1 To undertake a more detailed study on four randomly selected (6m x 5m) sites over a grid of 0.25m * 0.25m as compared with all other studies undertaken mostly over a grid of 1m * 1m. These post-mortem studies were performed principally to determine why the bridge deck and the other elements deteriorated so prematurely (only over 34 years).

2 The data from the various in-situ tests are correlated with each other, and then with the results of the tests on concrete cores obtained from about 100 randomly selected locations for all four sites. These cores represented three different levels of deterioration in the bridge deck-low, medium and high levels of deterioration.

3 To study the qualitative and quantitative effects of the various influencing parameters on the corrosion deterioration process, and their relative importance in the design, construction of new and repaired concrete structures. The data base is

being used presently by Lounis and Mirza (1998, 2001) to develop reliability-based procedures for design of new concrete structures for durability against corrosion, and for repair and rehabilitation of existing structures, which have deteriorated due to corrosion of the reinforcing steel, and for service life prediction of new and existing deteriorated concrete structures.

4 One of the long-range objectives of this program is to undertake detailed nonlinear finite element analysis of the response of corrosion-deteriorated structures at different levels of corrosion. The presently well-established nonlinear finite element analysis program for detailed behaviour studies of new structural concrete systems will be modified to model the levels of deterioration in the concrete and the reinforcing steel due to corrosion and other causes before analysing the behaviour of the system. Once appropriate models have been developed for the various microclimates acting on the structure and the transport of the aggressive elements into the concrete system, and the resulting deterioration, these will be incorporated into the basic program, which will eliminate the need to input the geometry of the deteriorated system. The program will be able to determine the level of deterioration at any time during the life of the structure subjected to a given microclimate and for the transport characteristics with the associated levels of deterioration.

This investigation along with the accompanying detailed tests on standard pullout and tension tests will assist with establishing of the accelerated corrosion technique, by direct comparison of the nature of the corrosion products developed during corrosion of the steel rebars in the field and due to accelerated corrosion in the laboratory. In addition, the pullout and the tension tests on specimens corroded to different levels of corrosion, will enable evaluation of the deterioration of the bond at the steel-concrete interface which will be incorporated in the nonlinear finite element analysis program. Development of the various subroutines and modification of the existing program are beyond the scope of this thesis. However, the results of this investigation will assist considerably and they will represent a major step with the development of the program for analysis of nonlinear response of a concrete

structure, deteriorated due to the microclimate acting on it and the ingress of aggressive elements and the associated varying levels of deterioration at different stages of the service life of the system.

5.3 Dickson Bridge Post-Mortem

The influence of the severe environmental conditions, poor quality control in construction practices and materials is manifested in the results of an extensive condition survey carried out from 1997 to 1999 on the abandoned Dickson Bridge. The results from several different electrochemical, chemical, physical and mechanical tests on this reinforced concrete structure, which had been exposed to a corrosive environment for about 35 years, are presented. The superstructure of the bridge, 366 m long by 27 m wide, located in the east end of Montreal, consists basically of a 150 mm thick heavily reinforced concrete deck over continuous heavily reinforced concrete beams, 1500 mm x 1200 mm in section, on spans of 12 to 18 meters, except for the central three spans over the CN railway tracks, where the reinforced concrete deck is supported on steel plate girders.

5.4Corrosion of Reinforcing Steel

Corrosion of steel embedded in concrete is an electrochemical process that depends mainly on the electrical resistivity of the concrete, extent of chlorides, the availability of oxygen and moisture at the steel-concrete interface, and pH of the pore liquid in the hydrated cement paste (hcp) around the steel bar. These factors are strongly influenced by the concrete quality and therefore its pore structure and permeability, and the concrete cover depth to the reinforcement.

Presence of oxygen is essential for cathodic depolarisation, while moisture is essential for the exchange of ions between the anode and the cathode, which promotes electrochemical corrosion activity by decreasing the electrical resistivity of the concrete. Ingress of carbon dioxide to the steel level can result in the carbonation of

the concrete due to reactions with the calcium hydroxide in the hydrated cement paste, thereby reducing its pH below 9 locally, resulting in destruction of the alkaline protective layer on the steel bar.

The extensive use of de-icing salts in cold climate countries on pavements and bridge decks during the winter reduces the alkalinity of the concrete and causes dissolution of the passive film on the reinforcing steel. The ice melt-salt mixture readily penetrates the more or less dry concrete by diffusion through totally or partially water-filled pores to the interior of the concrete, or by rapid capillary suction, which can cause penetration to the extent of a few millimetres in a few hours, or by direct flow through the cracks. Salt deposits are retained in the pores after evaporation. Pockets of salts within the concrete tend to create a microclimate, which promotes corrosive action, because the salt is hygroscopic and it attracts and retains moisture even when the external humidity is low.

In summary, the corrosion causing aggressive agents must penetrate through the concrete cover to reach the reinforcing steel, therefore, the permeability of the concrete, and the concrete cover thickness and its quality are important in controlling the rate of deterioration of reinforced concrete. It should be noted that the overall quality of the concrete and its permeability are affected by basically the same parameters.

5.5 Field Tests

The techniques used to investigate the cause and extent of corrosion of the steel reinforcement are detailed by Amleh and Mirza (2000), along with the detailed results of all of the tests undertaken. Only a summary of the results is presented here. A brief description of the number of tests undertaken or the site areas covered is presented in Table 5.1, while a summary of the spot tests undertaken is presented in Table 5.2. The various tests undertaken on the cores are summarized in Table 5.3.

As mentioned earlier, the parameters known to influence the corrosion of the steel reinforcement are concrete quality, concrete cover depth to the reinforcement, severity and duration of exposure, electrical resistivity of the concrete, and the chloride content near the reinforcement. The measurements are analysed individually for each test using the univariate analysis and then in selected groups by applying the multivariate analysis to investigate the degree of correlation between the various test results. Table 5.4 shows the results of the univariate analysis for all of the variables. It should be noted that the tests were carried out over the steel rebars at locations where the concrete cover was intact; consequently, some patches with reinforcing steel exposed due to cracking, spalling and decomposed concrete were not considered. The results of univariate analysis for all of the variables studied on the North, Central and the South sections of the Dickson Bridge and the entire Dickson Bridge are presented in Table 5.5

Following the discovery of large variations in the results of some of the tests, it was decided to investigate the condition of the bridge deck further. This was accomplished by extracting concrete cores from the same locations where the linear polarisation tests had been undertaken, on top of the rebar and exposing the steel reinforcement to measure the mass loss and then to relate it to the results of the other tests. The corrosion rate can be measured electrochemically using the linear polarisation method, or using the physically measured mass loss. The latter can be established more accurately than the electrochemical observations. The embedded reinforcing steel bar from each core was cleaned and scrubbed with a stiff non-metallic brush to ensure that the bar was free from any adhering corrosion products and then cleaned with a chemical solution according to the ASTM Standard G1-90. This chemical cleaning solution consisted of 500-ml hydrochloric acid, HCl, with a specific gravity of 1.19, 3.5 g of hexamethylene tetramine and 500 ml of distilled water. The corrosion products were removed after 5 to 6 cleaning cycles of about 10 minutes each. The reinforcing bar was then carefully examined for its general condition as a result of the corrosion effects in terms of pitting, rib degradation, and then weighed for the determination of the mass loss.

5.6 Visual and Delamination Test

A general visual inspection and delamination survey was first undertaken before carrying out the various tests (Tables 5.1 and 5.2), accompanied by comprehensive recording and photographic documentation. The visual examination showed an alarming deck condition in many areas with soft or crumbling concrete. Figure 5.1 shows a typical disintegrated area. The existing reinforcing steel had corroded severely and in some locations, it had disintegrated completely. Figure 5.2 demonstrates the extensive corrosion deterioration; excessive scaling and spalling were also observed. The disintegrated areas were spread around but concentrated mostly on the sides of each exterior concrete lane, mainly due to the cracking and debonding of the asphalt layer, as water and aggressive agents infiltrated through the interface between the concrete and the asphalt and got trapped underneath the asphalt cover for a long time. The underside of the bridge deck also displayed considerable cracking and spalling of the concrete cover.

5.7 Concrete Cover Thickness

The thickness and quality of the concrete cover influence the corrosion of the reinforcing steel and the associated spalling of the concrete cover. A covermeter survey was performed over a grid of 0.25m by 0.25m to locate the position of the embedded steel in the concrete and the concrete cover thickness to the rebar. The nominal cover depth was 25 mm, which is highly inadequate for reinforced concrete decks that are subjected to de-icing salts. The average measured cover depth was 35mm; approximately 18 percent of the cover depth measurements were less than 25mm and this implies that corrosion could have initiated much sooner at these locations than was expected. The minimum and maximum values of the concrete cover thickness were 6 mm and 64 mm, respectively; the coefficient of variation of the concrete cover thickness for the four sites was 34 percent, compared with a value of 45 percent for the entire bridge, and 48 percent, 39 percent and 34 percent for the North, Central and South sections, respectively. Therefore, the accuracy of the

measurements in this investigation is comparable with those from the different sections of the bridge.

Figure 5.3 attempts to correlate the steel bar mass loss with the concrete cover depth. The results are quite scattered showing that the thickness of the concrete cover alone does not provide adequate protection against corrosion of the reinforcing steel. An increase in the cover thickness did not lead to any reduction in corrosion due to the deficiency of the concrete quality, which had a significant effect on its permeability. The thickness of the concrete cover remains relevant so long as the concrete is relatively impermeable and of high quality. Amleh and Mirza (1998) also noted that if the concrete quality is not adequate, the concrete cover thickness did not have any significant effect on protecting the steel from corrosion.

It is now well recognised that one of the most important factors, which controls the rate of reinforcement corrosion is the availability of oxygen at the cathode of the corrosion microcell. An increase in good quality concrete cover thickness will result in a decrease in the supply of oxygen, and it will also result in a decrease in the ingress of other aggressive agents, such as moisture and salts. Diffusion of oxygen to the concrete-steel interface is necessary for cathodic depolarisation. Within a cathodic area, the steel is obviously in a good condition and it stays that way as long as it continues as a cathode, which explains the contradiction between the variation in the mass loss, or the corrosion rate with the cover depth.

The correlations were not distinct, within the places with relatively good quality concrete. Some high cover depth locations corresponded with low corrosion potentials, corrosion rates and chloride contents. This indicates a progressive change to a smaller probability of corrosion as the cover thickness increases. However, even at larger covers, the potential measurements indicate a significant probability of corrosion occurring over a significant proportion of the Dickson Bridge. The chloride content and the corrosion rate measurements showed similar trends with an increasing cover depth. The results suggest that the cover depth alone provides only a rough

guide as to where the corrosion may be occurring, but when used in conjunction with the other techniques, they help to locate parts of the structure with active and passive reinforcing steel

5.8 Half-Cell Potential

The corrosion of the reinforcing steel is reflected in its half-cell potential with respect to a standard half-cell (e.g., $Cu/CuSO_4$ half-cell). After establishing the electrical continuity of the reinforcing steel, half-cell potential survey was conducted over the same grid of 0.25m by 0.25m, for determining the probability of the actively corroding regions of the steel reinforcement (ASTM C876-91). The field-testing resulted in over 2000 half-cell potential values, which were used to select locations for in-depth testing such as the linear polarisation tests, permeability, resistivity etc. Figure 5.4 shows the contours of the half-cell potential readings for one of the sites. Examination of the data (Fig. 5.4) reveals that most of the area readings are algebraically lower than -350 mV. Most of the readings were between -400 and -650 mV, which indicates an over 90 percent probability of corrosion at these locations. These potential measurements indicate that locally the steel is anodic and no longer passive, and that these sites are corroding quite actively. The results also show that the steel reinforcement in about 2 percent of the sites was very unlikely to corrode whereas at about 73 percent of the sites, the steel was very likely to be corroding. About 25 percent of the measured results fell in the intermediate zone reflecting uncertainty of the reinforcing steel state which may be passive at the time of testing, however, it can turn into active anodes at a later stage.

As a part of the corrosion rate measurements, the linear polarisation test also determines the corrosion potentials of the reinforcing steel at each location. As expected, the results from the conventional half-cell potential agreed well with the corrosion potential from the linear polarisation test. Therefore, the results of corrosion potentials from the linear polarisation test were used for correlation between the corrosion potentials and the results of the other tests, which were

performed at the same locations. The potential readings ranged from -497mV to –113 mV with an average value of –465mV and a coefficient of variation of 29%. All four selected sites displayed close mean and standard deviation for both the corrosion potential and the concrete cover depth, showing that the overall condition of the four sites and the regions from which they were selected randomly was similar. These trends were also consistent with those observed in the north, central and south parts of the bridge, with a coefficient of variation value of 28% for all of the half-cell potentials for the entire bridge from over 11,000 readings. It also established confidence in the experimental procedure.

The correlation between the rebar mass loss and the half-cell readings (Fig. 5.5) showed some relationship between the two parameters; however, it was not significant enough to predict the mass loss. The results show a larger scatter of the rebar mass loss at values lower than –300mV, demonstrating a lack of potential dependence on these values. The scatter plot shows a good relationship between mass loss and the half-cell potentials for lower magnitudes of the mass loss. For the half-cell potentials in the intermediate zone (between –200 and –350mV), the mass loss results indicate that about 80 percent of the steel rebars were corroding.

5.9 Corrosion Rate

The linear polarisation test is a non-destructive method for assessing the instantaneous corrosion current density. It has been used widely in monitoring corrosion of laboratory specimens, as well as in field structures. The linear polarisation measurements were performed using GAMRY PC3 (a potentiostat that conducts the linear polarisation test) to measure the rate of corrosion of the steel reinforcement. A total of 96 corrosion rate measurements were conducted on the four sites, representing locations with a wide range of deterioration conditions present at these sites (at locations with the highest and the lowest potentials and at the steepest gradients for each of the four sites). The corrosion rates are normally related to the current density conditions as shown in Table 5.6. Approximately 3% of the corrosion

rate measurements indicated passive reinforcement condition (less than 0.0012mm/yr), and 6% of the results indicate moderate to high corrosion rates, and the remaining 91% of the measured spots are corroding significantly. These results show that there is a reasonable general correlation between the half-cell potentials and the corrosion rates. The coefficient of variation for the rebar corrosion rate for the four sites was 70 percent, as compared with a value of 76 percent for the entire bridge.

The analysis results showed some relationship between (LPR) and mass loss but it is not significant enough to predict the mass loss (Fig. 5.6). The linear polarisation (LPR) detects the instantaneous corrosion rate, which can change with temperature, relative humidity and other factors. In addition, a significant amount of pitting corrosion was observed, and the LPR technique is unable to measure the rate of localised corrosion at the pit. The laboratory tests have shown that the corrosion rate in the pits can be up to ten times higher than the generalised corrosion rate. For pitting corrosion measurements, Vassie, (1991) suggested that it must be performed by direct observation of the state of the reinforcing steel, or by a careful study of the half-cell potentials and the chloride content.

The correlation between the results of corrosion rate and corrosion potential are not sufficiently strong to predict the extent of the rebar corrosion, but it suggests that the two sets of results should be reviewed together to evaluate the corrosion activity.

5.10 Electrical Resistivity

The electrical resistivity of the concrete strongly influences the corrosion rate of the reinforcing steel, as a potential difference along the reinforcing bar is necessary to activate a current from the anode to the cathode. Thus, the magnitude of the corrosion current is primarily controlled by the resistivity of the concrete, which is dependent on the amount of moisture within the concrete pores, the pore size

distribution and its tortuosity. Therefore, it is affected significantly by the concrete quality. Also, the chlorides affect the concrete resistivity, as they help with the retention of water in the concrete. Thus, the rate of corrosion becomes increasingly related to both the resistivity of the concrete and the rate at which the oxygen can reach the steel.

A commercially available instrument, Nilson 400, which is similar to the Wenner probe that was developed for measuring the soil resistivity, was used to measure the electrical resistivity on the four sites. The normal interpretation for the resistivity measurements is shown in Table 5.7. Previous studies showed that in general, the risk of corrosion increases with a decrease in the electrical resistivity. The average value of the electrical resistivity for the four sites was 4715 ohm-cm with a coefficient of variation of 40 percent, as compared with an average value of 3537 ohm-cm for the entire bridge with a coefficient of variation of 68 percent.

Figure 5.7 attempts to correlate the mass loss with the concrete electrical resistivity. The field results of the electrical resistivity of the concrete indicate that the concrete resistivity is one of the controlling factors in the corrosion process. An increase in the concrete resistivity leads to a reduction in the corrosion of the steel reinforcing bars. A value of about 11,000 ohm-cm for moist concrete helps in reducing the corrosion to acceptable limits and the resulting loss of metal after 35 years of exposure is not more than 1 percent. Reduced values of the resistivity for moist concrete in the range of 2000 to 3000 ohm-cm are related with approximately 70 percent loss of the metal.

5.11 Chloride Content

The chloride content of concrete is critical to the service life of the reinforcement, because small amounts of chloride can disrupt the passive layer of the oxides of iron that protect the steel from corrosion. Therefore, to assess the condition of the deteriorating concrete, it is essential to determine the chloride content of the hydrated

cement paste. The rate of corrosion is strongly influenced by the rate at which the chloride ions reach a critical concentration at the steel surface and the degree of binding of the chloride in the hydrated cement paste (Rosenberg *et al.* 1989), which influences the rate at which the chlorides reach the steel surface.

Although it is the quantity of free and weakly bound chlorides which is the operative parameter in the corrosion process, its determination in concrete is rendered uncertain by the sensitivity of the test to a large number of procedural parameters such as temperature, soaking time, sample size, extraction technique, etc. Therefore, the total amount of chlorides in the concrete was chosen as the parameter in this investigation. Samples of concrete powder at the surface of the steel were obtained from each spot where the linear polarisation test was conducted. The total chloride content was determined using the methodology in the SHRP Publication S-/FR-92-108, using a chloride ion selective electrode. The chloride levels at the steel bar varied considerably and they were all above the generally accepted threshold of 0.2 percent of chloride ions by the weight of cement, except for one value. The significant influence of the chloride ion concentration at the steel-concrete interface on the corrosion deterioration is demonstrated in Fig. 5.8, which shows a direct relationship between chloride ion content and the metal mass loss. The average value of the chloride content at the steel bar level was 0.40 percent by the weight of cement with a coefficient of variation of 45 percent. The minimum and maximum values of the chloride content at the steel bar level were 0.01 percent (almost no chloride) and 1.36 percent with an average value of 0.18% and a coefficient of variation of 103 percent, showing a more consistent distribution of the chlorides over the four sites than over the entire bridge.

Difficulties arise in quantifying the threshold chloride levels for the onset of corrosion, due to the interactive influence of the other factors. However, for the condition of the concrete represented by the other tests, the threshold value is 0.15% by the weight of cement. This value is in good agreement with those obtained by Stratfull, *et al.* (1975) who proposed a chloride threshold value of the order of 0.6

kg/m^3 of concrete (0.15% by the weight of cement). The study by Lewis (1962) also gave similar corrosion threshold values. The U.S Federal Highway Administration obtained a threshold value of 0.2% by the weight of cement in the concrete mix. The results of this study show an overriding effect of chloride concentrations on the metal loss, cracking, and concrete spalling.

5.12 Concrete Cores

All concrete cores were examined visually, photographed as seen in Fig. 5.9 and then they were subjected to the following tests.

5.12.1 Petrographic Examination

The alkalinity of the concrete increases with the cement content of the concrete mix; it also depends on the cement type and it decreases with replacement of the cement with supplementary cementing materials. The higher the alkalinity of the concrete, the greater is the chloride threshold value. In addition, the proportion of the total chlorides in the form of chloride ions, which cause corrosion of the reinforcement, depends on the cement type. In general, an increase in the C_3A content in the cement reduces the free chloride content, which in turn increases the chloride threshold value.

To assess the quality control and supervision of workmanship, petrographic examinations were conducted on six concrete cores obtained from the four sites (Lafarge Canada Inc. 1999). These tests provide the information related to the bridge concrete mix specifications and other relevant information. The cement content varied from 320 to 721 kg/m^3 (ASTM C1084 Portland Cement Content of Hardened Concrete: SiO_2 method). This large variation in the cement content and the related water/cement ratio suggests the possibility of poor quality control during construction. This could also result from some patch repairs, which had to be undertaken within less then 35 years of the commissioning of the bridge.

5.12.2 Permeability

Mechanisms of rebar corrosion, which dominate concrete deterioration in the Canadian environment, are strongly dependent on the concrete permeability, which plays an important role in the durability of concrete because it controls the movement and the rate of entry of water. Despite considerable research efforts, rapid evaluation of the concrete permeability in the field has met with little success. Water absorption measurements are known to be closely connected with the permeability characteristics. This investigation used two types of absorption tests, the 30-minute absorption test in accordance with the British Standard 1881: Part 5, Methods of Testing Hardened Concrete for Other than Strength, and the ASTM C642, "Standard Test Method for Specific Gravity, Absorption, and Voids in Hardened Concrete" to determine the water absorption after immersion, and the volume of permeable voids in the concrete. Figure 5.10 shows the correlation of the steel rebar mass loss to the ASTM absorption test, while Figure 5.11 shows the relationship between the steel rebar mass loss to the 30-minute water absorption. It can be noted that the corrosion rate of the concrete with about 4 percent 30-minute water absorption is about 3.5 times more than that of the concrete with 2 percent water absorption.

The chloride ions migrate faster within the pores of the concrete with a higher absorptivity. Also, for the same degree of saturation, the specific electrical resistance is found to be lower for the more absorptive concrete. In addition, the more absorptive concrete will enhance the concentration polarisation and hence the corrosion rate by the increased diffusion of dissolved oxygen through the concrete cover to the steel rebar surface. There is a degree of arbitrariness associated with the results of these tests as they are not in accordance with the generalized results that are documented by BS 1881: Part 122. The concrete permeability is related to its absorptivity as shown in Table 5.8. On the basis of a large number of measurements, Table 5.9 has been formulated for interpretation of the concrete quality on the Dickson Bridge.

These lower values of absorption can be explained by the fact that the Dickson Bridge suffered from extensive corrosion of the reinforcement and the corrosion products have blocked the connecting paths between the pores. These observations were found during the test of the chloride ions, as a magnetic stirrer used for mixing, had a considerable amount of iron particles adhering to the magnet, even with the powder from the concrete slices that were farther away from the steel bar surfaces.

Midgley and Illston (1984) studied the penetration of chlorides into the hydrated cement paste and observed from their study of the pore size distribution of the hydrated cement paste by mercury intrusion porosimetry that the penetrating chlorides reduce the size of the small pores thus reducing the concrete permeability. In a similar study, Kayyali (1989) noted that high concentration of chlorides in the cement paste influences the cement matrix in the concrete as the capillaries in the hardened cement paste may become discontinuous leading to a reduction in the permeability of the concrete.

5.12.3 Depth of Carbonation

Carbonation depth is easily measured on a freshly exposed section of the concrete, by spraying the concrete with a chemical indicator, such as phenolphthalein, which changes color according to the alkalinity of the concrete. This phenolphthalein turns to a strong pink color (this is reflected by the darker regions in Fig. 5.12) when the concrete is alkaline (pH > 9.2) but remains colourless at locations where the concrete is carbonated (this is reflected by the lighter regions in Fig. 5.12). It should be noted that the pH at which the colour of phenolphthalein changes is lower than that at which the steel passivity is lost which occurs progressively below a pH value of about11 (Roberts, 1981).

Penetration of carbon dioxide, CO_2, changes the concrete cover chemically by neutralisation, with a reduction in pH of the concrete. In addition, carbonation

changes the microstructure of the cement paste by reacting with the hydration products in the hydrated cement paste, especially with $Ca(OH)_2$ which is the cause of high pH in the concrete. The $CaCO_3$ and Na_2CO_3 precipitate in the pores of the hydrated cement paste, thereby decreasing its permeability and also reducing pH of the pore solution. Excessive permeability can result from a high water/cement ratio, but it can also result from migration of moisture and air from the interior of the concrete to the faces near the formwork and poor curing of the concrete cover.

The results show that the concrete was deeply carbonated from the underside of the deck, to depths as high as 50 mm, which had sometimes caused the chloride content to be higher at the steel bar level than at the surface as seen in Fig 5.12. This phenomenon is often observed and is attributed to the release of the chemically bound chlorides by carbonation with the chlorides being pushed ahead of the carbonation front. Where the steel reinforcement was present in both carbonated and chloride-contaminated concrete, the corrosion problems were noted to be more severe.

5.12.4 Compressive Strength

The compressive strength test was conducted in accordance with the CSA Standard A23.2-9C, and the ASTM Standard C 42-90 (1990). Table 5.4 shows that about 48 percent of the compressive strength values were below 35MPa. A scatter plot for the compressive strength against the mass loss is shown in Fig.5.13, which indicates that the compressive strength has no influence on the corrosion deterioration. This indicates that strength alone is not a good measure to assess the durability of the concrete, as it is portrayed in many of the national codes. Though some of this scatter probably results from sampling, it shows clearly that there is substantial non-uniformity in the properties of the as-compacted concrete. This was borne out by the petrographic tests on six concrete cores taken from the four sites.

5.12.5 Pulse Velocity

The Ultrasonic Pulse Velocity Test is an in-situ non-destructive test carried out to determine the concrete quality and its composition. It is used primarily in assessing the uniformity of the concrete, i.e. detecting the presence of cracks, voids, and weak layers in the concrete structures. It makes use of the relationship between the measured velocities of the ultrasonic waves propagated through a medium and the physical properties of that medium, which is the concrete in this case. The ultrasonic pulse velocity test is one of the most widely used in-situ, non-destructive methods for assessing the quality of concrete. This is because of its field worthiness and capability to penetrate deep into the concrete. A scatter plot for the pulse velocity against the mass loss is presented in Fig. 5.14, shows wide variation of the results, however, it indicates a general trend of lower mass loss with a lower pulse velocity.

5.13 Multivariate Analysis Results

Table 5.10 shows the results of the squared multiple correlation coefficients, R^2, which demonstrates how well each variable predicts the mass loss due to the corrosion of the reinforcing steel. The very small values of R^2 indicate that there is no correlation among these parameters. The results of multivariate analyses suggest that the variables that played the most important role in the prediction of the corrosion rate are the electrical resistivity of the concrete and the chloride ion content of the cement paste. The rest of the variables did not play a significant role, consisting of (in a decreasing order) the half-cell potential followed by the water absorption rates (ASTM and BS), and the corrosion rate, pulse velocity, the compressive strength and finally the concrete cover thickness.

5.14 Summary and Conclusions

The study has provided valuable data on the effects of the de-icing salts on the rate of chloride ingress in concrete structures, which influences their durability. It has also

demonstrated the high variability resulting from the lack of uniformity in the mix composition and compaction (quality control), which must be considered in both the investigative work and durability design. It is suggested that other reinforced concrete structures (bridges, highways, and parking garages, off-shore structures) should be studied similarly to understand and predict the long-term chloride ingress, the corrosion phenomenon and the resulting distress in these structures.

- Data from this field investigation show that the chloride content, quality of the concrete cover to reinforcement, and the electrical resistivity of the concrete have a significant effect on the rebar corrosion severity.
- Very severe corrosion and concrete cracking/spalling were observed in the 62 sample cores, which had more than the recommended concrete cover thickness of 25mm. It was found that in the aggressive conditions of the local region, corrosion is not reduced to acceptable limits when the cover thickness is increased using low quality concrete.
- The variation in the concrete mix characteristics, its compaction and the variation due to local surface conditions observed in this investigation, is a dominant parameter in the vastly varying field behaviour of this bridge. Usually, this factor is not studied in research programs.
- Concrete electrical resistivity plays a key role in determining the reinforcement condition. Electrical resistivity values of about 1000 ohm-cm for moist concrete increased corrosion to a level where the loss of metal was more than 65 percent after only 35 years of exposure.
- Several national codes emphasise specific material quality requirements such as the minimum concrete strength, minimum cement content, maximum water/cement ratio, minimum concrete cover thickness, placing, compaction and curing of the concrete, to ensure durability of the system. However, because the quality of workmanship, including placing of the concrete, its compaction and curing can vary from site to site, the use of a minimum cement content, minimum concrete strength and maximum water/cement ratio is less than adequate to assure

durability and to attain the design or service life of the system (Mirza and Amleh 1995).

- The results of the various electrochemical, electrical, and chemical and physical tests show a considerably larger coefficient of variation than in the traditional strength and other parameters presently used in the concrete design and technology. However, these values of the coefficient of variation are consistent with the values obtained by other researchers on the same project. This shows the inherent nature of the various phenomena, which must be considered in the design of both new structures for durability against corrosion of the reinforcing steel, and for the design of repair and rehabilitation of concrete structures damaged by corrosion or other phenomena.

Table 5.1 Description of site tests

Test	Number of Tests, Or Area Covered	Results
Visual Inspection	All of the area	Preliminary deck assessment
Delamination	All of the area	Debonding between steel and concrete
Cover Depth	2000	Adequacy of concrete cover.
Half-Cell Potential	2000	Corrosion potential.

Table 5.2 Description of spot tests

Test	Number of Tests	Results
Cover Depth	96	Adequacy of concrete cover.
Half-Cell Potential	96	Corrosion potential.
Linear Polarization	96	Corrosion rate
Electrical Resistivity	96	Electrical resistance of the concrete.
Chloride Content, at Rebar	96	Chloride content at rebar level.
Chloride Diffusion, Apparent	74	Profile of chloride in concrete cover.

Table 5.3 Description of tests on cores

Test	Number of Tests	Results
Petrographic	6	Air content, cement content and type
Mass loss	37	Mass loss of rebar due to corrosion.
Absorptivity (ASTM)[b,c]	61	Absorption after full saturation.
Absorptivity (BS)[d]	61	Surface absorption after 30 minutes.
Pulse Velocity (Pundit)	61	To assess cracks, and uniformity.
Compressive strength	60	Concrete strength and its variability.
Carbonation depth	45	Extent of carbonation at top and bottom deck surfaces.

[c] Absorptivity test according to ASTM-C 642-90.

[d] Absorptivity test according to BS 1881: Part 122.

Table 5.4: Descriptive statistics of tests results for the four sites

Test	No. of readings	Minimum value	Maximum value	Mean value	Standard deviation	Coefficient of Variation (%)
Concrete Cover (mm)	96	6	64	35	12	34
Half-Cell Potential (mV)	96	-497	-113	-305	87	29
Corrosion Rate (mm/yr)	96	0.0035	0.28	0.1	0.07	70
Electrical Resistivity (ohm-cm)	96	757	11000	4715	1907	40
Chloride Content at Steel Level (%)	96	0.03	0.95	0.40	0.18	45
Steel Bar Mass loss (%)	37	2	65	13	2	16
Absorption _BS (%)	61	2.0	5.0	3.0	0.6	20
Absorption _ASTM (%)	61	11	16	13	1.0	8
Pulse Velocity (km/s)	61	3.0	5	4	0.4	10
Compressive Strength (MPa)	60	21	47	35	7	20
Carbonation Depth (mm)	45	5	50	17	8	47

Table 5.5: Descriptive statistics from Dickson Bridge test results

Tests	Bridge Section	Number Of Test	Minimum Value	Maximum Value	Mean Value	Standard Deviation	Coefficient of Variation
Half-Cell Potential (mV)	North	2688	-750	-44	-415	109	26
	Central	1181	-720	-144	-435	82	19
	South	2021	-920	-25	-354	115	32
	Total	5890	-920	-25	-398	111	28
Half-Cell Potential (Deck suffet and repeated tests) (mV)	North (1999)	1832	-729	-116	-436	96	22
	North suffet Deck (1999)	1630	-619	-35	-367	100	27
	South suffet Deck (1999)	1584	-673	613	-378	149	39
Half-Cell Potential (mV)	North	137	-700	-124	-444	147	33
	Central	31	-441	-229	-327	68	21
	South	66	-545	-68	-283	99	35
	Total	234	-700	-68	-383	146	38
Linear Polarization, Corrosion Rate (mm/yr)	North	137	0	0.13	0.05	2.87E-02	55
	Central	31	0.04	0.28	0.14	6.18E-02	44
	South	66	0.01	0.31	0.07	5.39E-02	82
	Total	234	0	0.31	0.07	5.15E-02	76
Electrical Resistivity (ohm-cm)	North	137	1602	30473	7477	5370	72
	Central	32	1885	13823	6543	2620	40
	South	66	1885	10996	4643	1711	37
	Total	238	1602	13823	3537	2423	68
Concrete Cover (mm)	North	137	1	90	35	17	48
	Central	32	26	120	43	17	39
	South	23	10	72	39	13	34
	Total	192	1	120	37	17	45
Chloride Content,Percent (Cement Weight) (%)	North	35	0.01	0.35	0.11	0.08	72
	Central	32	0.02	1.36	0.23	0.26	109
	South	23	0.03	0.62	0.22	0.17	77
	Total	90	0.01	1.36	0.18	0.19	103
Water Permeabilty Index ($m^3/(min)^{1/2}$)	North	34	5.10E-09	2.40E-07	4.73E-08	5.58E-08	118
	Central	16	8.43E-09	4.60E-07	5.88E-08	1.12E-07	190
	South	37	6.22E-09	2.40E-07	5.05E-08	5.85E-08	116
	Total	87	5.12E-09	4.60E-07	5.08E-08	6.94E-08	137
Chloride Migration (cm^2/s)	North	35	1.60E-08	1.40E-07	6.32E-08	3.16E-08	50
	Central	16	4.17E-08	2.12E-07	9.83E-08	5.40E-08	55
	South	66	2.85E-09	4.36E-07	6.35E-08	8.63E-08	136
	Total	117	2.85E-09	4.36E-07	6.82E-08	7.06E-08	104
Chloride Apparent (cm^2/s)	North	32	1.40E-09	5.20E-08	9.34E-09	9.53E-09	102
	Central	16	1.28E-09	6.59E-07	1.04E-07	1.84E-07	177
	South	25	5.53E-09	2.74E-06	1.74E-07	5.43E-07	312
	Total	73	1.28E-09	2.74E-06	8.65E-08	3.33E-07	385

Table 5.6. Linear Polarization Test Data Interpretation (Broomfield, 1997).

Corrosion Current Density	Corrosion Rate	Corrosion Condition
< 0.20 $\mu A/cm^2$	< 0.0046 *mm/yr.*	Passive corrosion rate
0.2 to 0.5 $\mu A/cm^2$	0.0046 to 0.012 *mm/yr.*	Low to moderate corrosion rate
0.5 to 1.0 $\mu A/cm^2$	0.012 to 0.023 *mm/yr.*	Moderate to high corrosion rate
> 1.0 $\mu A/cm^2$	> 0.023 *mm/yr.*	High corrosion rate

Table 5.7: Electrical Resistivity Test Interpretation (Broomfield, 1997)

Concrete Resistivity	Corrosion Condition
> 20 $k\Omega cm$	Low corrosion rate
10-20 $k\Omega cm$	Moderate corrosion rate
5-10 $k\Omega cm$	High corrosion rate
<5 $k\Omega cm$	Very high corrosion rate

Table 5.8: General relationship between permeability and absorption test

Concrete Absorption	Concrete Permeability
< 3 %	Low permeability
3-5 %	Moderate permeability
>5 %	High permeability

Table 5.9: Modified relationship between permeability and absorption tests based on Dickson Bridge data

Concrete Absorption	Concrete Permeability
< 2 %	Low permeability
2-2.5 %	Moderate permeability
2.5-4	High permeability
>4 %	Very high permeability

Table 5.10: Descriptive Statistics of all the Variables

Test	Number of readings	R^2
Concrete Cover (mm)	37	0.003
Half-Cell Potential (mV)	37	0.201
Corrosion Rate (mm/yr)	37	0.092
Electrical Resistivity (ohm.cm)	37	0.720
Chloride Content at Steel Level (%)	37	0.696
Absorption _BS (%)	37	0.308
Absorption_ASTM (%)	37	0.589
Pulse Velocity (km/s)	37	0.098
Compressive Strength (MPa)	37	0.011

Fig. 5.1: Typical bridge deck disintegrated area

Fig. 5.2: Typical extensive corrosion in the reinforcing bar.

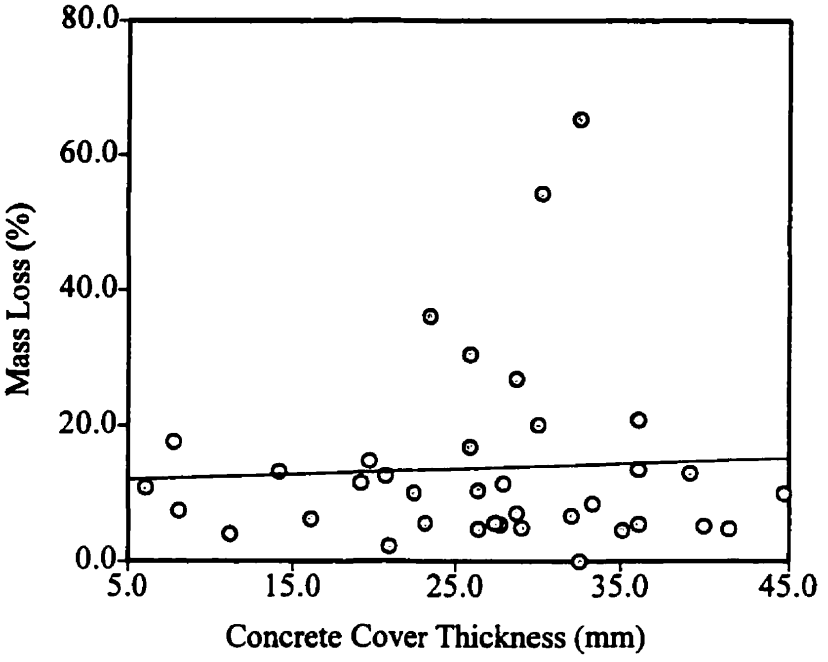

Fig. 5.3: Variation of mass loss with concrete cover thickness for the four sites

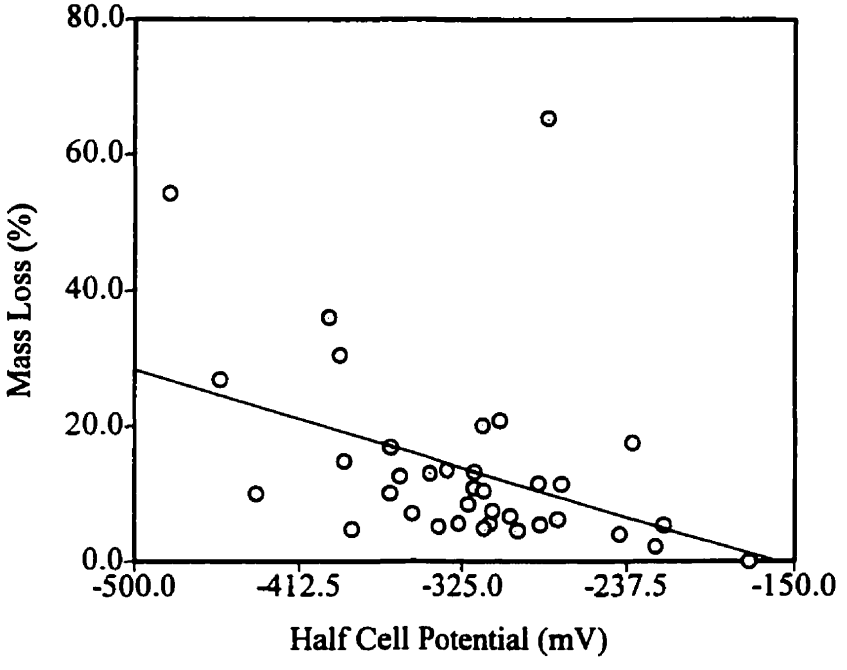

Fig. 5.5: Variation of mass loss with half cell potential readings for the four sites

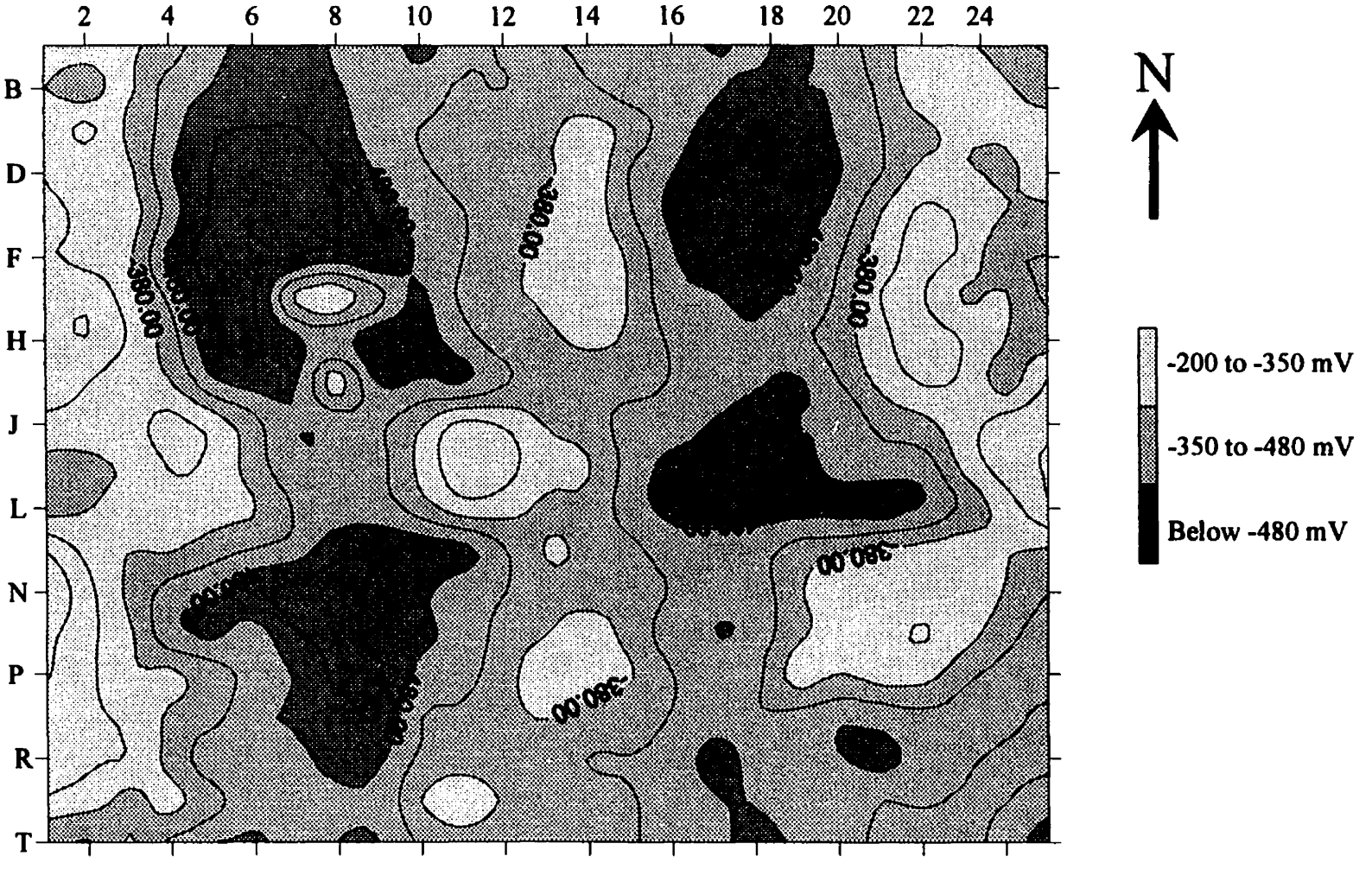

Fig. 5.4: Half-cell potential readings for Site M2

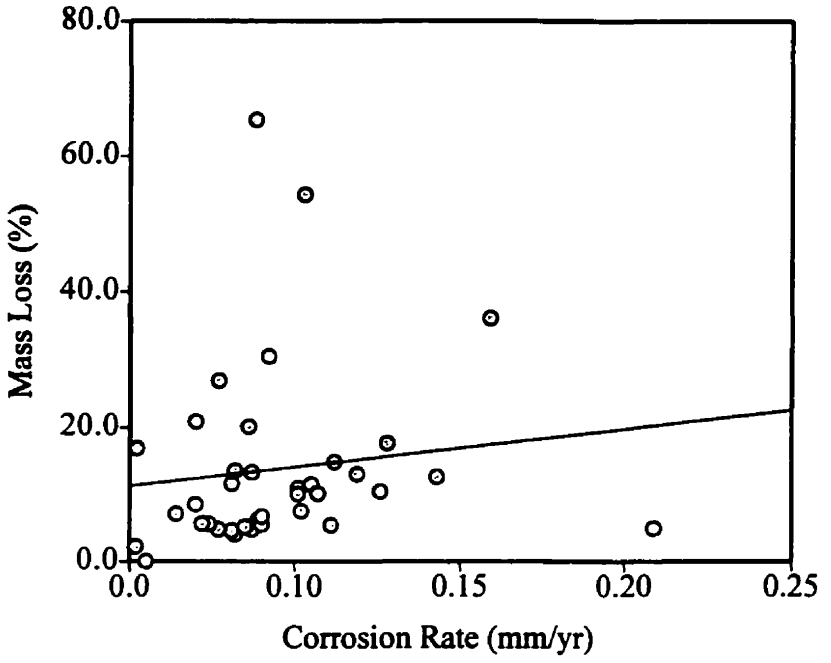

Fig. 5.6: Variation of mass loss with linear polarization resistance results for the four sites

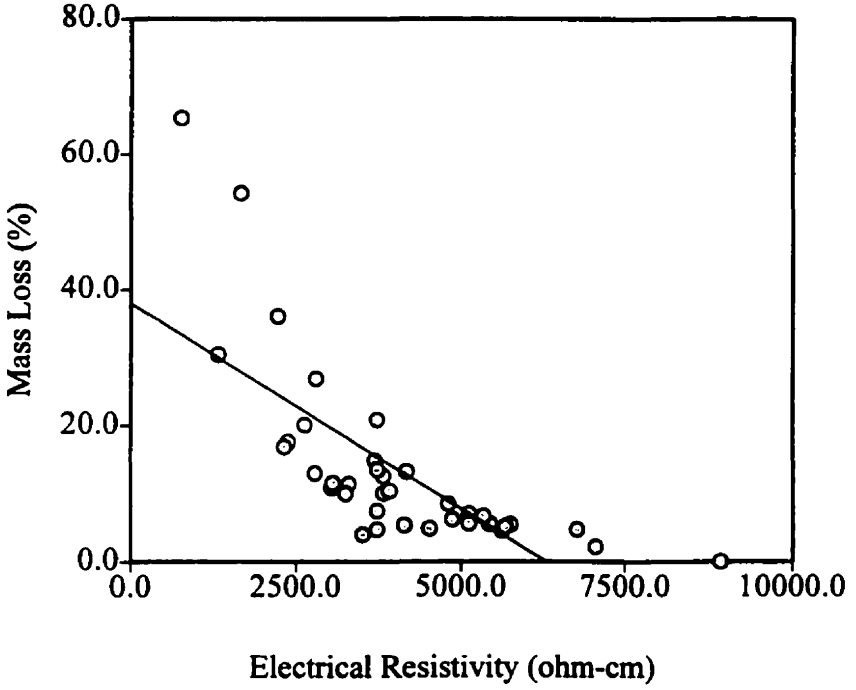

Fig. 5.7: Variation of mass loss with concrete electrical resistivity for the four sites

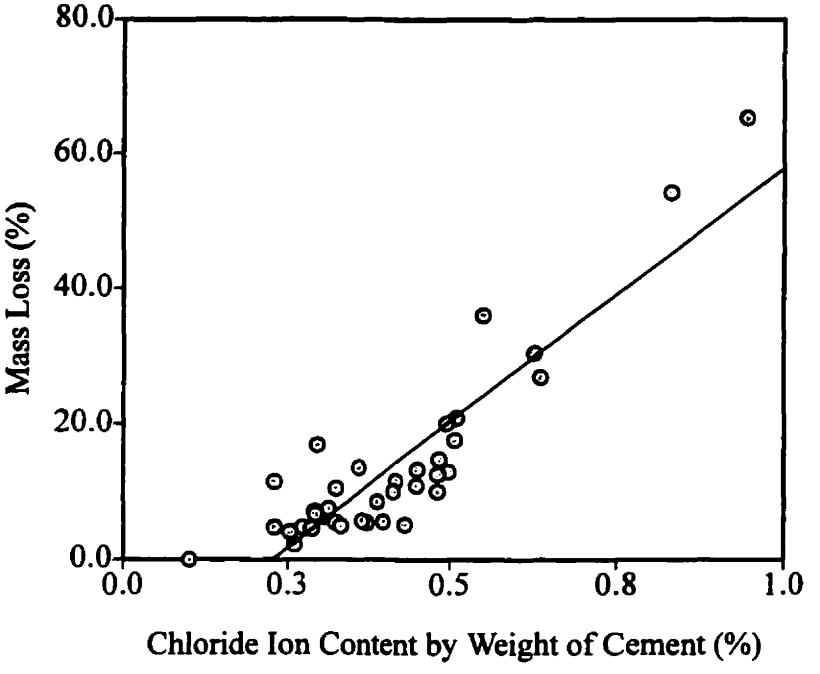

Fig. 5.8: Variation of mass loss with concrete chloride content for the four sites

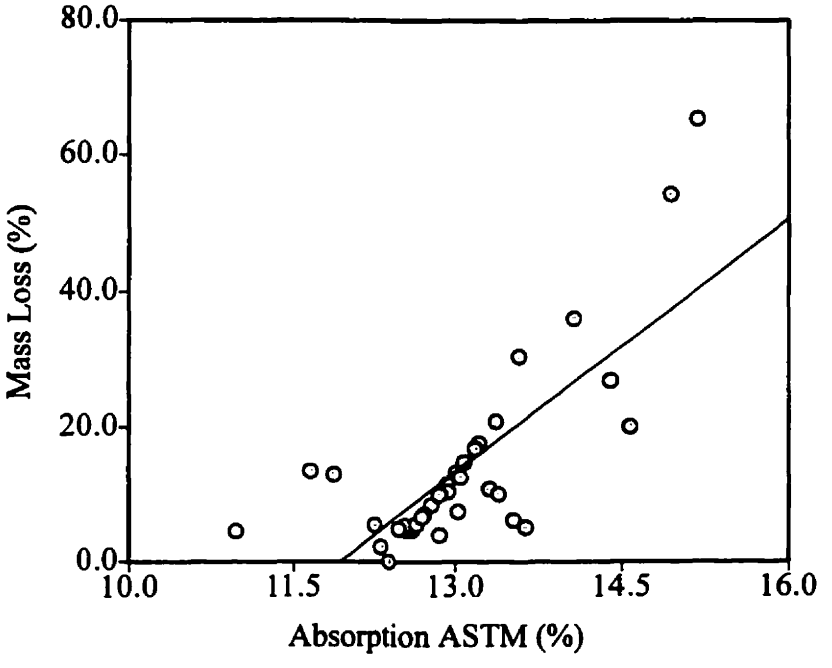

Fig. 5.10: Variation of mass loss with concrete absorption for the four sites

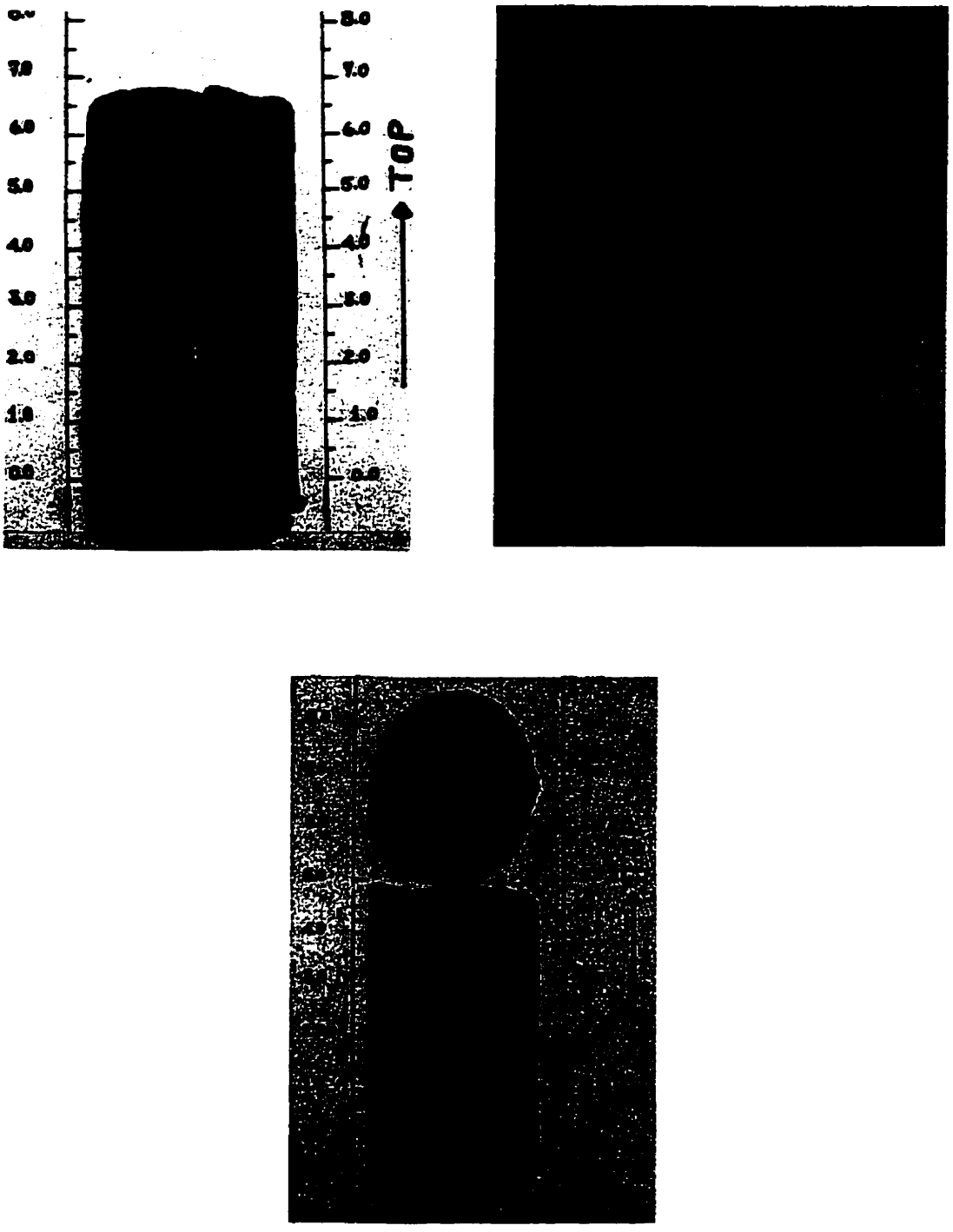

Figure 5.9: Extent of delamination and corrosion found in typical cores

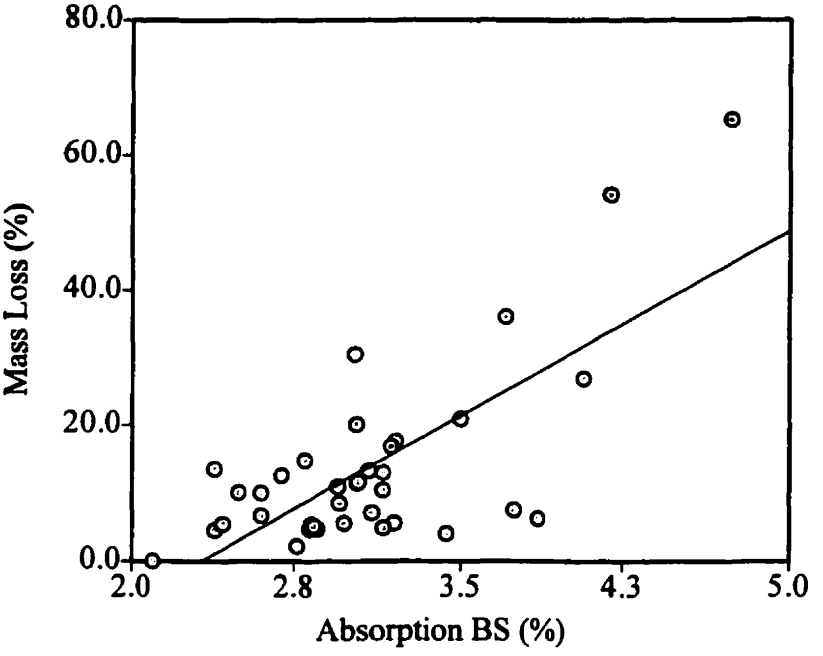

Fig. 5.11: Variation of mass loss with 30 minute water absorption (British Standard) for the four sites

Figure 5.12: Typical carbonation tests on collected cores

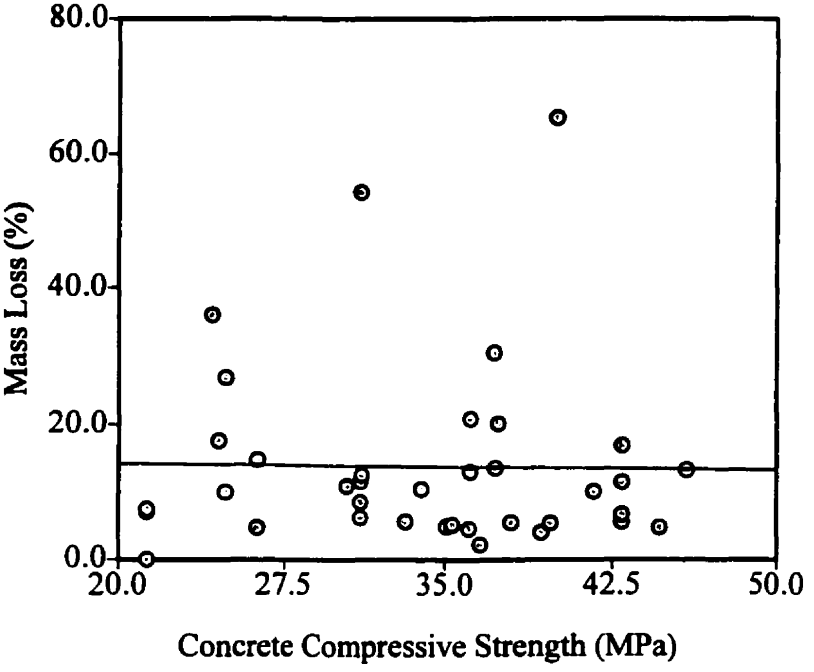

Fig. 5.13: Variation of mass loss with concrete compressive strength for the four sites

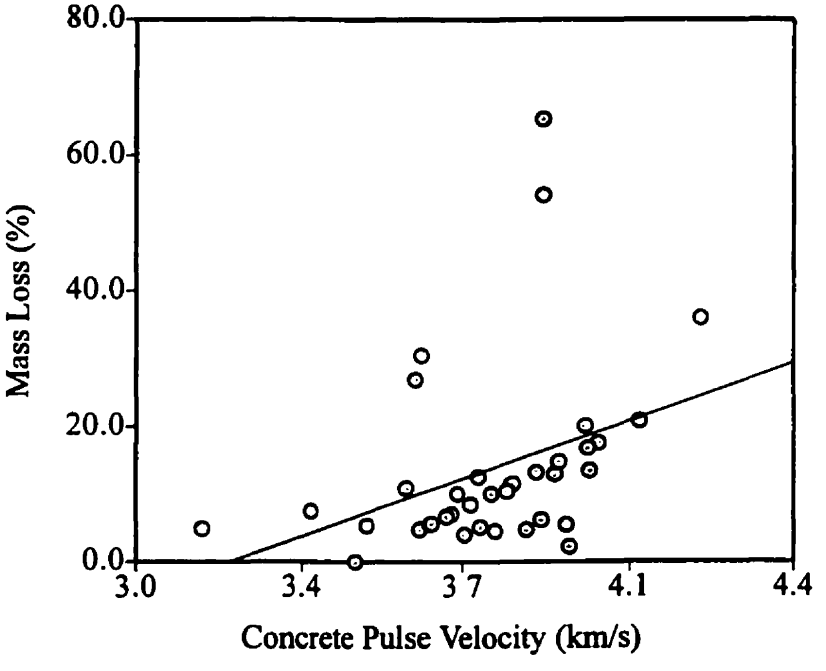

Fig. 5.14: Variation of mass loss with concrete pulse velocity for the four sites

Chapter 6

Laboratory Studies: Pullout and Tension Test

This chapter describes the test program to simulate the prevalent conditions of severe local corrosion environments, which cause significant changes in the surface conditions of the bar and the ribs. The criteria to establish the different levels of corrosion for different bar diameters, the method adopted to evaluate the corrosion rate and the determination of the chloride-ion concentration along the concrete cover depth are summarized.

In addition, this chapter describes the main experimental program, which was designed to investigate the influence of corrosion on the bond behaviour at the reinforcing steel-concrete interface. Pullout and tension specimens, reinforced with a single bar, were subjected to eight different stages of corrosion, and then subjected to axial tensile forces to determine the deterioration of bond between the concrete and the reinforcing steel bar.

6.1 Design Philosophy

The availability of new additive materials provides great incentive to examine their effect on concrete durability. In the current investigation, two series of tests were carried out.

Series I: Pullout specimens for the investigation of the following parameters:

1. Concrete composition
2. Compressive strength
3. Water/cement ratio
4. Concrete cover thickness

Six different mixtures of concrete were studied in the pullout testing program, with four different concrete cover thicknesses (25, 50, 75 and 100 mm) over the steel reinforcing bar. While 50 and 75 mm cover thicknesses are normally recommended in steel reinforced concrete structures that are exposed to severe environments, 25mm cover is being used here to provide an additional insight into the corrosion process. In addition, three different mixtures of concrete are studied for the tension testing program, using only one concrete cover size of 50 mm for all of the specimens.

Series II: Tension specimens for the investigation of the effect of the concrete mixture:

1. Concrete composition
2. Compressive strength
3. Water/cement ratio

In order to limit the extent of the investigation, some variables were kept constant, such as the steel strength, bar diameter, and the embedment length. The following arrangements were adopted for the pullout specimens:

1. Bar diameter = 19.5mm (No. 20 bar)
2. Embedded length = 280mm
3. Length of specimen = 305mm

The following arrangements were adopted for the tension specimens:

1. Bar diameter = 19.5mm (No. 20 bar)
2. Length of specimen = 1000mm
3. Concrete cover thickness = 50mm

The following parameters were varied in this investigation:

1. Concrete cover thickness (pullout specimens)
2. Type of concrete (pullout and tension specimens)
3. Corrosion rate (pullout and tension specimens)

The total number of specimens in series I was therefore: 6 (types of concrete) x 4 (concrete covers) x 4 (corrosion stages) x 2 (specimens per corrosion stage) = 192 specimens.

The total number of specimens in series II was therefore: 3 (types of concrete) x 5 (corrosion stages) x 2 (specimens per corrosion stage) = 30 specimens.

The specimen nomenclature was derived as follows:

1. The first letter and the second numeral indicate the type of concrete mixture used in the specimen as follows

Mixture Number	Concrete Type
C1	Point Tupper (fly ash w/scm = 0.32)
C2	Thunder Bay (fly ash w/scm = 0.32)
C3	Sundance (fly ash w/scm = 0.32)
C4	Normal portland cement (w/c = 0.32)
C5	Normal portland cement (w/c = 0.42)
C6	High aluminum cement (w/c = 0.37)

Mixture Number	Concrete Type
C4	Sundance (fly ash w/scm = 0.32)
C3	Normal portland cement (w/c = 0.32)
C7	Normal portland cement (w/c = 0.52)
	Dickson Bridge concrete mix

2. The third number indicates the number of the specimen.

3. The fourth letter indicates the size of the specimen in terms of concrete cover:

   A = 100 mm

   B = 75 mm

   C = 50 mm

   D = 25 mm

For example, Specimen C1-1A is a specimen cast from concrete mixture No.1 which has the Point Tupper fly ash as the supplementary cementing material, 1A is the first specimen with a 100 mm cover thickness.

6.2 Properties of Materials

6.2.1 Reinforcing Steel

The 20M size reinforcing steel bars used in the tests were obtained locally, and they conformed to the Canadian Standard Association (CSA) Standard G30.14-M83 (1983) which is equivalent to ASTM Standard A615-72 (1972). To determine the mechanical properties of the reinforcing steel, tension tests were performed on six randomly obtained deformed 20M steel bars, with a nominal diameter of 19.5 mm, and 195 mm in length, with a specified normal yield strength of 400 MPa. All of the coupons exhibited a yield plateau, with an average experimental yield strength of 432 MPa. Figure 6.1 shows the tensile stress-strain relationship obtained. The strains were measured over a 50mm gauge length with an extensometer. Table 6.1 reports the various mechanical properties of the bars.

6.2.2 Concrete Mix Parameters

6.2.2.1 Series I: Pullout Specimens

The concrete mixtures were provided by CANMET for this investigation. Six different mixtures of concretes were studied in this program using pullout specimens,

three concrete mixtures, incorporating different fly ashes to the extent of 58% of the mass of the total cementitious materials, with a water-to-cementitious materials ratio [(W/C+FA) or (w/cm)] of 0.32. Two control portland cement concrete mixtures were made for comparison, including one with the same w/c ratio of 0.32. High alumina cement concrete mixture was also used with a w/c ratio of 0.37.

The CSA Type 10 or the ASTM Type I normal portland cement was used, and its physical properties and chemical composition are summarized in Table 6.2.

The fly ash samples tested were obtained from the various regions of Canada. Fly ashes from Point Tupper (Nova Scotia), the CSA or the ASTM Class F ash, contained 2.8% CaO and had a specific surface of 236 m^2/kg (Blaine). Thunder Bay (Northern Ontario) fly ash, which met the general requirements of the CSA or the ASTM Class C ash, had a CaO content of 15.8% and alkali content (Na_2O equivalent) of 7.27%. The specific surface of the ash was 240 m^2/kg (Blaine). Sundance fly ash (Alberta) had a CaO content of 12.5%, but its combined (SiO_2 +Al_2O3 + Fe_2O_3) content was higher than 70%, thus meeting the requirement of the CSA or the ASTM Class F fly ash, and it had a relatively high specific surface of 408 m^2/kg (Blaine). The physical properties and chemical composition are given in Table 6.2.

The fine aggregate was natural sand from the Ottawa region, and the coarse aggregate used was crushed limestone with a maximum nominal size of 19mm. The physical properties of the aggregates are summarized in Table 6.3, while the grading of the aggregates is presented in Table 6.4.

A sulphate, naphthalene formaldehyde condensate type superplasticizer with negligible chloride content, which is a dark brown solution containing 42% solids, was used for all of the concrete mixtures. A synthetic type air-entraining admixture was used in all of the concrete mixtures.

The six concrete mixture proportions that were prepared at CANMET for this investigation are summarized in Table 6.5. The properties of the fresh concrete including the slump, air content and unit weight were determined, also by CANMET, (Table 6.6), immediately after the mixing according to relevant CSA and ASTM Standards, and are given in Table 6.6. The compressive strength of the hardened concretes at different concrete ages of one, seven, 28, 91 and 365 days are presented in Table 6.7.

6.2.2.2 Series II: Tension Specimens

Three different mixtures of concrete were studied in this program using the tension specimens, one concrete mixture incorporated 58% of Sundance fly ash by mass of the total cementitious materials with a water-to-cementitious materials ratio (w/cm) of 0.32. One portland cement concrete mixture was made for comparison purposes, with the same w/c ratio of 0.32. The concrete mixture used for the Dickson bridge using normal portland cement with a w/c ratio of 0.52 was also used. The details of the concrete mixes and proportions used in the various samples are presented in Table 6.3. Again, Tables 6.4 and 6.5 present the grading and the physical properties of the aggregates. Table 6.2 shows the properties of the fresh concrete, while Table 6.7 presents the compressive strength of the hardened concrete obtained from the compression tests on standard cylinders, with a height of 300 mm and a diameter of 150 mm.

6.3 Specimens Preparation

6.3.1 Pullout Specimens

The pullout specimens consisted of a pre-weighed single No. 20 bar embedded in a 300 mm long, cylindrical concrete specimen, with the bar protruding at one end only. As mentioned earlier, four different specimen diameters, giving cover thicknesses of

25 mm, 50 mm, 75 mm and 100 mm, were used. Figure 6.2 shows the geometry of a typical pullout specimen.

The concrete was mixed in a laboratory counter-current mixer for 6 minutes. The properties of the fresh concrete including the slump, air content, and unit weight were determined immediately after the mixing according to relevant CSA and ASTM Standards, and are presented in Table 6.5. The concrete specimens were cast in specially designed metal moulds which had one socket affixed to the mould top to allow the steel bar to pass. The reinforcing bar extended about 300mm outside the upper-face of the concrete. All of the test specimens were compacted on a vibrating table. After casting, the specimens were covered and left in the casting room for 24 hours. The specimens were then demoulded and cured in a standard moist curing room at 23±2° C and 100% relative humidity until they were ready to be shipped to Montreal for accelerated corrosion to different stages, followed by pullout tests.

To protect the interface between the protruding steel bar and the surface of the concrete specimen from corrosion, 50 mm of the extension part of the bars along with another length of 25mm within the specimen end, was epoxy-coated and taped with an electrical tape. In addition, the bottom of the specimens plus another 25mm was painted with several coats of concrete epoxy coating. The epoxy coatings were monitored carefully for damage, and if any damage was noted, the specimen was removed and the rebar was cleaned and epoxy coated again.

For each of the mixtures, fifteen 100 x 200mm auxiliary specimens were cast for determining the compressive strength according to the CSA or the ASTM Standard C39 for 1, 7, 28, and 365 days.

6.3.2 Tension Specimens

Thirty concrete cylindrical specimens, 1000 mm long by 125 mm diameter, each reinforced with a pre-weighed single 20M reinforcing deformed bar and with a

concrete cover of approximately 52mm, were cast. Figure 6.3 shows the geometry and instrumentation for a typical tension specimen.

The concrete specimens were cast in specially designed plastic molds, which had two sockets affixed at the top and bottom of the mold to allow the steel bars to pass. The reinforcing bar extended 150 mm outside the ends of the concrete. Just outside the concrete, an electrical wire (about 1 m in length) was connected to the steel bar by means of clips on each of the 24 specimens. The remaining two specimens for each mixture were used as control specimens (uncorroded conditions).

The extensions of the bars plus another length of 20mm within the specimen ends, were epoxy-coated and then covered with two layers of tape, first with an electrical tape followed by a duct tape, in an attempt to protect this part of the steel from corrosion. A silicon layer was added on top of the electrical wire and the clip for the same reason. Each specimen was marked with a number and a grid, 100 mm x 100 mm, drawn on the specimen surface before immersion in the tanks for accelerated corrosion, for measurement purposes as shown in Fig. 6.3.

The reinforcing bars of two tension specimens of each concrete mixture were instrumented with five strain gauges along the length of each bar. Strain gauges with a small gauge length of 6mm were glued to the surface of the reinforcing bars to minimize the reduction of bond surface area due to the presence of the gauge, which was less than 1% reduction in bar surface area.

The tension specimens along with the accompanying auxiliary specimens (cylinders) were moist-cured in the plastic molds for 48 hours, after which they were removed from the mold and cured for 91 days before positioning them in the immersion tank. Biczok (1972) suggested that the concrete exposed at an early age has less resistance to chemical attack than the concrete hardened over an extended period. Therefore, the concrete specimens and cylinders were cured for 91 days before exposing them to the accelerated corrosion process. This period

accommodated both the cement hydration reactions, and the pozzolanic reactions with the fly ash which started at a later stage.

6.4 Accelerated Corrosion

The various service and field corrosion tests normally require long exposure durations. Therefore, for design of structural components for durability against corrosion, and selection of suitable materials and appropriate protective systems, it is useful to use accelerated corrosion tests to obtain qualitative information on their corrosion behaviour in a relative shorter period of a few months. This data are especially useful in situations where the member or the system service life is endangered by the severe corrosive environment. Several electrochemical test procedures have been developed, including some, which have been standardized, and are available in the literature. Some of these methods such as the anodic polarization tests utilize closed circuit testing, while others rely on the chemical exposure in an open circuit. Accelerated corrosion tests have been used successfully to determine the susceptibility of the reinforcing and other forms of structural steel to localized attacks such as pitting corrosion, stress corrosion and other forms of corrosion. These tests provide qualitative data, which provides the designer with relative material performance indicators for the various localized forms of corrosion.

It is important that the accelerated testing conditions do not differ significantly from the service environment except for the time scale, otherwise the corrosion products from the accelerated tests could differ considerably from the products developed during the normal corrosion activity. Also, the accelerated testing could lead to misleading results [Biczok, (1972)]. Suitable increases in temperature, applied voltage or current and an increased concentration of the corrosive agent can achieve acceleration of corrosion activity in these tests.

6.4.1 Accelerated Corrosion Experimental Set-Up

A corrosion cell was designed, similar to that in a flashlight battery, to simulate the corrosion conditions in the system under the "normal" environmental conditions. As mentioned earlier, corrosion of the reinforcing steel embedded in the concrete occurs by the electrochemical process with the formation of an anode where electrochemical oxidation takes place, and a cathode where electrochemical reduction occurs, and an electrolyte capable of conducting the ionic current.

Once the 192 pullout specimens were cast and cured, 144 specimens were subjected to accelerated corrosion by placing them in the accelerated corrosion tanks, while the rest of the 48 specimens (2 specimens per concrete cover per concrete mixture) served as the control specimens (uncorroded stage). For Series II, 24 specimens were placed in the corrosion tanks and 6 specimens served as the control (2 specimens per concrete mixture). Figures 6.4 and 6.5 illustrate the schematic drawing of the set-up for both the pullout and tension specimens, respectively. The tanks were filled with an electrolytic solution [5% sodium chloride (NaCl) by the weight of water]. As seen in Fig. 6.4, the pullout specimens were partially immersed while for the tension specimens, the tank was filled to cover the top of the specimens by approximately 50 mm. The electrolyte solution was changed on a weekly basis to eliminate any change in the concentration of the NaCl and pH of the solution.

A copper electrical wire was soldered and connected by stainless steel anchors to the reinforcing bar of each specimen. These wires were permitted to protrude from the specimen surface and were used to make electrical connections to the circuit of the corrosion cell. The specimens were placed in the tank at a clear distance of 50 mm apart from each other by means of wooden spacers. The wires were then connected to a power supply with an in-built voltmeter within the electrical circuit required to impress the necessary voltage. To close the circuit, a steel bar is connected to a steel mesh was placed at the tank bottom.

The electrodes and the specimens were placed under water and the direction of the current was arranged so that the reinforcing bar served as the anode while the free steel bar served as the cathode. For connection, a jumper for each specimen wire was used to facilitate the connection and the measurements. The jumper was connected to the positive terminal of a direct current power supply and it was used as a switch, to open or close the electrical circuit. The negative terminal was connected to the bare bar electrode by a different electrical wire; the schematic drawing of the arrangement is also shown in Figures 6.4 and 6.5. A constant voltage of 5 V was applied as in the previous research programs to stimulate accelerated rebar corrosion, (Amleh 1996).

6.5 Measurements

6.5.1 Current

The current measurements for each specimen were recorded periodically (every 48 hours) by means of a SMART Digital Multimeter that read both the current and the voltage. The current readings were recorded by removing the jumper and then connecting the positive terminal probe of the ammeter to the specimen (anode), while the negative terminal probe was connected to the bare steel bar (cathode). When the readings stabilized after approximately 5 to 10 minutes, the current readings were recorded.

6.5.2 Half-Cell Potentials

Two sets of half-cell potential measurements were taken for each specimen periodically, one set every 48 hours and the other set on a monthly basis by using ASTM Standard C 876-80 method, as described earlier. The 48 hour half-cell measurements were taken after setting the power supply off for one hour. While the monthly readings were taken after the specimens were taken out from the corrosion tank and left to dry for five days.

6.5.3 Corrosion Rate (Linear Polarization)

The corrosion rate measurements were taken for each specimen on a monthly basis for the pullout specimens by using ASTM Standard G1-90 method, as described earlier. Again, the corrosion rate measurements were performed after taking the specimens out from the corrosion tank and allowing them to dry for five days. Figure 6.6 demonstrates the measurement set-up. The simplified schematic diagram in Figure 6.7 illustrates the typical circuitry.

For the tension specimens, the corrosion rate was measured after the specimens reached the specified corrosion stage. The corrosion rates were measured at three locations for each specimen.

6.5.4 Testing for Chlorides

The chloride content of concrete is critical to the life of the reinforcement, because small amounts of chloride can disrupt the passive layer that protects the steel from corrosion. Therefore, to assess the condition of the deteriorating concrete, it is essential to determine the chloride content in the concrete.

A chloride ion selective probe was used to determine the chloride ion profile for each specimen according to the ASTM Standard C 1152-90 method, as mentioned in Chapter 4.

For pullout and tension specimens, samples were obtained from each specimen at three different locations along the length of the specimens (same location as for the corrosion rate measurements) to determine how the chloride content changed with depth from the surface. The concrete cover of each specimen was sliced into three depths (15, 35, and 52 mm) and then each slice of concrete was pulverized and the concrete powder was collected in a small plastic bag that was

properly sealed and marked. The concrete powder was collected across the diameter of each specimen with due consideration for the cracks as follows:

- Along the crack (to investigate the effect of cracks)
- Away from the crack (to investigate the effect of diffusion)

6.6 Development of the Various Corrosion Levels

The levels of corrosion achieved in the various specimens varied from no corrosion (control specimens) to extensive corrosion. One important aspect of this observation was the organization of experimental data in a longitudinal crack width framework so that the levels of corrosion could be defined for a given specimen under a given set of environmental conditions. While the example cited in this chapter uses the longitudinal cracking as the basis for ascertaining the level of corrosion desired, or achieved, other methods such as the definition of current readings have been and can also be used to define the level of corrosion. It must be noted that this approach can be combined with other methods for defining the various levels of corrosion.

Evaluation of the corrosion attack after exposure of the test piece was undertaken by inspection (it was used for assessing the level of corrosion earlier), measurement of corrosion (pit) depth, or changes in the steel ultimate tensile strength. However, the evaluation was normally carried out by determination of the weight loss after the corrosion products had been removed by cleaning the bar with an acid.

In summary, four criteria were used to determine the various corrosion levels in this study:

1. The current measurements coupled with the width and the propagation of the longitudinal concrete crack(s), which is the result of the formation of expansive corrosion products on the steel bar. The onset of cracking in the concrete cover and the increase of the crack width were very carefully monitored through visual

observations of the specimens and recorded as this formed a reference for selecting precracking and subsequent postcracking levels of corrosion. The crack width was measured with a crack width comparator at 50 mm intervals along each crack length. An average crack width was then obtained for establishing the level of corrosion as:

2. Loss of metal relative to the original reinforcing steel bar weight. The mass loss of the steel reinforcing bar was obtained as the difference between the mass of the corroded bar (after the removal of the loose corrosion products) from its mass before corrosion. For this purpose, the specimens were broken open for the retrieval of the reinforcing bar after the completion of the test. The reinforcing bar, for each specimen was cleaned and scrubbed with a stiff nonmetal brush to ensure that the bar was free from any adhering corrosion products and then cleaned with a chemical according to the ASTM Standard G1-90 method. The chemical cleaning solution was made of 500 ml hydrochloric acid, HCl, with a specific gravity of 1.19, 3.5 g of hexamethylene tetramine and 500 ml of reagent water. The corrosion products were removed after 5 to 6 cleaning cycles where the duration of each cycle was 10 minutes. The reinforcing bar was then carefully examined for its general condition as a result of the corrosion effects in terms of pitting, ribs degradation, and then weighed for the determination of the weight loss. The percentage weight loss was determined as follows:

$$percentage\ weight\ loss = \frac{[(uncorroded\ weight) - (corroded\ weight)]}{[uncorroded\ weight]} x\,100 \qquad \textbf{(6.2)}$$

3. The loss of the cross-sectional area relative to the original cross sectional area of the reinforcing bar is obtained from the results of the mass loss due to corrosion for each specimen, as was described in Chapter 3.
4. Another approach was used to determine the loss of the cross-sectional area around the "pit". This loss of cross sectional area relative to the original cross sectional area of the reinforcing bar is obtained from the results of the load-deflection response for each specimen. Based on the assumption that the yield

strength of steel does not change with the corrosion of the reinforcing steel bar, and from the load-deformation response curves, the yield load for each specimen is compared with the yield load of the control specimen, to determine an equivalent cross-sectional area using the equation:

$$T_{(uc)s} / A_{(uc)s} = T_{(c)s} / A_{(c)ys} \qquad (6.3)$$

where
$T_{(uc)s}$ = yield load of the uncracked control specimen.
$A_{(uc)s}$ = area of the steel bar in the uncorroded specimen
$T_{(c)s}$ = yield load of the corroded specimen
$A_{(c)ys}$ = equivalent area of the bar after corrosion

where the subscript *'uc'* relates to the uncorroded specimen, the subscript *'c'* stands for the corroded specimen, and *'y'* stands for the yield load.

The results obtained for the four criteria were used on a comparative basis to ensure selection of an appropriate corrosion level.

6.7 Mechanical Experimental Procedure

This investigation was carried out for eight different stages of corrosion including two specimens of each concrete mixture constituting the uncorroded stage. In each stage, the bond behaviour was studied through an examination of both the longitudinal splitting cracks and the transverse cracks. The corrosion stages were chosen according to the width of the longitudinal splitting cracks.

6.7.1 Pullout Test Program

After establishing that a given lollipop specimen had reached the specified level of corrosion, the specimen was removed from the accelerated corrosion facility and supported on an appropriate base plate in the universal testing machine for the standard pullout test.

The pullout tests were performed in the Materials Laboratory at McGill University. The Material Testing System (MTS) Sintech 30/G Workstation electronic-controlled machine, with a capacity of 150 kN in tension with a built-in linear voltage differential transducers (LVDT) for deformation measurements, connected to a PC workstation, was used to test the pullout specimens. The data were stored automatically in the PC, analyzed and the relevant information was easily accessible.

A tensile force was applied to the protruding bar end and increased monotonically in about 20 load increments until failure by either yielding of the bar, or its pullout. The displacement of the bar was measured using an LVDT to plot the load-slip curves for the specimens prepared from each of the six concrete mixtures and concrete cover thickness, and subjected to eight different levels of corrosion. Figure 6.8 portrays the overall test set-up

6.7.2 Tension Test Program

The tension tests were performed in the Structures Laboratory at McGill University. The Material Test System (MTS) hydraulic servo-controlled machine, with a capacity of 1000 kN in tension with a built-in linear voltage differential transducers (LVDT) for deformation measurements, connected to a PC workstation, was used to test the tension specimens. The data were stored automatically in the PC, analyzed and the relevant information was easily accessible.

The test specimens were installed and centred to subject the specimens to pure tension. Figure 6.9 portrays the overall test setup. The test set-up of the MTS machine consisted of a loading frame that transmitted the load through the tension grips at both ends of the reinforcing bar.

6.7.2.1 Testing Procedure and Loading Sequence

The specimens were subjected to an incremental axial loading, using displacement control. An automatic data acquisition system determined the axial force (N) and the strains at every deformation stage. The MTS machine is able to register the measurements with different options. The data were acquired from displacement, time, load, and one strain channel. To obtain a complete and precise response, loads, deflections and strains were recorded every 5 seconds during the loading phase controlled by deformation using the computerized data acquisition system. In order to accurately determine the strains, an external MTS extensometer, that read the strains in the steel bar, was mounted along the side of the specimen, by clamping the extensometer to the reinforcing steel bar just on the outside of the concrete as shown in Fig. 6.9. The elongations were measured over a gage length of 1010 mm.

The specimen was subjected to a predetermined deformation using displacement control, however, the load would drop over a short holding period required to examine the specimen thoroughly and to take photographs for the different key load stages during testing and to record the crack development. Cracks were traced over the concrete surfaces as soon as they became visible, and the corresponding load levels, at which the cracks initiated were marked on the surface beside each crack. A hand microscope (10X) was used to follow the crack propagation, when it was needed. At each cracking stage, the crack widths were measured using a crack width comparator. The maximum loads applied exceeded the yield strength of the reinforcing bars.

The data acquired during the test were stored in the PC and were used to provide information about all of the relevant characteristics of the tests, for example, the load-deformation (or elongation) curves.

Table 6.1: Properties of reinforcing steel

Bar Size	Area (mm^2)	f_y *(MPa)*	ε_y (mm/mm)	f_{su} *(MPa)*	*Es (MPa)*
20M	300	433.0	0.0028	676.4	200000

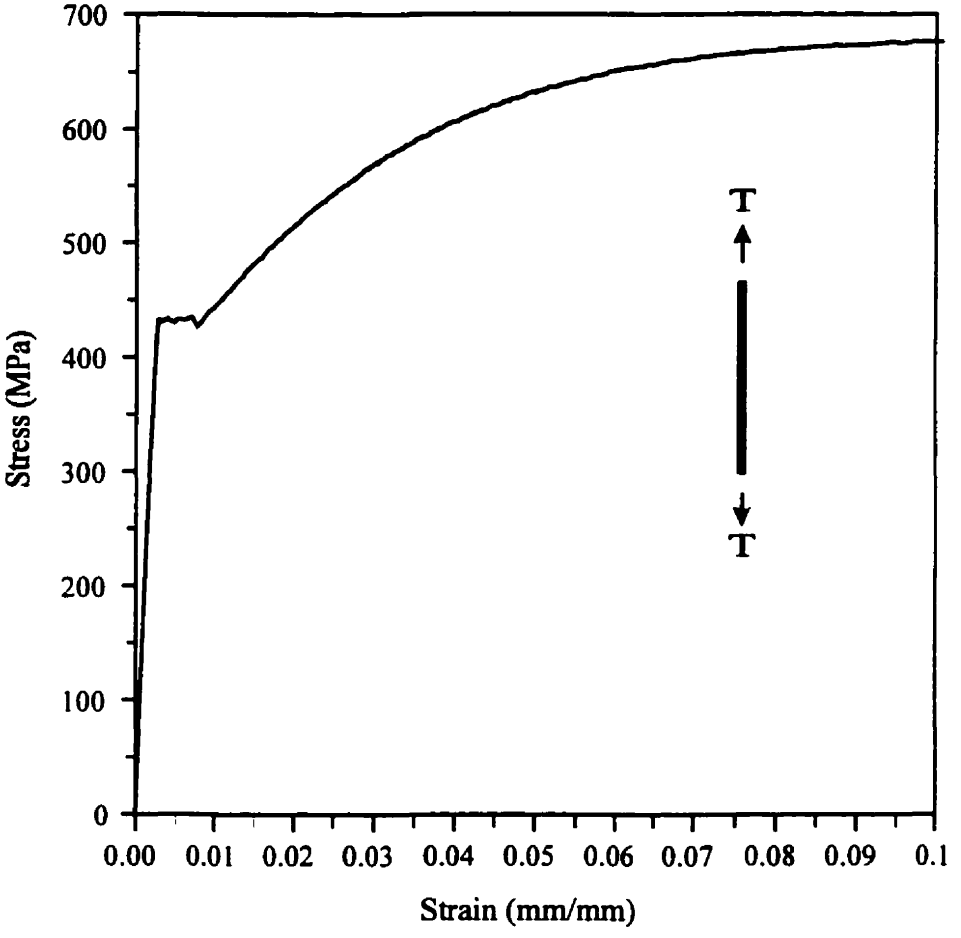

Figure 6.1: Stress-strain relationship for steel reinforcement

Table 6.2- Physical properties and chemical composition of the cements and fly ashes used

	ASTM Type I Cement	Fly Ash			High Alumina Cement
		Point Tupper	Thunder Bay	Sundance	
Physical Tests					Not
Specific gravity	3.13	2.67	2.43	2	available
Fineness				90.9	
-passing 45 mm sieve, %	93.1	90.2	89.7	408	
-specific surface, Blaine, m^2/kg	400	236	240	10.5	
-median particle size, mm	-	11.1	13.2		
Compressive strength of 50 mm cubes,					
MPa	34.8	-	-	-	
- 7 days	41.2	-	-	-	
- 28 days	-	95	93	93.8	
Water requirement, %					
Pozzolanic Activity Index, %	-	75.2	85.1	80	
- 7 days	-	92.8	104.3	106.9	
- 28 days					
Chemical Composition, %					
Silicon dioxide (SiO_2)	21.36	40.71	41.99	53.3	6.82
Aluminum oxide (Al_2O_3)	3.98	17.93	21.44	23.63	38.26
Ferric oxide (Fe_2O_3)	3.15	29.86	4.45	4.4	14.96
Calcium oxide (CaO)	62.41	2.8	15.81	12.45	36.37
Magnesium oxide (MgO)	2.57	1.09	3.18	1.15	0.58
Sodium oxide (Na_2O)	0.2	0.73	7.03	3.03	0.03
Potassium oxide (K_2O)	0.8	1.56	0.36	0.42	0.1
Equivalent alkali ($Na_2O+0.658K_2O$)	0.73	1.76	7.27	3.31	0.1
Phosphorous oxide (P_2O_5)	0.21	0.17	0.58	0.12	0.2
Titanium oxide (TiO_2)	0.19	0.85	1.05	0.71	1.75
Sulphur trioxide (SO_3)	3.43	1.27	1.79	0.2	0.03
Loss on ignition	1.72	1.95	0.75	0.71	1.01
Bogue Potential Compound Composition				-	-
Tricalcium silicate, C_3S	51	-	-	-	-
Dicalcium silicate, C_2S	23	-	-	-	-
Tricalcium aluminate, C_3A	5	-	-	-	-
Tetracalcium aluminoferrite, C_4AF	10	-	-	-	

Table 6.3: Physical properties of the aggregates

	Coarse Aggregate*	Fine Aggregate**
Specific Gravity	2.7	2.7
Water Absorption, %	0.6	0.8

* Limestone
** Natural sand

Table 6.4: Grading of the aggregate

Coarse Aggregate		Fine Aggregate	
Sieve Size (mm)	Cumulative % Retained	Sieve Size (mm)	Cumulative % Retained
19	0	4.75	1.9
12.7	35	2.36	11.5
9.5	60	1.18	25.3
4.75	100	0.6	47.9
		0.3	76.4
		0.15	93.2
		pan	100

Table 6.5: Concrete Type and Mix Propotions

Mix No.	Cement Type	Fly Ash Type	Fly Ash Content (%)	W/C +SCM	Quantities (kg/m³)						A.E.A** mL/m³
					Water*	Cement	Fly Ash	Fine agg.	Coarse agg.	Sp**	
C1	NPC	Point Tupper	58	0.32	118	156	216	743	1115	5.5	422
C2	NPC	Thunder Bay	58	0.32	117	153	213	726	1089	2.5	228
C3	NPC	Sundance	58	0.32	121	157	218	720	1083	6.0	558
C4	NPC	-	0	0.32	119	371	0	750	1127	10.1	401
C5	NPC	-	0	0.42	154	168	0	173	1071	1.3	149
C6	HAC	-	0	0.37	165	451	0	730	1093	0.0	0

NPC- Normal portland cement
HAC- High aluminum cement
* including water in the superplasticizer
**Sp superplasticizer, naphthalene based
***A.E.A air-entraining admixture

Table 6.5a: Concrete Mix Propotions

Mix No.	Cement Type	Fly Ash Type	Fly Ash Content (%)	W/C +SCM	Quantities (kg/m³)						A.E.A** (mL/m³)
					Water*	Cement	Fly Ash	Fine agg.	Coarse agg.	Sp**	
C4	NPC	Sundance	58	0.32	121	157	218	720	1083	6.0	558
C3	NPC	-	0	0.32	119	371	0	750	1127	10.1	401
C7	NPC	-	0	0.52	219	420	0	720	1020	0	300

NPC- Normal portland cement
* including water in the superplasticizer
**Sp superplasticizer, naphthalene based
***A.E.A air-entraining admixture

Table 6.6: Properties of the Fresh Concrete

Mix No.	Cement Type	Fly Ash Type	Fly Ash Content (%)	W/C +SCM	Slump (mm)	Air Content (%)
C1	NPC	Point Tupper	58	0.32	200	6.0
C2	NPC	Thunder Bay	58	0.32	150	7.2
C3	NPC	Sundance	58	0.32	225	5.0
C4	NPC	-	0	0.32	175	6.4
C5	NPC	-	0	0.42	100	6.6
C6	HAC	-	0	0.37	75	1.7

Table 6.7: Compressive Strength of the Hardened Concrete

Mix	Compressive strength (MPa)				
	1-d	7-d	28-d	91-d	365-d
C1	4.9	22.3	39.0	52.2	62.3
C2	7.2	31.5	39.1	44.1	47.1
C3	5.1	28.5	49.8	59.2	66.6
C4	22.2	38.2	46.9	51.0	60.2
C5	16.7	30.4	35.8	41.5	51.0
C6	38.7	47.2	49.2	49.7	50.0

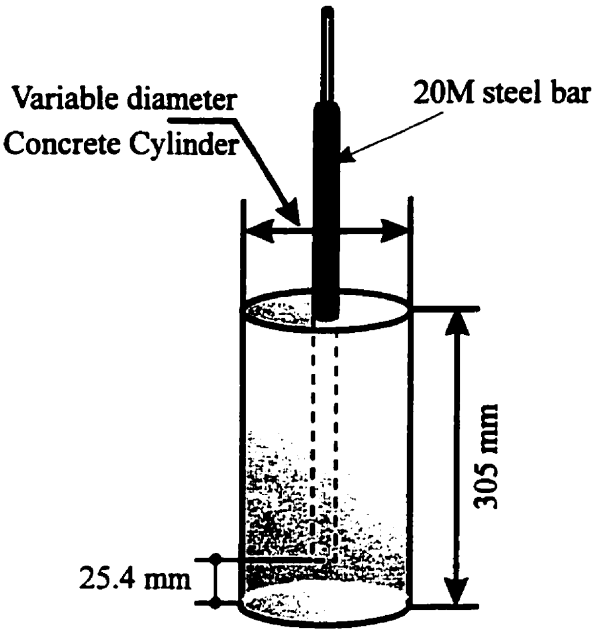

Figure 6.2: Typical pullout specimen geometry

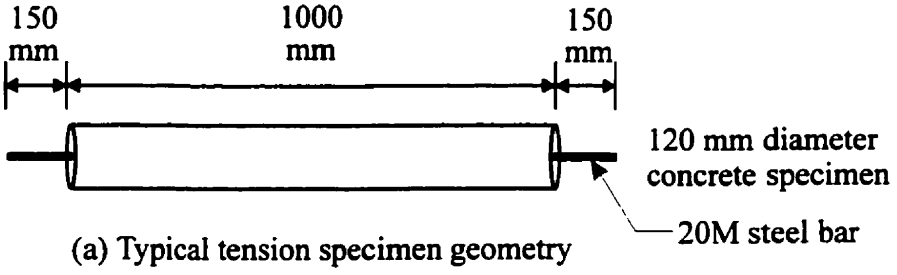

(a) Typical tension specimen geometry

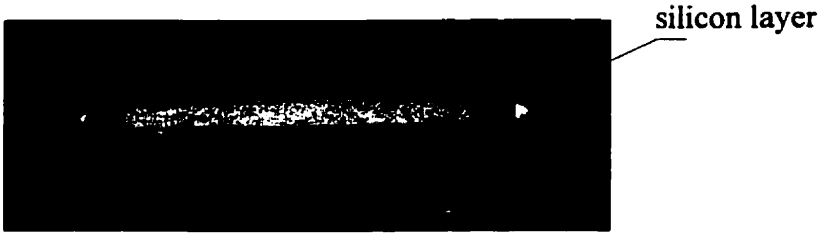

(b):10 mm x 10 mm grid on the cylinder

Figure 6.3: Typical tension specimen

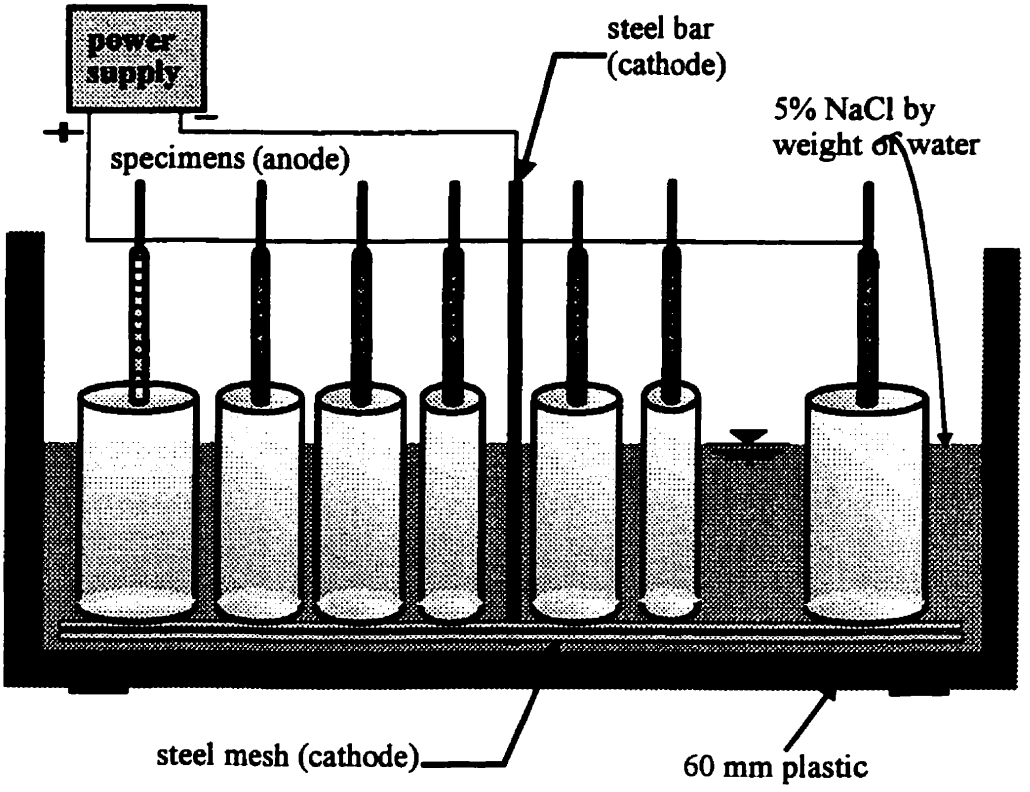

Figure 6.4: Accelerated corrosion set-up for pullout specimens

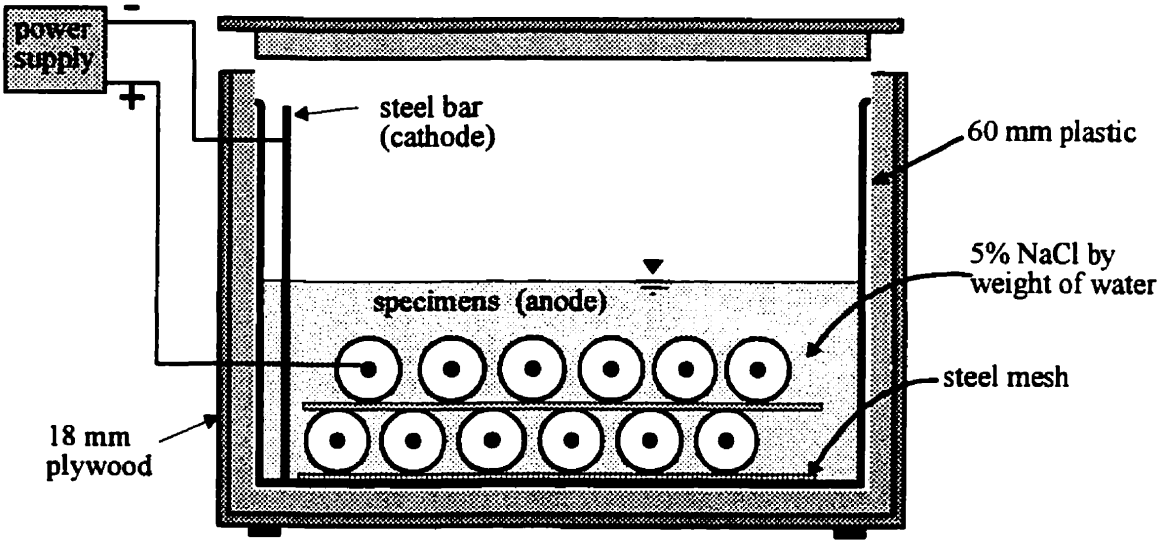

Figure 6.5: Corrosion tank set-up for tension specimens

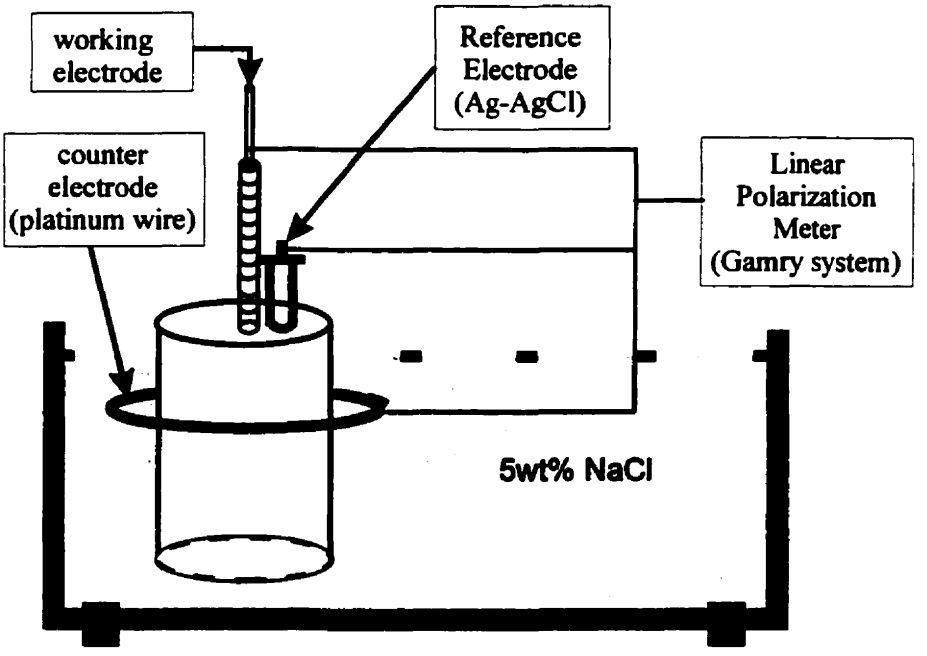

Figure 6.6: Linear polarization set-up

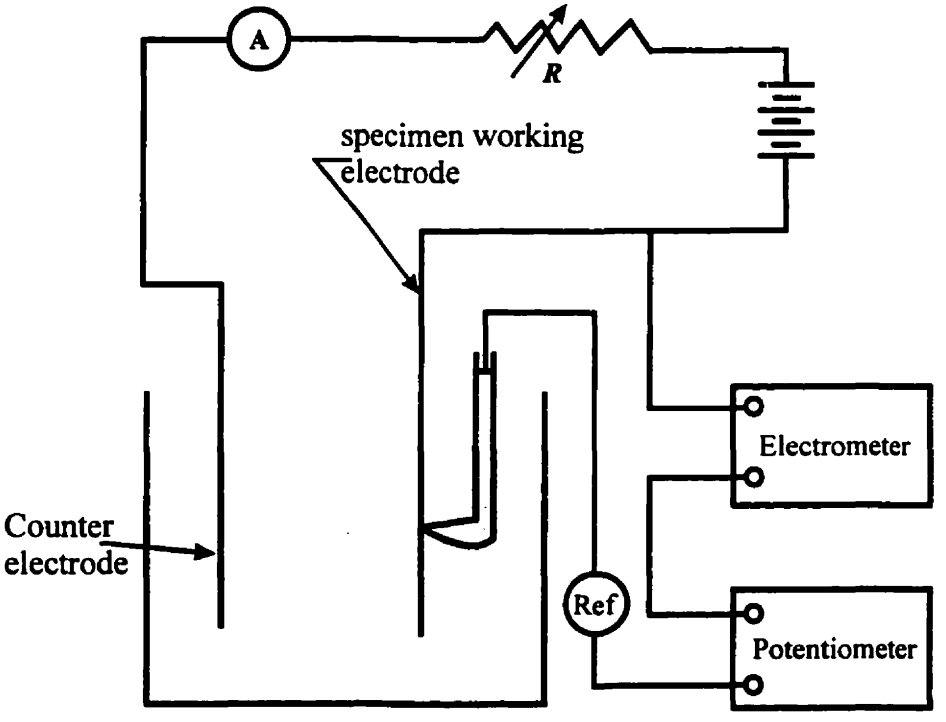

Figure 6.7: Schematic set-up for linear polarization

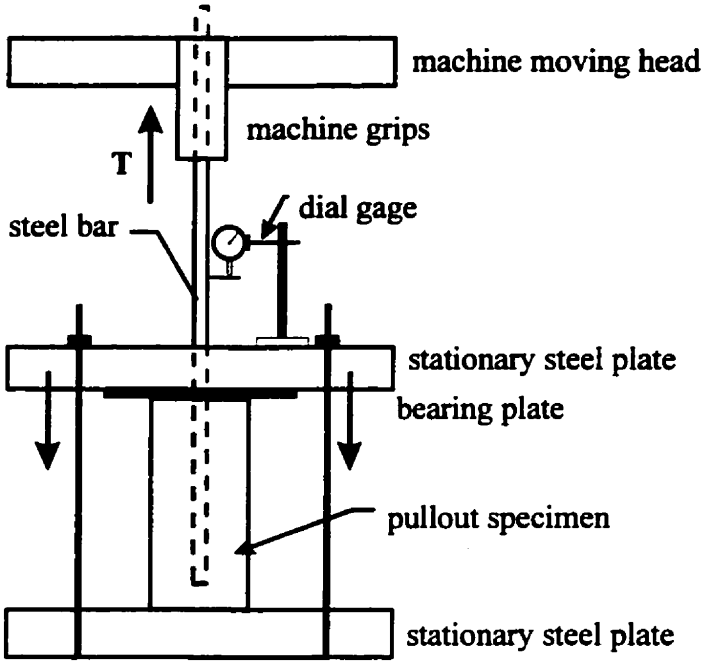

Figure 6.8: Pullout test set-up

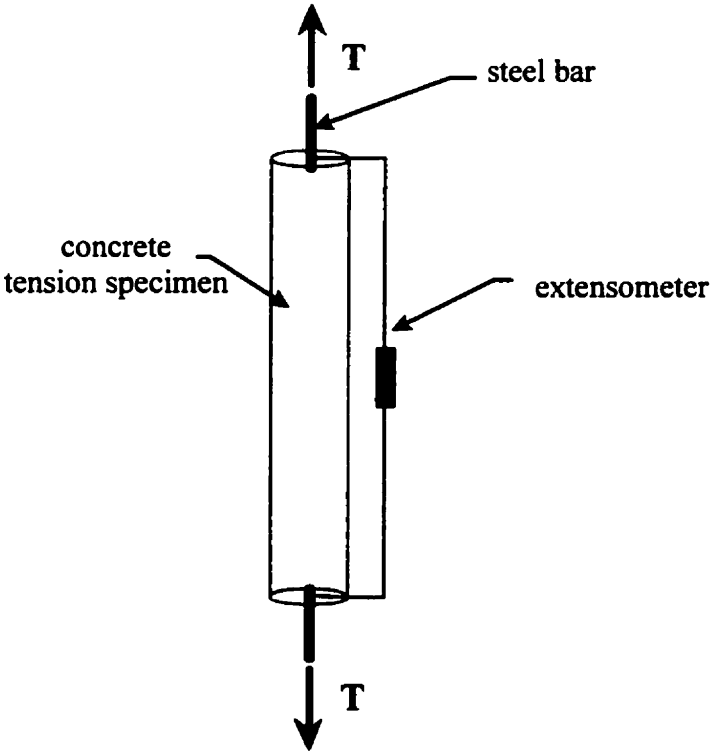

Figure 6.9: Tension test set-up

Chapter 7

Accelerated Corrosion Monitoring Results

The accelerated corrosion experimental program was designed principally to investigate the influence of steel reinforcement corrosion on the bond behaviour between the reinforcing steel and concrete. The accelerated corrosion method was used to achieve the various corrosion levels. The results of the main monitoring techniques are presented and discussed.

Considerable electrochemical testing was undertaken on each of the 192 lollipop and 30 tension specimens. Only some of the experimental results, and the visually observed specimen conditions, including cracking, corrosion of steel bar, etc. are reported here.

7.1 Current Measurements:

The measured current due to the applied voltage is one of the indicators of the corrosion activity occurring in the lollipop and tension specimens.

7.1.1 Effect of Concrete Type and W/C on Current Measurements

The variation of the current with the immersion time, due to an applied voltage of 5 volts, is shown in Figures 7.1 through 7.6. As seen from the data, the current passing

through the specimens starts at a very low level at an early age of one day, basically because the steel was still passive and the concrete resistivity was high. This current increased with an increase in exposure time, and this increase is related to the concrete type, concrete cover thickness and the resistivity of the concrete specimen, which decreases with its gradual deterioration. In addition, the rapid increase in the current values indicates the likelihood of cracking of the concrete cover leading to an increased corrosion rate. The trend of the current-time relationship in most of the cases showed a decrease in the current for some time, followed by a sudden increase. The decrease of current for the first few days is an indication of the formation of the passive film around the reinforcing steel bar, and the sudden increase in the current was observed to coincide generally with the specimen cracking.

As expected, the rate of corrosion of the steel bars in the specimens was very slow at first, until depassivation of the steel occurred when corrosion started, and then the rate of corrosion increased significantly. The initial current densities monitored were of the order of 10^{-4} A/m^2 and these remained unchanged for a long time, until the chlorides penetrated the concrete cover and initiated corrosion at which time the current increased by over three orders of magnitude within a few days.

The results in Fig. 7.1 through 7.6 show the variation of current with the immersion time. It is noted that the immersion in the 5% sodium chloride (NaCl) solution was undertaken only after a few weeks of the casting of the specimens when considerable hydration of the cement in the NPC specimens with water/cement ratios of 0.32 and 0.42 had occurred. Similarly, for the different fly-ash concretes, a considerable portion of hydration of the portland cement and the pozzolanic reactions due to the use of the fly ash had been completed. Comparison of the results in Figures 7.1, 7.2, and 7.3 (for Point Tupper, Thunder Bay and Sundance fly ash concretes, respectively) with those for the normal portland cement (NPC) concretes in Figure 7.4 (water/cement ratio = 0.32) clearly show that excepting for the concrete cover thickness of 25mm, all of the specimens displayed considerably high resistivity and small current values associated with the resulting low corrosion activity as noted in

the visual observations of these specimens. However, as expected the NPC concrete with higher w/c ratio of 0.42 demonstrated higher current values (approximately 10 mA) showing that the higher w/c ratios of 0.42 resulted in the lowest resistivity in this NPC concrete.

Fly ash affects the resistivity of concrete to a great extent, Bamforth and Pocock (1990) investigated the effect of incorporating fly ash by replacing cement in a concrete mix on the resistivity of concrete, and found that at age 2 years, fly ash concrete exhibited resistivities of the order of 1000 ohm-m or greater. The normal portland cement concrete (NPC) had values of resistivity in the range of 100-300 ohm-m. They concluded that the extremely high values of resistivity for the fly ash are most likely a consequence of the gradually decreasing porosity and pore continuity.

The Thunder Bay (C2) and Sundance fly ash mixtures displayed the highest resistivity (Fig. 7.2 and 7.3), although all of the specimens were subjected to the same voltage of 5 Volts. As seen from Fig. 7.6, the HAC concrete mixtures exhibits considerably higher resistance to corrosion as compared with the NPC concrete with a water-cement ratio of 0.42 (Fig. 7.5).

7.1.2 Effect of Concrete Cover Thickness

It should be noted that the measured value of the current was related to the concrete cover thickness and the tensile resistance of the concrete mix. As seen from the results in Figures 7.1 through 7.6 and Fig. 7.10, initially, the current density and the rate of corrosion of the steel bars was very slow for all specimens with the 25mm thick concrete cover. The initial current monitored was of the order of 1.5 and 3 mA for the Sundance and Thunder Bay fly ash concretes and remained unchanged for a period of about 45 days, at which time the chlorides penetrated the concrete cover and initiated corrosion when the current rate increased considerably within a few days.

An examination of Figures 7.1 through 7.6 shows that for each of the six concrete mixtures, the resistivity of the concrete increases with the concrete cover thickness. The corrosion of the steel bars is delayed with the larger concrete covers until the chlorides penetrate through the concrete cover to the level of the steel bars. The corrosion currents show dramatic increases in the final 7 to 14 days, when the reinforcing steel commences to corrode rapidly. In these final stages of corrosion, the values of the maximum corrosion current are not related to the concrete cover thickness. Again, the superior corrosion resistance of Sundance and Thunder Bay fly ash mixtures as compared with the Point Tupper fly ash mixture is quite obvious from Figures 7.1, 7.2 and 7.3. For normal portland cement concrete mixtures, the superior corrosion response of concretes with a lower w/c ratio (0.32) is quite obvious from Figures 7.4 and 7.5 for both the thickness of the concrete cover and an increase in the immersion time. It can also be noted for all concrete types and cover thicknesses that in the "final stage" when there is a multifold increase in the corrosion current or decrease in the resistivity, the reinforcing steel corrodes irrespective of the concrete quality and the cover thickness; the steel reinforcing bar commences to corrode quite rapidly. Moreover, at this stage, there is no correlation between the corrosion current or resistivity, and the other parameters.

The results show that the 25 mm concrete cover pullout specimens made from the Sundance and Thunder Bay fly ash concrete mixtures displayed the largest concrete resistivity and consequently the lowest value of the current and the lowest corrosion activity. This was confirmed by a visual examination of the specimens, with no traces of corrosion products or cracks. The Point Tupper fly ash mixture specimens (25mm thick concrete cover) demonstrated a much higher current (20 mA), which started to increase after an immersion period of 15 days, followed by a sudden jump in the current value to about 130 mA within about 5 days. Figure 7.10 clearly reveals the significant superiority of Sundance and Thunder Bay fly ash mixtures as compared with Point Tupper fly ash concrete mixture. The response of the high alumina cement (HAC) concrete (25mm cover thickness) was superior than that of the Point Tupper fly ash with the maximum current value being about 50 mA

after an immersion period of 45 days. Again, the superior response of the NPC concrete with w/c ratio of 0.32 is obvious as compared with the response of NPC with a w/c ratio of 0.42. This shows that the resistivity of the concrete decreases with an increase in the water/cement ratio.

Similar responses were observed for concrete cover thickness of 50, 75, and 100mm (Fig. 7.7, 7.8 and 7.9) with the immersion times to extended corrosion increasing with the concrete cover thickness. It should be noted that the NPC concrete mixture with a w/c ratio of 0.42 displayed the worst corrosion response irrespective of the concrete cover thickness. Thus, greater emphasis needs to be placed on both the thickness and the quality of the concrete cover in terms of its resistivity.

7.2 Half Cell Potentials:

As mentioned earlier, the electrochemical corrosion monitoring technique for corrosion potential mapping method, the ASTM Standard (C 876-87): Half-Cell Potential of Uncoated Reinforcing Steel in Concrete, detects only the likelihood of corrosion (potential) and does not measure the rate of corrosion, and may even be misleading since the corrosion potential depends upon the surrounding environmental conditions. As was mentioned earlier, two types of measurements of the half cell potential were recorded, one type on a daily basis, where the accelerated corrosion cell was disconnected for one hour and then the half-cell measurements were recorded, and the other measurements were undertaken on a 2-weeks basis where the specimens were removed completely from the immersion tank causing a cessation of the corrosion cell activities and dried for four days.

The daily measurements were used only for monitoring, and they did not indicate the "actual" half-cell readings due to the accelerated corrosion electrical set-up. In addition, other than the slow response time in providing a stable output voltage when contact is established between the electrode and the concrete surface, the half-cell

potential does not provide reasonable readings. When the specimens has a high moisture content, due to the fact that they were immersed in the NaCl solution, readings gave a very negative potential due to the restricted access of oxygen, as explained by Popovics *et al.* (1983). Also, the presence of moisture could have resulted in the conduction of electricity over the entire area of the specimen, so that the area of corrosion activity was not identified [John *et al.* (1987)]. Some experimental work by Naish and Carney (1988), suggests that the degree of wetness of concrete has a pronounced effect on the measured corrosion potential and the associated current flowing through the reinforcement.

7.2.1 Effect of Concrete Cover Thickness (daily readings)

Half-cell potentials recorded over time for all specimens using a copper-copper sulphate half-cell, indicate that the intensity of corrosion increases considerably with a decrease in the concrete cover thickness. Limitations of space prevent presentation of several figures of detailed data, however, these results are quite similar to those obtained for the current in the previous section, using the half-cell potential test. A typical example is presented in Fig 7.11 and Fig. 7.12.

7.2.2 Effect of HVFA Concrete (daily readings)

The effect of high volume fly ash (HVFA) replacement of cement in concrete mixtures on corrosion initiation time in several figures of the detailed results (not presented here due to lack of space) shows the time of initiation of corrosion for reinforcing steel in concrete. Those data clearly show the significant beneficial effect of fly ash blending on the corrosion initiation time, and on the reinforcement corrosion protection (see Figures 7.11 and 7.12).

7.2.3 Corrosion-resistance characteristics of the different concrete mixes:

The effect of fly ash content on the corrosion initiation time Figures 7.13 to 7.16 shows the half-cell potential measurements for the different types of concrete specimens with concrete cover thicknesses of 25, 50, 75 and 100 mm, respectively.

Figure 7.13 shows the half-cell potential data for the pullout specimens made from different concrete types with 100 mm thick cover, with the normally accepted criterion that the probability of corrosion is low when the half-cell potential is algebraically higher than –200 mV, Sundance and Thunder Bay fly ash concrete demonstrate the best performance with the corrosion initiating after about 10 weeks of immersion time. After this stage, the Sundance fly ash concrete specimens were noted to be superior in corrosion propagation than the Thunder Bay fly ash concrete specimens. The corrosion initiation performance of Point Tupper fly ash concrete and NPC concrete with w/c ratio of 0.32 was nearly similar. Again, as expected, the performance of the NPC concrete (w/c ratio = 0.32) was superior than that of w/c ratio of 0.42. The high alumina cement concrete displayed the lowest corrosion initiation time and corrosion protection.

The time to initiation of corrosion and the following corrosion propagation are shown in Figures 7.17 to 7.22 for each type of concrete for the four concrete cover thicknesses. The superior performance of specimens with 100 and 75 mm thick concrete covers can be clearly noted from these figures with the corrosion initiation times of 15 weeks for Sundance and Thunder Bay fly ash mixtures, 8 and 12 weeks for Point Tupper fly ash mixture for 75 mm and 100 mm concrete cover thicknesses, respectively, 7 and 9 weeks for NPC concrete with w/c ratio of 0.32, and 2 and 5 weeks for NPC concrete with the w/c ratio of 0.42. The high-alumina cement concrete mixture demonstrated the worst corrosion initiation and propagation performance and this response was independent of the concrete cover thickness. All of the specimens with 25 mm thick concrete cover demonstrated early corrosion initiation and propagation performance, showing that such low cover thicknesses are inappropriate for aggressive environments. By comparison, the fly ash concrete

specimens with 50 mm thick concrete cover displayed somewhat better performance with corrosion initiation times of 7 weeks (Sundance and Point Tupper fly ashes) and 5 weeks (Thunder Bay fly ash). The NPC concrete specimens with 50 mm thick concrete cover (w/c ratio of 0.32) showed initiation of corrosion at 3 weeks compared with about one week for similar NPC concrete specimens (with a w/c ratio of 0.42), showing the improved corrosion resistant characteristics of NPC concretes with the lower w/c ratio. It is also clear that the use of fly ash in concrete provides an improved corrosion resistance performance.

It should be noted that there are concerns regarding the use of fly ash especially in high volumes due to the possible side effects of the pozzolanic reactions which results in reduction in the pH of the solution, leading to an interface with the steel passivation or reduced chloride threshold level. Such concerns are related mainly to the unfavourable pore solution chemistry of fly ash blended cements because of the removal of hydroxyl ions from the pore solution by the pozzolanic reactions, and to a lower degree due to the presence of carbon in the fly ashes. It is now well recognized (Rasheeduzzafar *et al.* 1991) that the passivation of steel is a function of the relative concentrations of chloride and hydroxyl ions in the pore solution, expressed in terms of Cl^-/OH^- ratio rather than the chloride concentration. The study of Hausmann (1968), on the basis of mild steel corrosion tests in concrete-simulated artificial calcium hydroxide solution with a pH value of around 12.5, has proposed a threshold depassivation Cl^-/OH^- ratio of 0.60. However, pH of the pore solutions in "actual" concrete is significantly higher than 12.5, and varies between 13.5 and 13.75. Diamond (1986), based on Gouda's (1970) work, conducted tests on alkaline solutions with pH ranging between 11.8 to 13.95, proposed a threshold depassivation Cl^-/OH^- ratio of 0.30, corresponding to a pH of 13.3, as being more appropriate to the concrete pore solutions. More investigative work is needed in this area.

However, the present investigation clearly shows the superior corrosion-protection performance of the fly ash concretes, which contradicts the notion of

increased susceptibility of steel to corrosion by the increased aggressivity of the pore solution. This contradiction can be explained by the fact that fly ash also brings about other significantly favourable changes in the physical characteristics of the cementitious binding matrix by providing a denser structure and very low permeability in the concrete, which overrides the increased corrosion risk posed by the elevated Cl^-/OH^- ratio of the pore solution, and results in an improved corrosion protection behaviour.

Significant refinement in the pore-size distribution of mature fly ash concretes have been reported by several investigators. In a study conducted on 30% fly ash blended cement paste, Manmohan and Mehta (1981) showed that, at the age of 1 year, the 30% fly ash blended cement paste contained appreciably more finer pores than that of the control normal portland cement paste. A significant reduction in the median pore size leads to a lower ionic diffusion rates and reduced water permeability. Another study of fly ash over no fly ash concrete at the age of 6 months by Davis (1954), reported a 3.5 to 5 times decrease in the permeability of the fly ash concrete, while Elfert (1973) reported a 7 to 10 times reduction in the permeability rates of fly ash over plain portland cement concrete. Kumar and Roy (1986) and Kumar *et al.* (1987) showed that the median pore size and chloride diffusion coefficient of a mature 0.35 water/solid fly ash blended cement paste were reduced to 2.75 nm and 13.5×10^{-13} m^2/s, respectively, compared to 15.00 nm and 129×10^{-13} m^2/s, respectively for the control cement paste. A study of a 30% fly ash blended cement conducted by Short and Page (1982) reported a chloride diffusion coefficient of 14.7×10^{-13} m^2/s for the 30% fly ash concrete compared to 44.7×10^{-13} m^2/s for the corresponding base portland cement.

Improvement in the electrical resistivity for the fly ash concrete due to the densification and refinement of its pore structure is another physical factor that would offset the unfavourable effect of the increased aggressivity of the pore solution on the corrosion of the reinforcing steel in fly ash concrete. Corrosion of steel in concrete is an electrochemical process, and an enhanced electrical resistivity of concrete strongly

influences the reduction of the corrosion activity of the steel reinforcement (Beaton *et al.* 1967; Rasheeduzzafar *et al.* 1985). The results from this investigation on the electrical resistivity characteristics from the fly ash and no fly ash concretes show a 3-fold increase over the electrical resistivity of the concrete with no fly ash. These results also alleviate the concern that the fly ash may increase the electrical conductivity of the concrete by introducing carbon as one of its constituents.

It is well recognized that fly ash contribution to the properties of the blended cement concrete differs significantly from the normal portland cement concretes, and requires definable terms reflecting their composition, origin, and fineness. Even within a particular classification, fly ashes vary widely and are at best conglomerations of particles of varied compositions and crystalline contents, which must be considered in planning concrete mixtures for improved corrosion protection.

7.2.4 Effect of Cover Thickness on Corrosion Initiation Time

Figure 7.23 shows the time to the initiation of corrosion for reinforcing steel in concrete against cover thicknesses of 25, 50, 75 and 100 mm for all of the concrete types.

This investigation shows the vital importance of the concrete cover and the concrete quality in providing protection to the steel reinforcement. As seen from Fig.7.23 for the NPC with a 0.32 w/c ratio concrete with a 100 mm cover provides 91, 65, and 30 percent better protection than that for 25, 50, and 75mm concrete cover thicknesses, respectively. However, for the NPC with a 0.42 w/c ratio concrete with a 100 mm cover provides only 83, 52, and 28 percent improved protection as compared with the 25, 50, and 75mm concrete covers, respectively. These data indicate that the same increase in the cover thickness for the lower quality 0.42 w/c ratio concrete is not as effective for corrosion protection as with the higher quality 0.32 w/c ratio concrete.

These results agree well with the generally accepted concept that the concrete quality and cover thickness significantly influence the effectiveness of the general defensive shield against corrosion, and underline the fact that in terms of design practice, cover to reinforcement has a very important effect on the extent and rate of reinforcement corrosion. The field study on Dickson Bridge (Chapter 5) confirms the predominant role of concrete cover quality on the widespread corrosion deterioration in the bridge deck and other elements.

The field data from the investigations by the Portland Cement Association, in conjunction with four State Highway Department in the U.S. (1965-66) and in Kansas by Crumpton *et al* (1969), on bridge decks as well as by Tyler (1960) and Wakeman *et al.* (1958) on marine structures in Massachusetts, Florida, Southern California, and Los Angeles Harbour also agree well with the results of this investigation demonstrating the overriding significance of the concrete quality and cover thickness as a corrosion-protection measure.

All of these results clearly show the significantly beneficial effect of the partial cement replacement by 58% fly ash on the corrosion initiation time. The corrosion of steel is more severe in the concrete made with the higher w/c ratio (0.42).

All results (current readings, half-cell potentials and corrosion rate) show that the intensity of corrosion increases considerably with a decrease in the concrete cover thickness. This conclusion is also confirmed from the data in Fig. 7.23 where the corrosive action of the chlorides is seen to be substantially mitigated by the concrete cover thicknesses larger than 25 mm. It is now well recognized that the availability of oxygen at the cathode of the corrosion microcell is one of the most important factors which controls the rate of reinforcement corrosion; concretes with low permeability cause thicker concrete covers to decrease the supply of oxygen at the cathodic areas considerably.

Cabrera (1985) showed that incorporation of fly ash in concrete considerably reduces the total porosity and volume of capillary porosity. Marsh *et al* (1985) concluded that permeability in concretes and mortars containing fly ash was reduced due to the pore refinement and pore blockage resulting from the additional volume of reaction products generated by the pozzolanic reactions between the fly ash and the lime present in hydrated cement paste.

7.3. Corrosion Cracking Time

Corrosion rate is an important parameter for quantitatively predicting the time to cracking and the subsequent deterioration processes. As mentioned earlier, corrosion rate is a "dynamic" parameter, which varies with changes of climate conditions (such as temperature and relative humidity), exposure time and chloride content. The measured corrosion rate from the linear polarisation tests represent only instantaneous values corresponding to a certain temperature and moisture content at the time of measurement. Hence, the measured corrosion rate should be adjusted to an equivalent value, depending on the service exposure conditions, which can be used to predict the service life of the reinforced concrete member and the structure.

As mentioned earlier, the mechanism of corrosion damage of reinforced concrete is due to the formation of corrosion products on the steel surface, which has about 6 to 7 times higher volume than that of the steel reinforcement, and it induces expansive stresses, which cause cracking and spalling of the cover concrete.

The corrosion products result in an expansive stress applied to the surrounding concrete. Not all of corrosion products are responsible for the expansive pressure; some of them may fill the voids around the steel/concrete interface or migrate away from the steel/concrete interface. Figure 7.24 shows that the normal portland cement concrete with a w/c ratio of 0.42 needs the highest amount of corrosion products to initiate cracking comparing to the other concrete mixtures, indicating that the NPC

with 0.42 w/c ratio has higher difusivity and permeability than that of the other concrete mixtures.

There are different parameters that are relevant in controlling the corrosion cracking time, which includes the severity of the environment, concrete quality, and the bar diameter. For a given environment, the bar diameter defines the magnitude of the corrosion current. A larger bar diameter will result in a lower electrical resistivity and consequently higher corrosion currents, which in turn results in the formation of corrosion products at the steel-concrete interface. As seen earlier, this would lead to larger bursting forces (similar to those in a pipe with water under pressure), which would cause splitting of the concrete cover. The tensile strength of the concrete cover thickness plays a significant role in the resistance to concrete cracking due to these bursting forces. It should be re-emphasised that the concrete cover strength is characterised by its quality, thickness and the tensile strength of the concrete.

It should be noted that there exists a higher water-cement ratio porous matrix zone around the steel/concrete interface at the transition from cement paste to steel, entrapped / entrained air voids and corrosion products diffusing into the cement paste capillary voids. The volume of this porous zone is directly related to the surface area of reinforcement, w/c ratio, degree of hydration and the degree of consolidation. As the corrosion takes place on the surface of the steel, the porous zone will gradually fill with the corrosion products. When the total amount of corrosion products, is less than the amount required to fill the porous zone around the steel/concrete interface by diffusion, the formation of corrosion products at this stage will not create any stress in the surrounding concrete.

The significance of the cover thickness/bar diameter, c/d_b, ratio is an important parameter affecting the reinforcement corrosion in concrete, which has also been emphasised qualitatively by other researchers (Atimtay and Ferguson 1974; Beeby 1983; Ravindrarajah and Ong 1987; Al-Sulaimani *et al.* 1990; Rasheeduzzafar

et al. 1992). In summary, the three parameters that control concrete cracking due to corrosion are the concrete quality, cover thickness, and reinforcing bar diameter.

The effect of c/d_b ratio on corrosion cracking time for all of the concrete mixtures is presented in Fig 7.25. Each value is an average of eight test results. It can be seen from the figure that for the Sundance fly ash concrete with 100-mm concrete cover thickness, the time to cracking is increased by factors of 4.7, 1.6 and 1.3, as compared with those for 25, 50 and 75 mm concrete cover thicknesses for the same concrete. While for the NPC with 0.32 w/c ratio, the 100 mm concrete cover, the time to cracking is increased by factor of 4.75, 1.9 and 1.2 times as compared with those for the 25, 50 and 75 mm concrete cover thicknesses, respectively. The effect of c/d_b ratio on the amount of corrosion required to cause concrete cracking for all of the concrete mixtures is shown in Fig. 7.24. For both of the normal portland cement concretes, with 0.32 and 0.42 w/c ratios, about 4 and 5 percent corrosion by loss of mass are needed to initiate cracking for a c/d_b of 5.13 (100 mm cover thickness), only about 1 percent corrosion by loss of mass is found sufficient to crack reinforced concrete components for a c/d_b ratio of 1.3 (25 mm cover thickness).

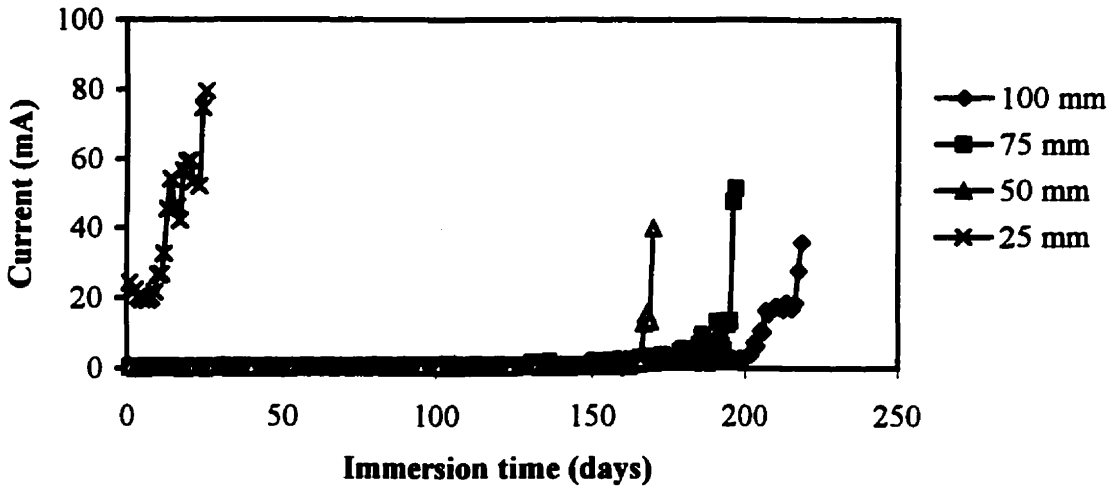

Fig. 7.1: Current readings for Point Tupper FA concrete specimens for different concrete cover thickness

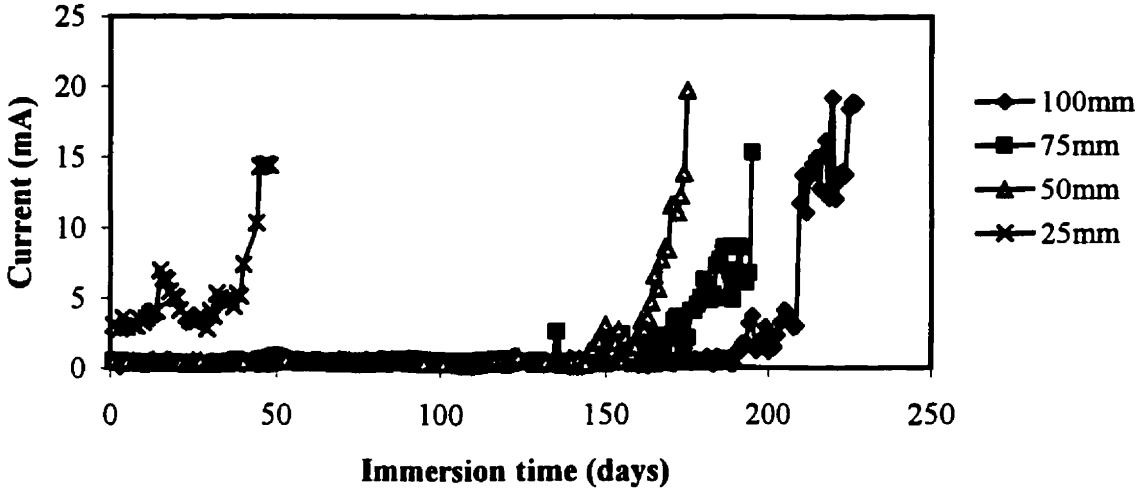

Fig. 7.2: Current readings for Thunder Bay FA concrete specimens for different concrete cover thickness

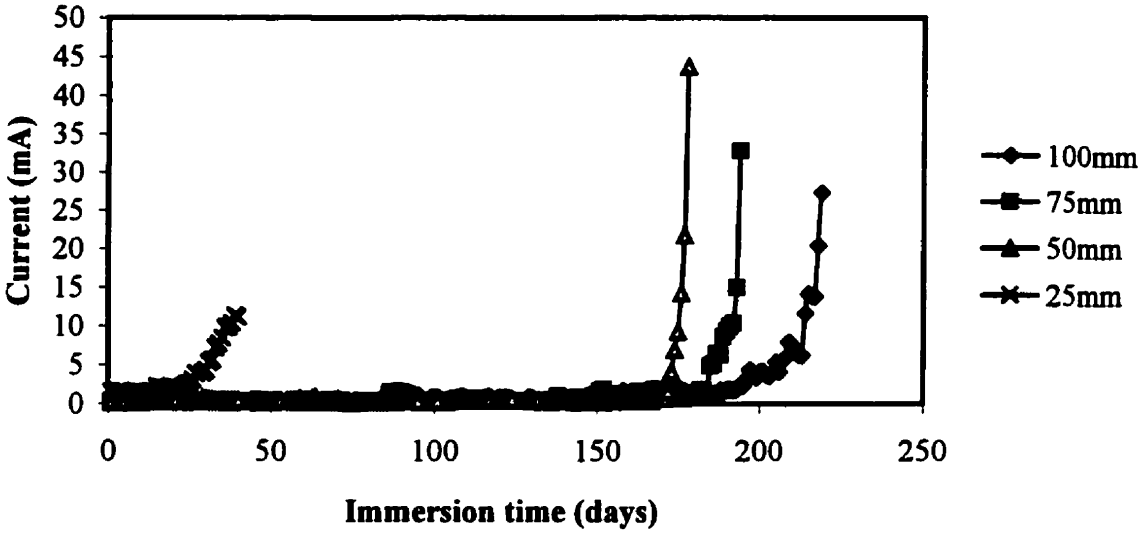

Fig. 7.3: Current readings for Sundance FA concrete specimens for different concrete cover thickness

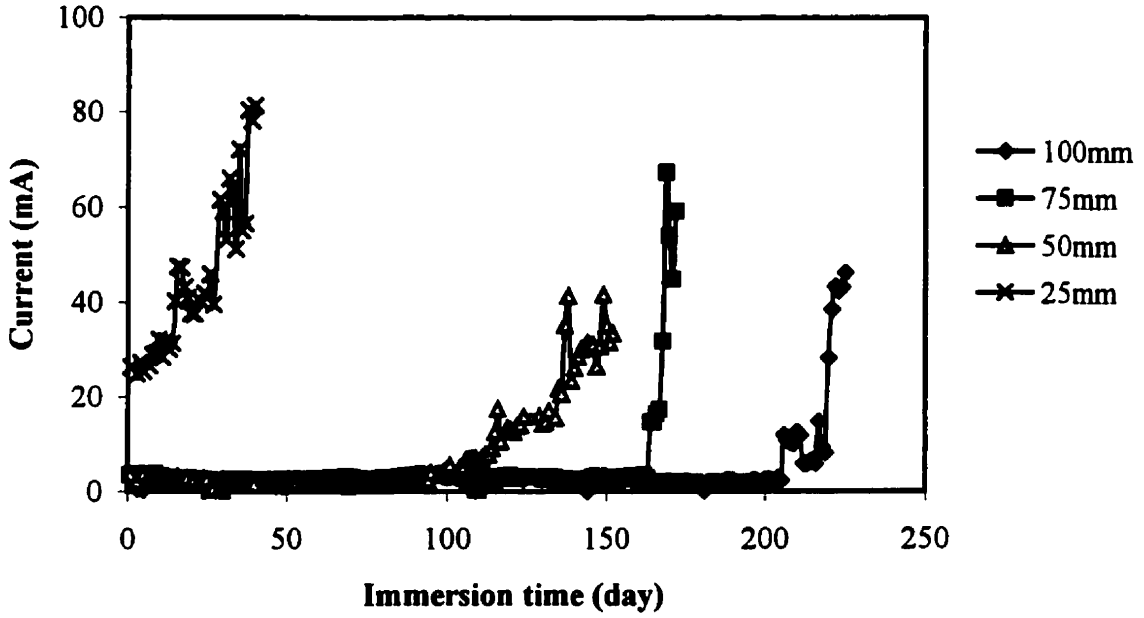

Fig. 7.4: Current readings for NPC with 0.32 w/c concrete specimens for different concrete cover thickness

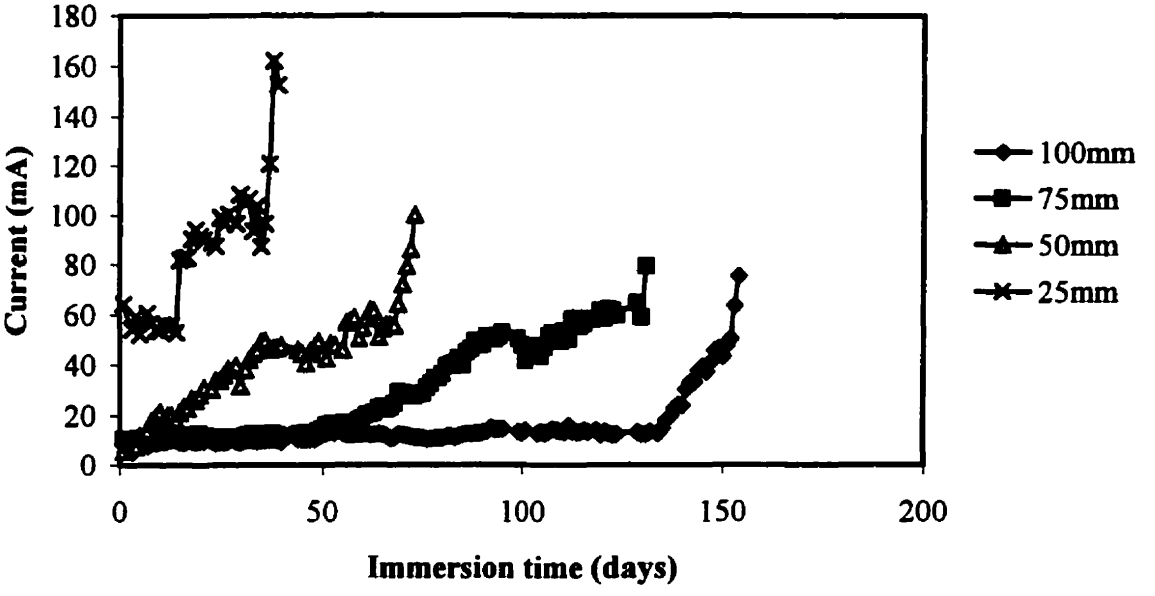

Fig. 7.5: Current readings for NPC with 0.42 w/c concrete specimens for different concrete cover thickness

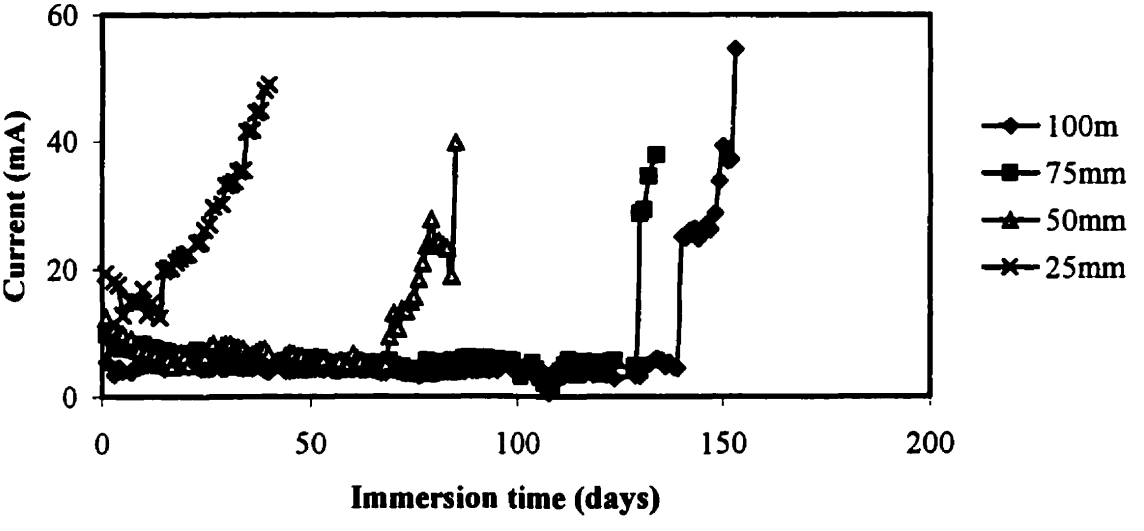

Fig. 7.6: Current readings for HAC concrete specimens for different concrete cover thickness

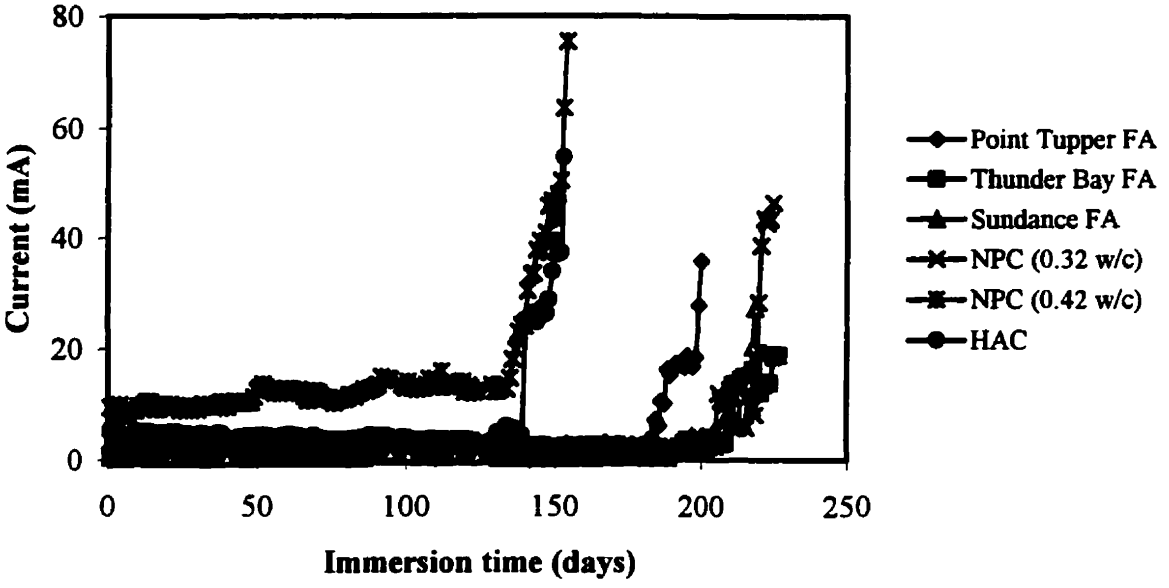

Fig. 7.7: Current readings for different concretes for 100 mm concrete cover thickness

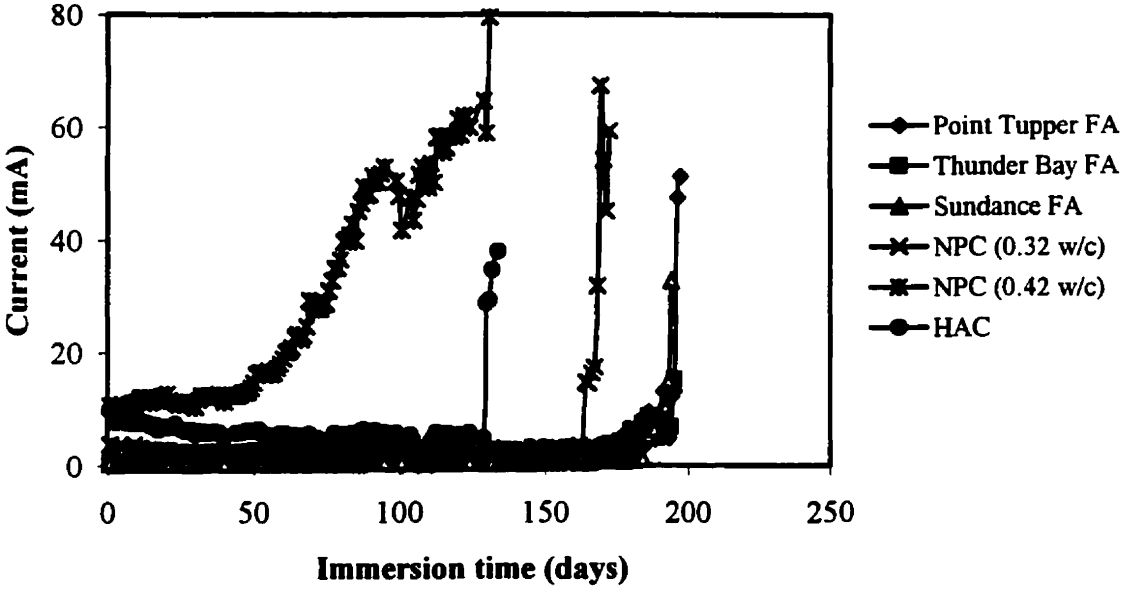

Fig. 7.8: Current readings for different concretes for 75 mm concrete cover thickness

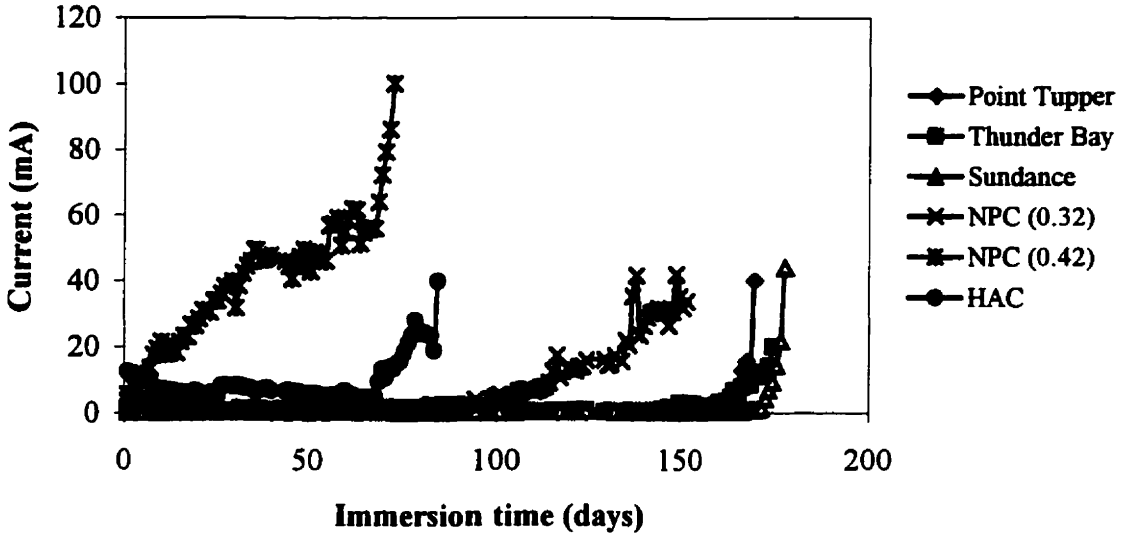

Fig. 7.9: Current readings for different concretes for 50 mm concrete cover thickness

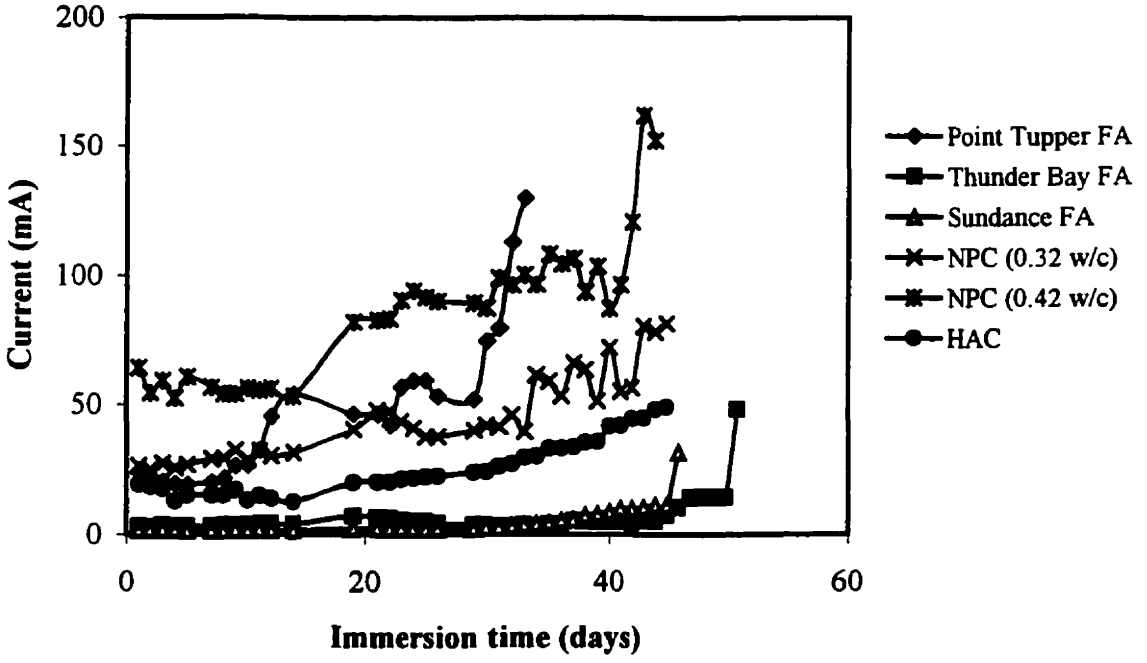

Fig. 7.10: Current readings for different concretes for 25 mm concrete cover thickness

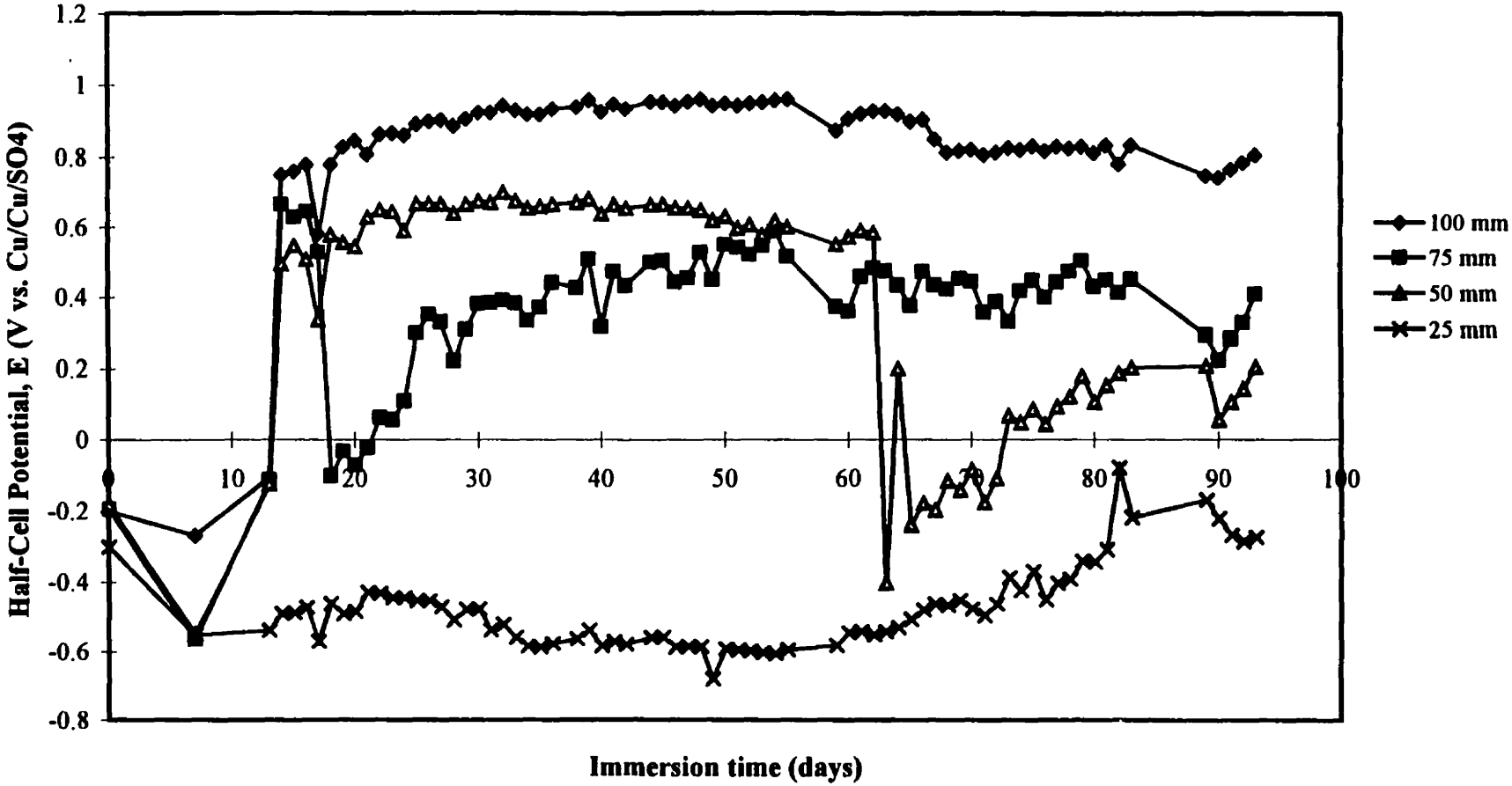

Fig. 7.11: Daily half-cell potential readings (one hour after shutting off the power) for Sundance FA concrete specimens for different concrete cover thickness

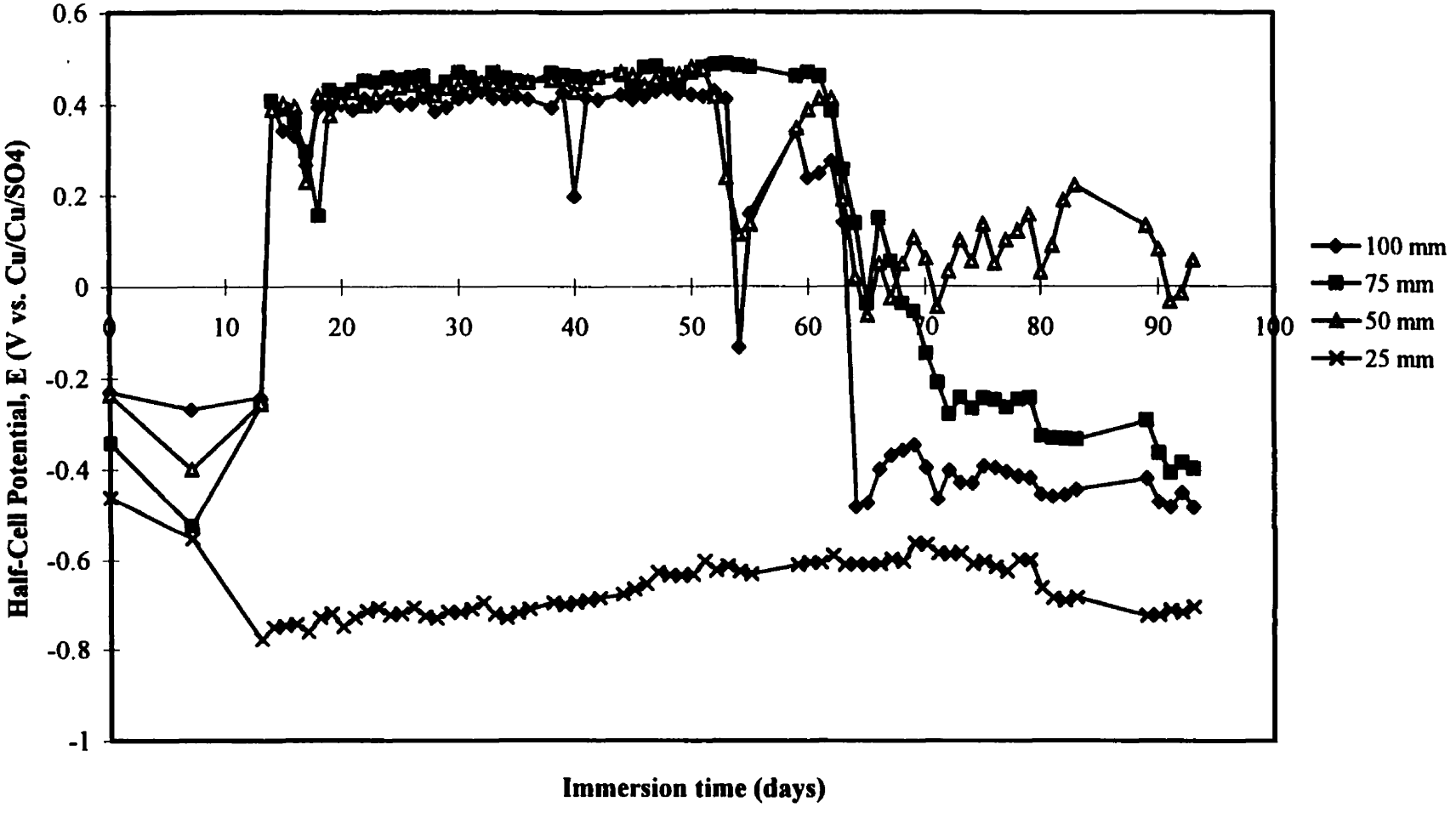

Fig. 7.12: Daily half-cell potential readings (one hour after shutting off the power) for NPC with 0.32 w/c ratio concrete specimens for different concrete cover thickness

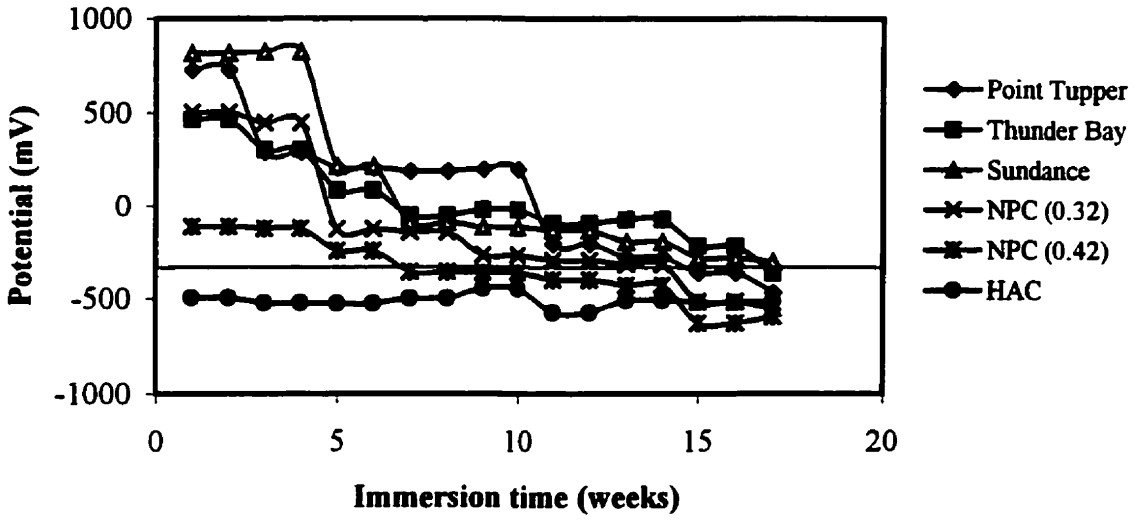

Fig. 7.13: Potential measurement for different types of concretes with 100mm concrete cover thickness

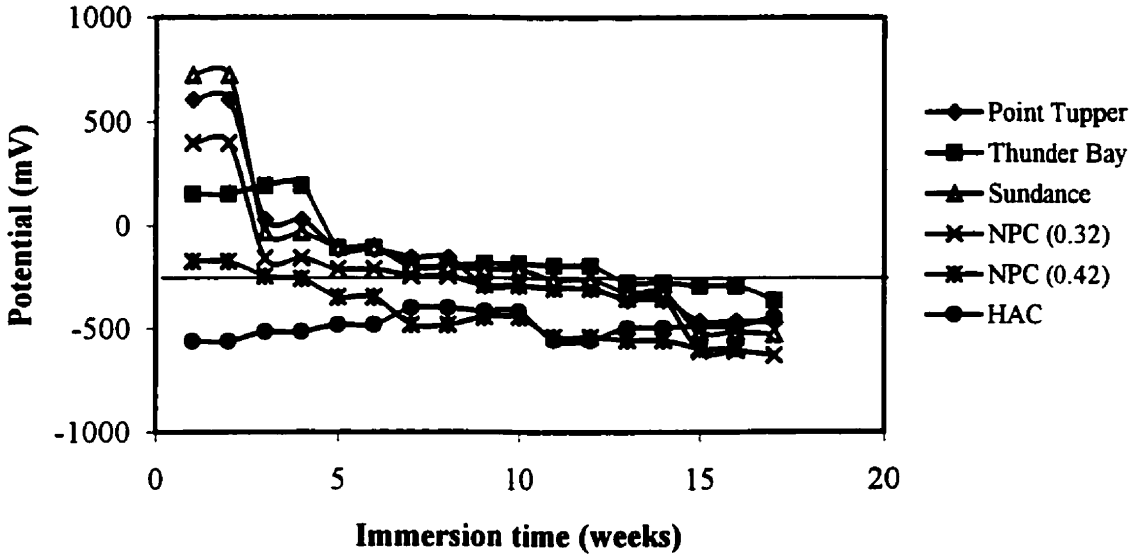

Fig. 7.14: Potential measurement for different types of concretes with 75mm concrete cover thickness

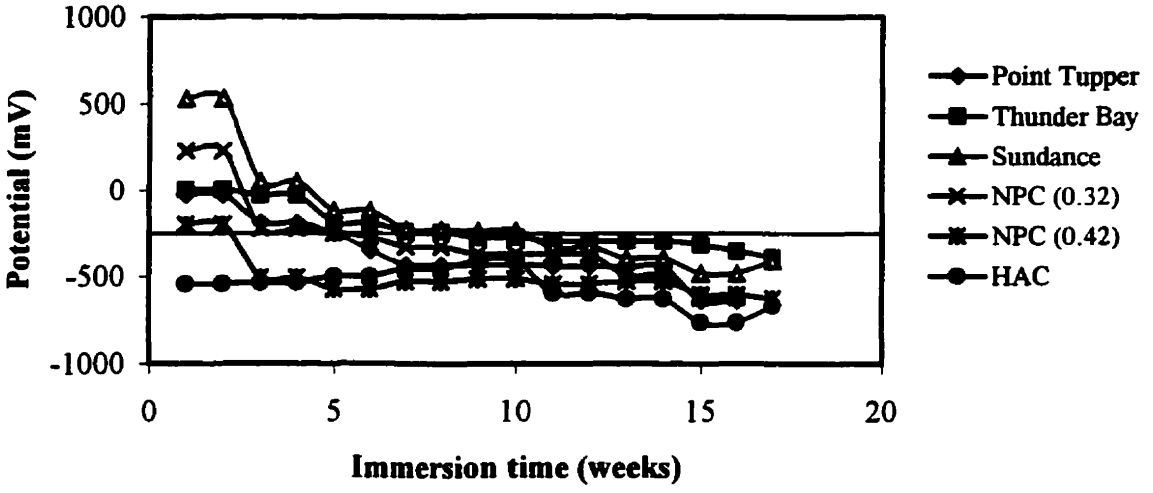

Fig. 7.15: Potential measurement for different types of concretes with 50mm concrete cover thickness

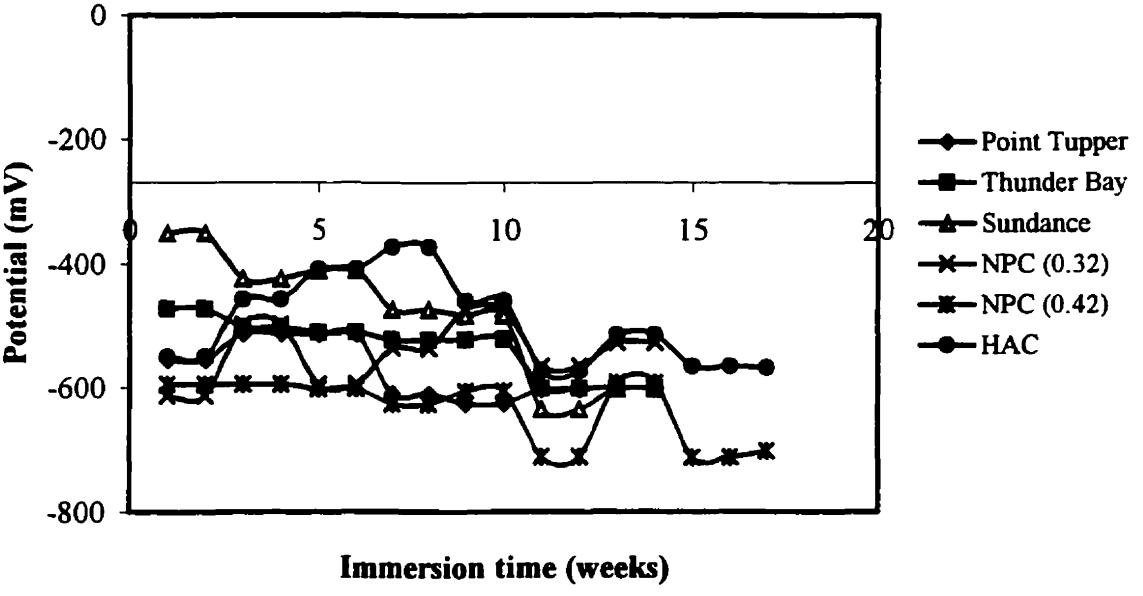

Fig.7.16: Potential measurement for different types of concretes with 25mm concrete cover thickness

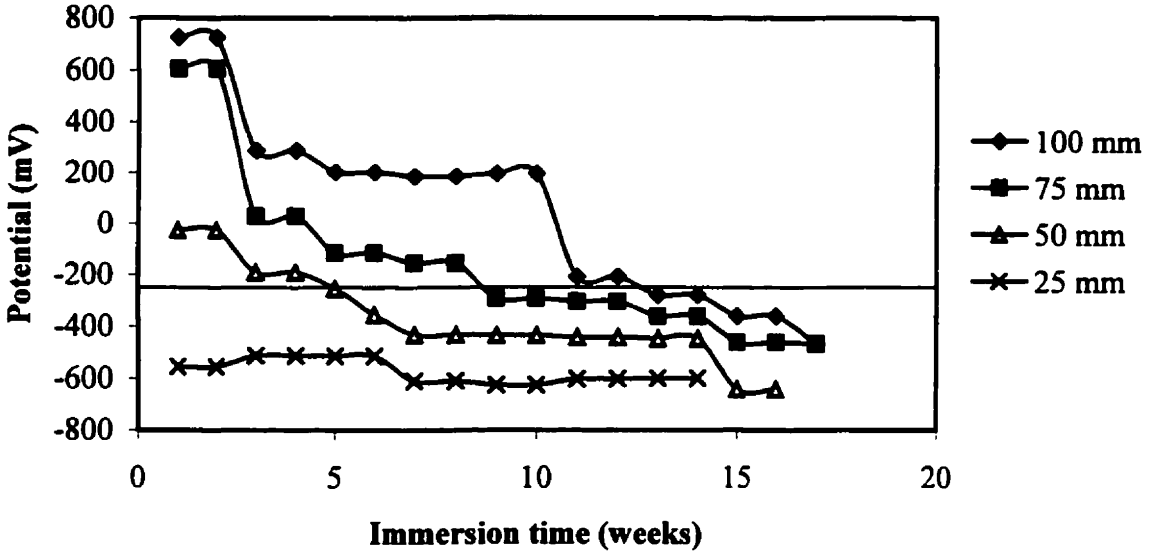

Fig. 7.17: Potential readings for the Point Tupper fly ash with all the different concrete cover thicknesses

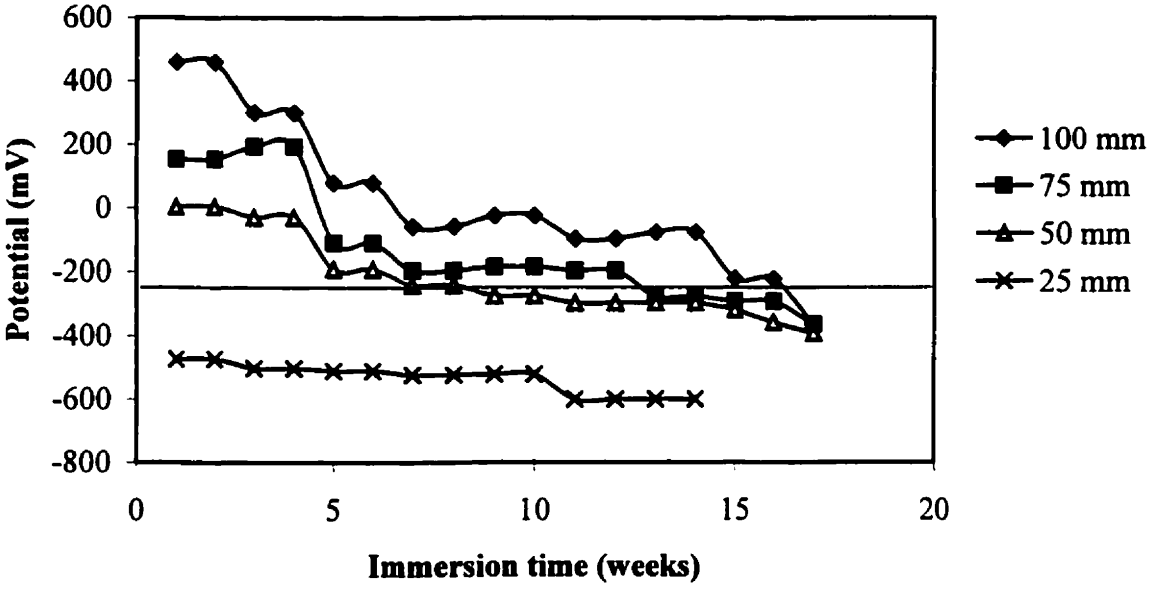

Fig. 7.18: Potential readings for the Thunder Bay fly ash with all the different concrete cover thicknesses

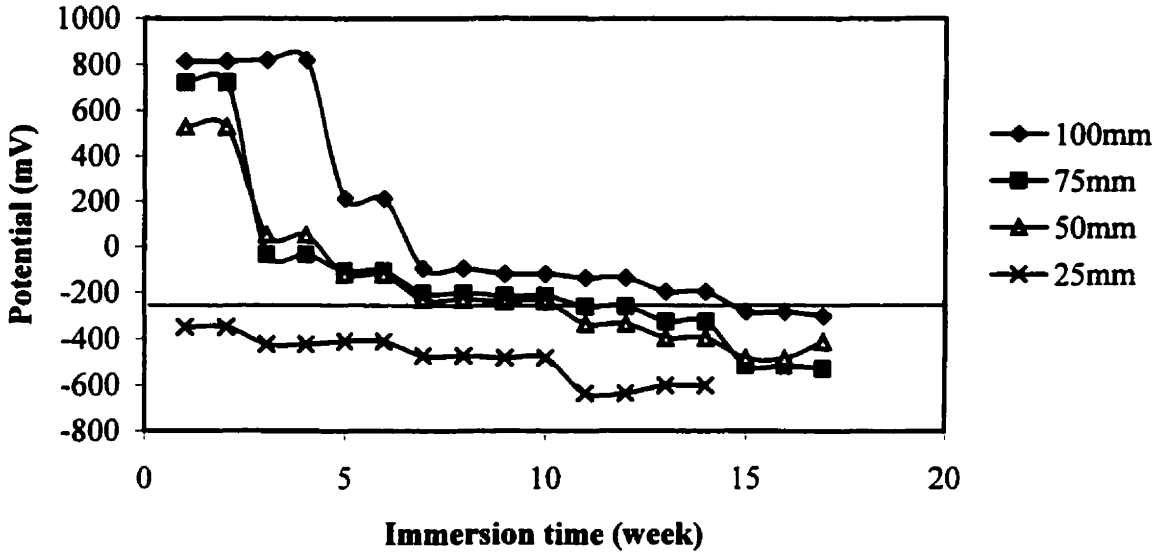

Fig. 7.19: Potential measurements for the Sundance fly ash concrete with all the different conccrete cover thicknesses

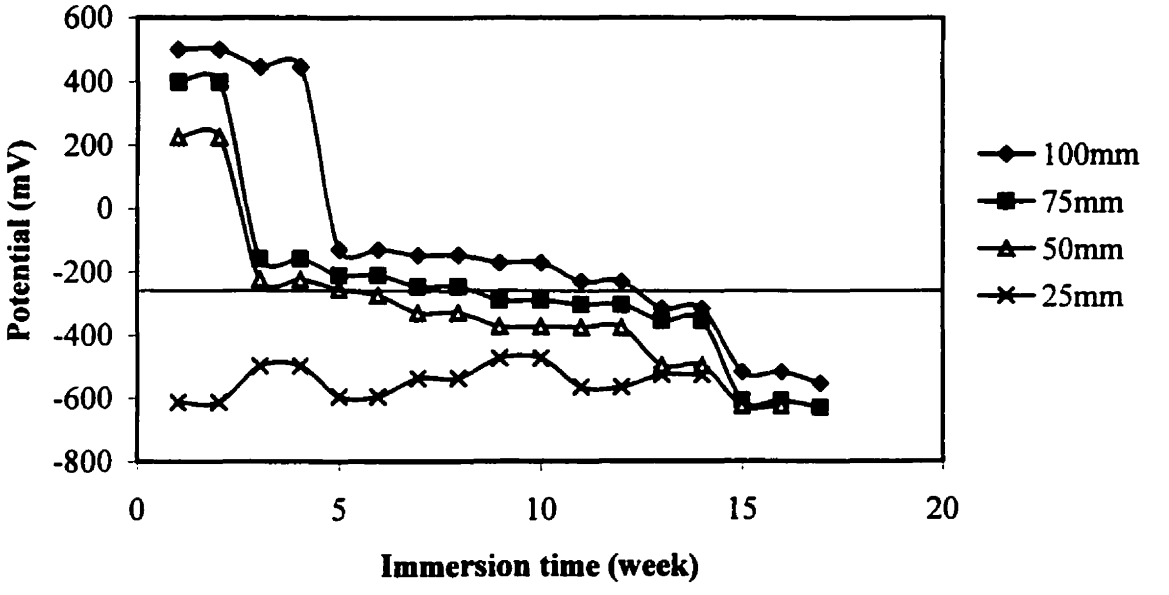

Fig. 7.20: Potential readings for the NPC with 0.32 w/c ratio with all the different concrete cover thicknesses

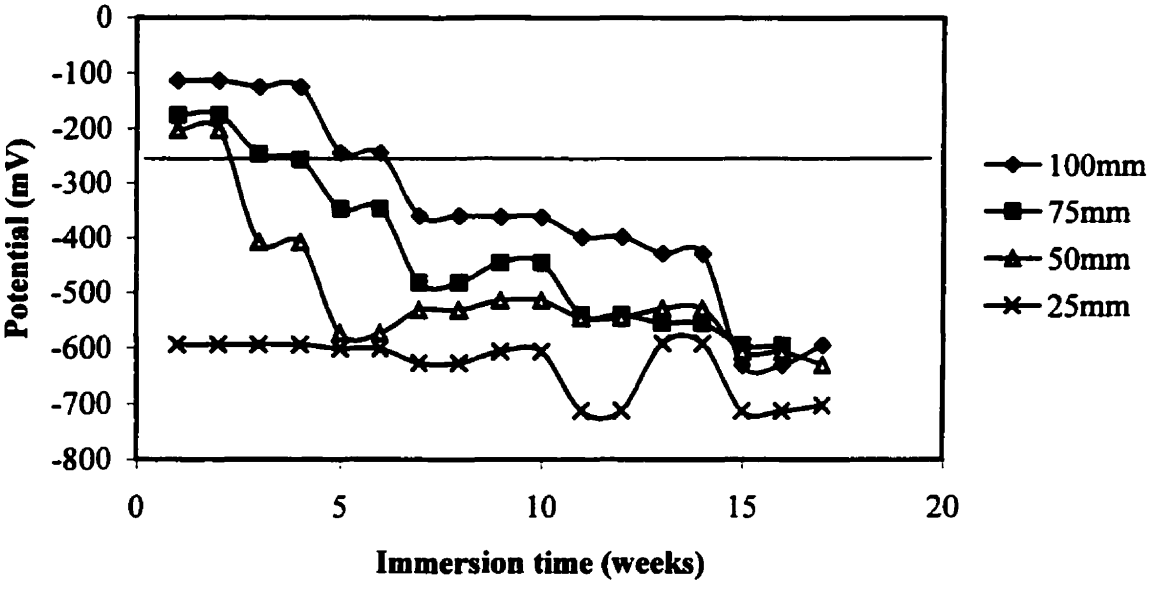

Fig. 7.21: Potential measurements for NPC with 0.42 w/c ratio with different concrete cover thickness

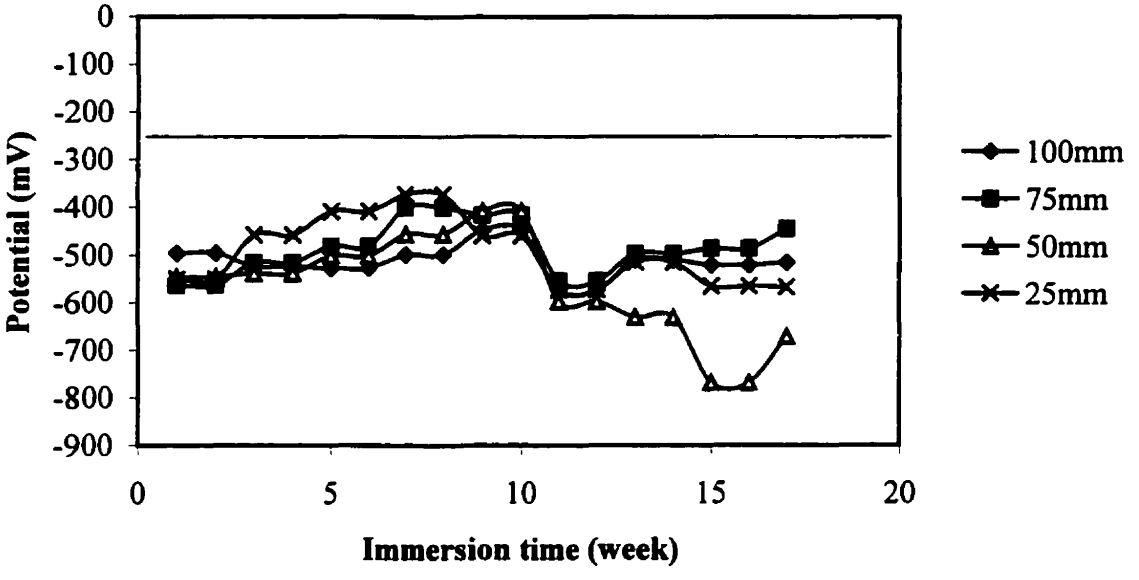

Fig. 7.22: Potential measurements for HAC with different concrete cover thickness

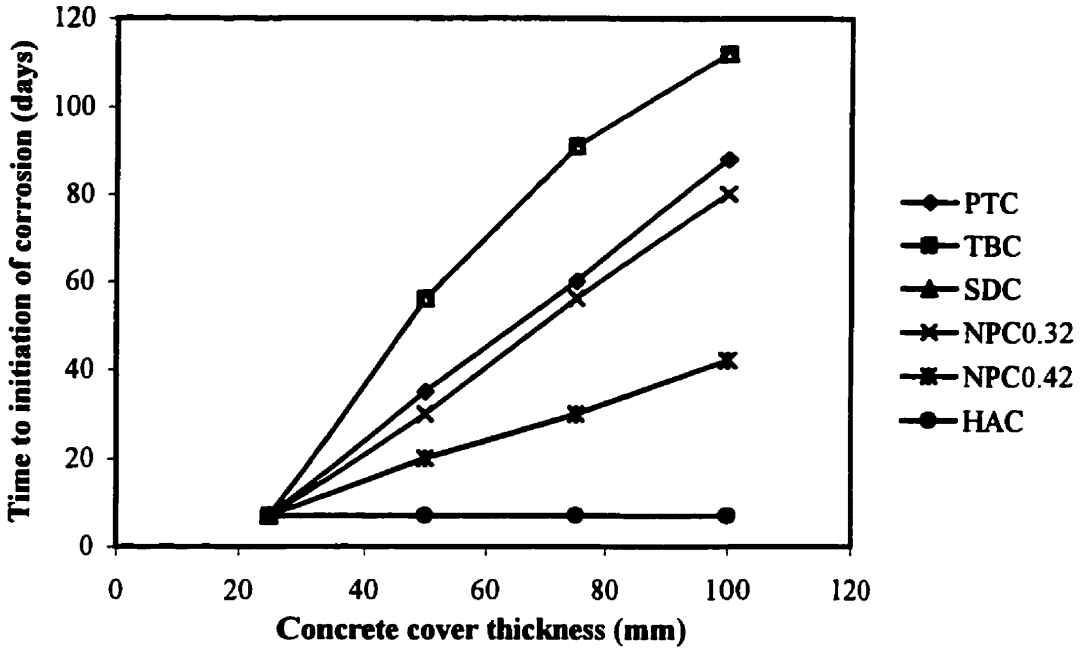

Fig. 7.23: Effect of concrete cover thickness and concrete mixture on time to initiation of corrosion

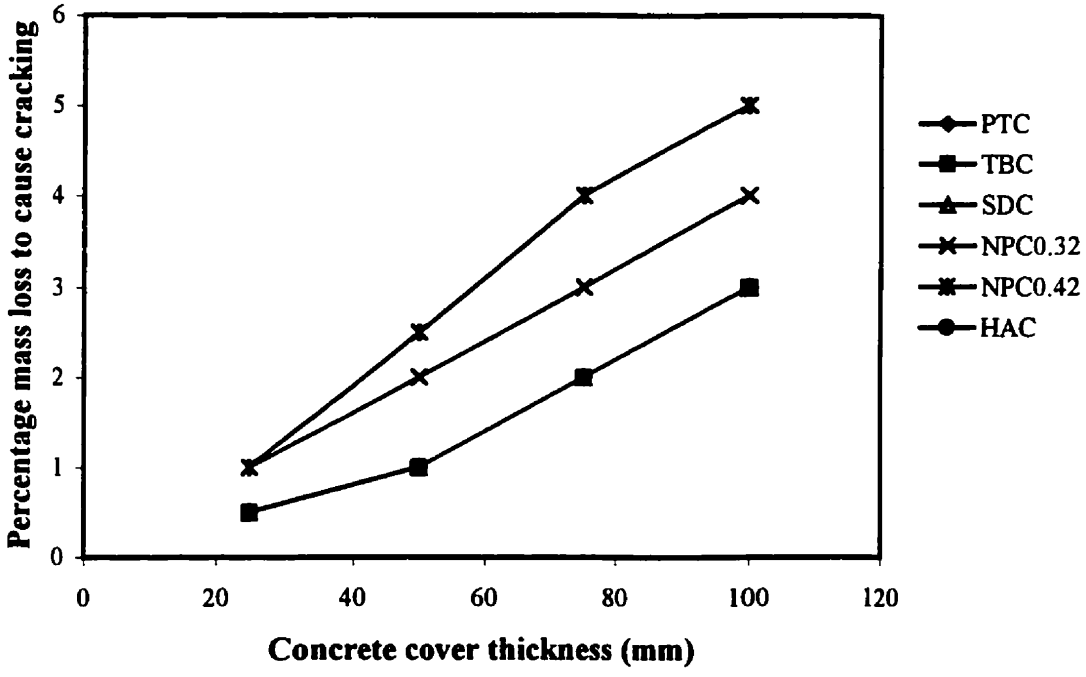

Fig. 7.24: Effect of concrete cover thickness and concrete mixture on the amount of corrosion to cause cracking

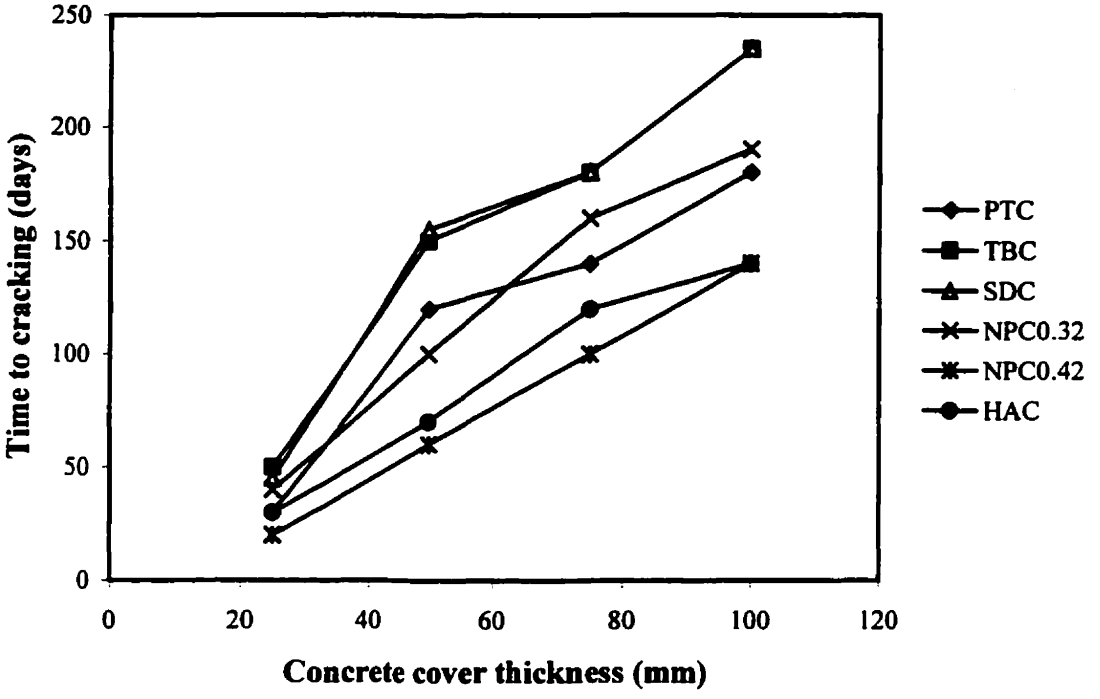

Fig. 7.25: Effect of concrete cover thickness and concrete mixture on time to cracking

Chapter 8

Pullout Test Results and Analysis

This Chapter reports the results of tests on a series of pullout specimens, which investigated different aspects of the bond strength between the reinforcing steel and concrete. The main variables in the experimental test series were the effect of the level of corrosion on the degree of bond between the reinforcing steel and concrete using six different concrete mixtures and four different concrete cover thicknesses.

8.1 Basic Testing Program

The fundamentals of the bond characteristics at the steel-concrete interface were presented in Chapter 3. It should be noted that different investigators have used the pullout, tension and other tests to evaluate the bond characteristics at the steel-concrete interface. The tension specimen, loaded at both-ends, with a properly instrumented steel bar can enable evaluation of the bond stress distribution along the length of the bar. Although the pullout tests on cylindrical specimens reinforced with a symmetrically placed steel bar, was used frequently by earlier researchers to evaluate the bond characteristics at the steel-concrete interface, it can provide only relative values of the bond characteristics. This is because one face of the specimen is supported and the bar is pulled out by applying force at this supported end. This results in the steel bar being in tension and the surrounding concrete being in compression (for equilibrium) near the loaded end, leading to a slightly higher slip than in the tension test where all of the concrete in the specimen is subjected to

different levels of tension. However, because of its simplicity, it is easier and less time-consuming to use the pullout tests to evaluate the various parameters being studied in this investigation. A total of 192 pullout tests were conducted to study the effect of the type of concrete, the concrete cover thickness and 7 to 8 different levels of corrosion. In addition, carefully planned tension tests were performed to study and evaluate the bond characteristics at the steel-concrete interface to study the influence of three selected concrete types and eight different levels of corrosion. The results of the tension tests are presented in Chapter 9. The specimen nomenclature is presented in Chapter 6.

8.2 Average Bond Strength

The average bond stress, u, for each load level was calculated as the average stress between reinforcing steel bar and the surrounding concrete along the embedded portion of the bar, using the relationship:

$$u = \frac{P}{L\,(\pi d_b)} \tag{8.1}$$

where P is the maximum measured load, L is the embedded length of the reinforcing steel bar (constant at 254mm), and d_b is the reinforcing bar diameter, No. 20 bars were used in all of the pullout and tension specimens.

8.2.1 Parameters Influencing Bond Strength

As mentioned in Chapter 3, the bond strength and the failure mode are affected by several variables, such as the tensile strength of concrete, f_t, concrete cover thickness, c, reinforcing bar diameter, d_b, and the embedment length, L, of the reinforcing bar. The bond characteristics of the reinforcing bars in the six different concrete mixtures with the control specimens (no-corrosion) are investigated first in terms of the effect

of concrete cover/bar diameter ratio, c/d_b, and the variation of the concrete tensile strength with the compressive strength.

It was shown by many researchers such as Orangun, *et al.* (1977), Kemp and Wilhelm (1979), and Jimenez, et al. (1979) that for a bar subjected to an axial force only, and without the confinement provided by stirrups, the average uniform bond stress at which splitting occurs is a function of the tensile strength of the concrete, f_t, the concrete cover thickness-bar diameter ratio, c/d_b, and the bar diameter-embedment length, d_b/L, ratio.

The values of the tensile strength of concrete, f_t, were estimated using the expression

$$f_t = 0.56 (f'_c)^{1/2} \qquad (8.2)$$

in SI units, as was explained in Chapter 3.

8.2.2 Bond Strength-Tensile Strength Ratio and Concrete Cover Thickness

The variation of the bond strength at the steel-concrete interface to the concrete tensile strength, u/f_t, ratio with the concrete cover thickness for the fly ash concrete mixtures is shown in Fig. 8.1, which shows the slightly superior performance of Thunder Bay (TBC) and Sundance (SC) fly ash concrete mixtures, as compared with the Point Tupper (PTC) fly ash concrete mixture. In all cases, the bond strength increases with an increase in the concrete cover thickness. Most of the control specimens with a cover thickness of 100mm for the six concrete mixtures failed due to yielding of the No. 20 bar, followed by fracture of the bar at the ultimate load. There was no bond distress in any of the specimens. The fly ash concrete specimens with 100 mm thick concrete cover exhibited different modes of failure at the ultimate load with some specimens failing due to the failure of the steel bar; some specimens

failed due to the splitting of the concrete cover. The variations in the mode of failure of the various fly ash concrete specimens did not enable a reliable correlation between their results and more experimental research is needed in this area. It should be noted that the present practice normally provides a 75 mm thick concrete cover for corrosion protection of the steel bars and the large concrete cover thickness of 100 mm is rarely used. It is for these reasons that the results of the specimens with 100 mm thick concrete cover are not included in Figures 8.1 through 8.3.

The variation of the bond strength-tension strength, u/f_t, ratio for the NPC concretes (w/c ratios of 0.32 and 0.42) and the HAC concrete (w/c ratio= 0.32) pullout specimens is shown in Fig. 8.2. As expected, the NPC concrete mixture with a w/c ratio of 0.32 showed better response, however, the differences between the three u/f_t ratio responses for the different concrete cover thicknesses were relatively small.

The responses of the pullout specimens for all six concrete mixtures and the different concrete cover thicknesses, excepting for the 100 mm thickness, are presented in Fig. 8.3. It is noted that the NPC concrete specimens with a w/c ratio of 0.32 displayed the best (u/f_t) ratio response compared with a lower response for the NPC concrete specimens with a w/c ratio of 0.42. Increasing the cover thickness from 25 to 50 mm resulted in an improvement of the bond strength for the TBC and SC fly ash concrete specimens by about 40 to 50 percent, while the strength augmentation for NPC concrete (w/c ratio = 0.32) was about 60%.

A strength increase of about 16 percent was noted for the PTC specimens. These results clearly show that both the quality of the concrete in the cover and its thickness are important for protection of the bar against corrosion. Increasing the concrete cover thickness from 50 to 75 mm displayed much smaller increase in the bond strength, with increases in the range of 16 to 19 percent for the TBC and SC specimens, 9 percent for the PTC specimens, 12 percent for the NPC specimens (w/c ratio = 0.32) and a relatively smaller increase (percent) for the NPC specimens (w/c

ratio = 0.42). This again emphasizes the need for high quality concrete covers for protection of steel reinforcement against corrosion.

8.2.3 Experimental Bond Strength and Concrete Properties

The previous section presented the results of the pullout tests in terms of the variation of the bond strength-tensile strength (u/f_t) ratios with the concrete cover thickness. The tensile strength of the NPC and fly ash concretes is known not to have the same relationship to the compressive strength of the concrete. The results of the measured ultimate bond strength are plotted against the concrete cover thickness in Fig. 8.4 for the different concrete mixtures. The results again show the superiority of the bond performance of NPC 0.32 (w/c ratio = 0.32) specimens and the inferiority of the PTC specimens, however, the bond performance of the other four mixtures are somewhat different in Figures 8.3 and 8.4. In evaluating these curves, the one-year compressive strengths at the time of the tests of the six concretes in-order of their relative bond strengths (see Chapter 6) were evaluated as follows:

Concrete mix.	Compressive strength, f'_c	Tensile strength, $0.56\sqrt{f'_c}$
NPC 0.32	60 MPa	4.34 MPa
SC	67 MPa	4.58 MPa
NPC 0.42	51 MPa	4.00 MPa
HAC	51 MPa	4.00 MPa
TBC	41 MPa	3.59 MPa
PTC	62 MPa	4.41 MPa

The differences in the variation of the bond strength u and the bond strength-tensile strength (u/f_t) ratio with the concrete cover thickness can be attributed to the calculated tensile strength values from equation 8.2. Since the measured bond strength is a function of the tensile strength of concrete, it is clear that equation 8.2 overestimates the tensile strength of the fly ash concretes. It can be seen from Fig. 8.1 that the compressive strength of the fly ash concrete mixtures has no clear

relationship to its bond strength/tensile strength ratio, the Sundance fly ash mixture with a compressive strength of the range of 67 MPa showed the best results followed by the Thunder Bay with the concrete compressive strength with the range of 47 MPa than the Point Tupper fly ash concrete mixture with the compressive strength of 62 MPa.

It may be noted that Bilodeau and Malhotra (1998), and Sirivivatnanon *et al.* (1994) studied the mechanical properties of high volume fly ash concrete, and they found that the tensile strength of the high volume fly ash concrete exhibited slightly lower values than that of the normal portland cement concrete with the same compressive strength. However, they provided no explanation for this phenomenon, which needs further research.

8.4 Bond Stress - Slip Relationships

In each pullout test, the slip at the loaded end is measured at the various load increments up to failure, which can be due to yielding of the reinforcing bar, splitting of the concrete, or pulling out of the bar from the concrete specimen.

The calculated bond stress at each load level is plotted against the loaded-end slip for each specimen in Figures 8.5 through 8.16. Failure was defined as the point of maximum bond strength, and the corresponding maximum slip value was then defined as the value at the point of failure. The test results are also summarized in Tables 8.1 through 8.6, along with the corresponding bond strengths.

8.4.1 Uncorroded Control Specimens

The results of the pullout tests are presented Table 8.1 through 8.6. A maximum load was reached, followed by a sharp drop in the applied load with longitudinal splitting cracks in all of the pullout specimens with concrete cover thicknesses of 25 and 50mm. However, for most of the specimens with 75 and 100mm concrete cover

thicknesses, a maximum load was reached, followed again by a sharp drop in the applied load. This load was then sustained by the specimen with increasing slip, finally resulting in a pull out failure. In addition, some specimens failed due to the failure of the steel bar, which reached its ultimate strength and fractured.

The results of the bond break down for the uncorroded specimens show behaviour similar to that presented in Chapter 3 in the literature review. The bond stress-slip relationship, which consisted of three distinct regions that adequately describes the complete bond stress-slip behaviour. The demarcation of the three regions would be based on the behavioural trends which would be similar to that of the CEB Model Code (where $s_1 = s_2$ in Equation 3.18). In this model, the shear stress initially increased with slip up to a maximum shear stress of u_m. The second region was then illustrated by an increase in the slip with a small drop in the applied load, or constant shear stress for a short distance (between s_1 and s_2) followed by a sharp drop in the applied load with longitudinal splitting cracks. The bond behaviour between s_1 and s_2 is associated with the concrete shearing off between the ribs and splitting open, hence, s_1 was associated with the breakdown of the bond.

8.4.2 Corroded Specimens

The variation of the calculated bond stress with the accompanying slip at various load levels is shown in Figure 8.5 through 8.7 for the different corrosion levels, concrete types and concrete cover thicknesses. The associated test data are presented in Tables 8.1 through 8.6. The test results in the various figures and tables clearly show that with slight corrosion (second level of corrosion; zero corrosion is the first level) improves the bond strength slightly because of the increased roughness at the bar surface due to corrosion. The growth of this thin firm layer of corrosion products causes an increase in the radial and hoop stresses, which in turn increases the friction bond. An increase in the corrosion level is manifested in an increase in the loaded-end slip due to the formation of the longitudinal cracks because of corrosion. An increase in the level of corrosion is accompanied by increased corrosion products at

the bar surface, which convert the initially firm layer of corrosion products into a flaky layer at the bar surface with very little strength and resistance to slip. This phenomenon is reflected in the bond stress-slip curves in Figures 8.5 through 8.16.

At advanced levels of corrosion (10 percent mass loss and more), the corrosion products at the bar surface are relatively loose. In addition, the bar ribs also get corroded thereby reducing the resistance to slip considerably. As the pullout force is applied to these specimens with heavily corroded bars, the bar slips at first (very low stiffness related to the slope of the bond stress-slip curve) until it grips the concrete at the interface which is reflected in a considerable increase in the stiffness, reflected in the slope of the bond stress-slip curve (for example, Specimen C1-3C in Fig. 8.5 and the Specimens C2-8C and C2-3C in Fig. 8.6).

At very advanced levels of corrosion beyond this stage, the corrosion products increase to such an extent that the steel bar is unable to grip the concrete and continues to slip at very low pullout load values (for example, Specimen C4-3C in Fig. 8.8, Specimens C5-4C and C5-7C in Fig. 8.9, and Specimen C1-6D in Fig. 8.11). At this stage, it is believed that the only bond mechanism that is still working is the friction bond stress. Figures 8.17 and 8.18 show pullout specimens with different level of corrosion, while Fig. 8.19 shows the effect of corrosion on the reinforcing bar and its ribs.

8.5 The Effect of Corrosion on Bond Strength

The effect of corrosion in terms of the bar mass loss on the calculated bond strength for the different concrete cover thicknesses is shown in Figures 8.20 through 8.25 for the six different concrete types. For each concrete type, it is clear that the bond strength decreases as the concrete cover thickness decreases from 100 to 25 mm. The influence of the concrete type on the bond strength with different concrete covers (100, 75, 50 and 25 mm) is shown in Figures 8.26 through 8.29 in terms of the bar mass loss. As seen earlier, the performance of NPC0.32 (w/c ratio = 0.32) specimens

is generally the best for all concrete cover thicknesses. The performance of the various fly ash concretes are reasonably close to each other for all concrete cover thicknesses.

It can be noted from the above figures that the bond strength generally increases with an increase in the concrete cover thickness. Also, the value of bond strength increases generally up to a mass loss value of 1.5 percent beyond which the bond strength deteriorates gradually with an increase in the level of corrosion, irrespective of the cover thickness.

Numerical relationship to calculate the reduction of bond strength caused by the level of corrosion can be obtained by a multiple linear regression analysis (to account for the change in the cover thicknesses) of the experimental results of the relationship between the bond strength and the mass loss due to corrosion, and by disregarding the values where slight corrosion leads to an increase in the bond strength.

Figures 8.20 through 8.25 show the correlation between the nominal bond strength of the steel bars in all of the different concrete mixtures and the mass loss obtained from this study. It can be seen from the figures that the nominal bond strength decreases linearly with an increase in the steel mass loss due to corrosion.

The equations obtained for the bond strength of corroded steel bars in different concrete mixtures are presented in Table 8.7, which also includes the correlation coefficients. Here, ML represents the percentage mass loss. It should be noted that the first term in each equation represents a specific experimental P value and therefore it has a different value for each type of concrete, including the fly ash concretes.

8.5.1 Effect of Concrete Cover Thickness

Concrete quality and cover thickness characterize the resistance to the high bursting forces generated by the corrosion products resulting from the rebar corrosion, which causes cracking of the concrete. These forces are dependent on the bar diameter, making the concrete cover thickness-bar diameter ratio, (c/d_b), a significant corrosion protection parameter.

The bond stress-slip relationship in Figures 8.5 through 8.16 show the response of the specimens in all stages, including the postcracking stage where each specimen had an initial longitudinal crack due to corrosion. The flexibility of the longitudinally cracked specimen is reflected in the tendency of the cracked specimen to open when the bar is loaded. This results in a "free slip" of the bar initially, because the bar is already slightly detached from the surrounding concrete, and under applied load, it slips until the ribs and the concrete keys come into contact again. In addition, this free slip is normally linearly proportional to the width and the number of the cracks due to corrosion. In some specimens, this phenomenon is observed to be repeated more than once within the test. Very weak and crushed concrete in front of the bar ribs in addition to the corrosion products tend to move along with the steel bar, and they tend to get accumulated at some locations and form a temporary key that would interlock with the "reduced" bar ribs. This phenomenon leads to a temporary stiffening at the steel-concrete interface, and as in the earlier load stages, this results in locally increased hoop and radial tensile stresses, resulting in an increase in the local bond resistance, however, it would not take much load to break these bonds again.

8.5.3 Effect of Corrosion Level on Bond with Fly Ash Concrete

The effect of fly ash on bond was noted earlier in Tables 8.1 through 8.6 and in Figures 8.5 through 8.16. It can be noted from this data that the fly ash concrete mixtures showed a larger increase in the bond strength initially with slight corrosion.

Basically, this very slight corrosion enhances the adhesive and cohesive properties of the fly ash concrete mixtures which are lower than that of the NPC and the HAC concrete mixtures.

The experimental data shows that the bond strength increases by about 6 to 18 percent for the various mixtures, with the exception of the Point Tupper (PTC) fly ash concrete and the normal portland cement mixtures, which demonstrated bond strength increase of 6 to 52 percent, and 2 to 8 percent, respectively. As explained earlier, the formation of the corrosion products, which at this stage are confined by the concrete and the steel bar, result in high radial and hoop (circumferential) stresses, which in turn augment the bond capacity at the steel-concrete interface.

In addition, it was shown in Chapter 7 that to induce the same level of corrosion in high volume fly ash (HVFA) concrete specimens as for NPC concrete specimens, the time required was 3 times higher in HVFA concretes. However, the data show that, for various stages of corrosion, the deterioration of bond was higher in the fly ash concrete than in the other concrete types. For the same corrosion percentage, the NPC concrete specimens developed higher bond resistance than the HVFA concretes.

As can be noted from Tables 8.1 through 8.6 and Figures 8.5 through 8.16, for the same bar mass loss and for the same concrete cover thickness, the slip of the steel bar and therefore, the widths of the cracks due to corrosion, are larger in the fly ash concrete mixtures as compared with the normal portland cement concrete mixtures. The larger crack widths in fly ash concrete mixtures suggest an inferior bond response, as compared with the NPC concrete mixtures, which is borne out by the experimental observations.

The results for the chloride ion content in Tables 8.1 through 8.6 show that the fly ash concrete mixtures are relatively impermeable as compared with the NPC concrete mixtures (w/c ratio = 0.32) that, in turn, is less permeable than the NPC

mixture (w/c ratio = 0.42). Therefore, there is a relatively lower diffusion of corrosion products in the fly ash concretes as compared with NPC concretes and this causes an increased confinement of the corrosion products, and hence larger bursting forces in the fly ash concretes. The chloride ion ingress in the three fly ash concretes before cracking is of the same order, which in turn is smaller than that in NPC concrete with a water-cement ratio of 0.32, which again is smaller than that in NPC concrete with a water-cement ratio of 0.42. This reflects the relative impermeability of the various concrete mixtures.

Further examination of Tables 8.1 through 8.6 shows that at an early stage of corrosion, as expected, it requires a higher mass loss to cause cracking in concrete specimens with a 100 mm thick concrete cover as compared with the specimens with a 25 mm thick concrete cover. There is a transition in the mass loss required to form cracks for intermediate cover thicknesses of 75 and 50 mm.

8.6 Effect of Crack Width on Mass Loss due to Corrosion

The effect of the width of cracks resulting from the corrosion of the reinforcing steel on the bond strength at the steel-concrete interface are shown in Figures 8.30 through 8.35 for the different concrete types. The results clearly show the trend of higher bond strengths for thicker concrete cover for any type of concrete, and the bond strengths decreases gradually as the cover thickness is decreased to 25 mm.

The influence of the crack width for a given concrete cover thickness (100, 75, 50, and 25 mm) for the different types of concrete is shown in Figures 8.36 through 8.39. As seen before in Figures 8.26 through 8.29, the results generally show the superiority of NPC concrete (w/c ratio = 0.32) and Sundance and Thunder Bay fly ash concrete mixtures for the various concrete cover thicknesses. The HAC concrete mixture generally displayed inferior performance for the various concrete cover thicknesses. It must also be noted, that the concrete cover thickness is reduced from 100 to 25 mm, the overall divergence between the different mixtures decreases

gradually until finally for the 25 mm thick concrete cover, the curves for the different concrete mixtures are almost overlapping.

8.7 Variation of Bond Strength with Chloride Content

The relationship between the chloride content at the steel bar level in specimens of different types of concrete for a given concrete cover thickness are shown in Figures 8.40 through 8.43. While no trends can be discerned definitely from the curves in these figures, it can be noted that the chloride content for the normal portland cement concrete mixture with a w/c ratio of 0.32 (NPC0.32) is low for all cover thicknesses, while that for NPC concrete (w/c ratio= 0.42), a concrete mixture with a higher w/c ratio, is a maximum for all concrete cover thicknesses, because of its higher permeability. The results for all Thunder Bay (TBC) and Sundance (SC) concrete mixtures are relatively low for the cover thickness of 100 and 75 mm, however, they tend towards higher values for smaller concrete covers, except for the Sundance (SC) concrete with a cover thickness of 25 mm.

The effect of the chloride content on a concrete mixture type with different cover thicknesses is shown in Figures 8.44 through 8.49. Again, the basic trend for all types of concrete mixtures is that for the same chloride content, the bond strength is higher for the larger concrete cover than for the lower cover thicknesses. Also, as expected, the chloride contents for all the smaller covers are generally higher than those for the larger concrete covers.

The variation of the chloride content was evaluated for each of the 144 specimens at three levels along the specimen height and at three depths up to the steel bar level. This data are too voluminous to be reported here, however, typical trends at the top, middle and bottom are shown in Figures 8.50 and 8.51. The results of the variation of the chloride-ion content with the concrete cover thickness showed that as expected, in the uncracked concrete specimens and parts of the specimens relatively free of cracks, the chloride ion concentration decreased from the exterior concrete surface to

the steel bar surface. This phenomenon is basically the migration of chloride ions into the concrete through diffusion.

8.8 Summary

The bond stress-slip response of the bar, as well as the bond stiffness, slope of the bond stress-slip curve, are adversely affected by the width of the crack due to corrosion. The maximum bond strength is significantly affected by the number of the cracks and their widths due to corrosion.

For a given value of the crack width due to corrosion, or the crack width to the concrete cover thickness ratio, bond strength is higher for larger concrete cover thicknesses than for the smaller cover thicknesses. This relationship holds even after some deterioration of the steel bar due to corrosion and shows the significance of larger concrete cover thickness for corrosion protection in structural concrete elements. Of course, the quality of the concrete in terms of its impermeability is equally important for the corrosion protection phenomenon.

Table 8.1: Test data for Point Tupper fly ash concrete (PTC) pullout specimen					
Specimen #	**Corrosion level**	**Mass loss due to corrosion (%)**	**Width of longitudinal crack due to corrosion (mm)**	**Chloride ion content at rebar level (%)**	**Bond strength (MPa)**
C1-1A	0.00	0.00	0.00	0.00	9.31
C1-2A	0.00	0.00	0.00	0.00	8.84
C1-3A	1.00	2.56	0.00	0.00	11.84
C1-7A	2.00	4.90	0.20	0.12	8.00
C1-6A	3.00	5.76	0.40	0.14	7.89
C1-8A	4.00	6.00	0.50	0.15	7.68
C1-4A	5.00	6.76	0.80	0.16	7.45
C1-5A	6.00	8.91	3.00	1.08	6.53
C1-1B	0.00	0.00	0.00	0.00	8.20
C1-2B	0.00	0.00	0.00	0.00	8.32
C1-6B	1.00	1.20	0.00	0.02	10.89
C1-5B	2.00	2.20	0.10	0.03	7.54
C1-4B	3.00	3.00	0.20	0.05	7.22
C1-7B	4.00	4.50	0.40	0.10	7.04
C1-8B	5.00	5.00	0.80	0.12	6.90
C1-3B	6.00	5.40	1.20	0.44	6.55
C1-1C	0.00	0.00	0.00	0.00	6.83
C1-2C	0.00	0.00	0.00	0.00	6.37
C1-7C	1.00	0.80	0.00	0.00	9.56
C1-5C	2.00	1.00	0.00	0.02	9.30
C1-8C	3.00	3.93	0.60	0.06	6.13
C1-6C	4.00	5.46	0.80	0.08	5.75
C1-4C	5.00	9.03	1.40	0.30	4.45
C1-3C	6.00	12.00	3.50	1.13	2.56
C1-1D	0.00	0.00	0.00	0.00	4.46
C1-2D	0.00	0.00	0.00	0.00	5.06
C1-5D	1.00	0.13	0.00	0.01	5.46
C1-4D	2.00	1.50	0.15	0.01	4.96
C1-7D	3.00	2.84	0.50	0.02	3.52
C1-8D	4.00	7.20	3.00	0.49	1.71
C1-3D	5.00	8.02	3.12	0.54	1.10
C1-6D	6.00	12.30	5.00	1.15	0.24

Table 8.2: Test data for Thunder Bay fly ash concrete (TBC) pullout specimen					
Specimen #	**Corrosion level**	**Mass loss due to corrosion (%)**	**Width of longitudinal crack due to corrosion (mm)**	**Chloride ion content at rebar level (%)**	**Bond strength (MPa)**
C2-1A	0.00	0.00	0.00	0.00	9.21
C2-2A	0.00	0.00	0.00	0.00	9.82
C2-4A	1.00	2.46	0.00	0.00	11.36
C2-5A	2.00	6.90	0.50	0.16	7.68
C2-8A	3.00	7.11	0.80	0.19	7.36
C2-3A	4.00	8.30	1.00	0.28	6.40
C2-6A	5.00	9.21	1.20	0.34	5.63
C2-7A	6.00	11.50	3.00	0.68	4.30
C2-1B	0.00	0.00	0.00	0.00	9.05
C2-2B	0.00	0.00	0.00	0.00	9.13
C2-3B	1.00	2.00	0.00	0.01	10.81
C2-4B	2.00	4.93	0.20	0.11	7.17
C2-5B	3.00	5.83	0.40	0.14	6.40
C2-8B	4.00	6.82	1.20	0.31	5.44
C2-7B	5.00	7.20	1.60	0.33	5.27
C2-6B	6.00	8.50	4.00	0.61	4.67
C2-1C	0.00	0.00	0.00	0.00	7.15
C2-2C	0.00	0.00	0.00	0.00	6.72
C2-5C	1.00	1.00	0.00	0.01	9.28
C2-7C	2.00	2.40	0.00	0.01	8.56
C2-4C	3.00	3.50	0.25	0.10	6.15
C2-8C	4.00	6.30	0.80	0.15	4.78
C2-6C	5.00	8.40	0.98	0.26	3.84
C2-3C	6.00	9.00	2.00	0.81	2.63
C2-1D	0.00	0.00	0.00	0.00	4.50
C2-2D	0.00	0.00	0.00	0.00	4.31
C2-4D	1.00	0.45	0.00	0.01	4.57
C2-8D	2.00	0.98	0.00	0.03	5.14
C2-5D	3.00	3.26	1.40	0.10	2.46
C2-6D	4.00	4.10	1.60	0.21	2.32
C2-3D	5.00	4.35	1.80	0.23	0.96
C2-7D	6.00	6.85	5.00	1.87	

Table 8.3: Test data for Sundance fly ash concrete (SC) pullout specimen					
Specimen #	**Corrosion level**	**Mass loss due to corrosion (%)**	**Width of longitudinal crack due to corrosion (mm)**	**Chloride ion content at rebar level (%)**	**Bond strength (MPa)**
C3-1A	0.00	0.00	0.00	0.00	12.22
C3-2A	0.00	0.00	0.00	0.00	12.00
C3-6A	1.00	2.11	0.00	0.00	12.50
C3-3A	2.00	5.50	0.30	0.10	8.64
C3-7A	3.00	6.00	0.40	0.13	8.12
C3-5A	4.00	7.00	0.60	0.14	7.63
C3-8A	5.00	7.50	0.90	0.15	7.24
C3-4A	6.00	8.00	2.40	0.29	7.17
C3-1B	0.00	0.00	0.00	0.00	10.33
C3-2B	0.00	0.00	0.00	0.00	10.56
C3-6B	1.00	1.68	0.00	0.00	11.52
C3-3B	2.00	3.90	0.20	0.04	8.70
C3-7B	3.00	4.40	0.90	0.08	8.00
C3-5B	4.00	7.70	1.00	0.23	6.08
C3-8B	5.00	7.20	1.40	0.25	5.09
C3-4B	6.00	10.60	4.00	0.40	3.39
C3-1C	0.00	0.00	0.00	0.00	9.37
C3-2C	0.00	0.00	0.00	0.00	8.64
C3-7C	1.00	0.95	0.00	0.01	9.60
C3-3C	2.00	1.90	0.08	0.01	8.71
C3-8C	3.00	4.15	0.40	0.07	5.64
C3-5C	4.00	4.45	0.60	0.08	5.44
C3-4C	5.00	7.56	1.60	0.26	3.97
C3-6C	6.00	8.32	2.00	0.49	3.71
C3-1D	0.00	0.00	0.00	0.00	4.53
C3-2D	0.00	0.00	0.00	0.00	4.34
C3-6D	1.00	0.53	0.00	0.01	5.03
C3-8D	2.00	1.00	0.20	0.02	4.26
C3-5D	3.00	2.30	1.20	0.08	3.20
C3-3D	4.00	3.00	1.60	0.29	2.83
C3-4D	5.00	3.40	3.00	0.48	2.42

Table 8.4: Test data for NPC with 0.32 w/c ratio concrete pullout specimen					
Specimen #	**Corrosion level**	**Mass loss due to corrosion (%)**	**Width of longitudinal crack due to corrosion (mm)**	**Chloride ion content at rebar level (%)**	**Bond strength (MPa)**
C4-1A	0.00	0.00	0.00	0.00	15.00
C4-2A	0.00	0.00	0.00	0.00	14.75
C4-4A	1.00	3.80	0.00	0.01	12.89
C4-3A	2.00	10.95	0.30	0.16	9.60
C4-5A	3.00	11.00	0.40	0.18	9.60
C4-7A	4.00	12.96	1.80	0.30	8.23
C4-8A	5.00	13.80	2.00	0.41	7.63
C4-6A	6.00	24.70	4.00	0.60	3.52
C4-1B	0.00	0.00	0.00	0.00	10.96
C4-2B	0.00	0.00	0.00	0.00	11.64
C4-4B	1.00	2.65	0.00	0.01	12.60
C4-7B	2.00	8.46	0.50	0.13	8.08
C4-5B	3.00	9.23	0.65	0.15	7.78
C4-6B	4.00	10.43	0.80	0.17	7.68
C4-8B	5.00	18.70	3.20	0.45	3.84
C4-3B	6.00	24.30	5.00	0.82	1.14
C4-1C	0.00	0.00	0.00	0.00	9.28
C4-2C	0.00	0.00	0.00	0.00	9.79
C4-6C	1.00	1.61	0.00	0.00	9.95
C4-8C	2.00	2.85	0.20	0.06	9.45
C4-5C	3.00	7.26	0.40	0.13	6.37
C4-4C	4.00	12.50	0.90	0.23	3.84
C4-3C	5.00	18.25	3.00	0.48	1.47
C4-7C	6.00	19.94	4.00	0.59	1.28
C4-1D	0.00	0.00	0.00	0.00	4.81
C4-2D	0.00	0.00	0.00	0.00	5.11
C4-5D	1.00	0.42	0.00	0.01	5.31
C4-6D	2.00	1.30	0.20	0.03	4.66
C4-3D	3.00	2.20	0.80	0.04	3.76
C4-7D	4.00	3.78	0.90	0.08	2.94
C4-8D	5.00	8.53	4.00	0.49	1.41
C4-4D	6.00	9.55	5.00	0.66	1.18

Table 8.5: Test data for NPC with 0.42 w/c ratio concrete pullout specimen					
Specimen #	**Corrosion level**	**Mass loss due to corrosion (%)**	**Width of longitudinal crack due to corrosion (mm)**	**Chloride ion content at rebar level (%)**	**Bond strength (MPa)**
C5-1A	0.00	0.00	0.00	0.00	13.51
C5-2A	0.00	0.00	0.00	0.00	13.85
C5-5A	1.00	3.70	0.00	0.02	11.28
C5-4A	2.00	9.93	0.20	0.15	9.60
C5-7A	3.00	12.82	0.35	0.21	8.30
C5-8A	4.00	19.40	1.20	0.63	5.78
C5-6A	5.00	20.40	2.00	0.98	4.48
C5-3A	6.00	21.11	2.40	1.59	3.74
C5-1B	0.00	0.00	0.00	0.00	9.53
C5-2B	0.00	0.00	0.00	0.00	9.80
C5-5B	1.00	2.25	0.00	0.04	11.52
C5-7B	2.00	4.95	0.08	0.13	9.79
C5-8B	3.00	9.86	0.60	0.17	7.74
C5-3B	4.00	18.34	1.20	1.00	3.20
C5-6B	5.00	20.85	2.00	1.23	2.58
C5-4B	6.00	21.85	3.00	1.45	2.18
C5-1C	0.00	0.00	0.00	0.00	9.12
C5-2C	0.00	0.00	0.00	0.00	8.60
C5-5C	1.00	1.30	0.00	0.01	9.60
C5-7C	2.00	2.50	0.00	0.10	9.60
C5-8C	3.00	5.10	0.20	0.15	8.14
C5-6C	4.00	13.23	1.00	0.82	4.16
C5-3C	5.00	17.56	1.40	0.97	3.13
C5-4C	6.00	28.48	3.00	1.13	0.64
C5-1D	0.00	0.00	0.00	0.00	3.26
C5-2D	0.00	0.00	0.00	0.00	3.13
C5-5D	1.00	0.50	0.00	0.09	3.71
C5-8D	2.00	2.17	1.60	0.09	2.88
C5-4D	3.00	2.53	3.00	0.39	2.37
C5-3D	4.00	9.74	5.00	0.48	0.97
C5-7D	5.00	9.95	6.00	1.50	0.70
C5-6D	6.00	24.01		2.30	

Table 8.6: Test data for High Alumina Cement concrete (HAC) pullout specimen					
Specimen #	**Corrosion level**	**Mass loss due to corrosion (%)**	**Width of longitudinal crack due to corrosion (mm)**	**Chloride ion content at rebar level (%)**	**Bond strength (MPa)**
C6-1A	0.00	0.00	0.00	0.00	7.98
C6-2A	0.00	0.00	0.00	0.00	8.13
C6-5A	1.00	0.63	0.00	0.00	8.36
C6-5A	1.00	0.63	0.00	0.01	8.36
C6-3A	3.00	7.40	0.60	0.10	7.20
C6-7A	4.00	10.70	0.80	0.30	5.40
C6-6A	5.00	24.00	3.00	0.70	1.02
C6-6A	6.00				
C6-1B	0.00	0.00	0.00	0.00	7.65
C6-2B	0.00	0.00	0.00	0.00	6.65
C6-4B	1.00	1.75	0.00	0.03	8.85
C6-3B	2.00	6.52	0.40	0.10	6.18
C6-7B	3.00	7.48	0.60	0.19	5.75
C6-5B	4.00	7.74	0.64	0.25	5.12
C6-6B	5.00	10.40	0.90	0.34	4.82
C6-8B	6.00	12.56	1.40	0.52	3.30
C6-1C	0.00	0.00	0.00	0.00	7.50
C6-2C	0.00	0.00	0.00	0.00	7.68
C6-4C	1.00	0.23	0.00	0.03	8.64
C6-7C	2.00	1.00	0.08	0.07	8.59
C6-6C	3.00	2.98	0.80	0.29	6.31
C6-8C	4.00	6.97	1.40	0.40	5.12
C6-3C	5.00	7.20	1.80	0.43	5.12
C6-5C	6.00	10.48	2.00	0.55	4.48
C6-1D	0.00	0.00	0.00	0.00	4.70
C6-2D	0.00	0.00	0.00	0.00	4.16
C6-5D	1.00	0.63	0.00	0.01	4.67
C6-8D	2.00	3.90	0.60	0.03	3.77
C6-7D	3.00	5.50	0.80	0.17	3.06
C6-4D	4.00	8.20	2.00	0.28	2.05
C6-3D	5.00	11.53	3.00	0.84	0.90
C6-6D	6.00	12.23	4.00	1.87	0.81

Table 8.7: Bond stress equations for pullout tests.

Concrete mixture	Bond strength of a corroded steel bar *(u)*	Correlation coefficient (r^2)
Point Tupper fly ash concrete	$u = \frac{P}{l\pi d_b} - 0.34(\%ML)$	0.95
Thunder Bay fly ash concrete	$u = \frac{P}{l\pi d_b} - 0.45(\%ML)$	0.93
Sundance fly ash concrete	$u = \frac{P}{l\pi d_b} - 0.58(\%ML)$	0.90
NPC (w/c ratio = 0.32)	$u = \frac{P}{l\pi d_b} - 0.42(\%ML)$	0.97
NPC (w/c ratio = 0.42)	$u = \frac{P}{l\pi d_b} - 0.33(\%ML)$	0.98
HAC (w/c ratio = 0.32)	$u = \frac{P}{l\pi d_b} - 0.31(\%ML)$	0.90

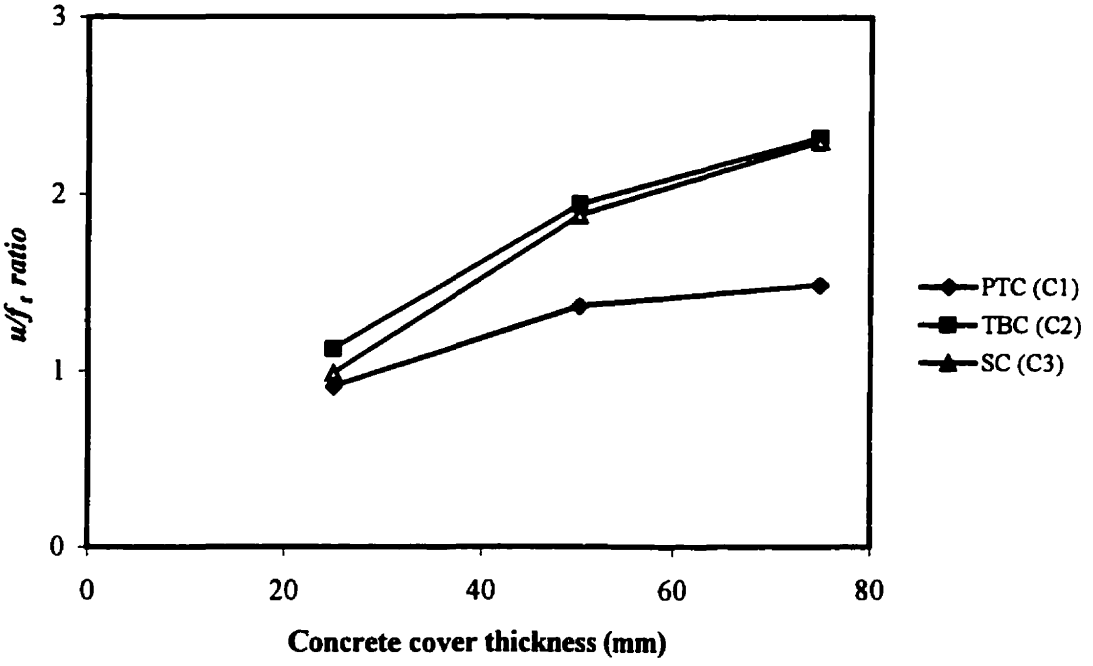

Fig. 8.1: Variation of u/f_t ratio with the concrete cover thickness, c, for fly ash concrete mixtures

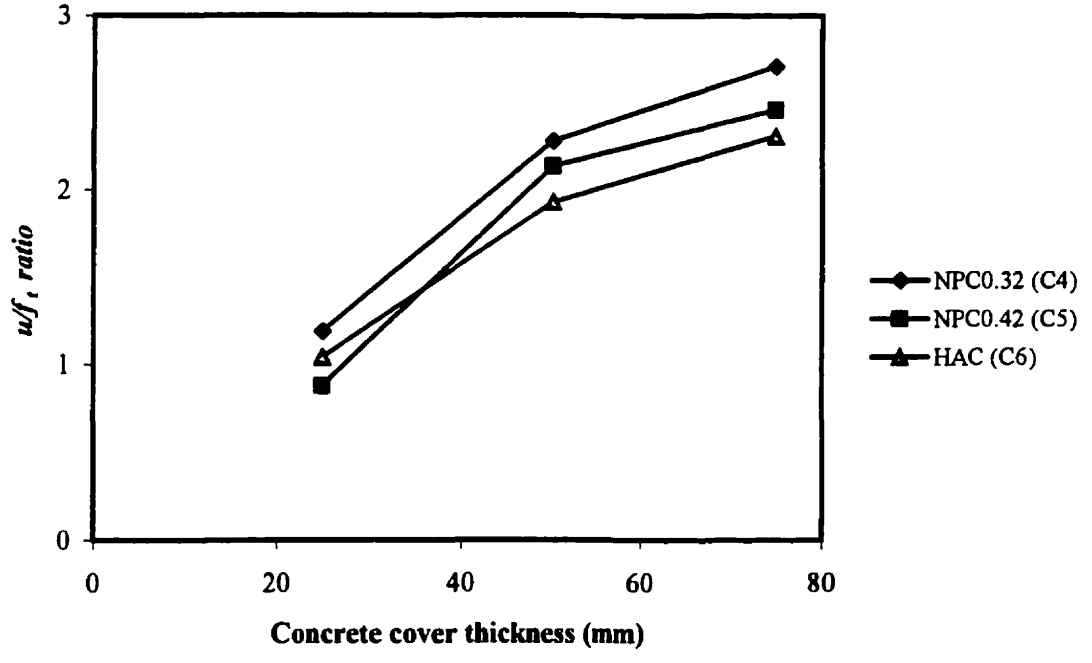

Fig. 8.2: Variation of u/f_t ratio with the concrete cover thickness, c, for NPC concretes and HAC concrete mixtures

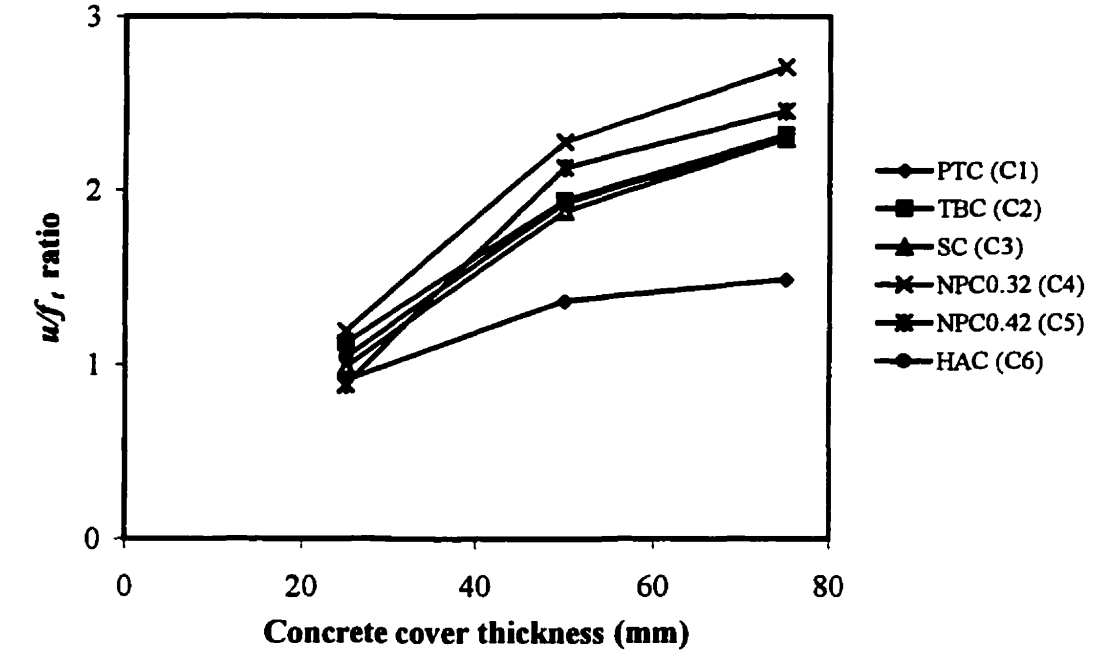

Fig. 8.3: Variation of u/ft ratio with the concrete cover thickness, c, for all of the concrete mixtures tested

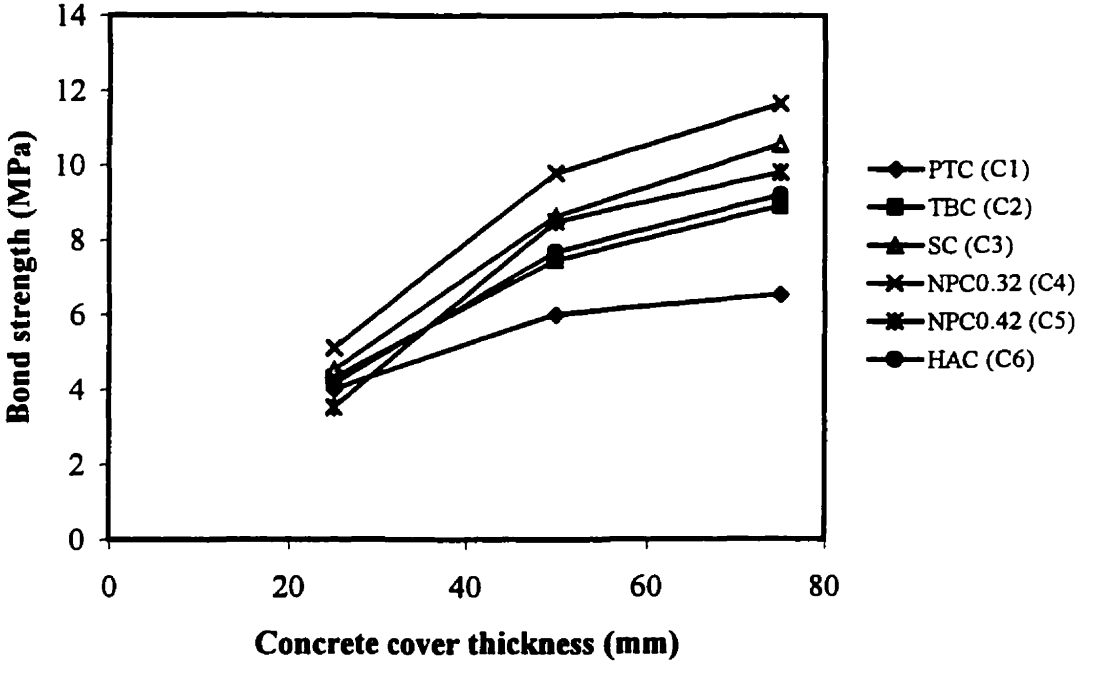

Fig. 8.4: Variation of bond strength with concrete cover thickness for all of the concrete mixtures tested

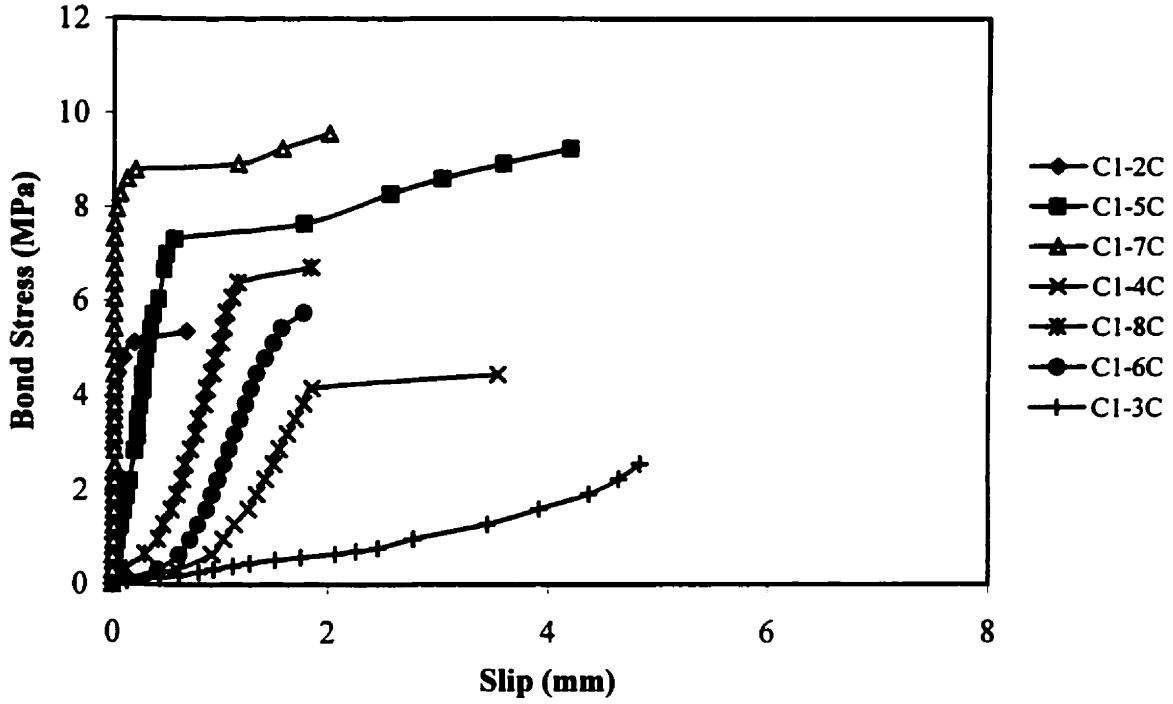

Fig. 8.5: Variation of bond stress with slip for Point Tupper fly ash concrete mix., cover thickness = 50mm for different levels of corrosion

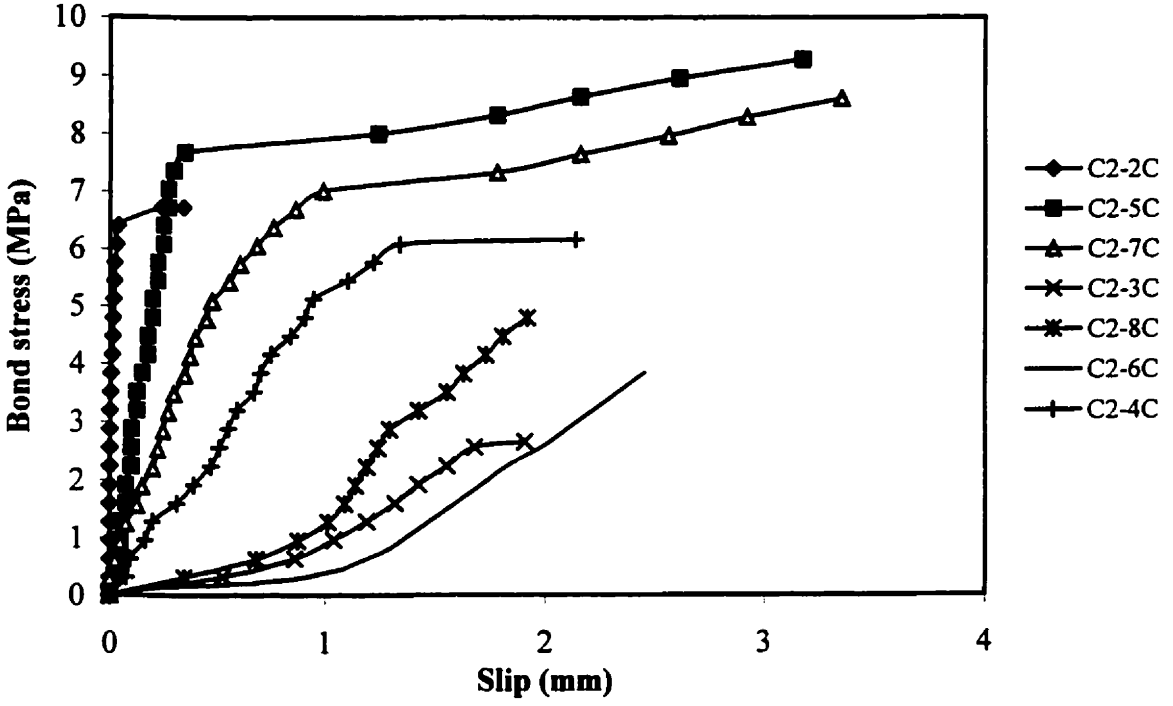

Fig. 8.6: Variation of bond stress with slip for Thunder Bay fly ash concrete mix., cover thickness = 50mm for different levels of corrosion

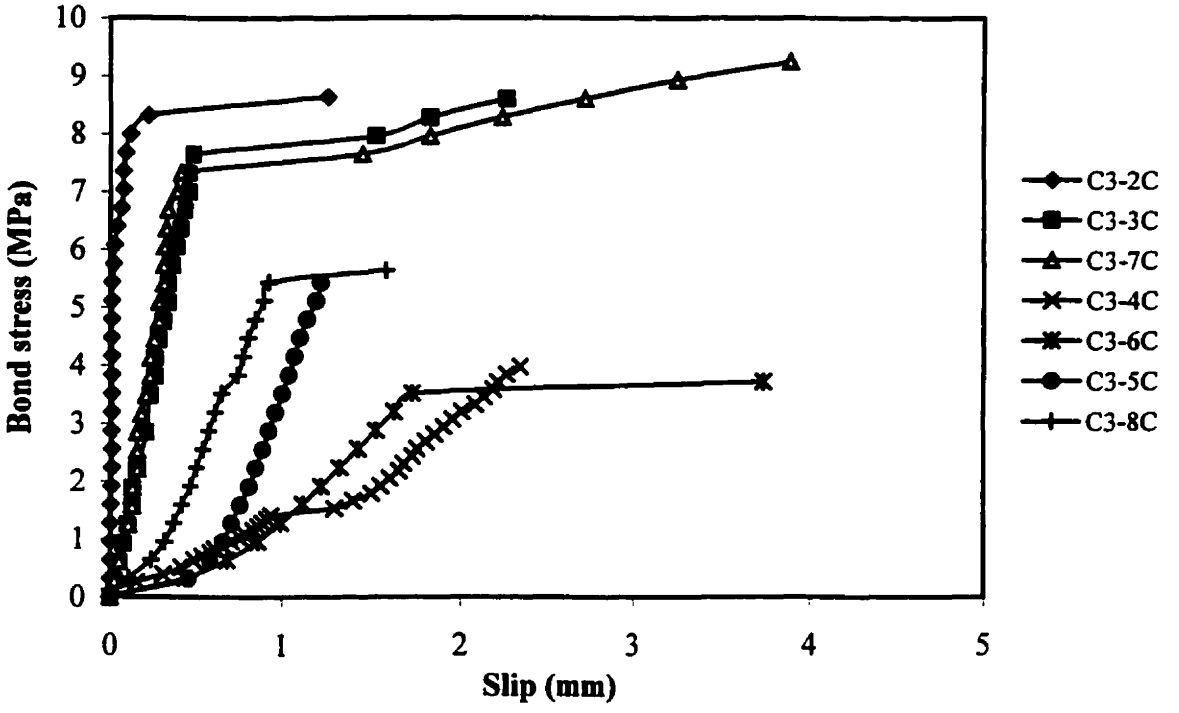

Fig. 8.7: Variation of bond stress with slip for Sundance fly ash concrete mix., cover thickness = 50mm for different levels of corrosion

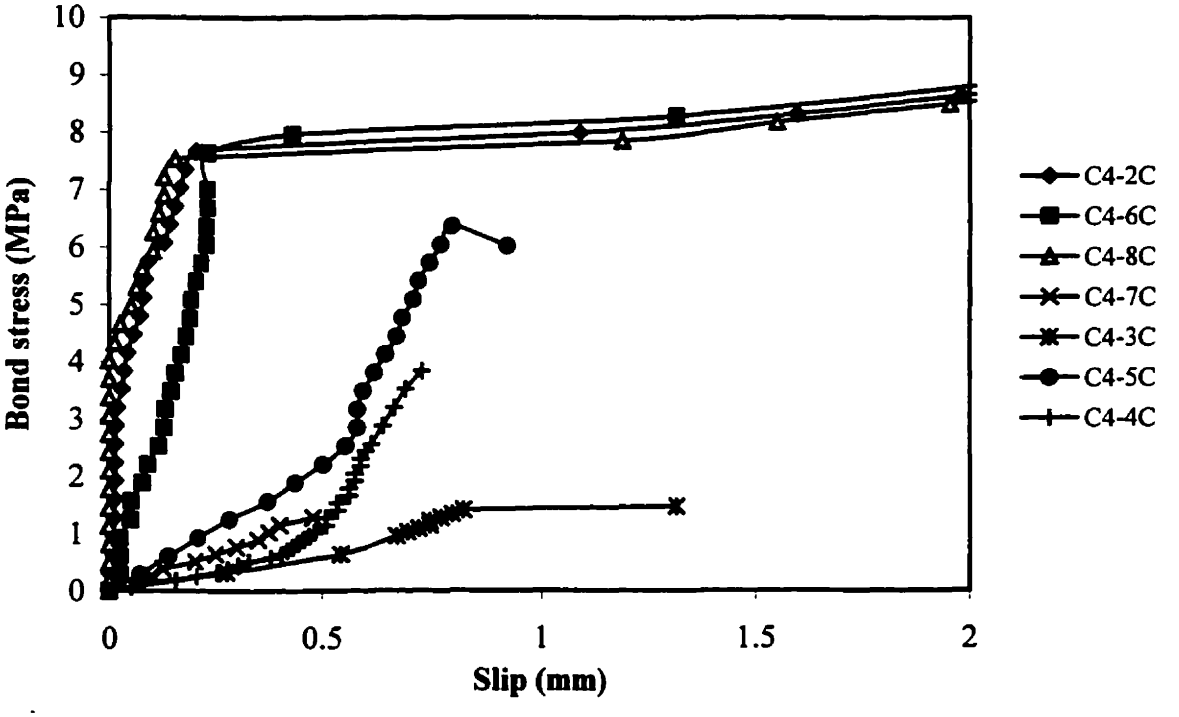

Fig. 8.8: Variation of bond stress with slip for NPC with 0.32 w/c concrete mix., cover thickness = 50mm for different levels of corrosion

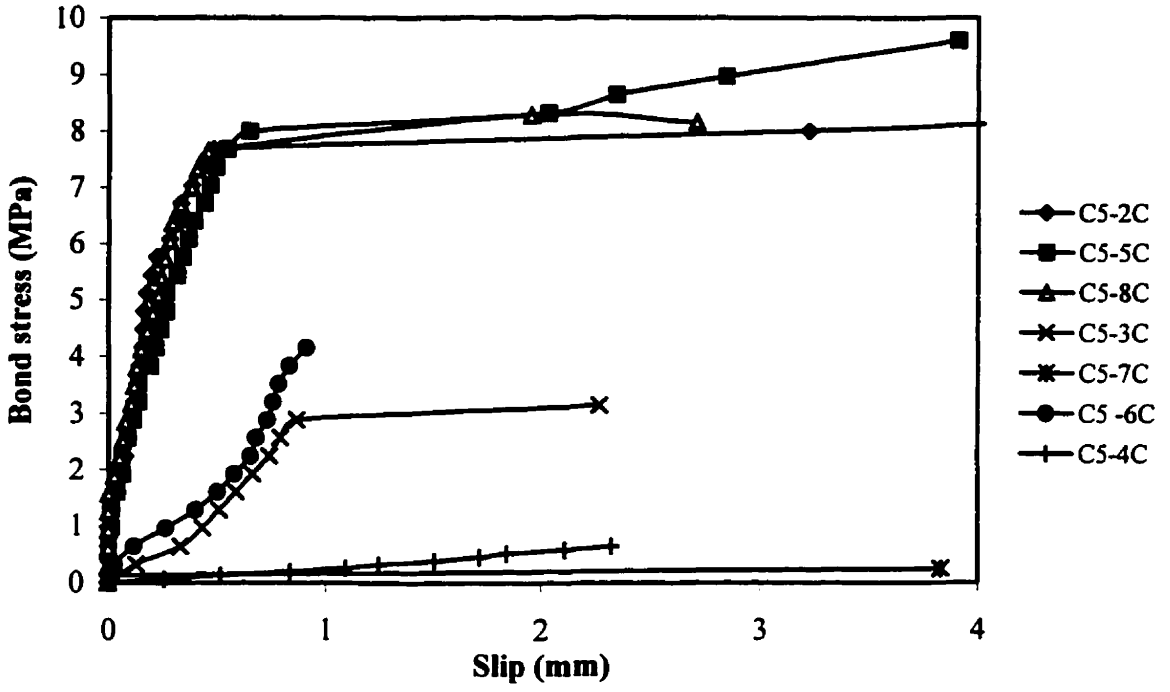

Fig. 8.9: Variation of bond stress with slip for NPC with 0.42 w/c concrete mix., cover thickness = 50mm for different levels of corrosion

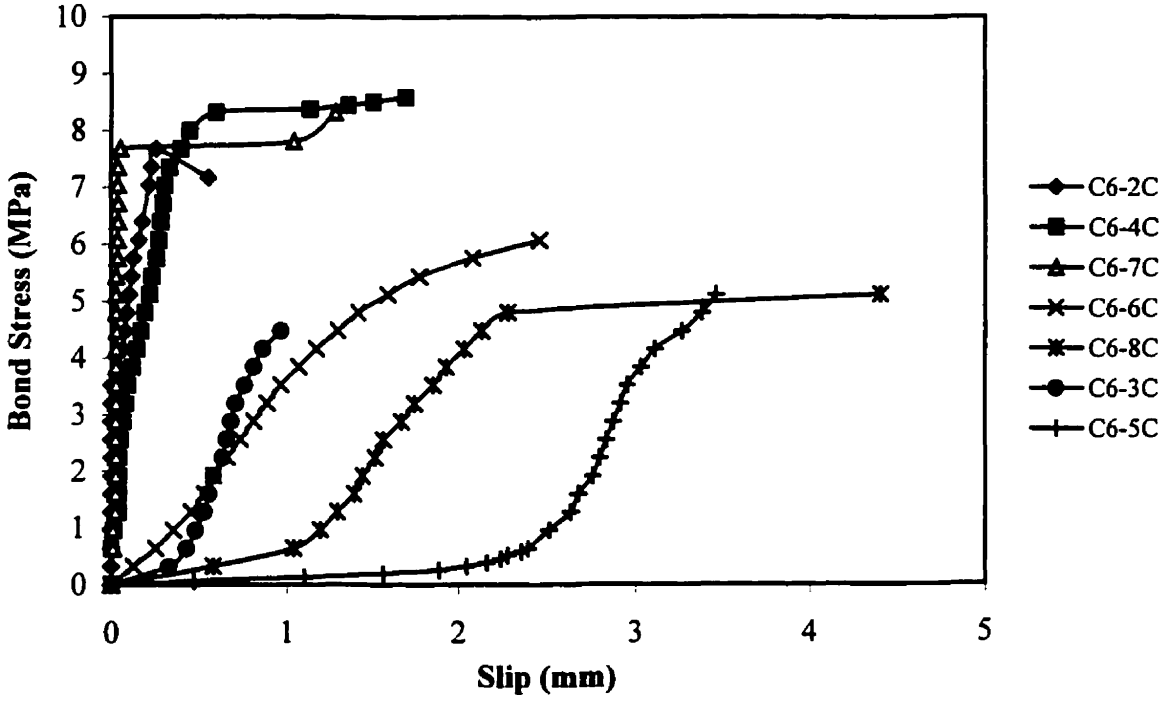

Fig. 8.10: Variation of bond stress with slip for High Alumina Cement concrete mix., cover thickness = 50mm for different levels of corrosion

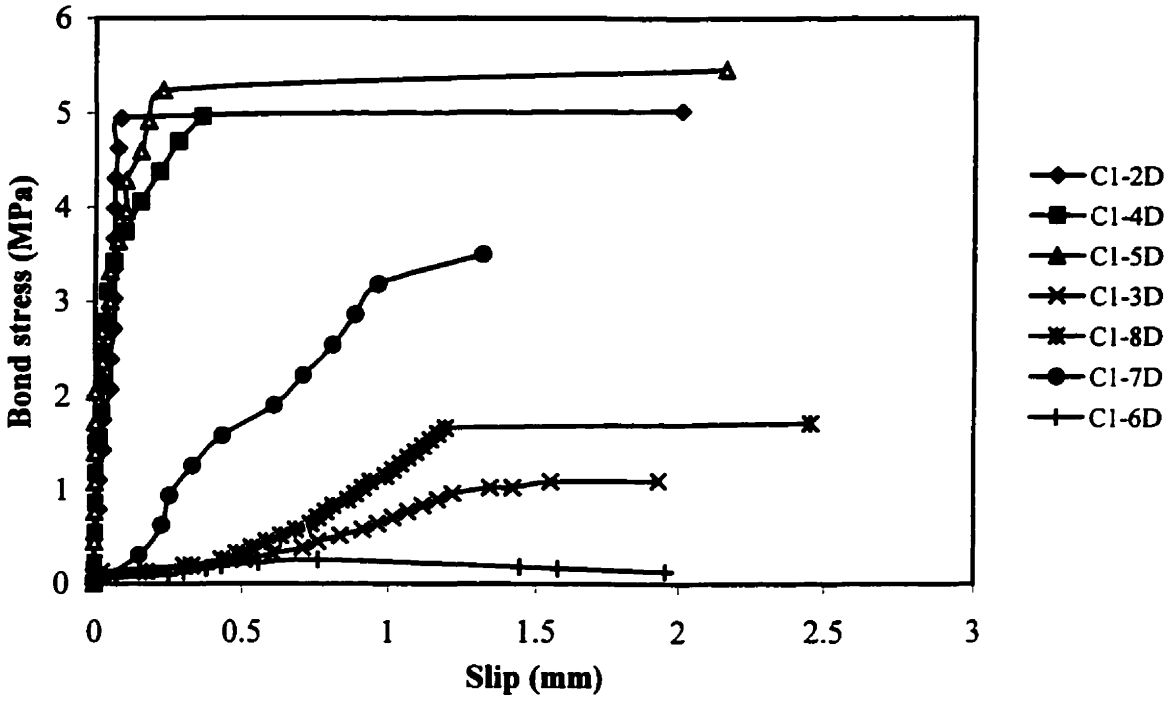

Fig. 8.11: Variation of bond stress with slip for Point Tupper fly ash concrete mix., cover thickness = 25mm for different levels of corrosion

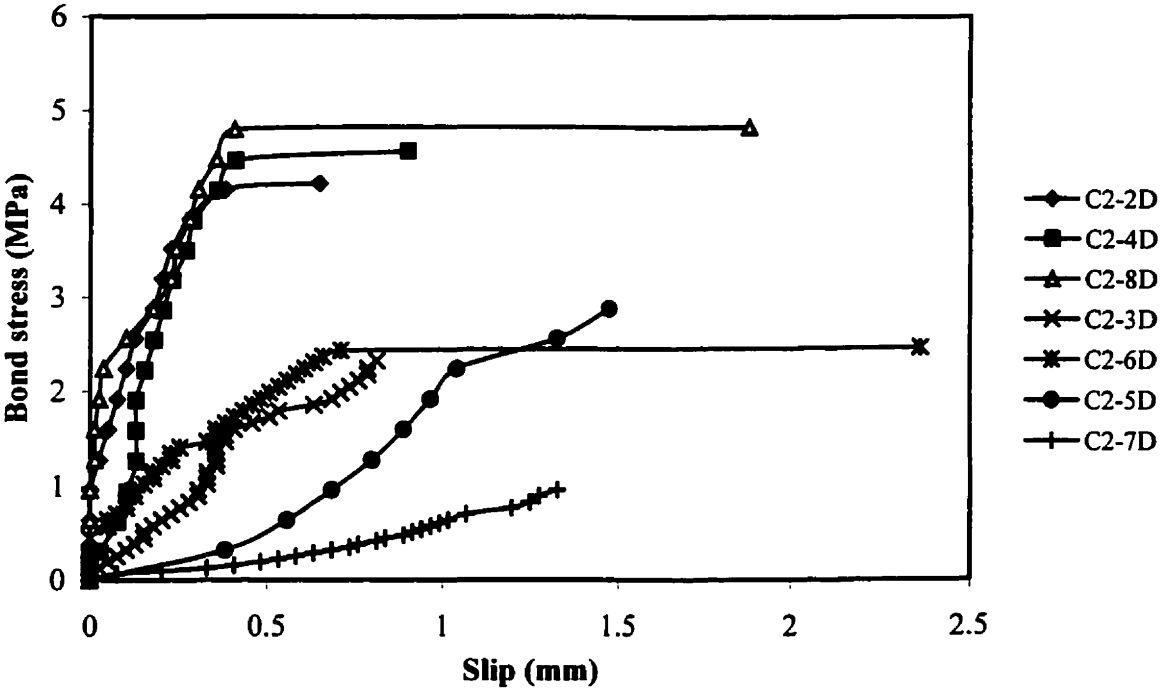

Fig. 8.12: Variation of bond stress with slip for Thunder Bay fly ash concrete mix., cover thickness = 25mm for different levels of corrosion

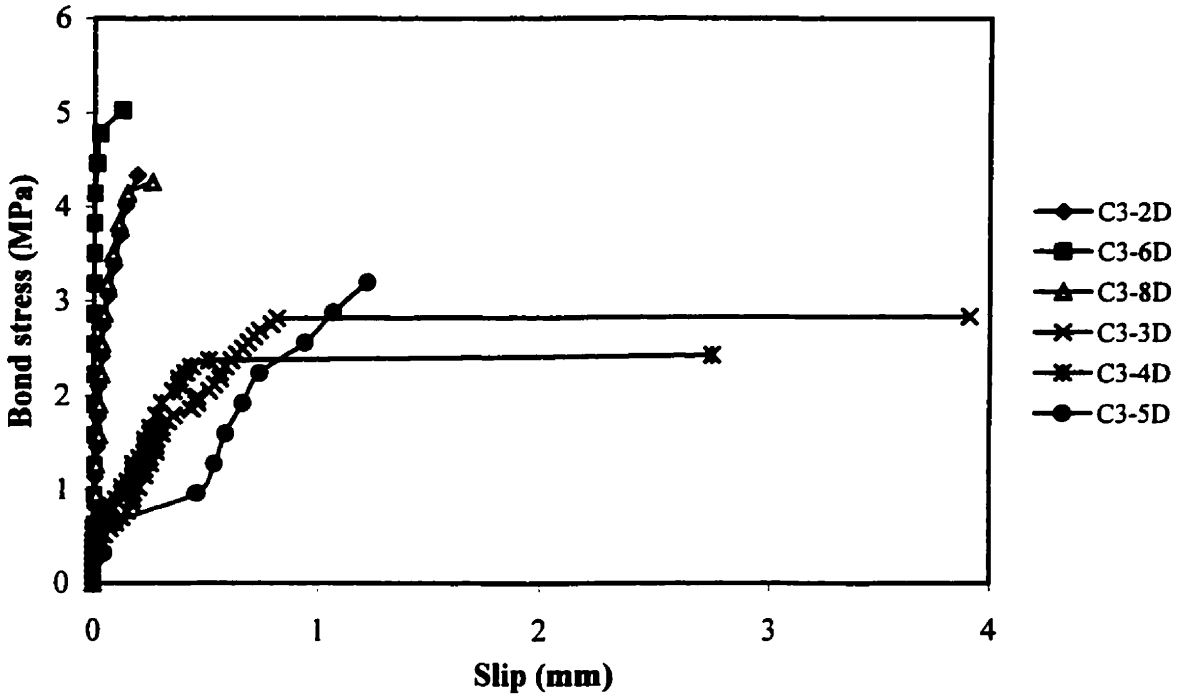

Fig. 8.13: Variation of bond stress with slip for Sundance fly ash concrete mix., cover thickness = 25mm for different levels of corrosion

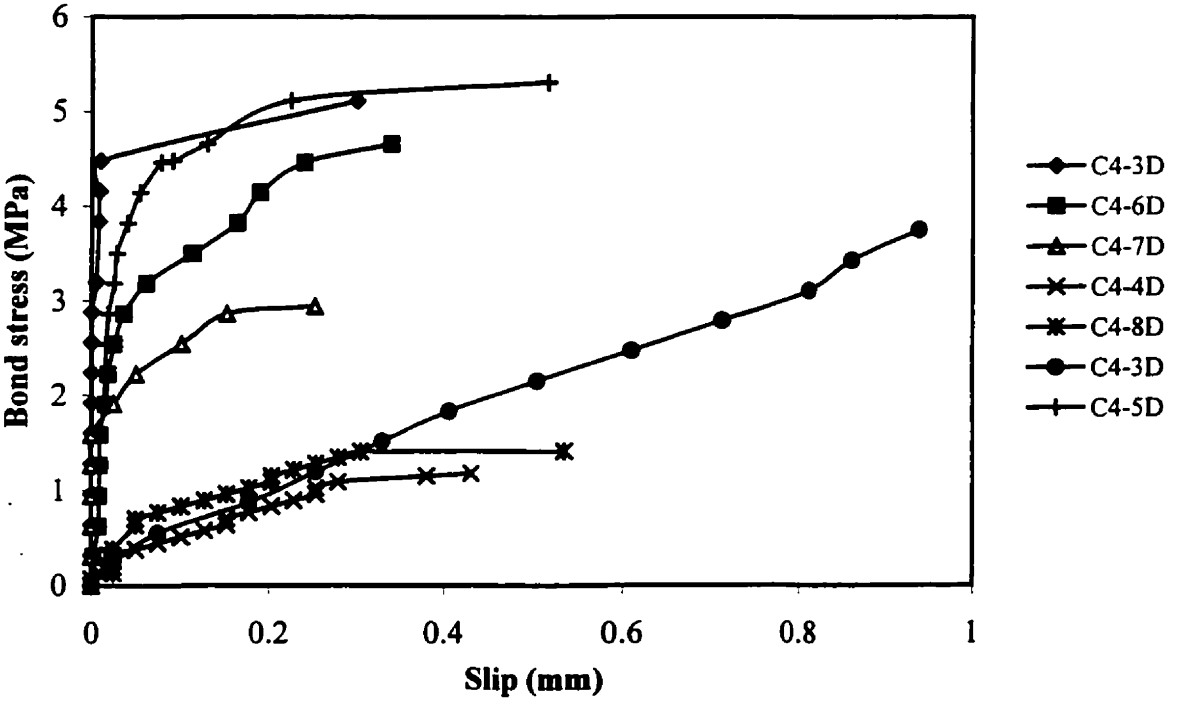

Fig. 8.14: Variation of bond stress with slip for NPC with 0.32 w/c concrete mix., cover thickness = 25mm for different levels of corrosion

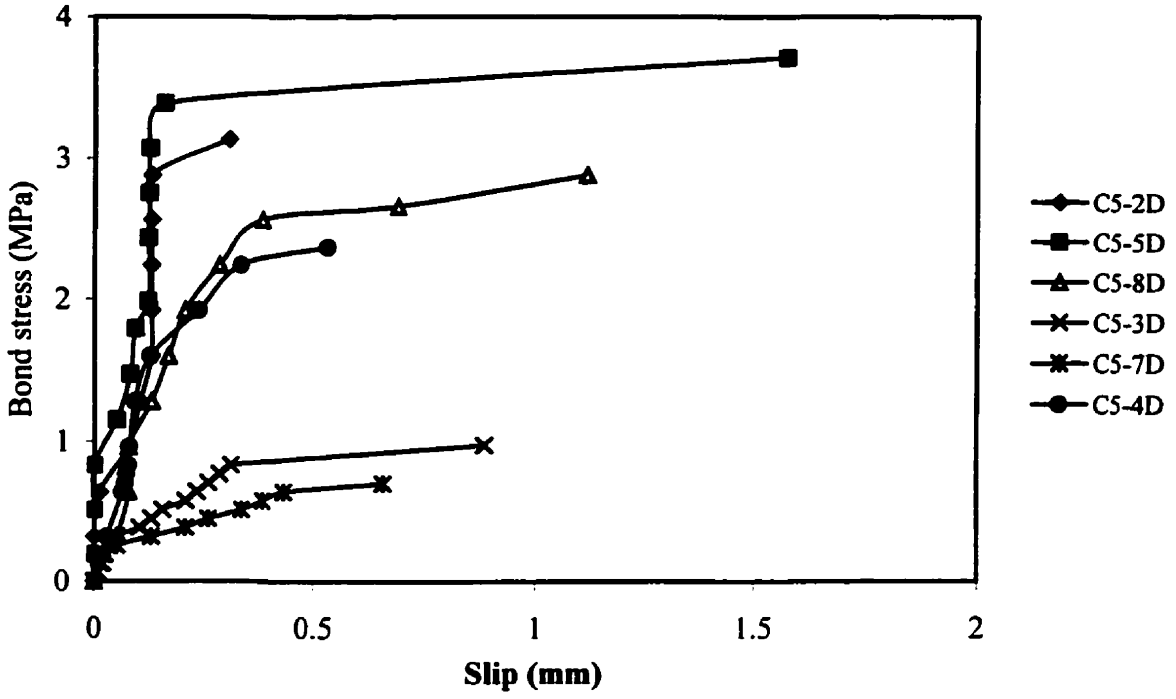

Fig. 8.15: Variation of bond stress with slip for NPC with 0.42 w/c concrete mix., cover thickness = 25mm for different levels of corrosion

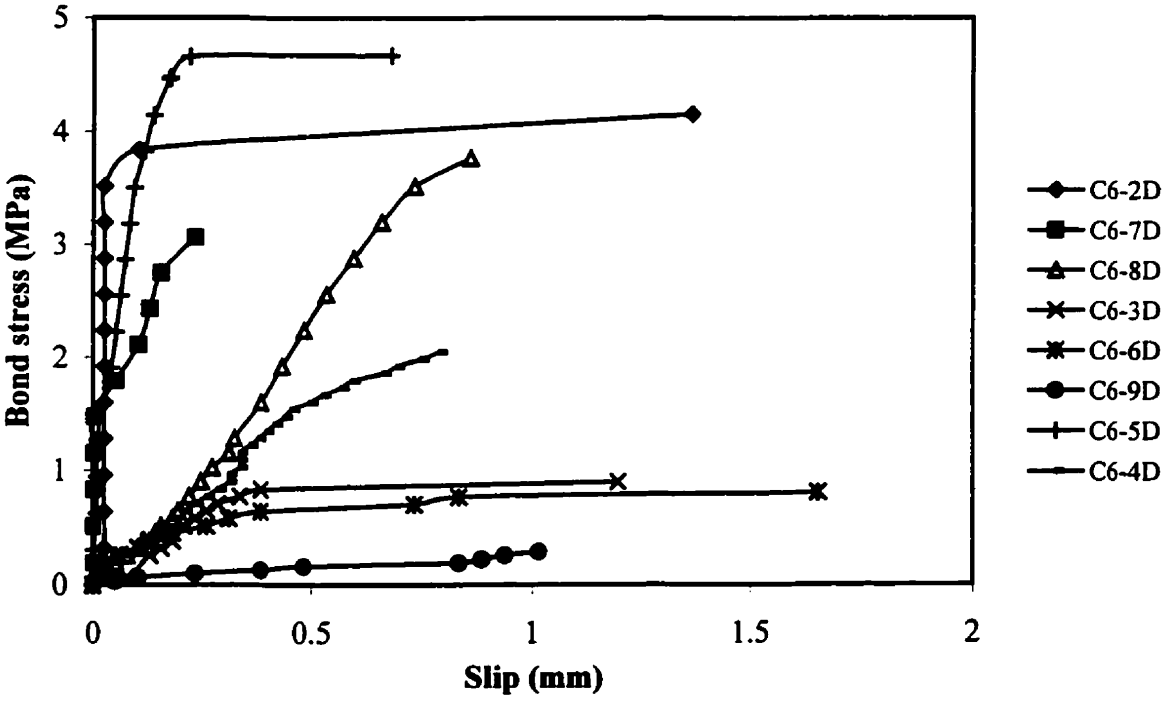

Fig. 8.16: Variation of bond stress with slip for High Alumina Cement concrete mix., cover thickness = 25mm for different levels of corrosion

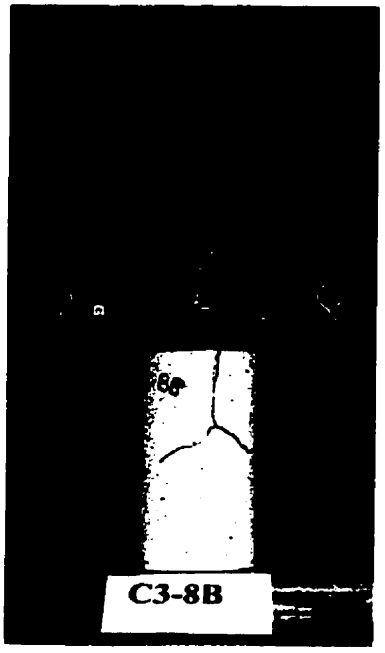

(a) moderate level of corrosion

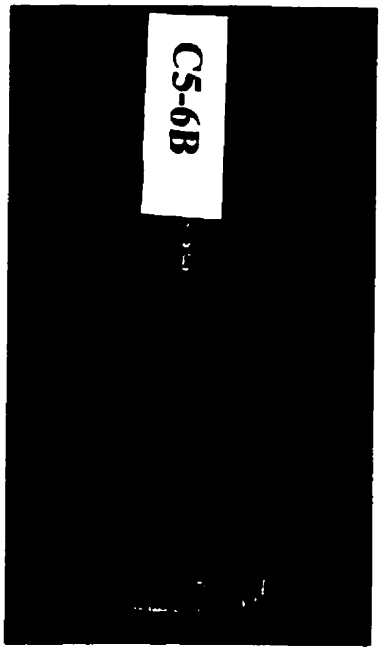

(b) Very advanced level of corrosion

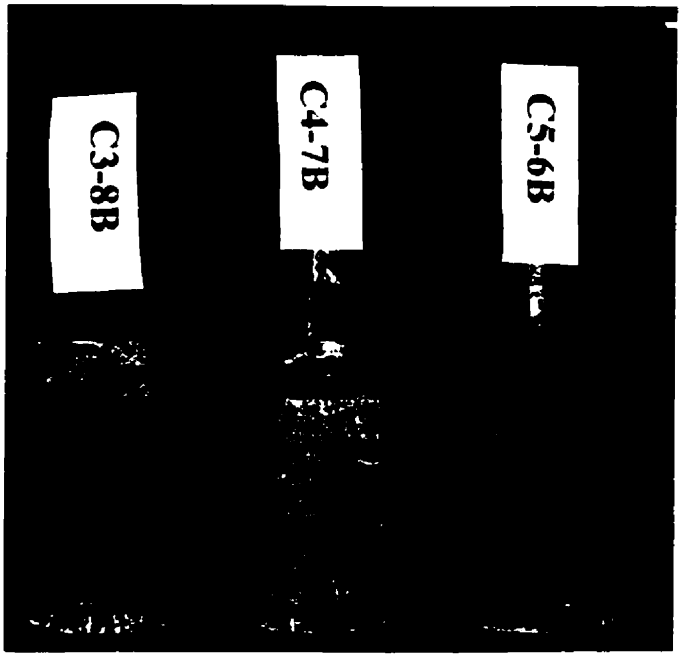

(c) Advanced level of corrosion

Figure 8.17: Influence of the different levels of corrosion on the specimen deterioration

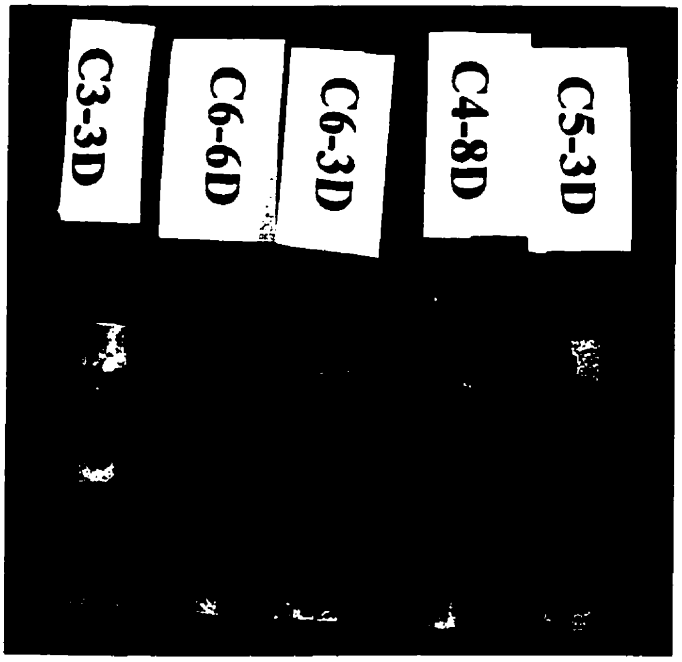

Figure 8.18: Very advanced level of corrosion in some pullout specimens

Figure 8.19: Severe localized corrosion "pitting" on the steel bar surface

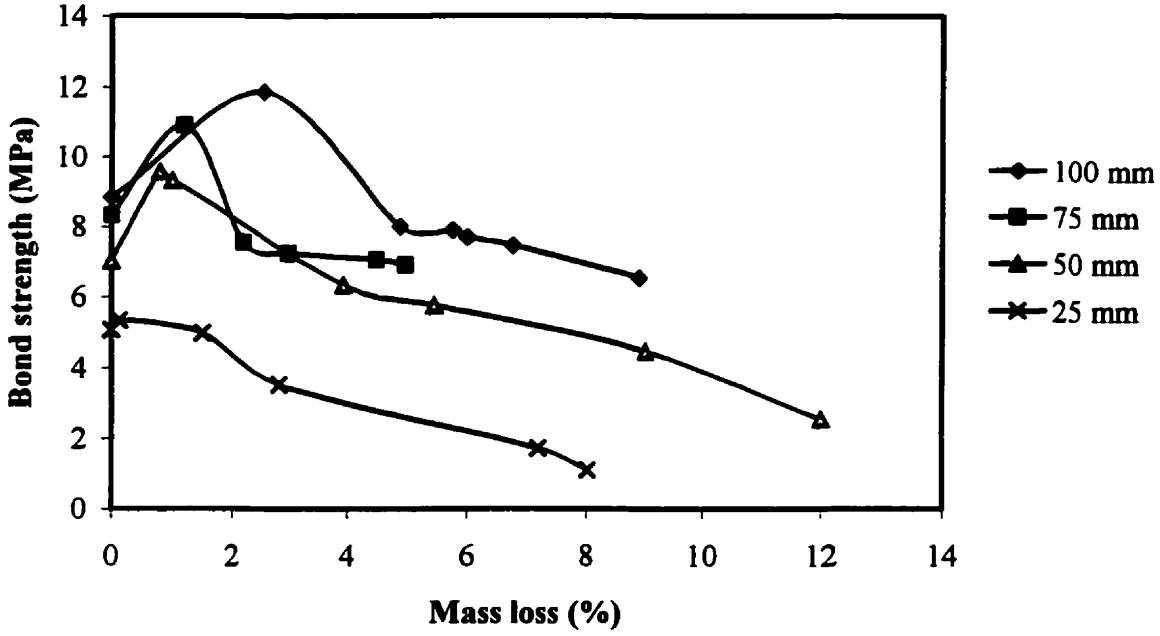

Fig. 8.20: Effect of corrosion on bond strength for Point Tupper concrete mix with different concrete cover thicknesses

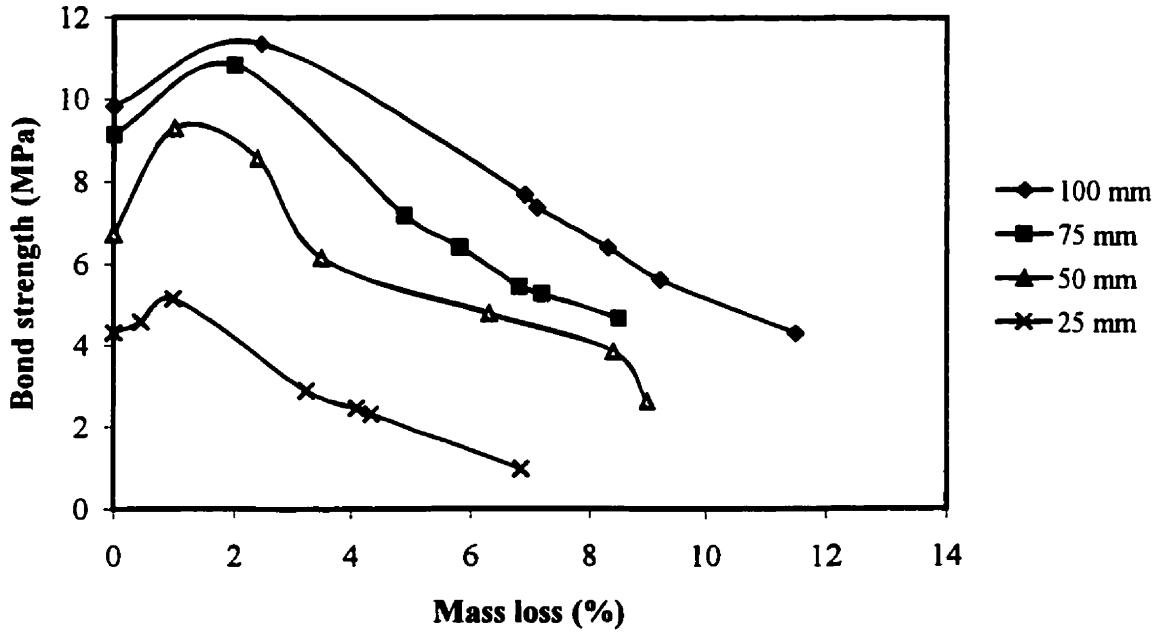

Fig. 8.21: Effect of corrosion on bond strength for Thunder Bay concrete mix with different concrete cover thicknesses

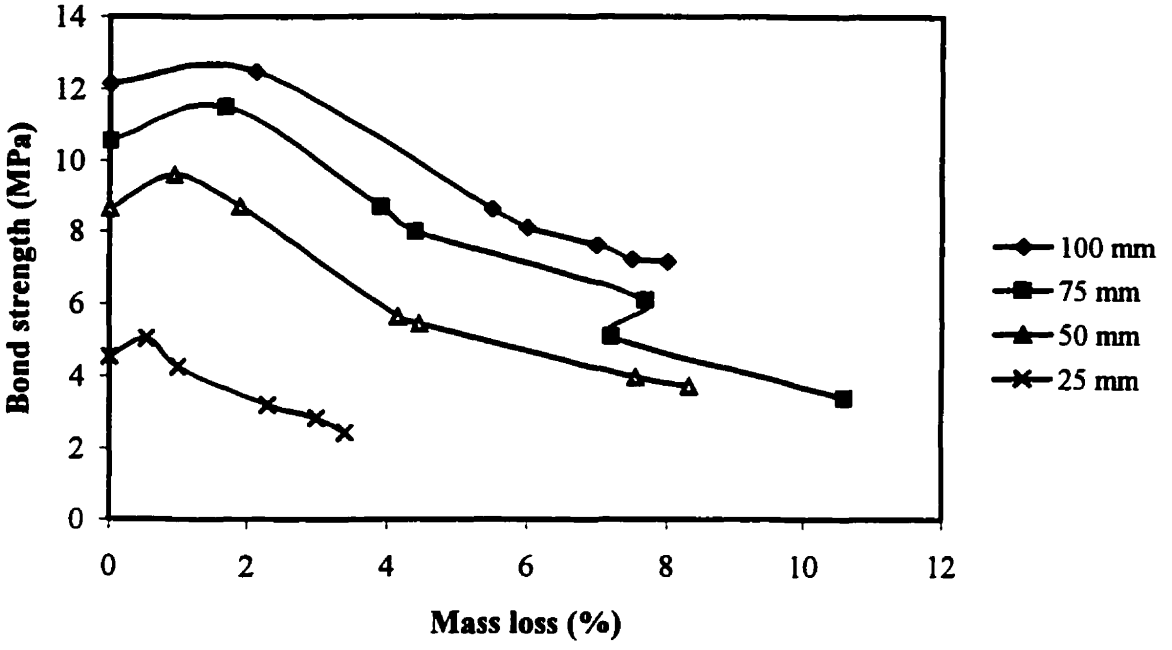

Fig. 8.22: Effect of corrosion on bond strength for Sundance concrete mix with different concrete cover thicknesses

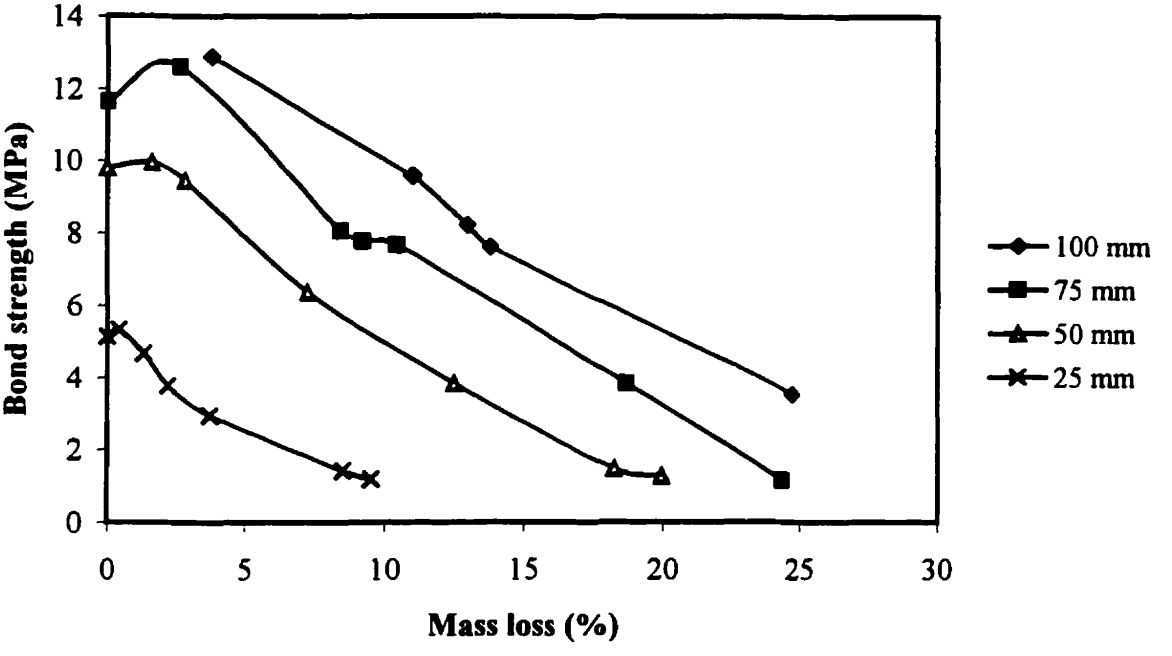

Fig. 8.23: Effect of corrosion on bond strength for NPC (0.32 w/c) concrete mix with different concrete cover thicknesses

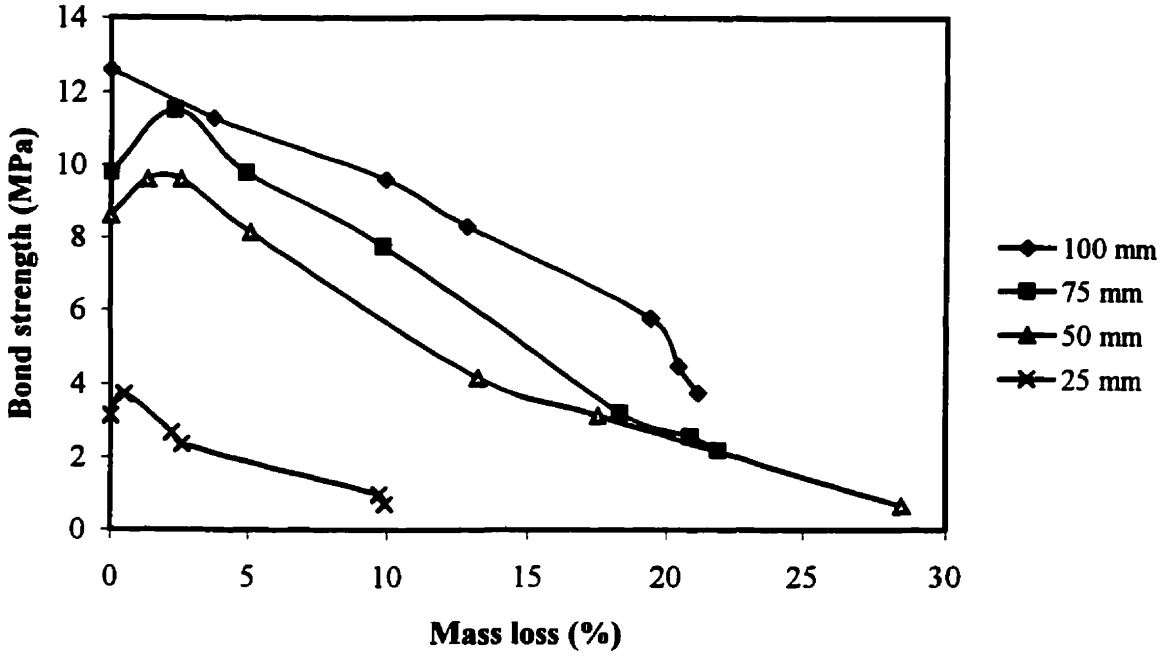

Fig. 8.24: Effect of corrosion on bond strength for NPC (0.42 w/c) concrete mix with different concrete cover thicknesses

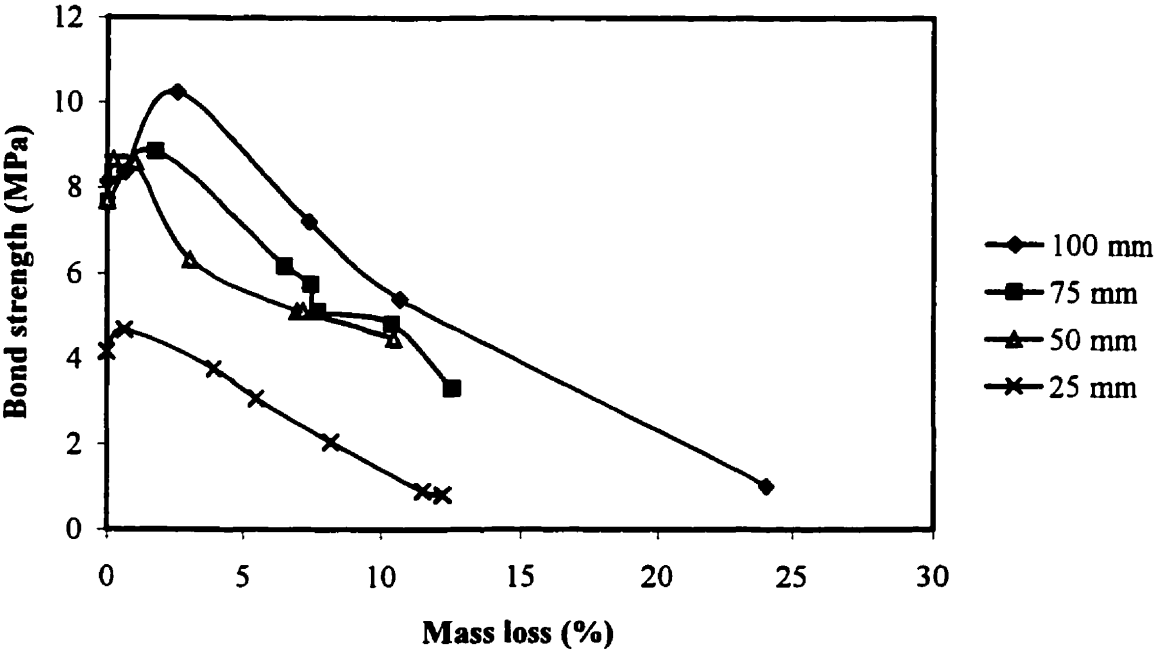

Fig. 8.25: Effect of corrosion on bond strength for HAC concrete mix with different concrete cover thicknesses

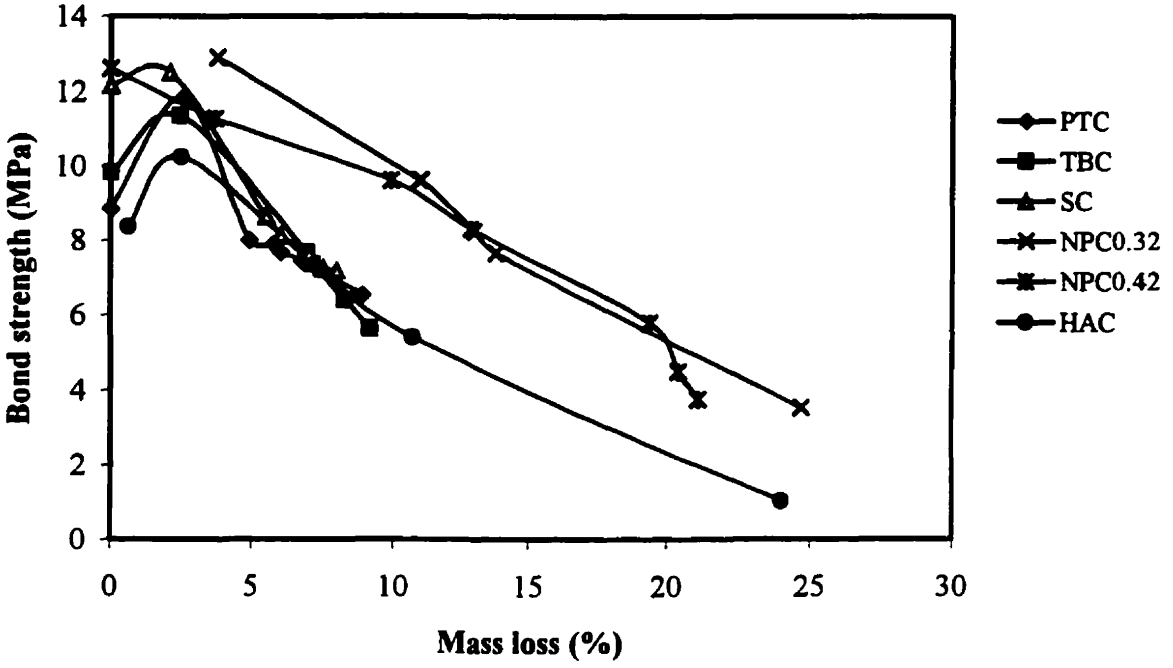

Fig. 8.26: Effect of corrosion on bond strength for 100 mm concrete cover thicknesses for different concretes

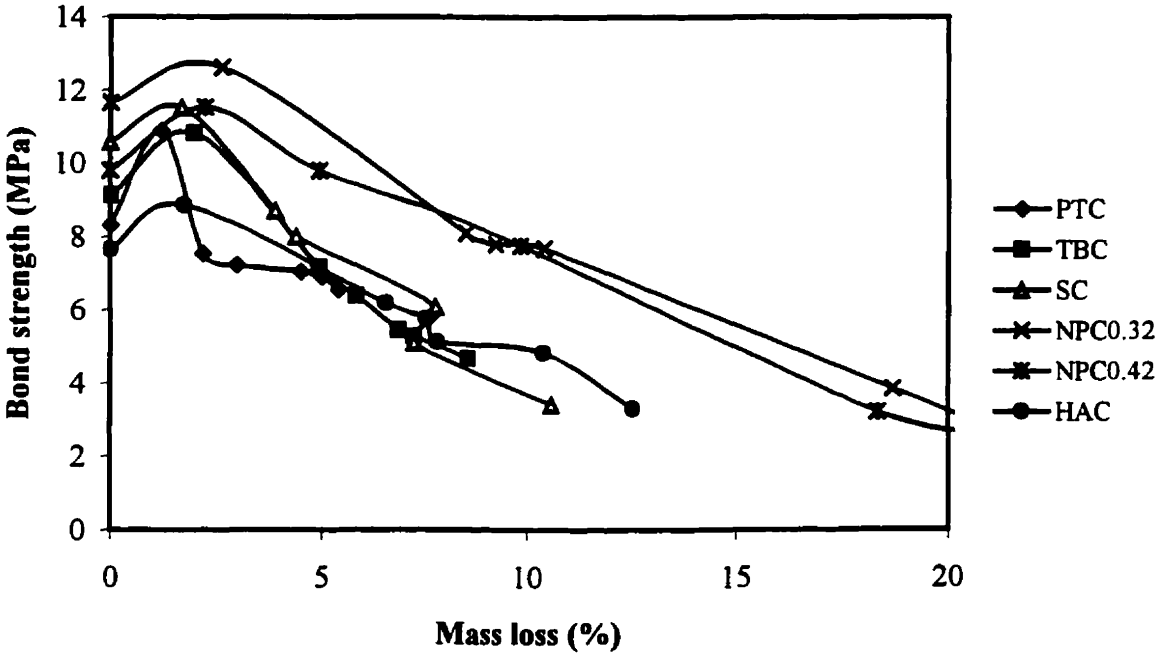

Fig. 8.27: Effect of corrosion on bond strength for 75 mm concrete cover thicknesses for different concretes

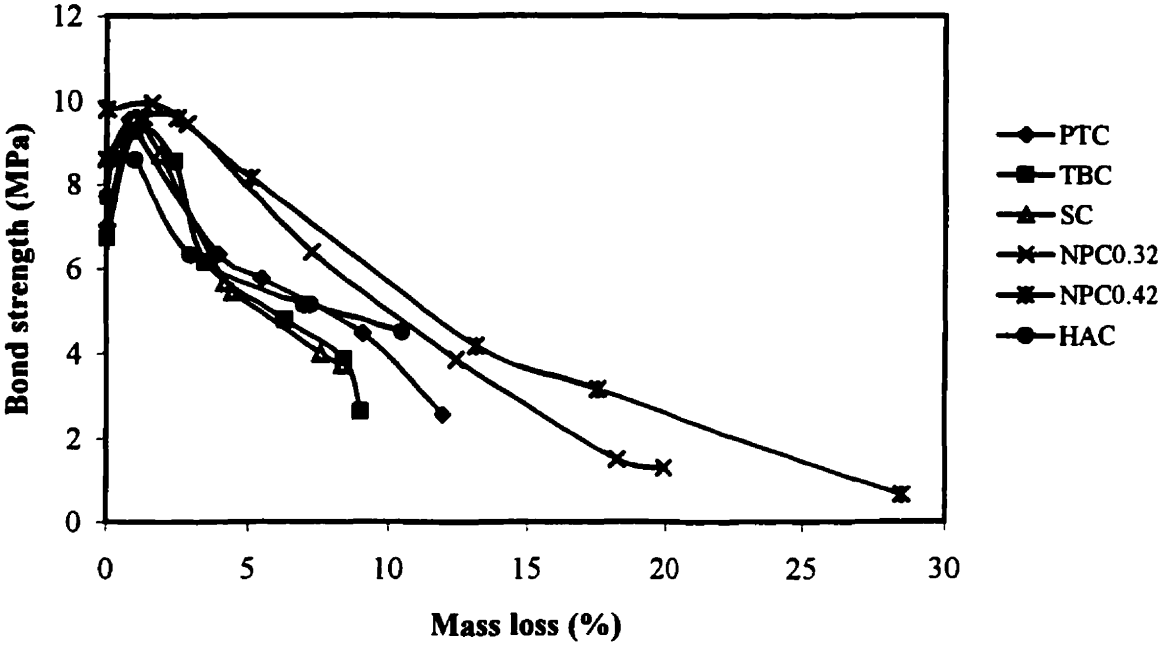

Fig. 8.28: Effect of corrosion on bond strength for 50mm concrete cover thicknesses for different concretes

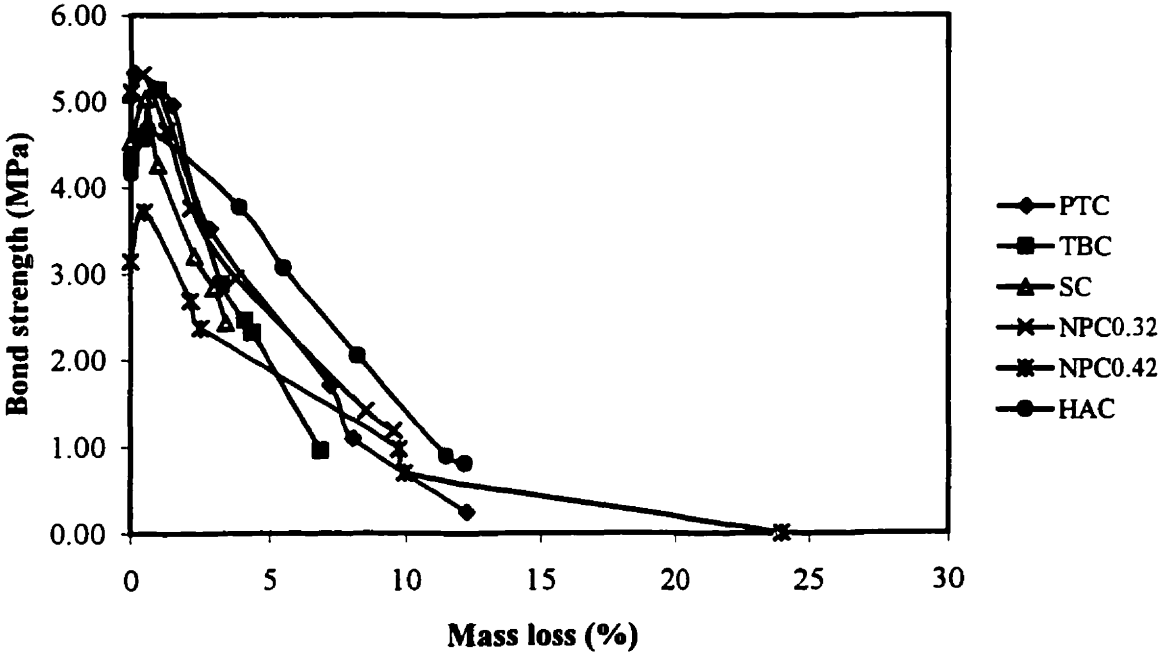

Fig. 8.29: Effect of corrosion on bond strength for 25 mm concrete cover thicknesses for different concretes

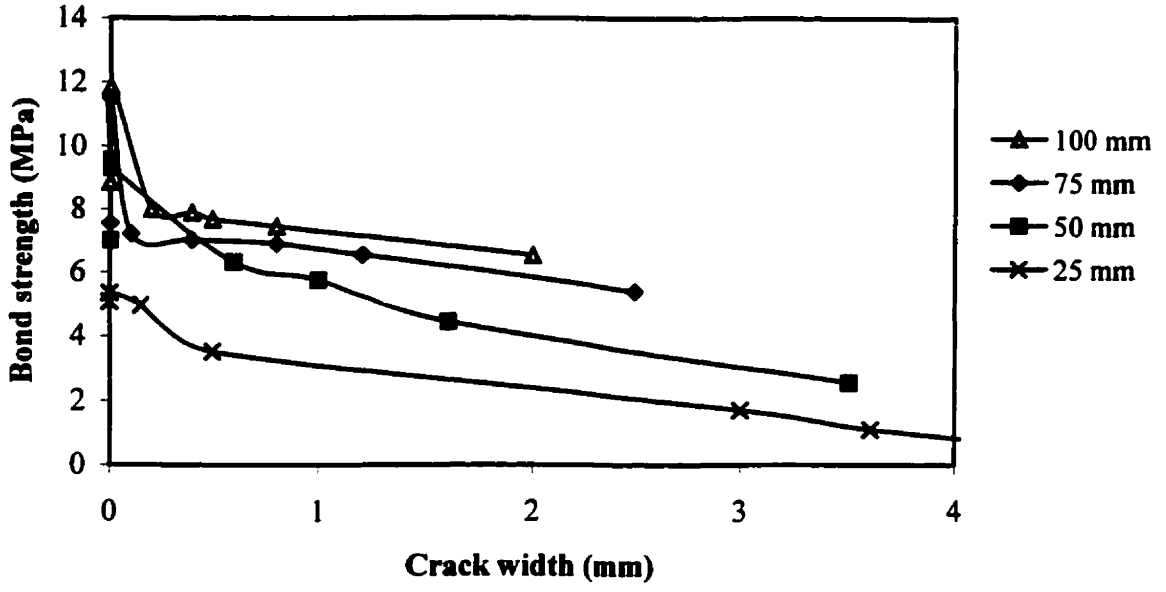

Fig. 8.30: Effect of crack width on bond strength for Point Tupper concrete mixture for different concrete cover thicknesses

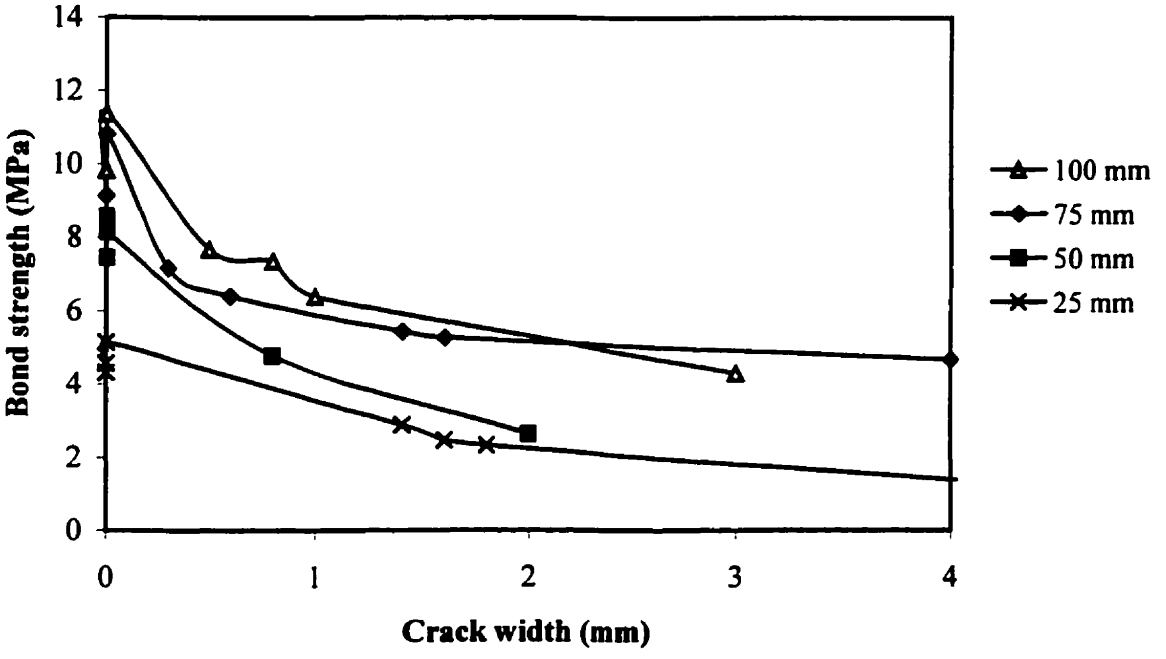

Fig. 8.31: Effect of crack width on bond strength for Thunder Bay concrete mixture for different concrete cover thicknesses

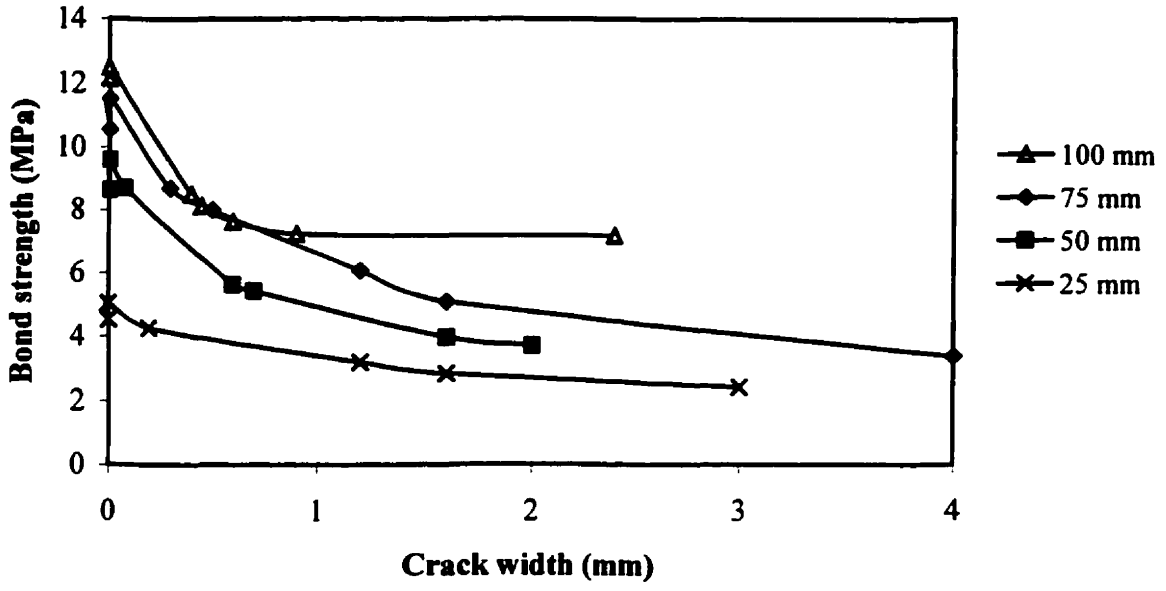

Fig. 8.32: Effect of crack width on bond strength for Sundance concrete mixture for different concrete cover thicknesses

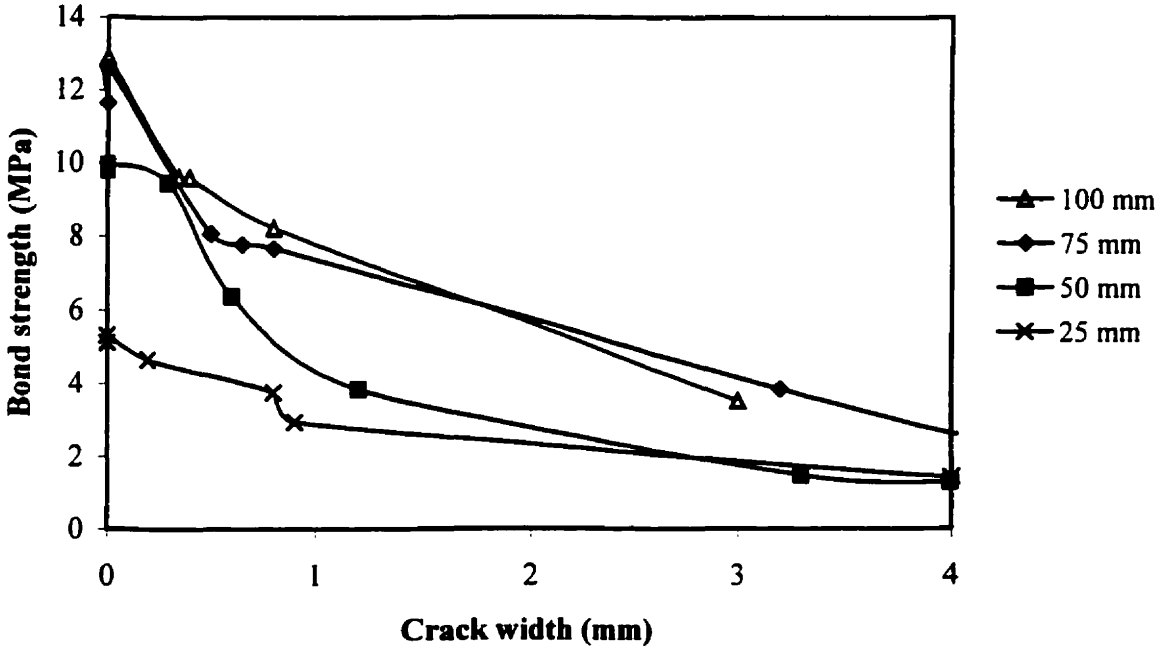

Fig. 8.33: Effect of crack width on bond strength for NPC (0.32 w/c) concrete mixture for different concrete cover thicknesses

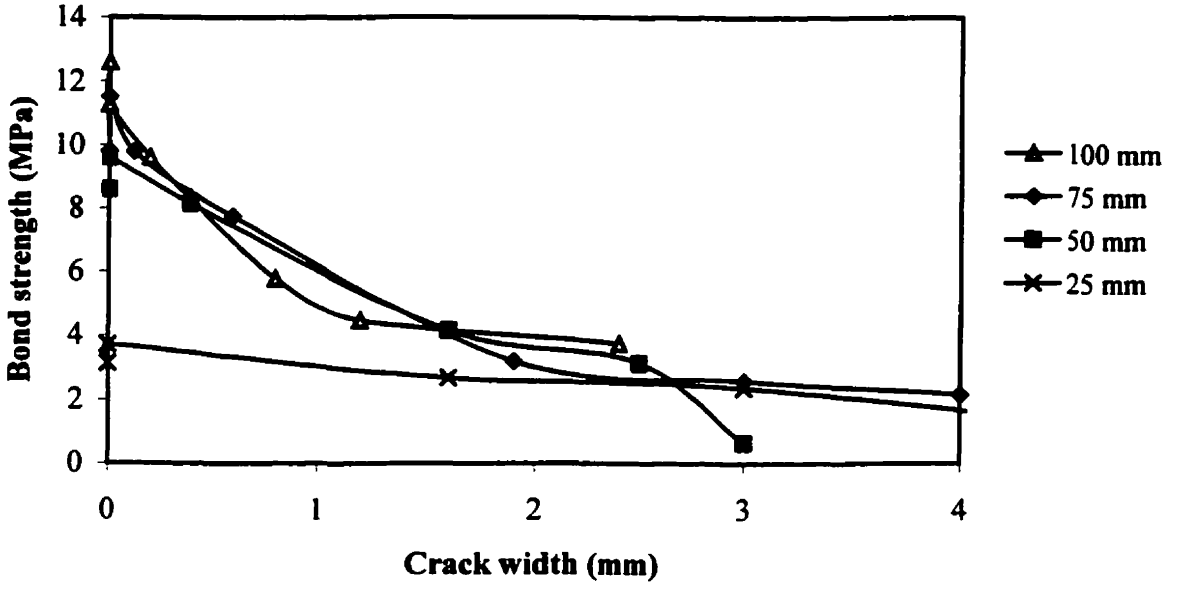

Fig. 8.34: Effect of crack width on bond strength for NPC (0.42 w/c) concrete mixture for different concrete cover thicknesses

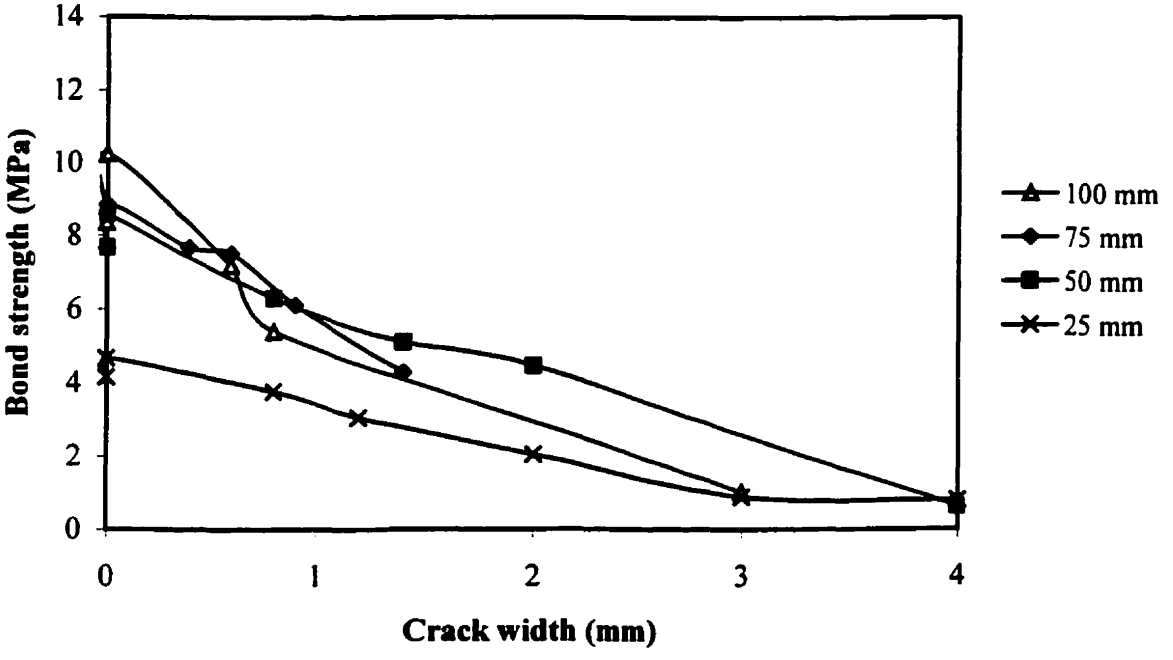

Fig. 8.35: Effect of crack width on bond strength for HAC concrete mixture for different concrete cover thicknesses

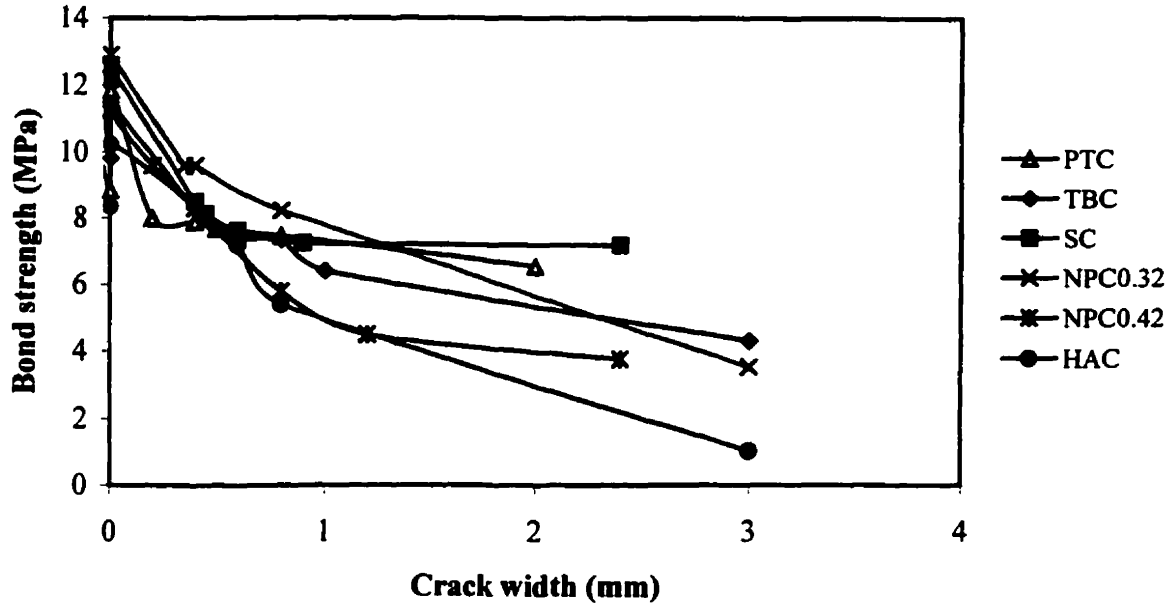

Fig.8.36: Effect of crack width on bond strength for all of the 100mm concrete cover thickness

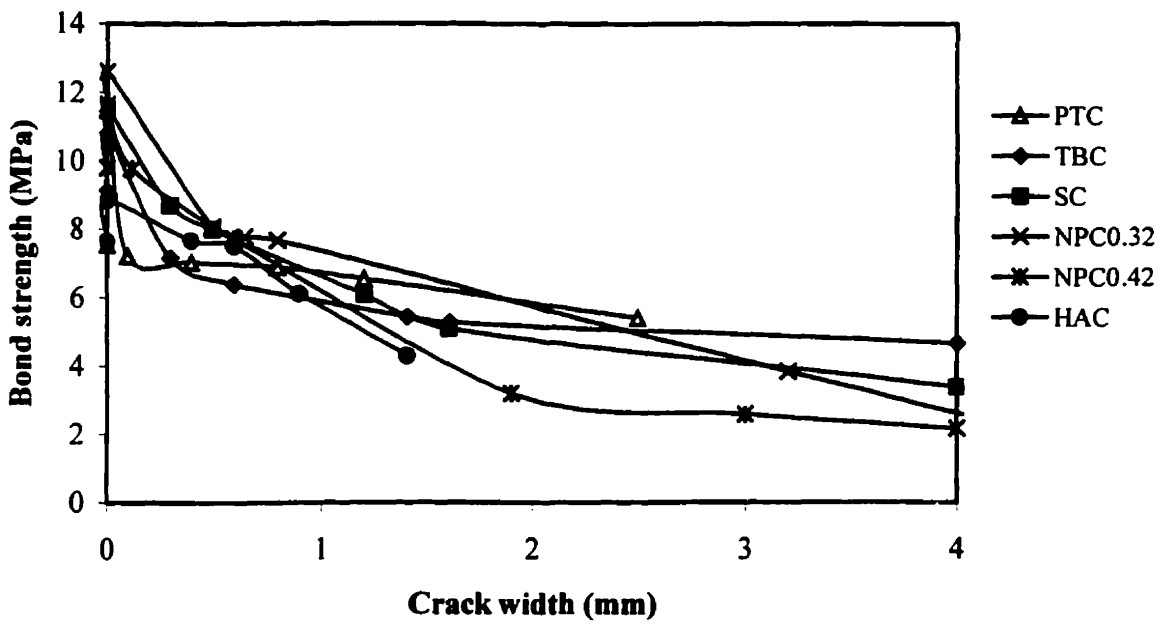

Fig. 8.37: Effect of crack width on bond strength for all of the 75mm concrete cover thickness

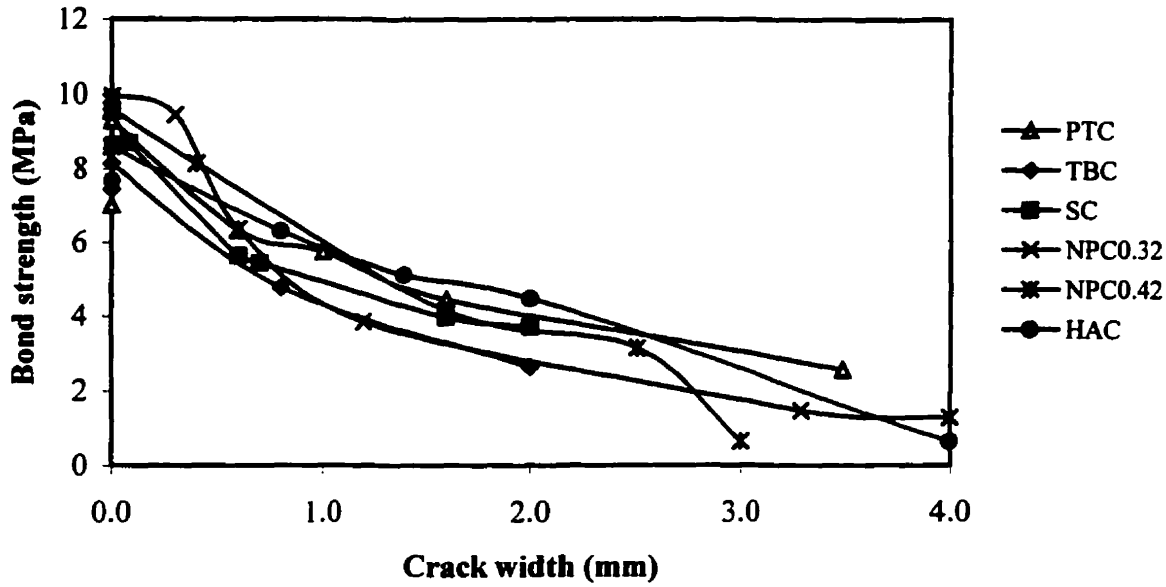

Fig. 8.38: Effect of crack width on bond strength for all of the 50mm concrete cover thickness for the different concretes

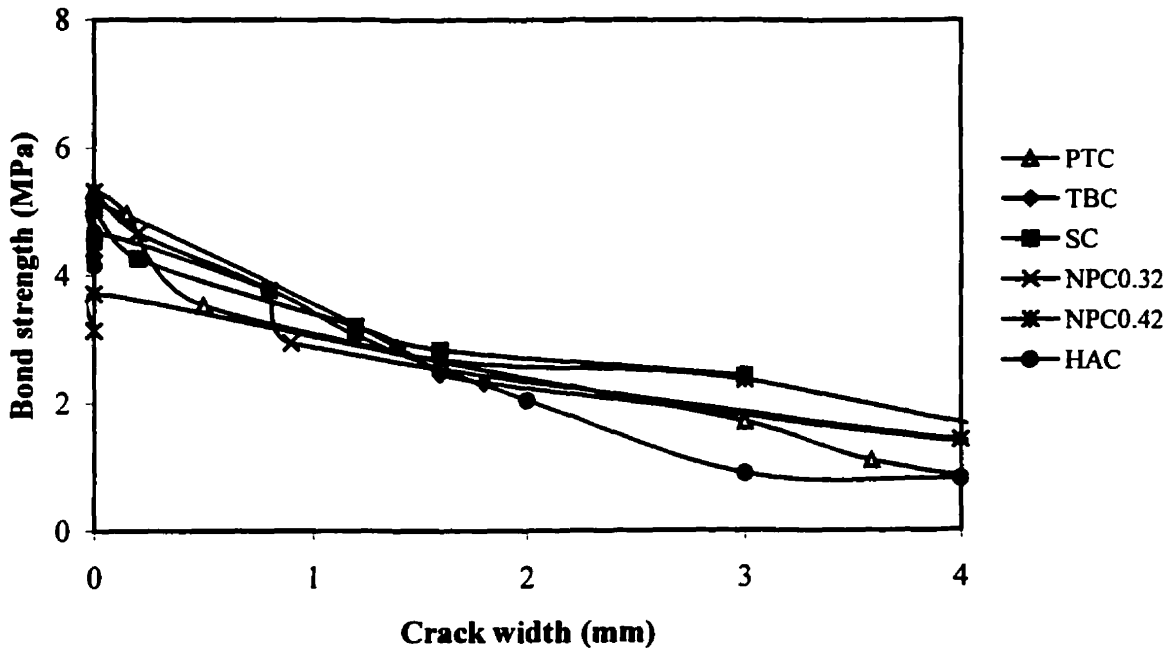

Fig. 8.39: Effect of crack width on bond strength for all of the 25mm concrete cover thickness for the different concretes

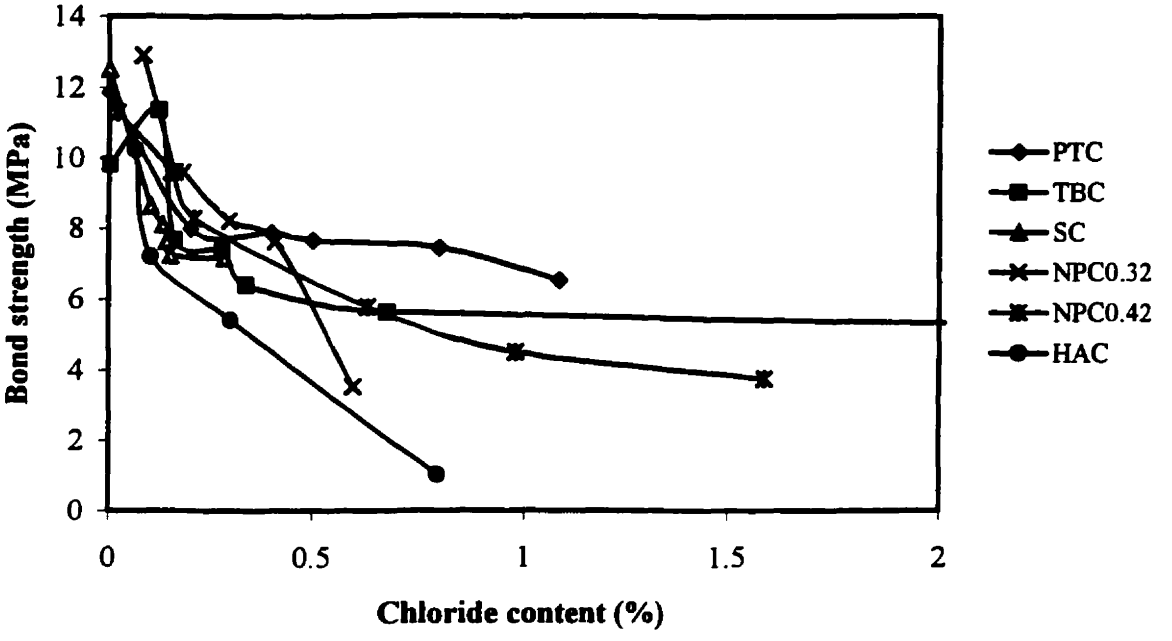

Fig. 8.40: Effect of chloride content at the steel bar level on bond strength with different concrete types and concrete cover thickness of 100 mm

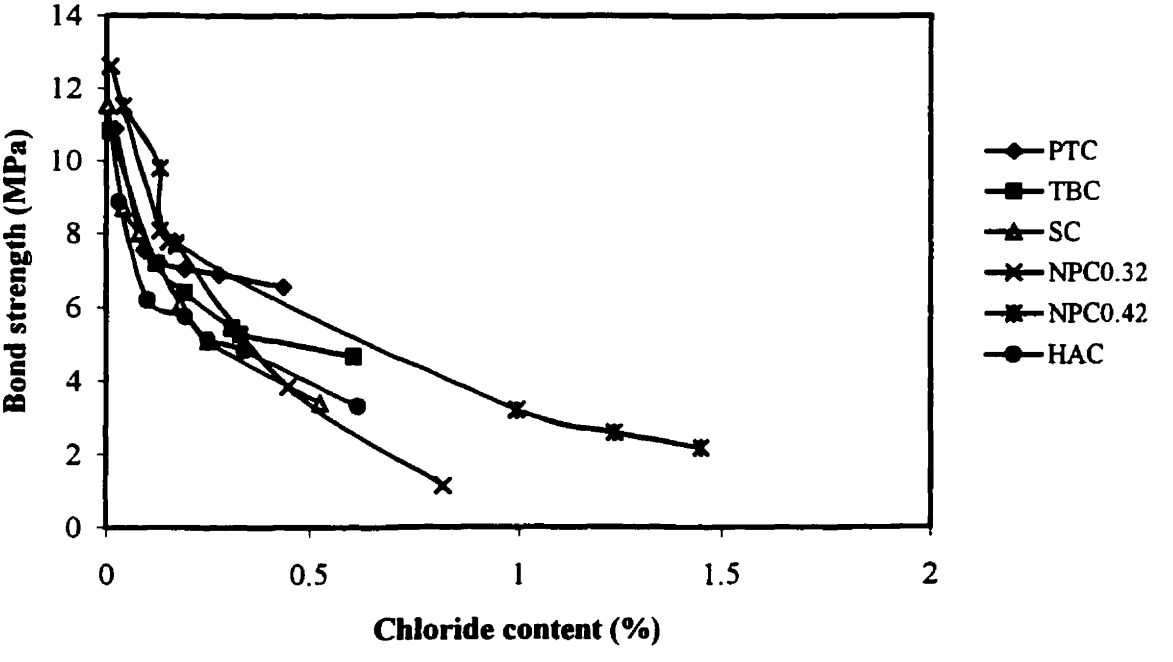

Fig. 8.41: Effect of chloride content at the steel bar level on bond strength with different concrete types and concrete cover thickness of 75 mm

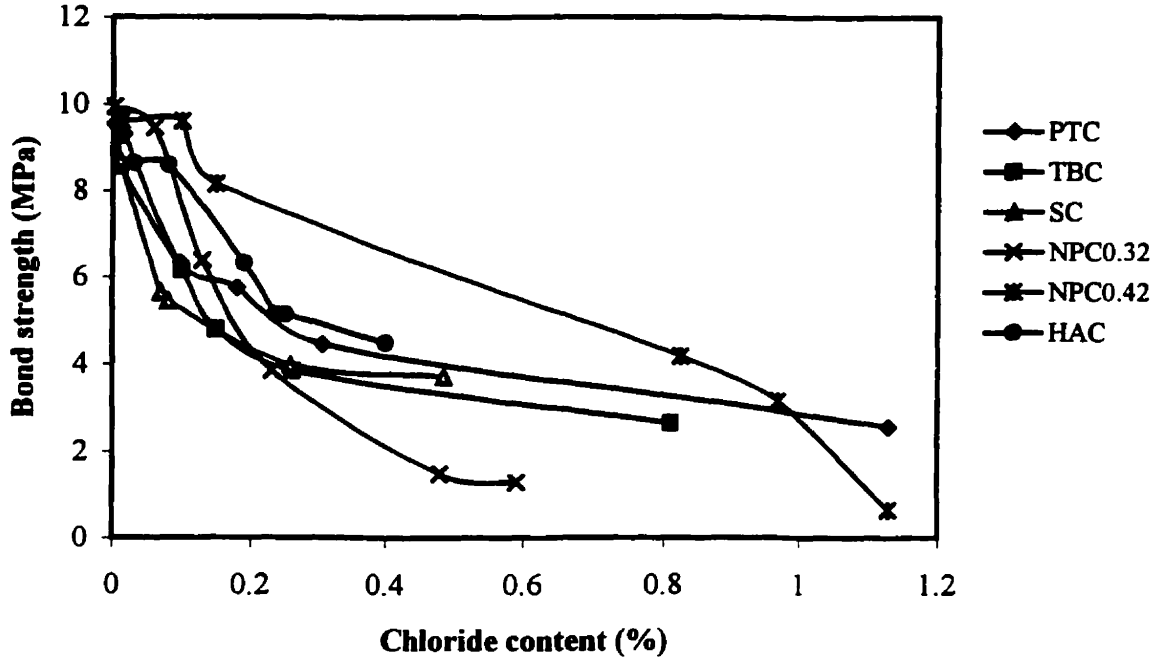

Fig. 8.42: Effect of chloride content at the steel bar level on bond strength with different concrete types and concrete cover thickness of 50 mm

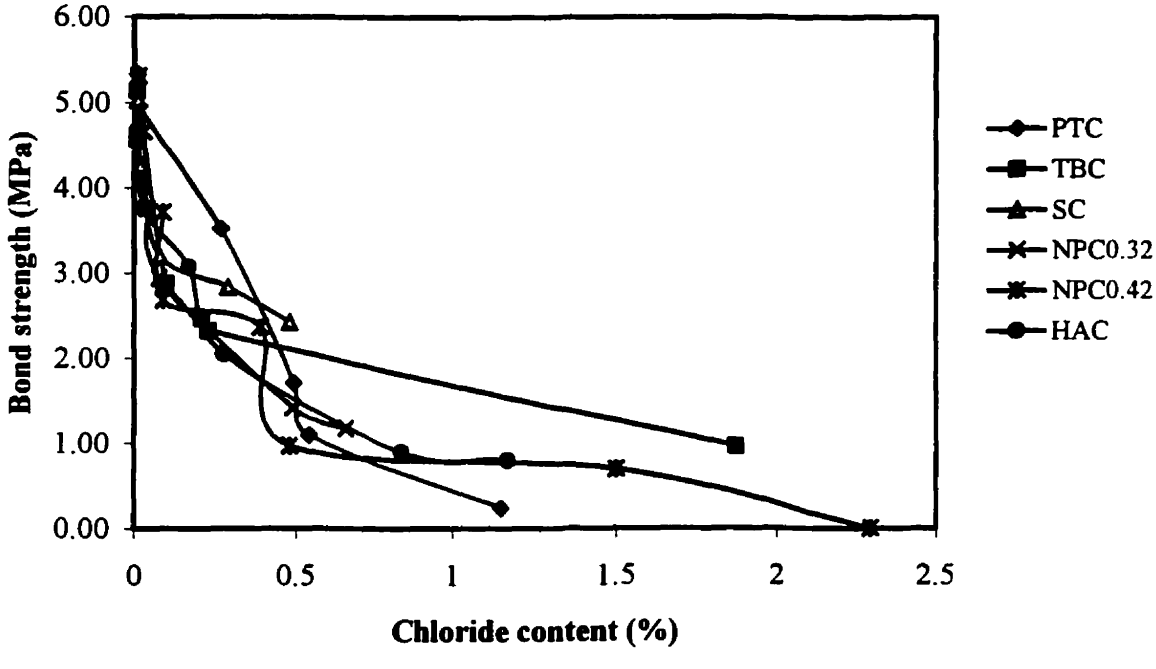

Fig. 8.43: Effect of chloride content at the steel bar level on bond strength with different concrete types and concrete cover thickness of 25 mm

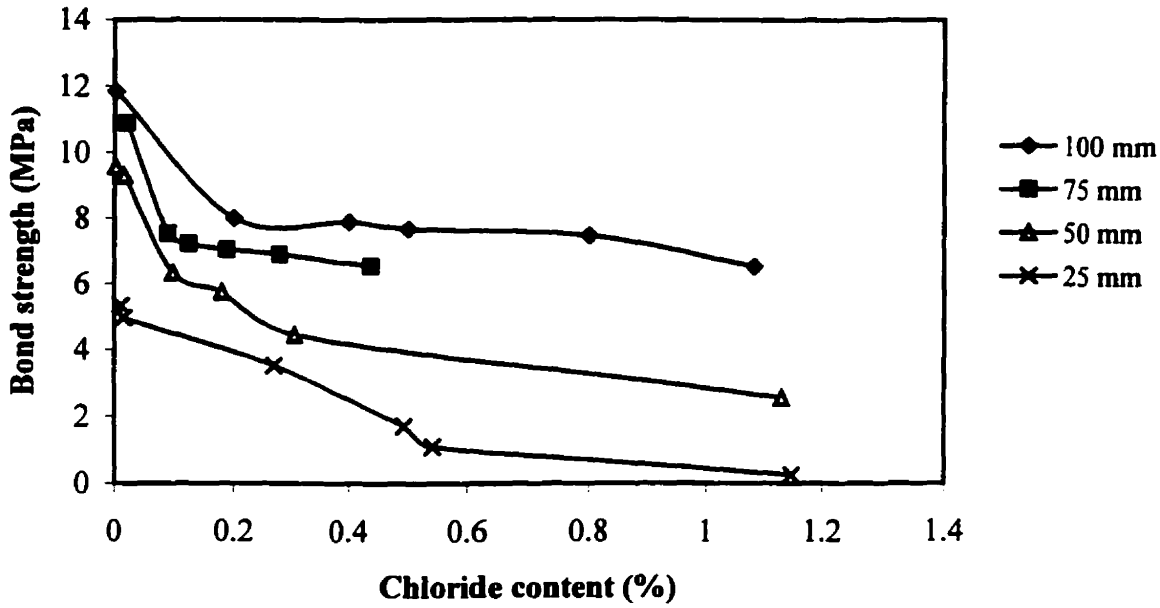

Fig. 8.44: Effect of chloride content on bond strength for Point Tupper fly ash concrete mixture (PTC) for different concrete cover thicknesses

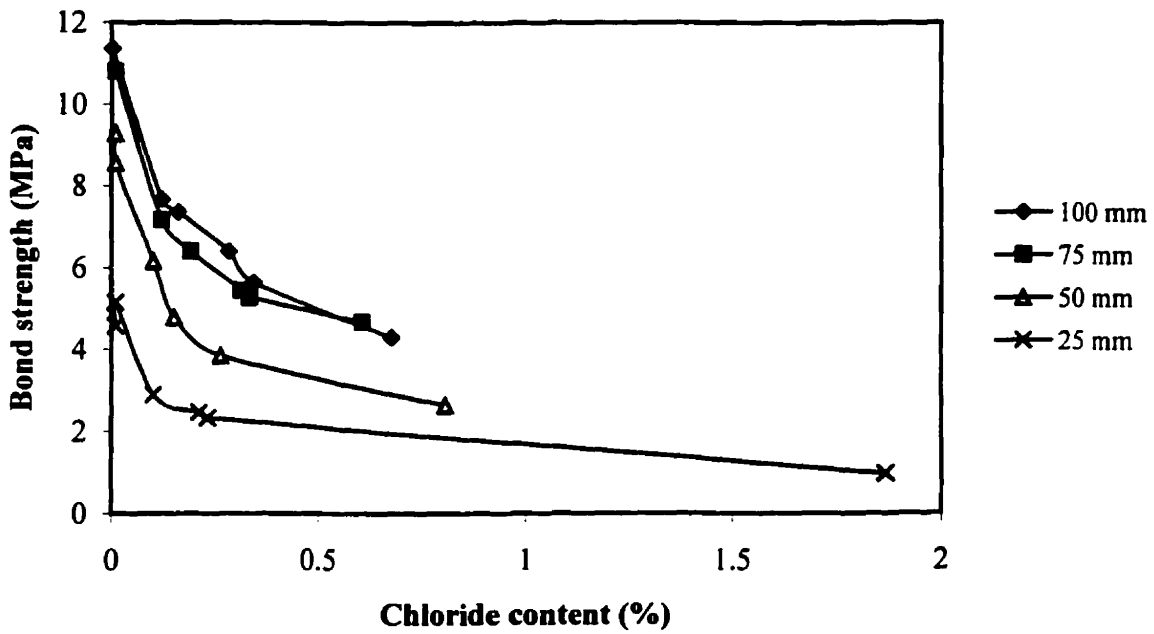

Fig. 8.45: Effect of chloride content on bond strength for Thunder Bay fly ash concrete mixture (TBC) for different concrete cover thicknesses

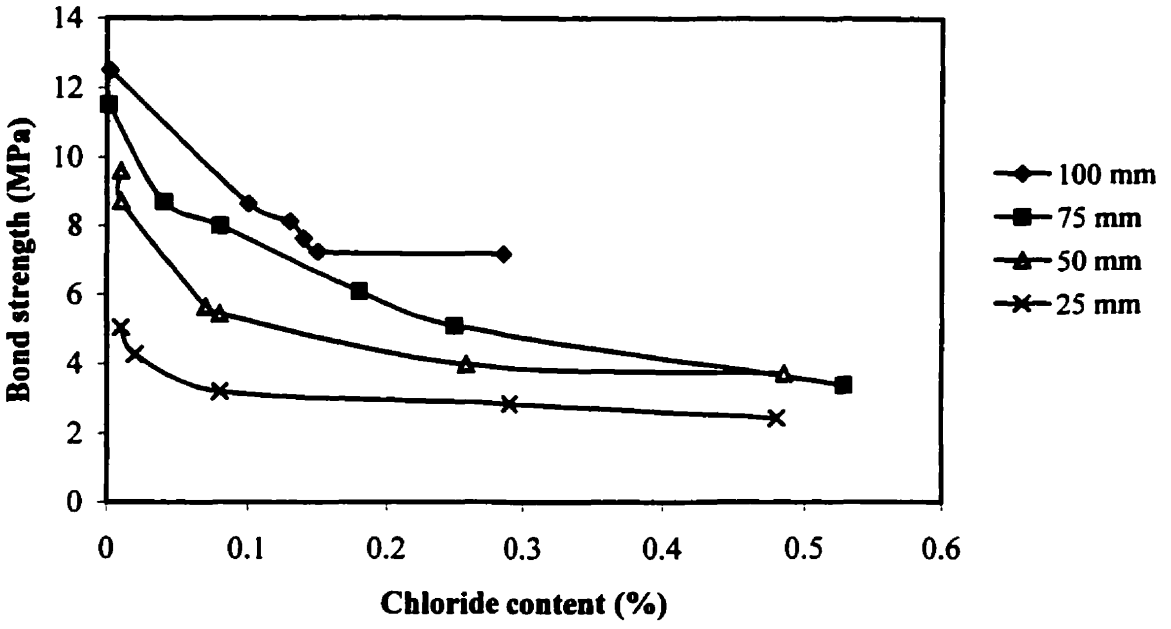

Fig. 8.46: Effect of chloride content on bond strength for Sundance fly ash concrete mixture (SC) for different concrete cover thicknesses

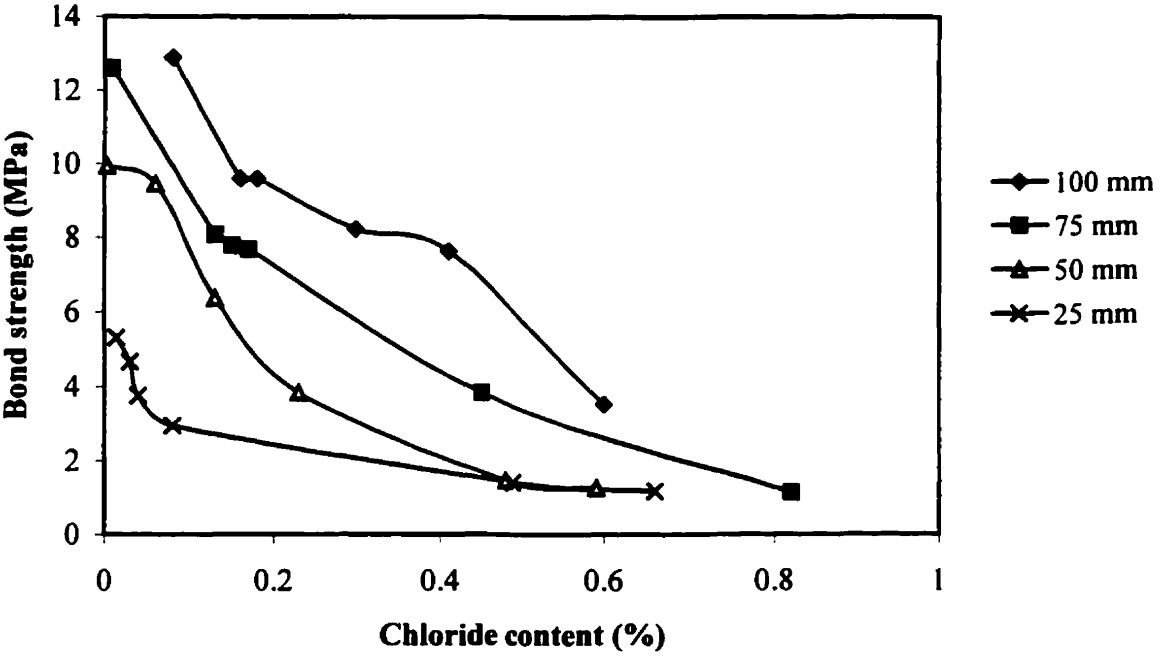

Fig. 8.47: Effect of chloride content on bond strength for Normal Portland Cement concrete mixture (NPC0.32) for different concrete cover thicknesses

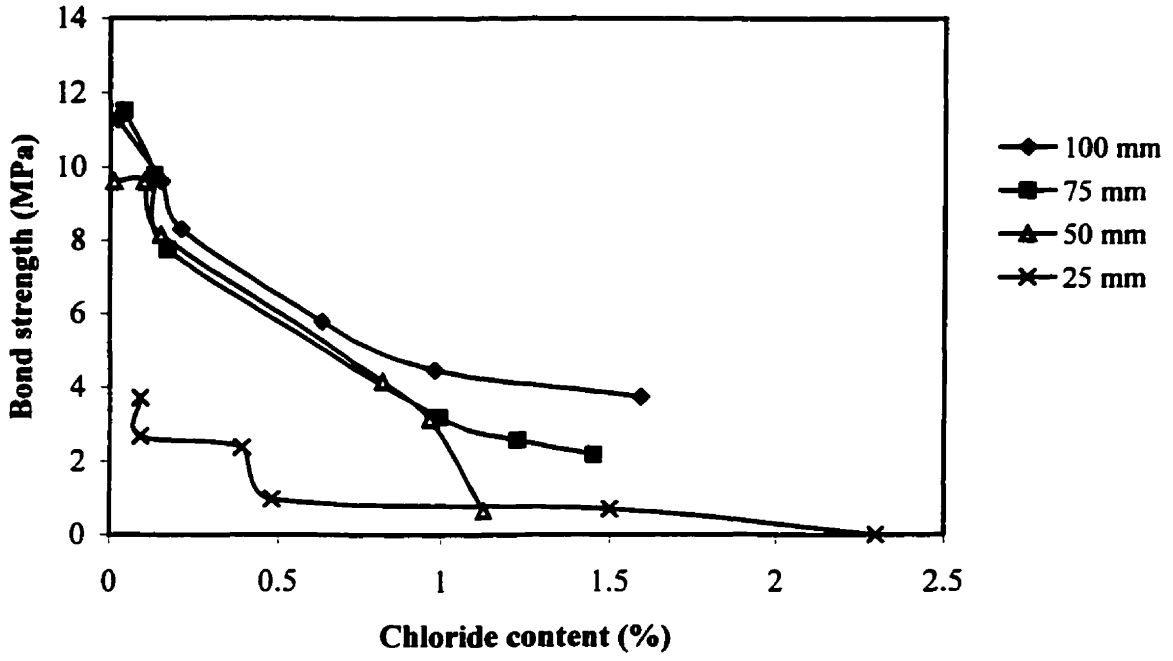

Fig. 8.48: Effect of chloride content on bond strength for Nromal Portland Cement concrete mixture (NPC0.42) for different concrete cover thicknesses

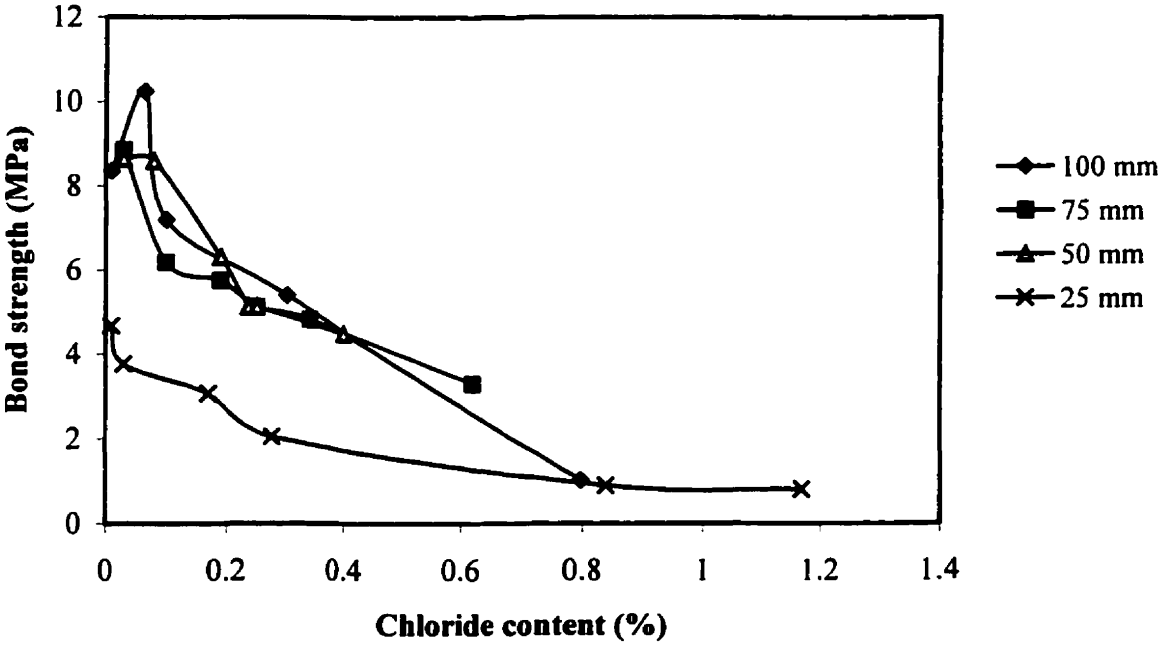

Fig. 8.49: Effect of chloride content on bond strength for High Alumina Cement concrete mixture (HAC) for different concrete cover thicknesses

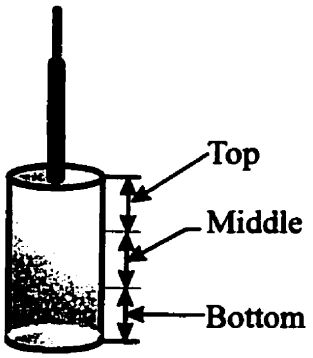

Typical pullout specimen

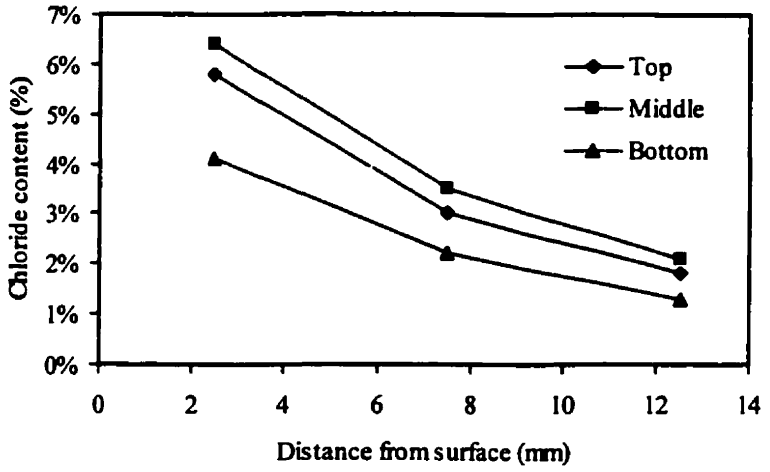

Figure 8.50: Chloride ion profile for Specimen C5-7D

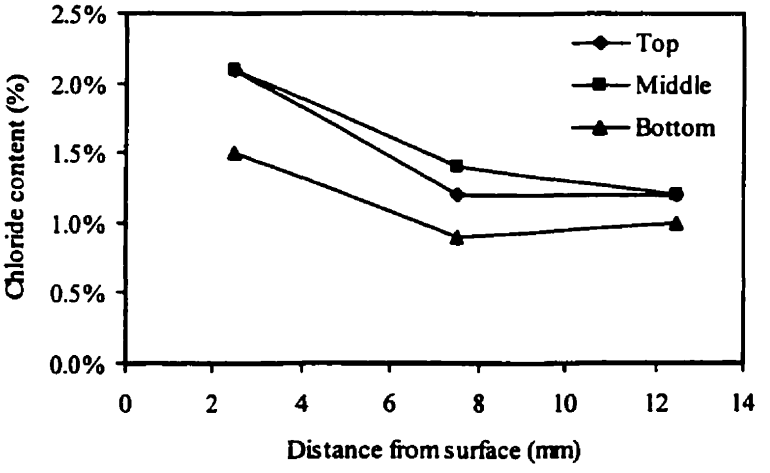

Figure 8.51: Chloride ion profile for Specimen C5-6B

Chapter 9

Tension Test Results and Analysis

This chapter reports the results of the complete responses until failure of thirty tension specimens, tested after the development of the different required levels of corrosion in twenty-four specimens. The remaining six specimens were used as control specimens.

9.1 Introduction

As mentioned earlier, the three concrete mixes used in this part of the investigation were as follows :

1. A replica of the normal portland cement concrete mix used for the Dickson Bridge (termed the Dickson Bridge Concrete), Montreal in 1959, consisting of:
    a) Water- cement ratio = 0.52
    b) Limestone coarse aggregates 1020 kg/m^3
    c) St.Gabriel de Brandon sand 720 kg/m^3

    This mix was used for tension Specimens C7- 1C through C7-10C.

2. Normal portland cement concrete mix (termed the Normal Cement Concrete) as used for the lollipops specimens with a water-cement ratio of 0.32. This mix was used for tension Specimens C3-1C through C3-10C.

3. The Sundance fly ash concrete mix (termed the Sundance Concrete) with a water-cementitious materials ratio of 0.32. The Sundance fly ash replaced 58 percent of the weight of normal portland cement, and it was used for tension Specimens C4-1C through C4-10C.

Beside the six control specimens, the remaining 24 specimens were subjected to different levels of corrosion using the accelerated corrosion technique described earlier in Chapter 6.

After completion of the tension tests, the specimens were tested for the chloride content at three depths along the concrete cover depth, including the chloride content at the steel bar level. Following the chloride content evaluation, the reinforcing bars were removed and tested to determine the percentage mass loss. The observed responses of the uncorroded and the corroded specimens were compared using the load-elongation behaviour of the tension specimens, the "derived" stress-strain relationships, and the information on crack widths and crack spacings used to derive the relative bond capacity of the bars at different levels of corrosion. The experimental results are analysed and quantified for the influence of the level of corrosion on the bond strength at the steel-concrete interface.

9.2 Elongation Responses

The load-elongation response of the various tension specimens commences with the uncracked elastic region, followed by the cracking of the element when the tensile strength of the concrete is exceeded. This is followed by the formation of cracks and their stabilization, a significant increase in deformations, and finally by the yielding of the steel bar, when the specimen is considered to have failed.

Two specimens of each concrete mixture were used as control specimens while the rest of the specimens were subjected to varying levels of corrosion. Note that the corrosion levels are not in the same sequence as the numbering of the

specimens, however, the following sections deal with these specimens in an ascending order of the level of corrosion.

In the load-elongation response of each specimen, the bare bar response is also shown. The phenomenon underlying the transfer of the force from the steel bar to the concrete and vice-versa is best understood by comparing the measured member response with that of the bare bar. Similarly, the influence of the level of corrosion can be established by comparing the response of the corroded specimens with the control specimens with uncorroded reinforcing bars. The control specimen elongation is negative prior to the load application because of the concrete shrinkage. Ignoring this member shortening could result in an underestimation of the tension stiffening effect, as confirmed in a recent study by Bischoff (1995), who noted an average free shrinkage strain of 0.3×10^{-3}. By comparison, the elongation of corroded members prior to the load application is zero because these specimens were continually immersed in water and hence, there was no shrinkage.

9.2.1 Normal Portland Cement Concrete Mix (w/c ratio = 0.52; Dickson Bridge Concrete)

All of the relevant experimental data (corrosion stage, number and width of major longitudinal crack due to corrosion, yield load and the mass loss) are presented in Table 9.1. The load-elongation characteristics of the control Specimens C7-1C and C7-2C were almost identical and therefore the response of only one of the specimens is presented in Figures 9.1 through 9.4 along with the response of selected corroded specimens and that of the bare bar for comparative purposes. The experimental responses of three specimens at three different selected corrosion levels are discussed and compared with the response of the Specimen C7-2C.

Both Specimens C7-1C and C7-2C behaved in basically the same manner, as was noted from their load-elongation responses. After the first cracking load, the load-elongation curve is noted to become parallel to the load-elongation curve for the

bare steel bar. As the load was increased, for both of the control Specimens C7-1C and C7-2C, eleven (11) transverse cracks formed with an average spacing of 83mm. The yield load of both of the specimens corresponds closely to the bare bar yield strength.

The Specimen C7-4C represented the first level of corrosion and developed a longitudinal splitting crack during the accelerated corrosion process, with an average width of 2 mm and a minor transverse crack with a maximum width of 0.1 mm. Figure 9.1 shows the load-elongation response for the corroded Specimen C7-4C along with the uncorroded Specimen C7-2C and the bare bar responses. As can be seen from the Fig. 9.1, the steel bar in the Specimen C7-4C yielded at a load of 116.0 kN, displaying a lower load bearing capacity than the uncorroded Specimen C7-2C. The first transverse crack appeared in the Specimen C7-4C at an applied load of about 23 kN which is higher than that for the Specimen C7-2C due to the lack of shrinkage because the specimen was continuously immersed in the sodium chloride solution. Also, Fig. 9.2 shows that the response curve for Specimen C7-4C is shifted to the right closer to the bare bar response, signifying less concrete contribution, i.e. a decrease in the tension stiffening effect. Apart from the difference in the concrete contribution and the yielding load, the Specimen C7-4C generally shows behaviour similar to that of the Specimen C7-2C.

The response of the Specimen C7-8C, which represented the third stage of corrosion is shown in Figure 9.2. The Specimen C7-8C had one splitting longitudinal crack, with a width of 1.2 mm, and two hair-line transverse cracks. The yielding load for the Specimen C7-8C was 96.0 kN which is much lower than that of Specimen C7-2C. The first cracking appeared at approximately 23 kN which again is higher than the first cracking load for Specimen C7-2C and six transverse cracks were formed during the tension testing with an average spacing of 143mm.

The Specimen C7-9C, which represented the eighth and the last stage of corrosion, had two major longitudinal splitting cracks ranging from 0.5 mm to 5.0mm

in width and 2 transverse cracks. A piece of concrete between two cracks had fallen off prior to testing. As shown in Fig. 9.3, the Specimen C7-9C had a yielding load of 45 kN which is obviously much lower than that of Specimen C7-2C. No transverse cracks appeared in this specimen until beyond the yield strength of the steel bar at a load of 46 kN when one transverse crack appeared, which was caused by the widening of an existing transverse crack. The specimen failed in a brittle manner at a load of 82 kN. The load-elongation curve for the Specimen C7-9C hardly shows any concrete contribution.

In summary, the load-elongation responses of all tension specimens commence with an uncracked elastic region when the concrete tensile strength is not exceeded. This initial cracking is followed by a slight drop in the applied load followed by stabilization of the cracks and by yielding of steel reinforcement as the load is increased further. At this stage, the specimen is considered to have failed.

The rest of the load-elongation curves for the specimens with varying levels of corrosion (Fig. 9.4) also show that after cracking, the load-elongation curves for all of the specimens become parallel to the load-elongation curve of the bare steel bar. It is also noted that the lower levels of corrosion (Specimen C7-4C, 8% mass loss) do not influence the load-elongation curve as much as the higher levels of corrosion (Specimen C7-9C, 27% mass loss). The difference between the load-elongation curve of any specimen and that for the bare bar provides a measure of the tension stiffening due to the concrete. As the level of corrosion increases, the extent of longitudinal cracking due to corrosion also increases, which in turn decreases the tension stiffening contribution from the concrete and brings the load-elongation response of the specimen close to that of the bare bar.

9.2.2 Normal Portland Cement Concrete Mix (w/c ratio = 0.32)

The Specimens C3-1C and C3-2C were used as control specimens, while the rest of the Specimens were subjected to varying levels of corrosion as shown in Table 9.2.

The Specimen C3-5C represents the first corrosion level and did not display any longitudinal splitting crack prior to testing, due to the corrosion of the steel bar. Figures 9.5 shows the load-elongation response for the slightly corroded Specimen C3-5C. As can be seen from Fig. 9.5, the steel bar in the Specimen C3-5C yielded at a load of 125.0 kN, displaying a very similar load carrying capacity as the uncorroded Specimen C3-1C and it is close to that of the bare bar, which had a yielding load of 127.0 kN. The first transverse crack appeared in the Specimen C3-5C at a load of about 34 kN which is higher than that for the Specimen C3-1C, again, due to the lack of concrete shrinkage because of the continued immersion of the specimen in the sodium chloride solution. As the load was increased, 12 transverse cracks formed with an average spacing of 77mm, which is similar to that of the uncorroded specimens. In addition, Specimen C3-5C showed a higher concrete contribution to the specimen resistance than that of the uncorroded Specimen C3-1C.

The response of the Specimen C3-6C, which represented the fifth stage of corrosion is shown in Fig. 9.6 along with the response of the Specimen C3-1C. The Specimen C3-6C had four longitudinal splitting cracks, three minor ones with an average size of 0.2mm and one major crack with an average width of 2mm, and also two transverse cracks that varied in width ranging from 0.15 mm to 0.3 mm. The yield load for the Specimen C3-6C was 115 kN which is lower than that for Specimen C3-1C. The initial cracking load was approximately 31 kN which is higher than the first cracking load for Specimen C3-1C; this was followed by the widening of an existing transverse crack. The Specimen C3-6C then developed four transverse cracks during the tension test, with an average width of 200mm. The load-elongation curve for the Specimen C3-6C shows lower concrete contribution.

The Specimen C3-4C, which represented the seventh and last stage of corrosion, had four longitudinal splitting cracks- one minor crack with a width of 0.2mm and three major cracks ranging from 1.0 mm to 5.0mm in width and 3 transverse cracks. A piece of concrete between two cracks had fallen off prior to

testing. As shown in Fig. 9.7, the Specimen C3-4C yielded at a load of 83 kN which is obviously much lower than that of Specimen C3-1C; this cracking was followed by widening of an existing transverse crack, at a load of about 37 kN, which is higher than the first cracking load for Specimen C3-1C, and developed only two transverse cracks during the tension test. The load-elongation curve for the Specimen C3-4C shows hardly any concrete contribution.

In Summary, the number of specimens in increasing order of the level of corrosion are: C3-5C, C3-8C, C3-10C, C3-9C, C3-6C, C3-3C, C3-4C and C3-7C. All of the relevant experimental data for this series are presented in Table 9.2. The specimen C3-7C failed due to malfunctioning of the MTS machine and it could not be tested. The load-elongation curves for the various specimens in this series are presented in Fig. 9.8, which exhibits the same features and trends as for the Dickson Bridge NPC Specimens.

9.2.3 Sundance Fly Ash Concrete Mix (w/cm ratio = 0.32)

Both of the standard control Specimens C4-1C and C4-2C behaved in basically the same manner, and the response of the Specimen C4-2C is shown in Figures 9.9 through 9.12. The Specimen C4-2C developed the first transverse crack at an applied load of about 22 kN and hence, the stress in the steel bar at first cracking. Again, after the first cracking load, the load-elongation curve is noted to become parallel to the load-elongation curve for the bare steel bar. As the load was increased, for both of the control specimens C4-1C and C4-2C, 10 transverse cracks formed with an average spacing of 91mm. The Specimens C4-1C and C4-2C developed yielding of the steel bars at approximately the same load of 127 kN; the steel stress at this stage was 423 MPa. The yield load of both of the specimens corresponds closely to the bare bar yield strength.

The Specimen C4-10C represented the first level of corrosion and did not display any longitudinal splitting cracks prior to testing. Figure 9.9 shows the load-

elongation response for the slightly corroded Specimen C4-10C. As can be seen from the Fig. 9.9, the steel bar in the Specimen C4-10C yielded at a load of 127.0 kN, displaying the same load carrying capacity as the uncorroded Specimen C4-2C. The first transverse crack appeared in the Specimen C4-10C at a load of about 31 kN, which is higher than that for the Specimen C4-2C, again, basically due to the lack of concrete shrinkage because the specimen was continuously immersed in the sodium chloride solution. As the load was increased, 11 transverse cracks formed with an average spacing of 83mm. The response of Specimen C4-10C in Fig. 9.9 shows that the curve of Specimen C4-10C is identical to that of the Specimen C4-2C, signifying a higher concrete contribution, i.e. about the same level of tension stiffening. Apart from the slight difference in the yielding load, the Specimen C4-10C shows behaviour similar to that of the Specimen C4-2C. Also, with the difference in the early parts of the load-elongation curves, the load-elongation responses are almost identical throughout.

The Specimen C4-4C represented the fifth stage of corrosion and again without any longitudinal cracks prior to testing. The first cracking load occurred at a load of 36 kN, and as the load was increased seven transverse cracks formed with an average spacing of 125mm. The overall response observed was similar to that for the Specimen C4-2C. Figure 9.10 shows the load-elongation curves for the Specimens C4-4C and C4-2C. The yielding load for the Specimen C4-4C was 124.5 kN, which is very close to the yielding load of the Specimen C4-2C.

The Specimen C4-8C represented the eighth stage of corrosion and again without any longitudinal cracks prior to testing. The first cracking occurred at a load of 30 kN, and as the load was increased six transverse cracks formed with an average spacing of 143mm. Figure 9.11 shows the load-elongation curves for the Specimens C4-8C and C4-2C. The yielding load for the Specimen C4-8C was 90 kN. The specimen also failed in a brittle manner at a load of 124 kN. The load-elongation curve for the Specimen C4-8C showed much lower concrete contribution.

In summary, as for the other series, the levels of corrosion were not in the same sequence as the numbering of the specimens. The number of specimens in increasing order of the level of corrosion are: C4-10C, C4-6C, C4-9C, C4-5C, C4-3C, C4-4C, C4-7C and C4-8C. All of the relevant experimental data for this series is presented in Table 9.3. The load-elongation curves for the various specimens in this series is presented in Fig. 9.12 and they behaved similarly (excepting that the Specimen C4-8C failed in a brittle manner with very little deformation), which exhibited the same features and trends as for the tension specimens in the other two series. It was noted that as for the other series, the contribution of the concrete to the tension stiffening of the specimen decreased with an increasing level of corrosion.

9.3 Stress-Strain Characteristics

Due to the loss of the cross-sectional area as a consequence of corrosion, the reported stresses were calculated from the equivalent cross-sectional area obtained by dividing the various loads by the new equivalent cross-sectional area, A_{ms}, (obtained from the loss of mass due to corrosion as explained in Chapter 6). As discussed earlier (Chapter 6), these calculated stress-strain responses represent the "actual" contributions of the reinforcing steel and the tension stiffening due to the concrete in the overall specimen response. The equivalent cross-sectional areas are summarized in Tables 9.4 through 9.6 for all of the specimens and the concrete mixtures along with the equivalent cross-sectional areas calculated from the yield loads.

Figures 9.13 through 9.21 show the "modified" stress-strain relationship for Specimens C7-2C, C7-4C, C7-8C, C7-9C, C3-1C, C3-5C, C3-6C, C3-4C, C4-2C, C4-10C, C4-4C and C4-8C, respectively. Again, each stress-strain curve obtained for the corroded specimens is presented along with the control specimen stress-strain curve for comparison purposes; these figures indicate the overall behaviour of the tension specimens and indicate the relative contribution from the tension stiffening effects.

This use of an "equivalent" cross-sectional area led to an apparent increase in the tension stiffening which was observed for each corroded specimen, including the last few stages of corrosion such as C7-9C, C3-4C and C4-8C, which showed no concrete contribution in their load-elongation curves. This observed difference between the load-elongation curves and the stress-strain relationship curves is due to the fact that in the load-elongation curve for the specimen with a clean uncorroded 20M bar was compared with that of the specimen with a corroded 20M bar. The ultimate load for the latter is obviously smaller than that for the first (uncorroded) specimen.

However, as can be seen, from the stress-strain curves, this tension stiffening decreases as the level of corrosion increases. The equivalent cross-sectional areas for each specimen are summarized in Tables 9.4 through 9.6.

9.4 Cracking Behaviour

This section will attempt to trace the development of cracks during the tension testing in terms of transverse cracks and longitudinal splitting cracks. A comparison between the uncorroded specimens and the corroded ones will also be included to study the influence of corrosion on cracking behaviour.

The number and average crack spacing of the transverse cracks for all of tension specimens was determined for the specimens from each concrete mixture and are summarized in Tables 9.7 through 9.9 for the different stages of corrosion and for the control specimens as well as the maximum crack spacing. The results for the number and spacing of the cracks clearly show that as the level of corrosion increases the crack spacing increases.

The effect of the longitudinal splitting cracks and the internal cracks formed during accelerated corrosion reduces the rate at which the force is transferred from

the reinforcement to the concrete and vice-versa, and hence it increases the distance from the crack over which the bond stresses are reduced.

The loads at which the first cracks appeared in the various specimens of Series C7, C3 and C4 are listed in Tables 9.1, 9.2 and 9.3, respectively. As mentioned earlier, the concrete in the uncorroded specimens from the three series was subjected to shrinkage and therefore, these cracking loads would be lower than the cracking loads which can be used to evaluate the tensile strength of the various concretes. Using the cracking load values for stage 1 corrosion for the three series (23, 34, and 31 kN for Series C7, C3, and C4, respectively) results in direct tensile strengths (uniform tensile strains across the cross-sections) of 1.92, 2.84 and 2.59 MPa. It should be noted that these direct tensile strength values are lower than the indirect tensile strength values which have a different strain gradient across them. These values are 2.48, 3.23, and 3.32 MPa, respectively. Thus the Sundance fly ash concrete with the same water/cementitious materials ratio as the normal portland cement concrete shows a slightly lower tensile strength. In addition, although the Sundance fly ash concrete tension specimens did not develop any longitudinal cracks due to corrosion, the bond strength developed at the steel-concrete interface was lower than that for the corresponding normal portland cement specimens with the same water/cementitious materials ratio.

9.4.1 Normal Portland Cement Concrete Mixture (w/c=0.52) used for the Dickson Bridge Concrete

The control specimens for the Dickson Bridge concrete mix, C7-1C and C7-2C, exhibited transverse cracks, well before the longitudinal splitting cracks formed at the later stages of the tests. By comparison, the corroded specimens exhibited only transverse cracks in addition to the widening of some of the existing longitudinal splitting cracks, as all of them had at least one splitting crack prior to the test due to corrosion.

Figure 9.22 shows the cracking behaviour in terms of the bar stress at the crack locations versus the crack width for the uncorroded Specimens C7-1C through C7-10C. The maximum crack width curve for the uncorroded specimen is also produced for comparison. The steel-stress vs. crack width curve was not obtained for Specimen C7-9C because it did not produce any cracking prior to the yielding of the reinforcing steel. As can be seen from Fig. 9.22, the steel stress vs. maximum crack width curve for the Specimens C7-6C and C7-10C, respectively, starts from zero load because of the fact that the cracks existed before the test. The influence of the corrosion level on the crack width can be clearly noted from the curves. The crack width increased with an increasing level of corrosion. Figures 9.23 (a) and (b) show the longitudinal splitting crack due to corrosion in a typical corroded Specimen C7-5C and its width before and after the test. Figure 9.24 shows the transverse tensile and longitudinal splitting cracks for different levels of corrosion for the specimens made from the normal portland cement (Dickson Bridge Concrete) and a water-cement ratio of 0.52.

9.4.2 Normal Portland Cement Concrete Mixture (w/c = 0.32)

The control specimens for the NPC concrete with a water/cement ratio of 0.32, C3-1C and C3-2C, exhibited transverse cracks, well before the longitudinal splitting cracks formed at the later stages of the tests. Also, the first stage of corrosion, the precracking stage, showed cracking behaviour that is similar to that of the uncorroded specimens. By comparison, for the post cracking stage, the corroded specimens exhibited only transverse cracks, in addition to the widening of some of the existing longitudinal splitting cracks, as these cracks had developed due to accelerated corrosion prior to the test.

As mentioned earlier, Figures 9.25 (a) and (b) show the longitudinal splitting crack due to corrosion in a typical corroded specimen C3-3C and its width before and after the test. Figure 9.26 shows the transverse tensile and longitudinal splitting cracks in all of the Series C3 specimens, due to corrosion for different levels of

corrosion. Figure 9.27 shows the steel stress at the crack versus the crack width for all of the specimens. Again, the influence of the corrosion level on the crack width can be clearly noted from Fig. 9.27. The crack width increased with an increasing level of corrosion.

9.4.3 Sundance Fly Ash Concrete Mixture (w/cm ratio = 0.32)

The control specimens for the Sundance fly ash concrete, C4-1C and C4-2C, exhibited transverse cracks, well before the longitudinal splitting cracks formed at the latter stages of the tests. The Sundance fly ash concrete mixture specimens exhibited more longitudinal splitting cracks than that for the specimens from the other NPC concrete mixtures.

The Sundance concrete specimens did not develop any longitudinal splitting cracks due to corrosion, however, two specimens experienced a high local corrosion in a very concentrated area, which resulted in spalling of small concrete pieces out of the specimens. Beside those two specimens, all of the other specimens behaved in a very similar manner, the yielding load was between 124 kN to 127 kN, and they exhibited between 7 to 9 transverse cracks.

Figure 9.28 shows the steel stress at the crack versus the crack width for all of the specimens. Again, the influence of the corrosion level on the crack width can be clearly noted from the Fig. 9.28. The crack width increases with an increasing level of corrosion. Figures 9.29 (a) and (b) show the longitudinal splitting crack due to corrosion in a typical corroded specimen (C4-2C) and its width before and after the test. Figure 9.30 shows the transverse tensile and longitudinal splitting cracks due to corrosion for different levels of corrosion.

9.6.4 Cracking Response of Specimens

The distress in the concrete is manifested as a series of internal cracks, and the following stages of cracking are normally noted as applied load is increased:

1. Initial corrosion would form a microscopic layer around the steel surface, which is the film of gamma ferric oxide. After the early stages of corrosion, this initial microscopic layer increases the bond strength which results from the precipitation of iron oxides which occupy larger volume than the original components and therefore increase the hoop-stress and radial compression so that friction bond increases.

2. Increasing corrosion would result in further accumulation of the corrosion products (iron oxides) along the steel bar. Because of the internal pressure caused in the increased volume of the corrosion products by confinement due to the increase in the volume of the uncorroded steel as it is converted to iron oxides and hydroxides, the tensile stresses in the concrete are much greater than the concrete tensile strength, which results in the longitudinal cracks that were observed in all of the corroded specimens. Figure 9.31 (a) and (b) display a specimen cut open after testing showing the heavy layer of the corroded metal that is adhering to the concrete surface. Therefore, any adhesion between the concrete and the reinforcing steel is lost within the corroded specimens before the specimen is tested. Furthermore, this layer of corrosion products also breaks down the friction mechanism, except for low levels of corrosion. The change in the level of roughness of the bar surface, as observed by Al-Sulaimani *et al.* (1990), can result in an increase in the bond strength with increasing levels of corrosion up to about 1% corrosion.

3. Further corrosion results in development of crack(s).

4. Additional corrosion causes loss of adhesion adjacent to the crack, transferring load to the ribs of the bar.

5. Internal cracks form around the steel bar.

6. Further corrosion causes more internal cracks

At corrosion stage (1), the bond strength increases, which results from precipitation of iron oxides which occupy larger volume than the original components and therefore increases the hoop-stress and radial compression so that frictional resistance increases. The effect of stages (2), (3), and (4) is to reduce the rate at which force is transferred from the reinforcement to the concrete and hence increase the distance from the transverse crack over which the surface stresses are reduced. In other words, the minimum crack spacing S_o, as was explained in Chapter 3, increases successively above the minimum value of the concrete cover as the applied loading increases, which again causes events (2), (3), and (4) above to occur in a tension test. Also, the main transverse cracks can form anywhere on the member except within a distance, $\pm S_o$ of existing cracks. It has also been explained that no intermediate cracks can form when two cracks are less than $2S_o$ apart, and the force transferred from the steel to the concrete is smaller than the load required to crack the concrete cross-section.

If, on further loading after crack forms, an adjacent crack develops before substantial amounts of internal distress would have occurred (events (2), (3), and (4)), a new crack will be able to form close to the previous crack, giving a minimum spacing approaching the cover thickness. However, if substantial internal failure has occurred before the adjacent crack forms, S_o will be substantially larger than the cover and thus the minimum possible spacing would have increased. The average spacing will be equal to a constant times the cover thickness plus the average increase in S_o resulting from the average amount of internal distress occurring prior to formation of the adjacent crack.

Corrosion of the reinforcing steel and the formation of the corrosion products are the key parameters that are likely to control the rate of development of internal distress.

9.5 Corrosion Percentage

After completion of the tension test, the steel bar was retrieved from the specimen and detailed observation and measurement of the changes in the diameter and of the depths of the corrosion pits were made to determine the loss of the cross-sectional area after exposure of the test specimen to the aggressive environment for varying periods of time. The weight loss after cleaning and brushing of the corrosion products was determined. The cross-sectional areas of the reinforcing bars were also determined and the results are summarized in Tables 9.10 through 9.12.

9.6 Chloride Ion Profile

The variation of the chloride ion content across the concrete cover thickness at depths of 7.5mm, 25mm and 42.5mm from the concrete surface and at locations near the crack, due to corrosion and away from the crack of the tension specimens were obtained using the method presented in Chapter 4.

Figures 9.32 and 9.33 show two typical examples (Specimens C7-5C and C3-3C) of how the average chloride ion profile was obtained for each specimen of each concrete mixture. The experimental results for the chloride profiles for the Dickson Bridge Concrete tension specimens (constructed using normal portland cement with a water/cement ratio of 0.52) are presented in Figure 9.34 for Specimens C7-3C through C7-10C. The results for tension specimens made from normal portland cement concrete with a water/cement ratio of 0.32 are presented in Figure 9.35 for Specimens C3-3C through C3-10C, along with the results for Specimen C3-7C which could not be tested. The results for tension specimens made from Sundance fly ash concrete with a water/cement ratio of 0.32 are presented in Figure 9.36 for Specimens C4-3C through C4-10C.

9.7 Analysis and Discussion-Influence of Corrosion on Bond Behaviour-

The specimens were designed according to the CSA Standard-A23.3-M84 and the ACI Standard 318 recommendations for the development length, l_d, for the bar extension required to transfer the bar force to the surrounding concrete by bond. While the test specimens fulfil the development length requirement, the deteriorated surface of the bar at the steel-concrete interface, and the associated opening of the longitudinal cracks within the corroded specimens represented a departure from the ideal conditions.

As a consequence of corrosion, corrosion products (iron oxides) accumulated along the steel bar surface. Because of the internal pressure caused by the increased volume of the corrosion products due to the bar confinement, the tensile stresses in the concrete were much greater than the concrete tensile strength and resulted in the longitudinal cracks that were observed in all of the corroded specimens. As was mentioned earlier, Figure 9.31 shows a specimen which was cut open after testing, with the heavy layer of the corroded metal adhering to the concrete surface along the bar indentations. Therefore, any adhesion between the concrete and the reinforcing steel was lost within the corroded specimens before the specimen was tested. Furthermore, this layer of corrosion products also broke down the friction mechanism, excepting at low levels of corrosion. The change in the level of roughness of the bar surface, as observed by Al-Sulaimani *et al.* (1990), can result in an increase in the bond strength with increasing levels of corrosion up to about 1% loss of mass or cross-sectional area.

9.7.1 Bar Profile

Examination of the steel bar embedded in the tension specimen showed 'localized corrosion', as the deterioration was more specific to the various parts or regions of the steel bar, resulting in deep pits on the surface of the steel bars, and its eventual severance, as illustrated in Figures 9.37 and 9.38. This altered the geometric shape and size of the steel bar and hence it had a significant effect on the transfer of the force from

the steel to the surrounding concrete by the mechanical interlocking of the bar ribs affected by corrosion. Therefore, this primary mechanism of bond in deformed bars, that of transfer of forces by mechanical interlocking of the ribs, gets weakened by the effect of corrosion of the ribs.

In summary, two significant phenomena influence the deterioration of the bond strength due to the corrosion of the reinforcing steel, firstly the formation of the corrosion products along the reinforcement, and secondly, the longitudinal cracking of the tension specimen.

9.7.2 Cracking Behaviour

Figures 9.23 through 9.30 show the crack patterns for the specimens after being subjected to different levels of corrosion and then subjected to the tension tests, these are compared with the crack patterns for the uncorroded specimens. The influence of corrosion is quite evident in these figures.

For NPC specimens (w/c ratio= 0.52), the control Specimens C7-1C and C7-2C, the cracks formed at spacings as expected, which is the formation of the additional primary cracks with an increase in the stress level until the crack spacing was approximately twice the concrete cover thickness, which was about 83 mm. The calculated initial cracking load (transverse cracks) for the concrete Specimens C7-1C and C7-2C is 15 kN, but the experimental initial cracking load, adjusted for the concrete shrinkage, was 14 kN for the uncorroded Specimens C7-1C and C7-2C. This is because of the induced tensile stresses (about 5 MPa) caused by the restrained concrete shrinkage, which influence the extent of cracking at a given tensile force level. Cusick and Kesler (1976) conducted tensile tests on concrete specimens using two different types of cements, Type I cement and Type K (shrinkage-compensating) cement and compared their cracking behaviour. The Type K specimens exhibited first cracking at a higher load level than the Type I specimen, which shows that the tensile stresses,

induced in the concrete due to shrinkage, are responsible for a decrease in the cracking loads.

The fact that the corroded specimens had fewer transverse cracks than the control specimens would indicate a reduction of bond between the concrete and the reinforcing steel. This could be explained by referring to the basic considerations in Chapter 4, that slip causes a further reduction in the bond stress, which in turn, increases the value of the minimum crack spacing, S_o, as in the case of plain bars, but in the case of deformed bars, this distance S_o is influenced by the internal cracks that are formed as a result of the increase in the loads after the primary crack had formed. A study by Goto (1971) on the cracks formed around the deformed bars in tension, notes that after forming a primary crack, further loading causes loss of adhesion adjacent to the crack, transferring the loads to the ribs of the bar, and then internal cracks form close to the main crack (primary crack), and further loading increases the internal cracking. Therefore, the effect of loss of adhesion and/or the internal cracking would result in reduction of the rate at which the force is transferred from the reinforcement to the surrounding concrete and hence an increase in the distance from the main crack over which the concrete stresses are reduced. The reduction of the interlocking phenomenon between the ribs and the concrete keys due to the reduction of cross-sectional area of the ribs is the primary cause of this breakdown of bond. However, the layer of corrosion products also causes loss of adhesion and cohesion between the two materials.

Furthermore, as corrosion progresses, the longitudinal cracking and the widening of the cracks, also contribute to the loss of bond because of the smaller area of the steel surrounded by the concrete (part being lost due to the longitudinal cracking) as well as the loss of cohesion and adhesion between them. In addition, the maximum crack widths in the corroded specimens are much larger than in the uncorroded specimens which also indicates a weakening of the bond.

Goto (1971), Houde and Mirza (1972), and others observed that for the concrete specimen to crack, the force transferred from the steel bar to the concrete through the

mechanical interlock between the bar ribs and the concrete must be large enough to cause the concrete to crack. Again, once one or more cracks have developed in the specimen, further cracking would occur only if enough force was transferred between the steel and the concrete over half of the distance between the two cracks (or a crack and a free end) to cause the concrete to crack. As mentioned earlier, the corrosion of the bar ribs has a significant influence on the mechanical interlocking between the steel ribs and the concrete leading to a deterioration of the bond at the steel bar-concrete interface. Thus, the force is not transferred as efficiently from the steel bar into the concrete, leading to a larger spacing between the cracks in a specimen with a corroded bar than in a specimen with an uncorroded bar. A hypothetical extreme would be an extremely corroded bar in which the ribs are completely corroded and the adhesion and cohesion between the reinforcing steel and the concrete has been completely destroyed. The crack spacing would be very large in such a specimen because of the significant loss of bond strength, for example, the specimen C7-9C, with a 27 percent mass loss due to corrosion, which did not exhibit any transverse crack until beyond the yield strength of the reinforcing steel.

In order to form a new crack between two existing cracks, the tensile force which causes cracking of the concrete should be introduced into the concrete by this bond at the steel-concrete interface. The significant degradation in the profile of the ribs indicates that the bond integrity of the bar has decreased considerably and that it takes a longer length of the steel bar to redistribute the forces and transfer them to the concrete where it would develop a new transverse crack.

9.7.3 Load-Elongation Response

In general, local bond failures are evidenced with increasing steel stresses, when full transverse cracks form. The bond stress value at the crack drops to zero. This can be noted on the load-elongation curves, where there is a slight dropping of the load. The experimental load-elongation curves show the contribution of the concrete in the specimens basically because this corrosion is normally scattered along the length of the

steel bar, leaving some areas, or some ribs not completely destroyed, therefore, transfer of force from the steel bar to the concrete occurs in these regions, contributing to the overall transfer of force from the steel to the concrete, and vice versa.

The observations from the load-elongation responses showed mainly a decrease in the load carrying capacity for the corroded specimens, indicating a 9 to 65 percent loss of the cross-sectional area around the pit (by using A_{ys} results) of the reinforcement, from the first level to the last level of corrosion, respectively. Figures 9.39 through 9.41 show the relationship between the ultimate load (yield load) versus the mass loss due to corrosion for each of the concrete mixtures. The decreasing effect of the ultimate load capacity with increasing levels of corrosion is obvious again. The data show that the ultimate load decreases gradually up to a mass loss of 8 percent due to corrosion, i.e. in NPC with 0.52 w/c ratio (Dickson Bridge concrete), the results show that for the 8.0 percent mass loss due to corrosion, the ultimate capacity is reduced by about 5 percent, while the ultimate load is reduced to the extent of 62 percent for about 27 percent mass loss due to corrosion. Since the bond stress is well below the ultimate load in all cases of corrosion, this capacity reduction is attributable to the loss of bond. The loss of ultimate load is most likely due to the reduction in the steel bar cross-sectional area as a result of corrosion. The ultimate load capacity reduction compares well with the "equivalent" cross-sectional area of the reinforcing steel bar due to the yield load (see Table 9.13 through 9.15).

Moreover, the load-elongation curves are shifted to the right closer to the bare bar response, signifying much less concrete contribution, i.e. a decrease in the concrete tension stiffening. In fact, the specimens with the fifth, sixth, seventh and eighth levels of corrosion, with mass losses of 20, 22, 24 and 27 percent, respectively, hardly showed any concrete contribution, which was expected after experiencing the loss in the steel bar mass; the bar ductility was also reduced significantly. However, after modifying the stress-strain relationship, the corroded specimens indicated a larger concrete contribution. The contribution of the concrete was less than that in the control specimens, decreasing gradually with the increasing level of corrosion. This could be

explained by the heavy layer of the corrosion products adhering to the concrete and the steel, keeping the two materials in contact. Also, the fact, that the reinforcing bar showed localized corrosion, implies that some areas of the bars are not as badly corroded as the others, and hence some ribs along the steel reinforcing bar are in fact interlocking with the surrounding concrete. In addition, the increasing number of the longitudinal splitting cracks and their increasing widths combined with the advancing corrosion also contribute to the loss of adhesion and cohesion between the concrete and the reinforcing steel.

9.7.4 Relative Bond Performance of Corroded Bars

If the bond stress, u, is assumed to be uniformly distributed over the length of the bar, l, which is half the distance between the cracks, i.e. the length over which the steel force is transferred, then

$$(\pi\, d_b l)\, u = (\frac{\pi\, d_b^2}{4})\, f_y \qquad \textbf{(9.1)}$$

where d_b is the bar diameter, and f_y is the steel yield strength.
This gives:

$$u = \frac{d_b\, f_y}{4l} \qquad \textbf{(9.2)}$$

If d_b and f_y are constant, then

$$u = \frac{k}{l} \qquad \textbf{(9.3)}$$

where k is a constant. Therefore, the average uniform bond stress is inversely proportional to the distance between the cracks.

If the bond stress in the uncorroded specimen is considered to be 100%, the relative percentage for the corroded specimens can be calculated using Equation 9.2. These values were calculated for all of the specimens and are summarized in Tables 9.16 through 9.18 and plotted in Figures 9.42 through 9.44. It can be noted from this qualitative plot that the bond between the concrete and the reinforcing steel deteriorates increasingly as the level of corrosion increases.

As can be seen, the relative bond stress of the NPC concrete specimen with a w/c ratio of 0.52, with 8 percent mass loss due to corrosion, represents a 24 percent loss of bond strength, while a 27 percent mass loss due to corrosion, results in an 88 percent loss of bond strength.

For the NPC specimen with a w/c ratio of 0.32, as expected, a 1.5 percent mass loss due to corrosion resulted in a 2 percent loss of bond strength, while a 14.5 percent mass loss due to corrosion, resulted in an 85 percent loss of bond strength. This investigation agrees well with the results of the study by Andrade *et al.* (1990), who suggested that a reduction of 10 to 25 percent in the bar section in the critical zones of the structure will result in the depletion of its service life, while a reduction up to 5 percent, even with cracking and spalling, will indicate an early stage of deterioration with the remaining service life not as significantly influenced, provided that adequate repairs are undertaken urgently.

The qualitative plot of the relative bond stress of the corroded Sundance fly ash concrete specimens with respect to the corresponding uncorroded specimens (Fig. 9.44) shows that the bond between the concrete and the reinforcing steel increases with corrosion rate up to a maximum mass loss value of 0.9 percent, after which the bond deteriorates increasingly as the level of corrosion increases. With about 0.9 percent mass loss due to corrosion, there is a 10 percent increase in the bond strength. However,

a mass loss of 1.5 percent causes a 10 percent loss of bond strength, while a 4.5 percent mass loss results in a 55 percent loss of bond strength.

The most significant deterioration of bond in the postcracking corrosion stage occurs with a 27 percent mass loss, resulting in a 88 percent loss of bond strength, i.e. the bond between the steel and the concrete is lost almost completely. This can be explained on the basis of several interactive factors. This significant degradation results from the severe localized corrosion of the rebar ribs, the formation of a heavy layer of the corrosion products along the rebar, causing a loss of adhesion and cohesion, and the reduction in the cross-sectional area. Therefore, the mechanical interlocking between the ribs of the reinforcing bar and the concrete deteriorates significantly with an increase in the corrosion level. Furthermore, the widening of the longitudinal cracks with an increase in the corrosion level have also contributed to the loss of adhesion and cohesion between the reinforcing bar and the surrounding concrete.

The analysis presented here does not consider directly the effect of the concrete permeability on the bond between the concrete and the reinforcing steel. The published results in the literature show that the permeability of the concrete mixture is very important in the ingress of chloride ions into the concrete specimen, however, an increase in the permeability accelerates the cracking due to corrosion. Therefore, the concrete permeability must be considered as a significant factor in comparing the bond strength of the interface between the steel and the concrete in different concrete mixture specimens and in different types of aggressive environments, causing different levels of corrosion. This is in agreement with the results of the pullout specimens, which show that the permeability of the Sundance concrete mixture is about two orders higher than that of the Normal Portland Cement with a w/c ratio of 0.32.

The chloride ion content results provide an indirect indication of the concrete permeability and show that introducing high volume fly ash into the concrete mixture resulted in lower diffusivities and permeabilities even though the water-cementations

materials ratios are constant. However, the difference between the fly ash concretes and the normal portland cement with a w/c ratio of 0.32 was less pronounced.

The reduction of bond strength caused by a given level of corrosion is quantified by regression analysis of the experimental results for the relationship between the bond strength and the mass loss due to corrosion. Also, by disregarding the values where slight corrosion leads to an increase in the bond strength (Chapter 10).

9.8 Correlation between Series C7 and Dickson Bridge Test Results

The mass loss of the reinforcing steel in the Dickson Bridge and the C7 Series tension specimens, constructed using the bridge deck concrete were correlated with the respective chloride contents at the steel levels. The results in Fig 5.8 show a larger cluster of the data between chloride contents of 0.3-0.5% and mass loss between 5 to 20%. The bridge deck had been subjected to deicing salts over the years until 1993 when the bridge was abandoned. The use of deicing salts was then discontinued and since the bridge was not being used, the snow and ice were not cleared. As this snow and ice melted each spring, the chlorides were leached from the upper part into the lower part of the deck, therefore, the chloride content at the steel level in the upper part of the deck would be lower than the chloride content that initiated it. Therefore, it was decided to compare the test results for the steel bar mass loss as the chloride content for the Dickson Bridge deck and the Series C7 specimens with steel bar mass loss less than 15%. These results are shown in Fig. 9.45 which shows that despite the scatter in the field test data very good agreement exists between the average of the two sets of data. It is clear that for steel bar mass loss values smaller than 15% (which is quite large by itself), it is possible to predict the mass loss for a given value of the chloride content. It should be noted that almost all of the chloride content values are larger than 0.2%, the threshold value for chloride content in a reinforced

concrete structure. It should also be noted that these projections have been made from limited field and laboratory data and more research is needed in this area.

9.9 Nonlinear Finite Element Analysis of Dickson Bridge Deck Using Series C7 Test Results

The results of the tests on Series C7 specimens, which had been constructed using the Dickson Bridge concrete. The parameters of the Dickson Bridge concrete were established from the contract drawings and specifications to build the new bridge in 1959 and confirmed by the petrographic studies performed as a part of this research program were formalized. Based on the field test data for the various tests and the results of similar tests on the Series C7 specimens in the laboratory, the Dickson Bridge deck steel was idealized for its level of corrosion, the remaining cross-sectional area and its mechanical properties (Palsson and Mirza, 2001). Nguyen is presently analysing the deteriorated bridge deck using the nonlinear finite element analysis program, NONLACS, which will provide the overall response of the bridge deck in terms of its load-deformation characteristics, stresses and strains at the various locations, the ultimate load and the final mode of failure. These computed values for the deteriorated bridge (as modeled from the field tests and the properties as modeled from the related laboratory tests) will be compared with the results for the same parameters computed for the "new" bridge (as constructed in 1959). In addition, the effect of the various levels of deterioration on the bridge deck response from 1959 to 1996 will be established. The results will be projected to the future with increased deterioration in both concrete and steel to a stage when the bridge would lose its structural integrity. These results would constitute a deterioration case history of the Dickson Bridge and will be presented by Nguyen in his MEng. thesis (2001).

Another study by Lounis and Mirza (2001) examined the service life of the Dickson Bridge based on the on-going environmental conditions and the statistical parameters for the various deterioration modes (Table 5.5 and other related tables). They determined independently that under these conditions, the bridge would have

deteriorated extensively over a period of about 35 years. More work is in progress to evaluate the service life of new infrastructure subjected to aggressive environmental conditions and the remaining service life of existing deteriorated infrastructure.

9.10 Summary

This chapter summarizes the results of 30 tests on tension specimens after the development of different levels of corrosion from three concrete mixtures, required in 24 of the specimens with the remaining six (two per concrete mixture) being used as control specimens. The experimental results are analyzed and quantified for the influence of the level of corrosion on the bond strength at the steel-concrete interface and compared with similar relationships for the tests on pullout specimens with six different concrete mixtures. These relationships can be adapted to enable design of concrete structures for the effect of corrosion over a given service period in an aggressive environment, which is reflected in the percentage steel bar mass loss. They will also enable evaluation of the service life of new infrastructure and the remaining service life of the existing infrastructure.

Table 9.1: Details of the results for tension specimens (Dickson Bridge Concrete; NPC w/c = 0.52)

Specimen	Corrosion stage	Number of major longitudinal crack(s) due to corrosion	Average width of longitudinal crack due to corrosion (mm)	Experimental load at First cracking (kN)	Experimental yielding load (kN)	Mass loss due to corrosion (%)
C7-1C	0	0	0	18	127	0
C7-2C	0	0	0	19	127	0
C7-4C	1	1	1.2	23	116	8
C7-5C	2	1	1.5	24	102.5	11
C7-8C	3	1	1.2	23	96	16
C7-3C	4	2	1.3	17	87.5	15
C7-7C	5	1	3	28	83	20
C7-10C	6	2	4	59	81.5	22
C7-6C	7	3	2	63	70	24
C7-9C	8	2	4	-	45	27

Table 9.2: Details of the results for tension specimens (NPC, w/c = 0.32).

Specimen	Corrosion stage	Number of major longitudinal crack(s) due to corrosion	Average size of longitudinal crack due to corrosion (mm)	Experimental load at first cracking (kN)	Experimental yielding load (kN)	Mass loss due to corrosion (%)
C3-1C	0	0	0	19	127	0
C3-2C	0	0	0	19	127	0
C3-5C	1	0	0	34	125	1.5
C3-8C	2	2	0.08	48	124	2.2
C3-10C	3	2	0.35	35	121	4.5
C3-9C	4	3	1.5	30	122	5.7
C3-6C	5	3	2	31	115	7.7
C3-3C	6	2	3	48	93	11.1
C3-4C	7	3	3	37	83	14.5

Table 9.3: Details of the results for tension specimens (Sundance Fly Ash Concrete w/cm = 0.32).

Specimen	Corrosion stage	Experimental load at first cracking	Experimental yielding load	Mass loss due to corrosion
		(kN)	(kN)	(%)
C4-1C	0	22	126	0
C4-2C	0	21	128	0
C4-10C	1	31	127	0.9
C4-6C	2	29	124	1.0
C4-9C	3	27	126	1.5
C4-5C	4	27	125	1.75
C4-3C	5	32	124	2
C4-4C	6	36	124.5	2.5
C4-7C	7	22	110	3.35
C4-8C	8	30	90	4.5

Table 9.4: Comparison between the different cross-sectional area evaluation

Specimen	Corrosion stage	Mass loss due to corrosion	Experimental yielding load	Equivalent cross-sectional of steel A_{ys}	Equivalent cross-sectional of steel A_{ms}	Loss of cross-sectional area due to concentrated corrosion
		(%)	(kN)	(mm^2)	(mm^2)	(%)
C7-1C	0	0	127	300	---	0
C7-2C	0	0	127	300	---	0
C7-4C	1	8	116	274	277	8.7
C7-5C	2	11	102.5	242	267	19.3
C7-8C	3	16	96	227	254	24.4
C7-3C	4	15	87.5	207	257	31
C7-7C	5	20	83	196	243	34.6
C7-10C	6	22	81.5	193	237	35.8
C7-6C	7	24	70	166	231	44.9
C7-9C	8	27	45	106	223	64.6

Table 9.5: Comparison between the different cross-sectional area evaluation

Specimen	Corrosion stage	Mass loss due to corrosion (%)	Experimental yielding stress. f_y (MPa)	Equivalent cross-sectional of steel A_{ys} (mm^2)	Equivalent cross-sectional of steel A_{ms} (mm^2)	Loss cross-sectional due to concentrated corrosion (%)
C3-1C	0	0	423	300	300	0
C3-2C	0	0	423	300	300	0
C3-5C	1	1.5	417	295	296	1.6
C3-8C	2	2.2	413	293	294	2.4
C3-10C	3	4.5	403	286	287	4.7
C3-9C	4	5.7	407	288	284	3.9
C3-6C	5	7.7	383	272	278	9.4
C3-3C	6	11.1	310	220	268	26.8
C3-4C	7	14.5	277	196	258	34.6

Table 9.6: Comparison between the different cross-sectional area evaluation

Specimen	Corrosion stage	Mass loss due to corrosion (%)	Experimental yielding load (kN)	Equivalent cross-sectional of steel A_{ys} (mm^2)	Equivalent cross-sectional of steel A_{ms} (mm^2)	Loss of cross-sectional area due to concentrated corrosion (%)
C4-1C	0	0	126	300	---	0
C4-2C	0	0	128	300	---	0
C4-10C	1	0.9	127	300	298	0
C4-6C	2	1.0	124	293	297	2.4
C4-9C	3	1.5	126	298	296	0.8
C4-5C	4	1.75	125	295	295	1.6
C4-3C	5	2.0	124	293	294	2.4
C4-4C	6	2.5	124.5	294	293	2.0
C4-7C	7	3.35	110	260	290	13.4
C4-8C	8	4.5	90	213	287	29.1

Table 9.7: Details of the cracking behaviour

Specimen	Corrosion stage	Mass loss due to corrosion (%)	Number of transverse crack due (tension test)	Experimental stress at first cracking (MPa)	Measured average crack spacing S_m (mm)	Measured maximum crack spacing (mm)
C7-1C	0	0	11	47	83	110
C7-2C	0	0	11	80	83	100
C7-4C	1	8	9	77	100	160
C7-5C	2	11	7	80	125	200
C7-8C	3	16	6	77	143	200
C7-3C	4	15	4	57	200	220
C7-7C	5	20	3	93	250	300
C7-10C	6	22	2	197	333	350
C7-6C	7	24	1	210	500	500
C7-9C	8	27	0	---	1000	150

Table 9.8: Details of the cracking behaviour

Specimen	Corrosion stage	Mass loss due to corrosion (%)	Number of transverse crack (tension test)	Experimental stress at first cracking (MPa)	Measured average crack spacing S_m (mm)	Measured maximum crack spacing (mm)
C3-1C	0	0	12	47	77	95
C3-2C	0	0	12	80	77	98
C3-5C	1	1.5	12	113	77	100
C3-8C	2	2.2	10	160	91	180
C3-10C	3	4.5	8	117	111	220
C3-9C	4	5.7	6	100	143	250
C3-6C	5	7.7	4	103	200	220
C3-3C	6	11.1	3	175	250	270
C3-4C	7	14.5	2	123	333	350

Table 9.9: Details of the cracking behaviour

Specimen	Corrosion stage	Mass loss due to corrosion (%)	No of transverse crack due (tension test)	Experimental stress at first cracking (MPa)	Measured average crack spacing S_m (mm)	Measured maximum crack spacing (mm)
C4-1C	0	0	10	424	91	110
C4-2C	0	0	10	426	91	100
C4-10C	1	0.9	11	103	83	112
C4-6C	2	1.0	9	97	100	140
C4-9C	3	1.5	9	90	100	135
C4-5C	4	1.75	8	90	111	150
C4-3C	5	2.0	8	107	111	153
C4-4C	6	2.5	7	120	125	158
C4-7C	7	3.35	7	40	125	190
C4-8C	8	4.5	6	100	143	150

Table 9.10: Comparison between the different criteria for corrosion evaluation

Specimen	Corrosion stage	Mass loss due to corrosion (%)	Loss of cross-sectional area due to concentrated corrosion (%)	Measured average crack spacing S_m (mm)	Chloride content at the steel level Cl (%)
C7-1C	0	0	0	83	---
C7-2C	0	0	0	83	---
C7-4C	1	8	8.7	100	0.37
C7-5C	2	11	19.3	125	0.48
C7-8C	3	16	24.4	143	0.72
C7-3C	4	15	31	200	0.94
C7-7C	5	20	34.6	250	1.16
C7-10C	6	22	35.8	333	1.12
C7-6C	7	24	44.9	500	1.44
C7-9C	8	27	64.6	1000	1.52

Table 9.11: Comparison between the different criteria for corrosion evaluation

Specimen	Corrosion stage	Mass loss due to corrosion (%)	Loss of cross-sectional due to concentrated corrosion (%)	Measured Average Crack Spacing S_m (mm)	Chloride content at the steel level Cl^- (%)
C3-1C	0	0	0	77	---
C3-2C	0	0	0	77	---
C3-5C	1	1.5	1.6	77	0.04
C3-8C	2	2.2	2.4	91	0.11
C3-10C	3	4.5	4.7	111	0.19
C3-9C	4	5.7	3.9	143	0.28
C3-6C	5	7.7	9.4	200	0.29
C3-3C	6	11.1	26.8	250	0.35
C3-4C	7	14.5	34.6	333	0.46

Table 9.12: Comparison between the different criteria for corrosion evaluation

Specimen	Corrosion stage	Mass loss due to corrosion (%)	Loss of cross-sectional area due to concentrated corrosion (%)	Measured average crack spacing S_m (mm)	Chloride content at the steel level Cl^- (%)
C4-1C	0	0	0	91	---
C4-2C	0	0	0	91	---
C4-10C	1	0.9	0	83	0.002
C4-6C	2	1.0	2.4	100	0.003
C4-9C	3	1.5	0.8	100	0.013
C4-5C	4	1.75	1.6	111	0.004
C4-3C	5	2.0	2.4	111	0.02
C4-4C	6	2.5	2.0	125	0.01
C4-7C	7	3.35	13.4	125	0
C4-8C	8	4.5	29.1	143	0.006

Table 9.13: Percentage loss of ultimate load for NPC (w/c ratio= 0.52)

Specimen	Corrosion stage	Mass loss due to corrosion (%)	Ultimate load capacity (kN)	Percentage loss of ultimate capacity
C7-1C	0	0.0	200	0.0
C7-4C	1	8	190	5.0
C7-5C	2	11	169	15.5
C7-8C	3	16	154	23.0
C7-3C	4	15	128	36.0
C7-7C	5	20	125	37.5
C7-10C	6	22	121	39.5
C7-6C	7	24	104	48.0
C7-9C	8	27	76	62

Table 9.14: Percentage loss of ultimate load for NPC (w/c ratio= 0.32)

Specimen	Corrosion stage	Mass loss due to corrosion (%)	Ultimate load capacity (kN)	Percentage loss of ultimate capacity
C3-1C	0	0.0	200	0.0
C3-5C	1	1.5	202	0.0
C3-8C	2	2.2	199	0.5
C3-10C	3	4.5	193	3.5
C3-9C	4	5.7	193	3.5
C3-6C	5	7.7	189	5.5
C3-3C	6	11.1	147	26.5
C3-4C	7	14.5	127	36.5

Table 9.15: Percentage loss of ultimate load for Sundance concrete mixture.

Specimen	Corrosion stage	Mass loss due to corrosion (%)	Ultimate load capacity (kN)	Percentage loss of ultimate capacity
C4-1C	0	0.0	200	0.0
C4-10C	1	0.9	198	1.0
C4-6C	2	1.2	196	2.0
C4-9C	3	1.5	197	1.5
C4-5C	4	1.8	197	1.5
C4-3C	5	2.0	195	2.5
C4-4C	6	2.5	196	2.0
C4-7C	7	3.4	173	13.5
C4-8C	8	4.5	128	36.0

Table 9.16: Nominal bond stress percentage.

Specimen	Corrosion stage	Mass loss due to corrosion (%)	Measured average crack spacing S_m (mm)	Nominal bond stress (%)
C7-1C	0	0	83	100
C7-2C	0	0	83	100
C7-4C	1	8	100	83
C7-5C	2	11	125	67
C7-8C	3	16	143	58
C7-3C	4	15	200	42
C7-7C	5	20	250	33
C7-10C	6	22	333	25
C7-6C	7	24	500	17
C7-9C	8	27	1000	8

Table 9.17: Nominal bond stress percentage.

Specimen	Corrosion stage	Mass loss due to corrosion (%)	Measured average crack spacing S_m (mm)	Nominal bond stress (%)
C3-1C	0	0	77	100
C3-2C	0	0	77	100
C3-5C	1	1.5	77	100
C3-8C	2	2.2	91	85
C3-10C	3	4.5	111	69
C3-9C	4	5.7	143	54
C3-6C	5	7.7	200	39
C3-3C	6	11.1	250	31
C3-4C	7	14.5	333	23

Table 9.18: Nominal bond stress percentage.

Specimen	Corrosion stage	Mass loss due to corrosion (%)	Measured average crack spacing S_m (mm)	Nominal bond stress (%)
C4-1C	0	0	91	100
C4-2C	0	0	91	100
C4-10C	1	0.9	83	110
C4-6C	2	1.0	100	91
C4-9C	3	1.5	100	91
C4-5C	4	1.8	111	82
C4-3C	5	2.0	111	82
C4-4C	6	2.5	125	73
C4-7C	7	3.4	125	73
C4-8C	8	4.5	143	64

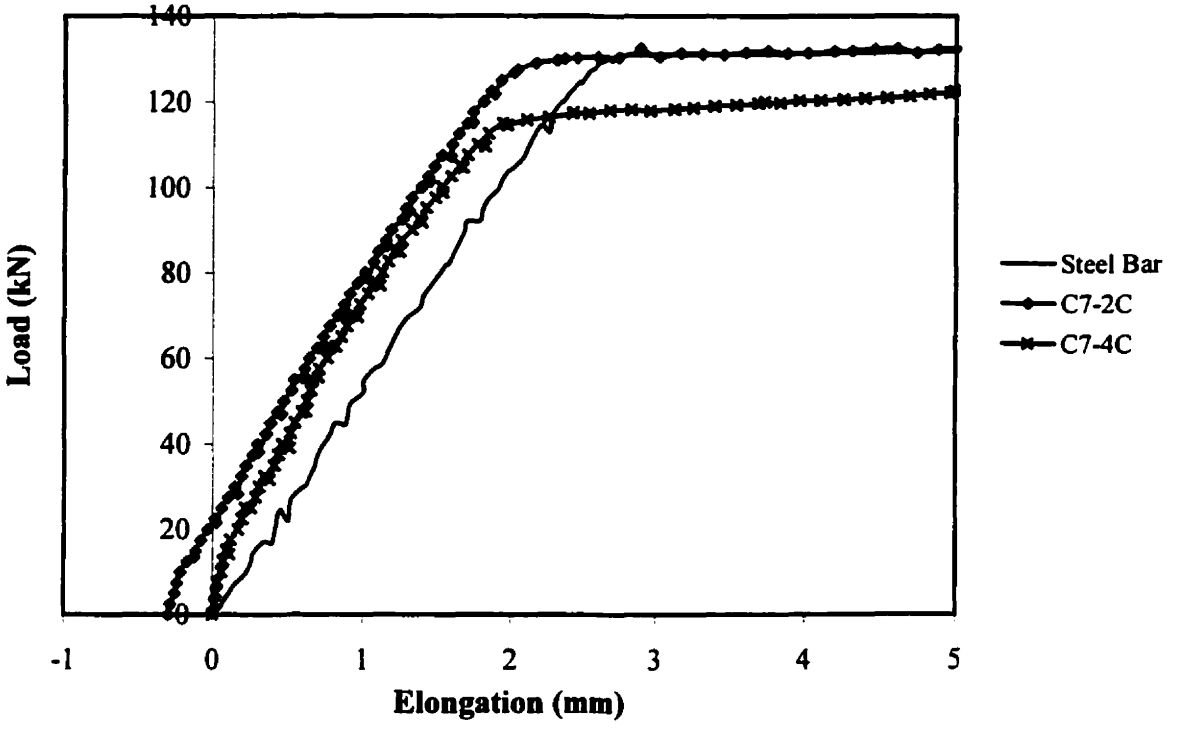

Fig. 9.1: Load-elongation response for Specimen C7-4C
(Normal Portland Cement with w/c ratio = 0.52)

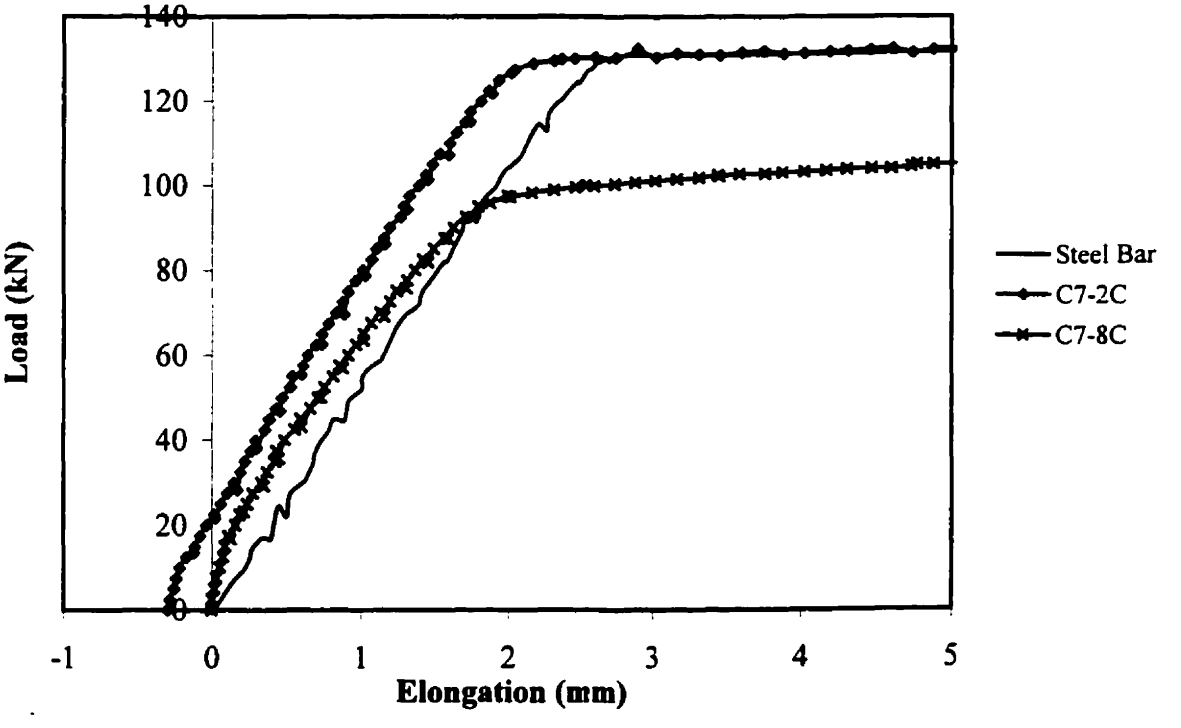

Fig. 9.2: Load-elongation response for Specimen C7-8C
(Normal Portland Cement with w/c ratio = 0.52)

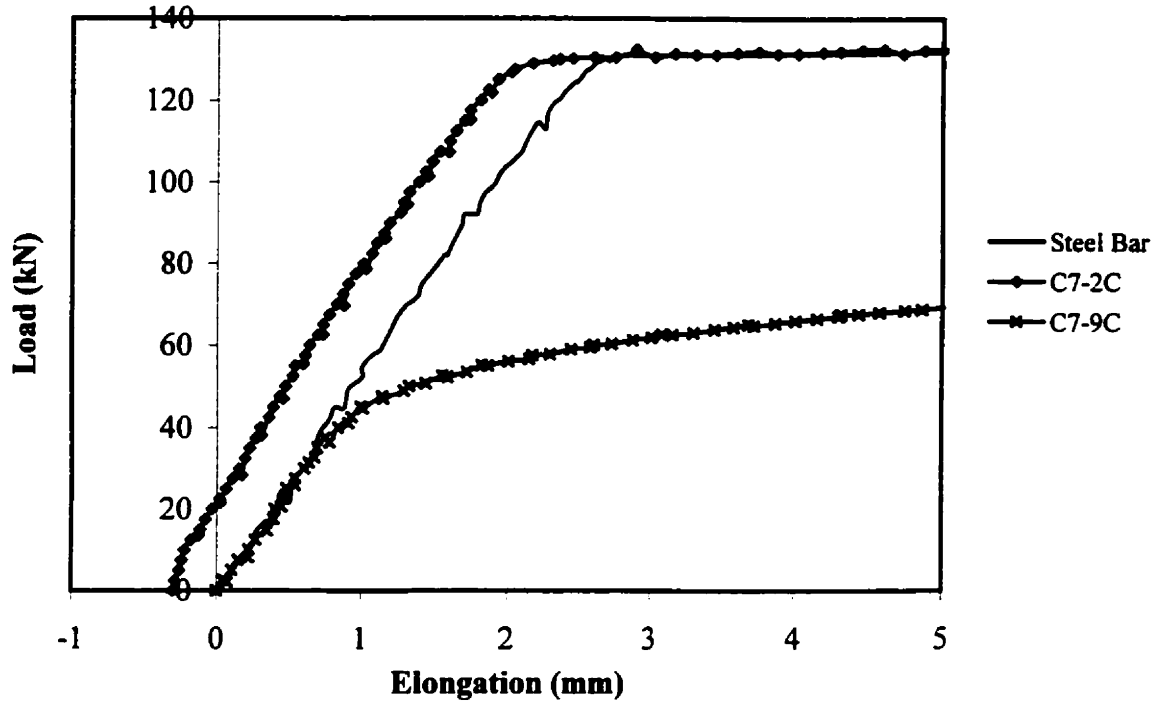

Fig. 9.3: Load-elongation response for Specimen C7-9C
(Normal Portland Cement with w/c ratio = 0.52)

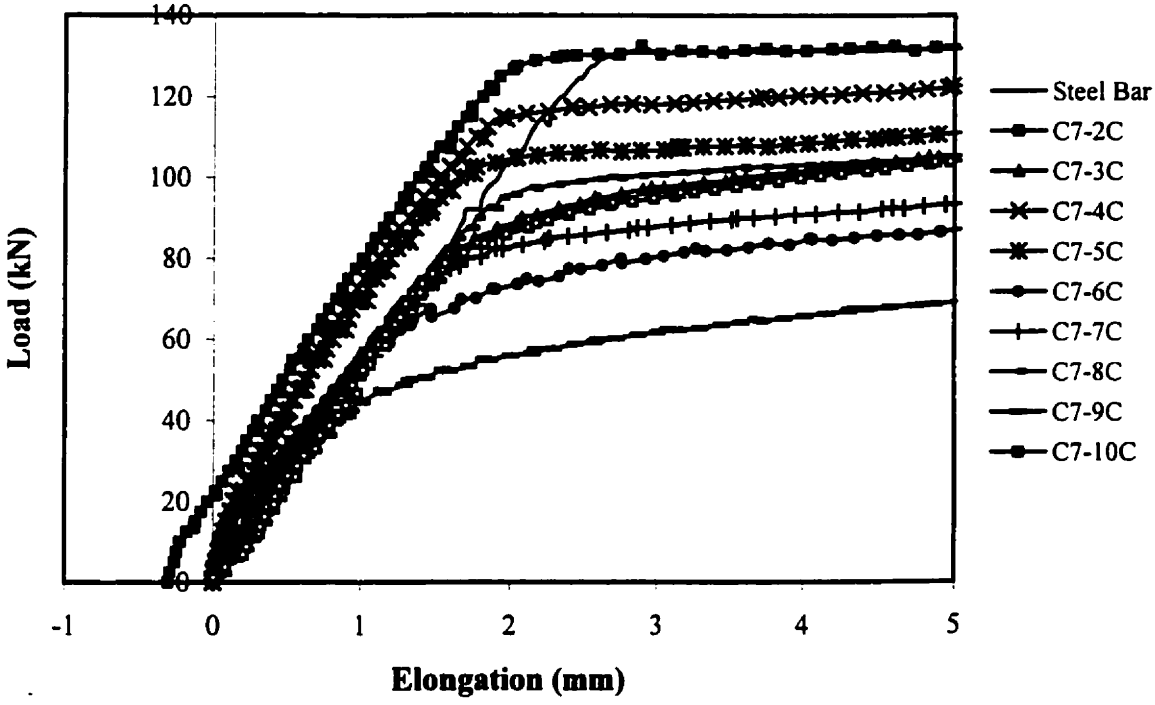

Fig. 9.4: Load-elongation response for all of the Specimens
(Normal Portland Cement with w/c ratio = 0.52)

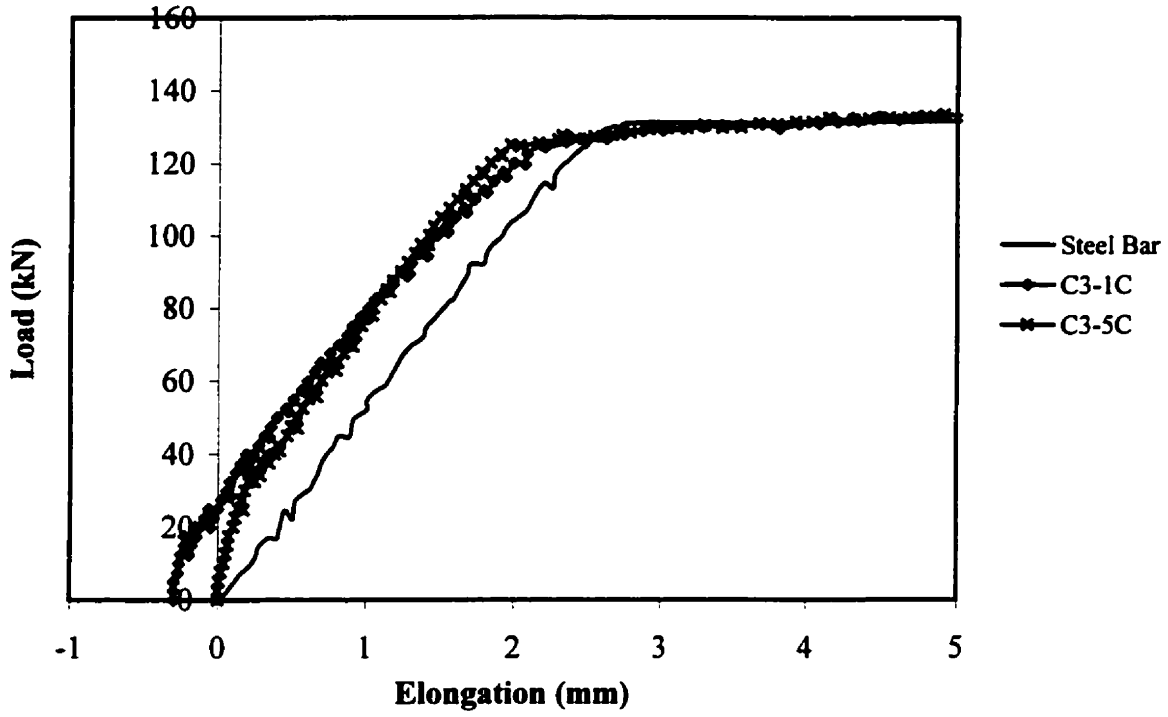

Fig. 9.5: Load-elongation response for Specimen C3-5C
(Normal Portland Cement with w/c ratio = 0.32)

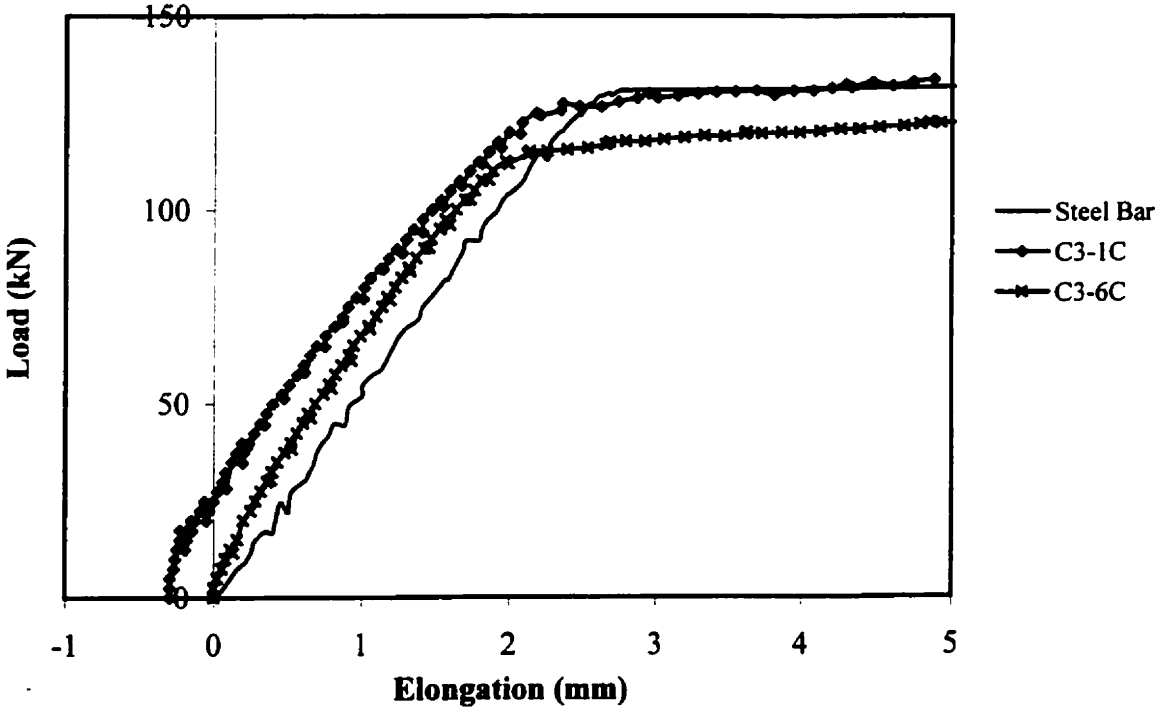

Fig. 9.6: Load-elongation response for Specimen C3-6C
(Normal Portland Cement with w/c ratio= 0.32)

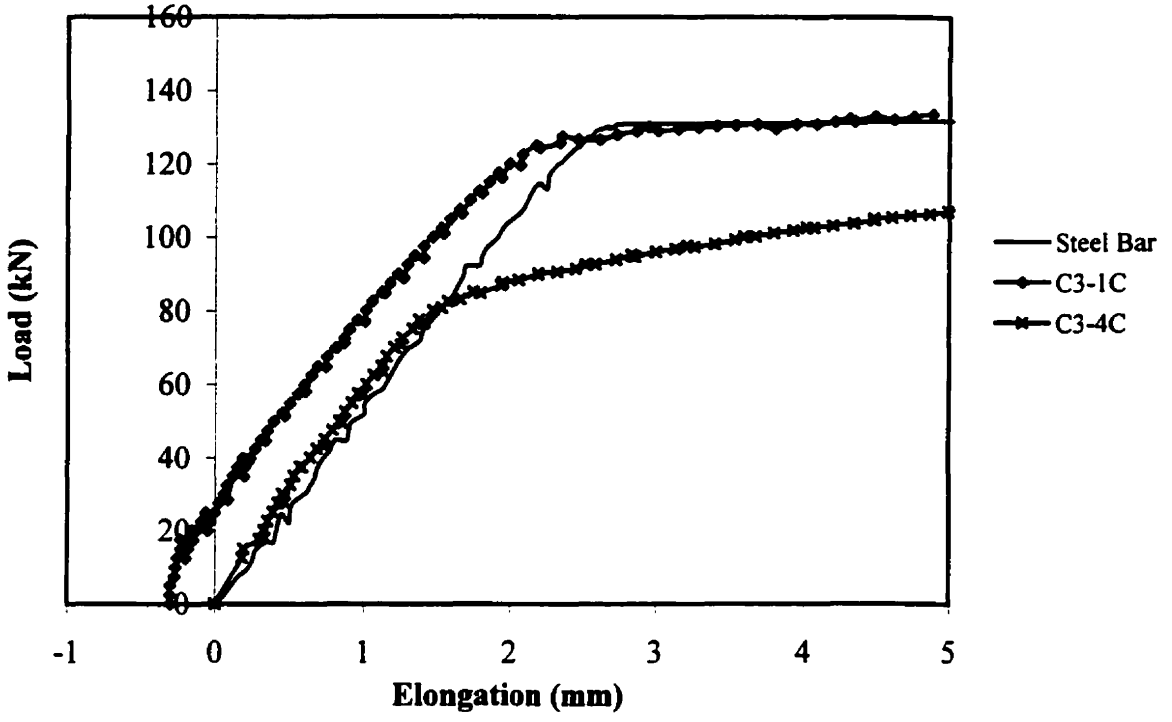

Fig. 9.7: Load-elongation response for Specimen C3-4C
(Normal Portland Cement with w/c ratio = 0.32)

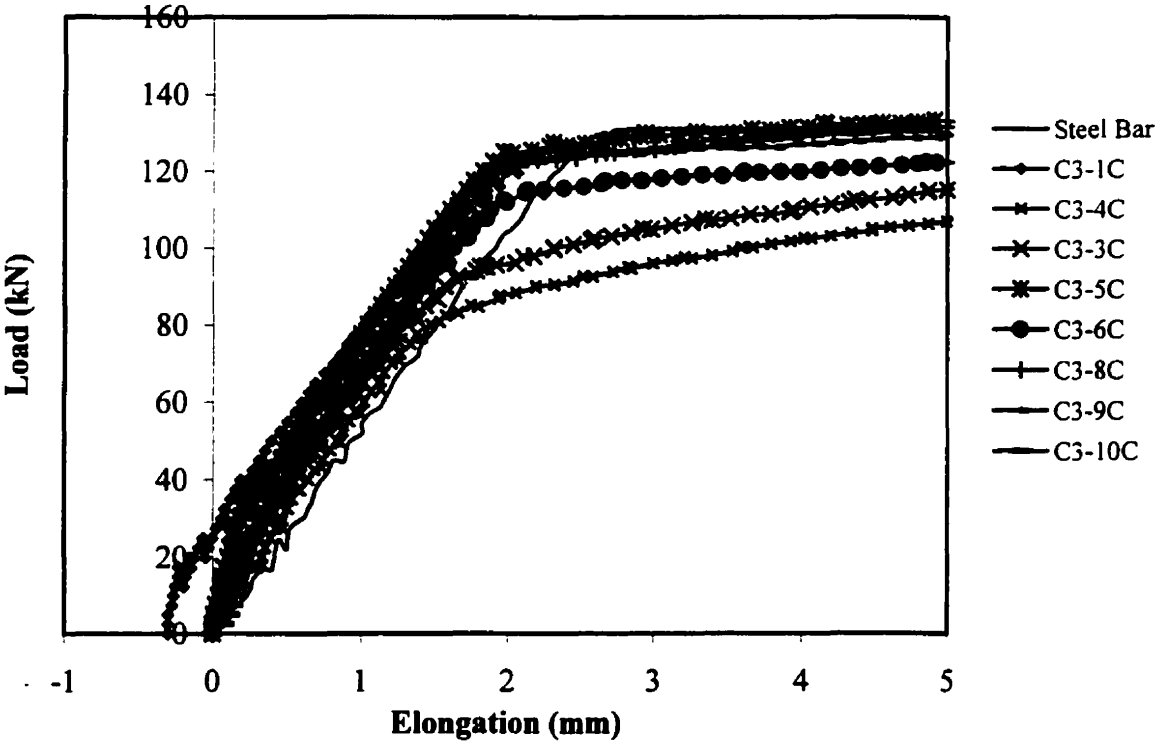

Fig. 9.8: Load-elongation response for all of the Specimens
(Normal Portland Cement with w/c ratio = 0.32)

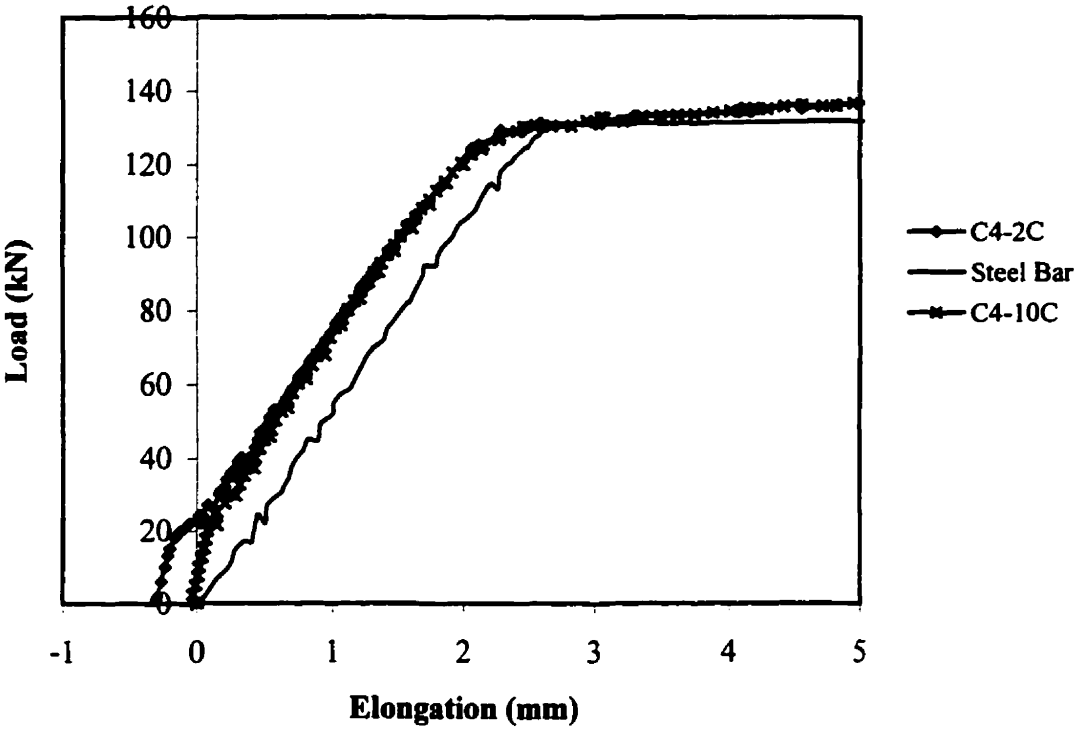

Fig. 9.9: Load-elongation response for Specimen C4-10C
(Sundance fly ash concrete)

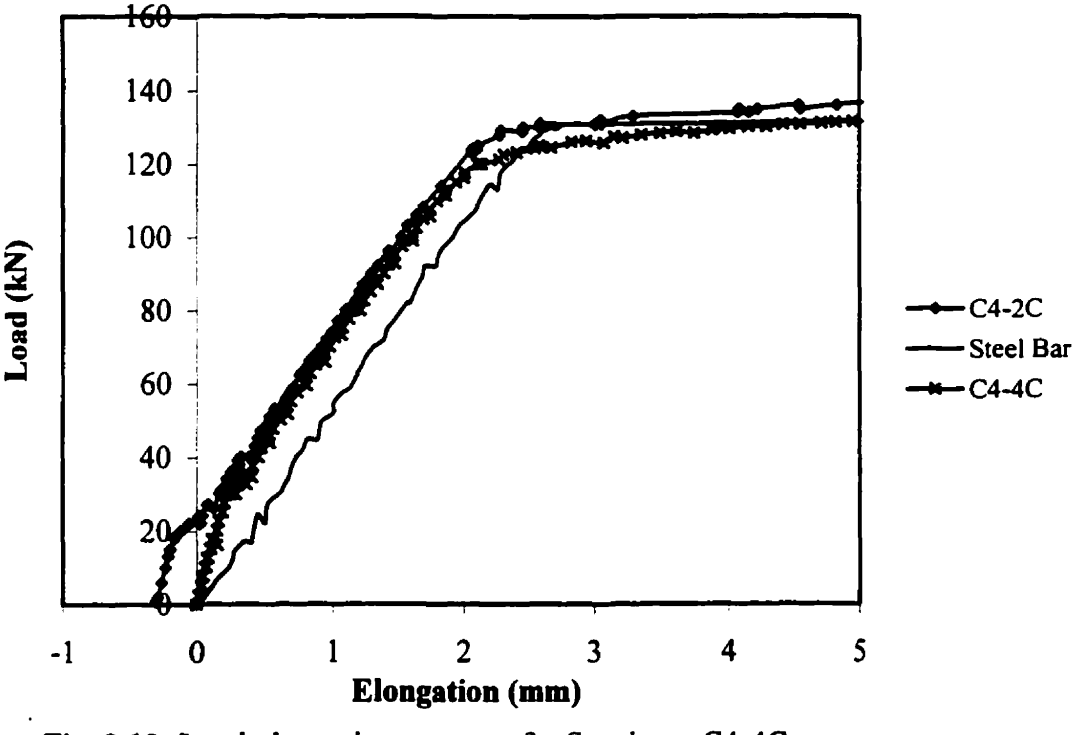

Fig. 9.10: Load-elongation response for Specimen C4-4C
(Sundance fly ash concrete)

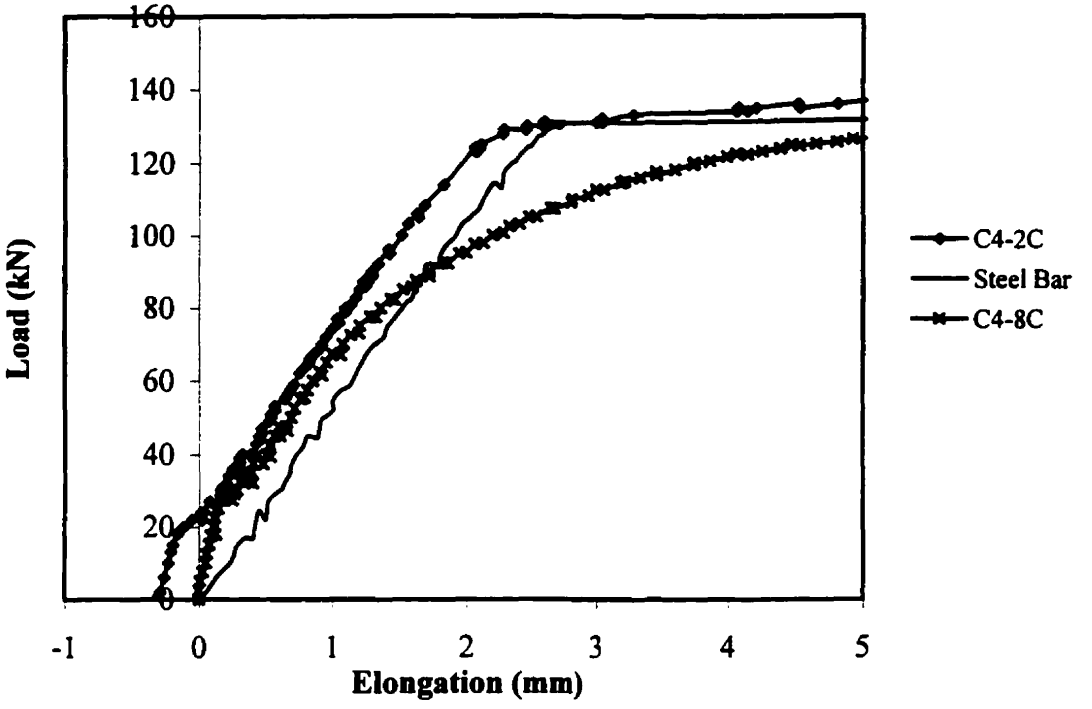

Fig. 9.11: Load-elongation response for Specimen C4-8C
(Sundance fly ash concrete)

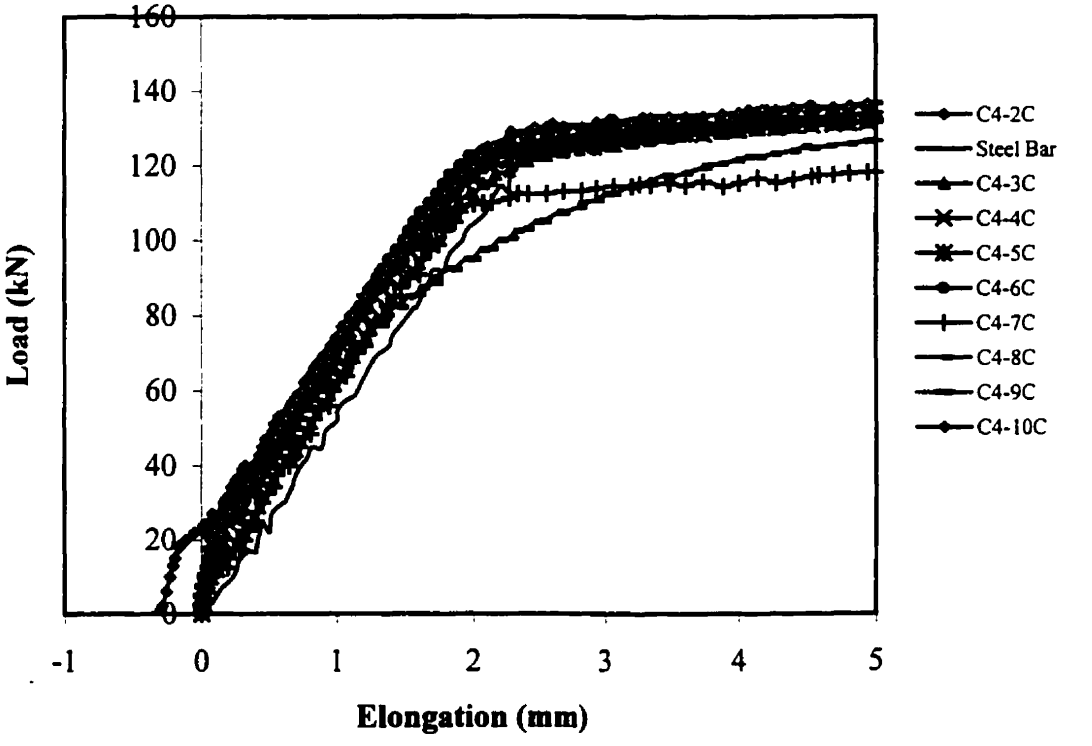

Fig. 9.12: Load-elongation response for all of the Specimens
(Sundance fly ash concrete)

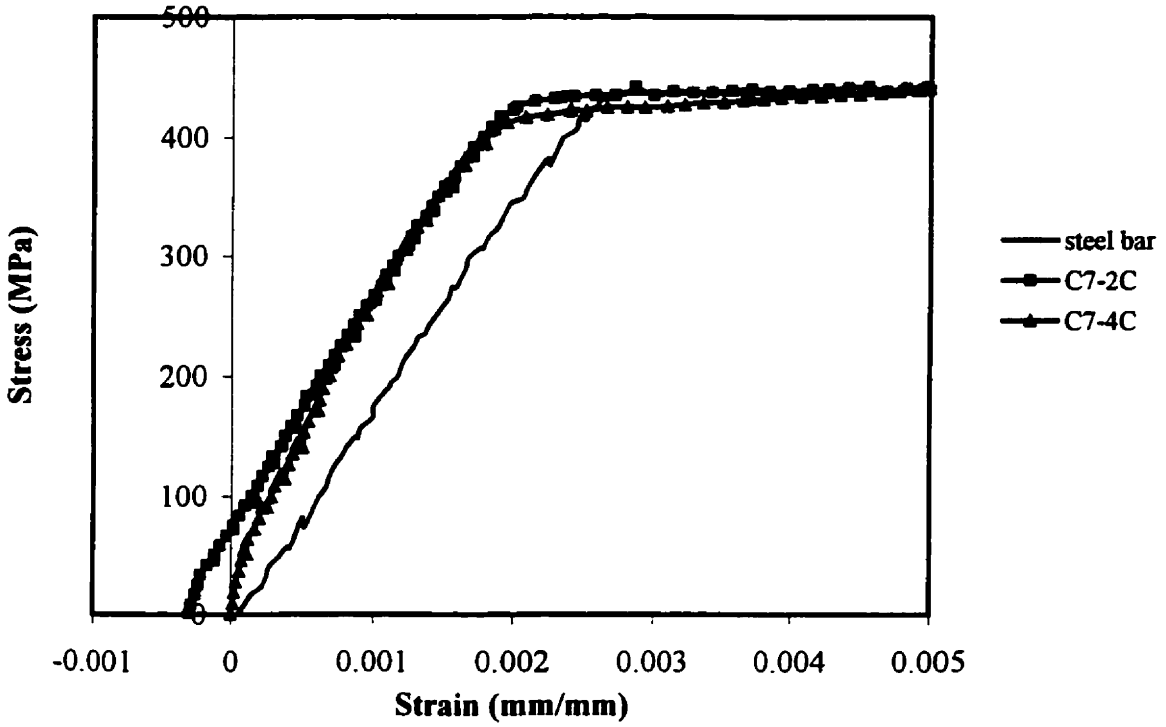

Fig. 9.13: Comparison of calculated stress-strain relationship for Specimen C7-4C (Normal Portland Cement with w/c ratio = 0.52)

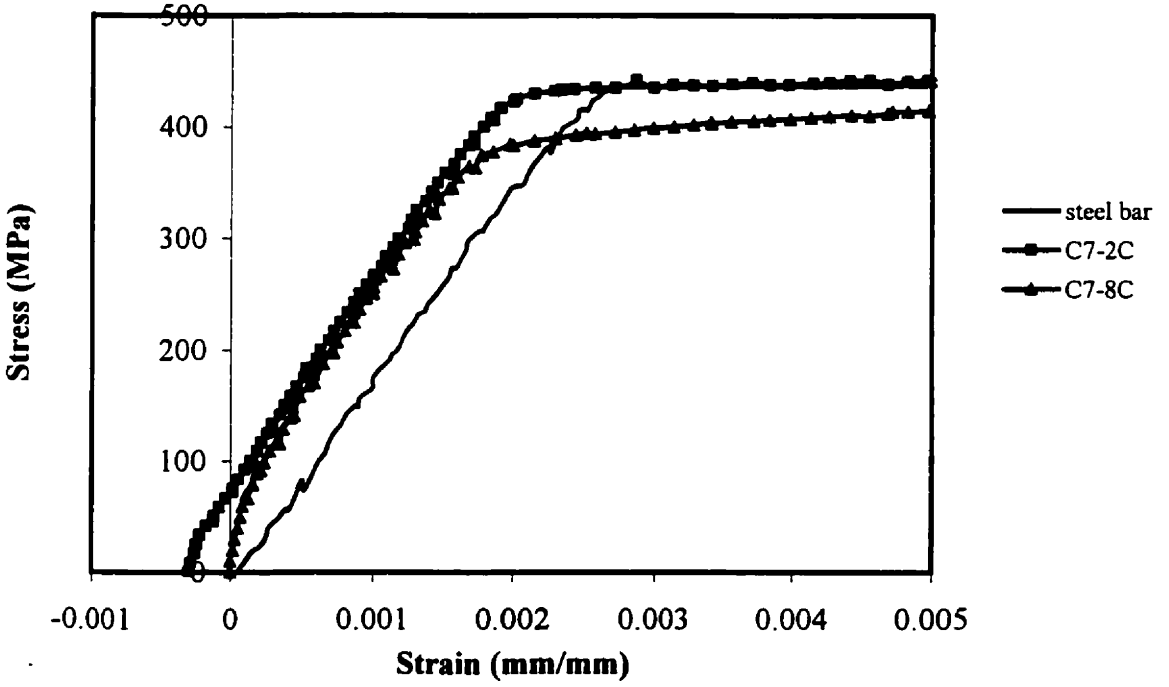

Fig. 9.14: Comparison of calculated stress-strain relationship for Specimen C7-8C (Normal Portland Cement with w/c ratio = 0.52)

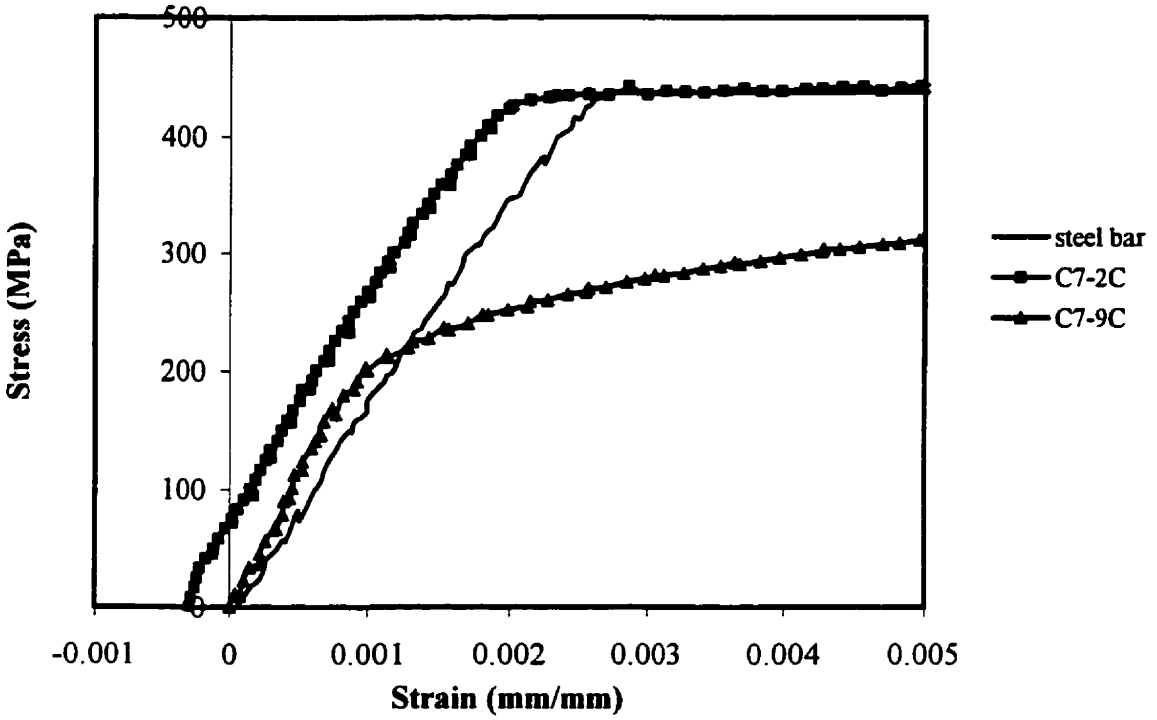

Fig. 9.15: Comparison of calculated stress-strain relationship for Specimen C7-9C (Normal Portland Cement with w/c ratio = 0.52)

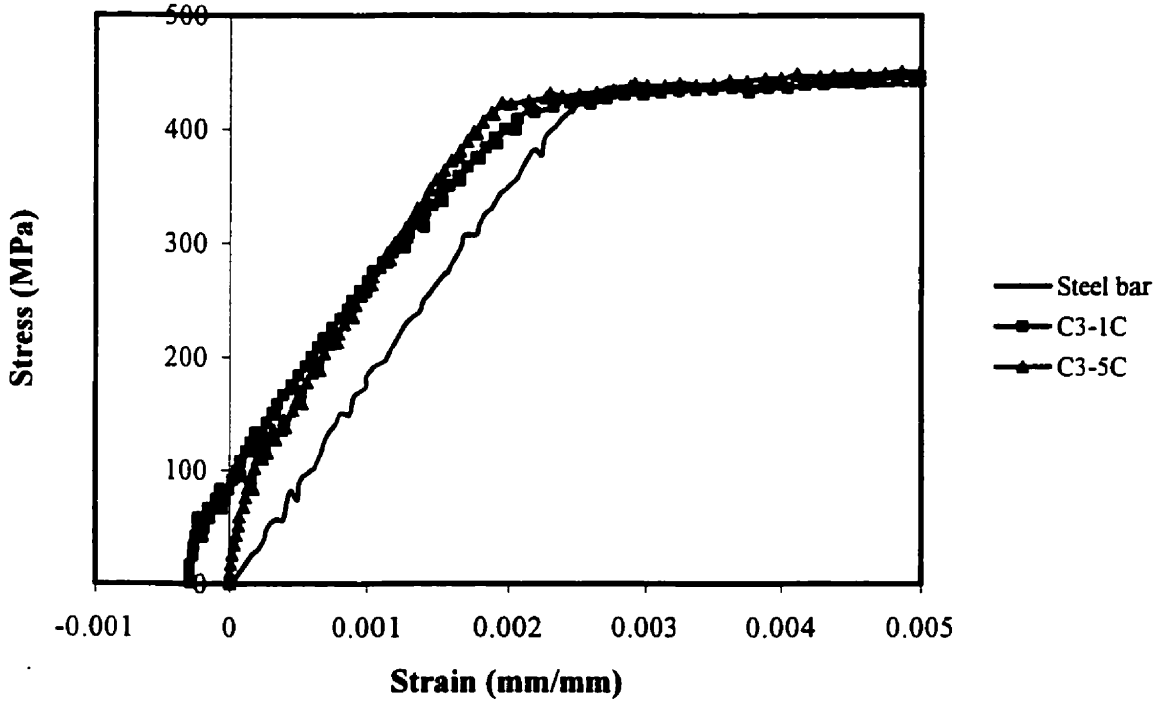

Fig. 9.16: Comparison of calculated stress-strain relationship for Specimen C3-5C (Normal Portland Cement with w/c ratio = 0.32)

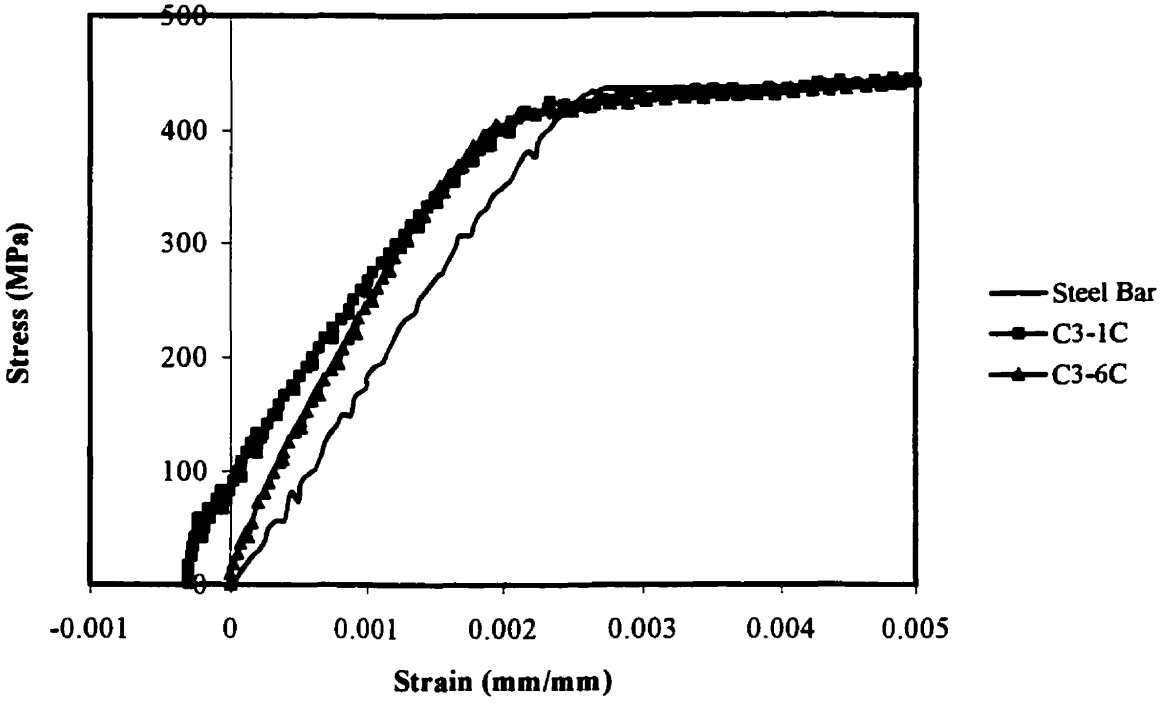

Fig. 9.17: Comparison of calculated stress-strain relationship for Specimen C3-6C (Normal Portland Cement with w/c ratio = 0.32)

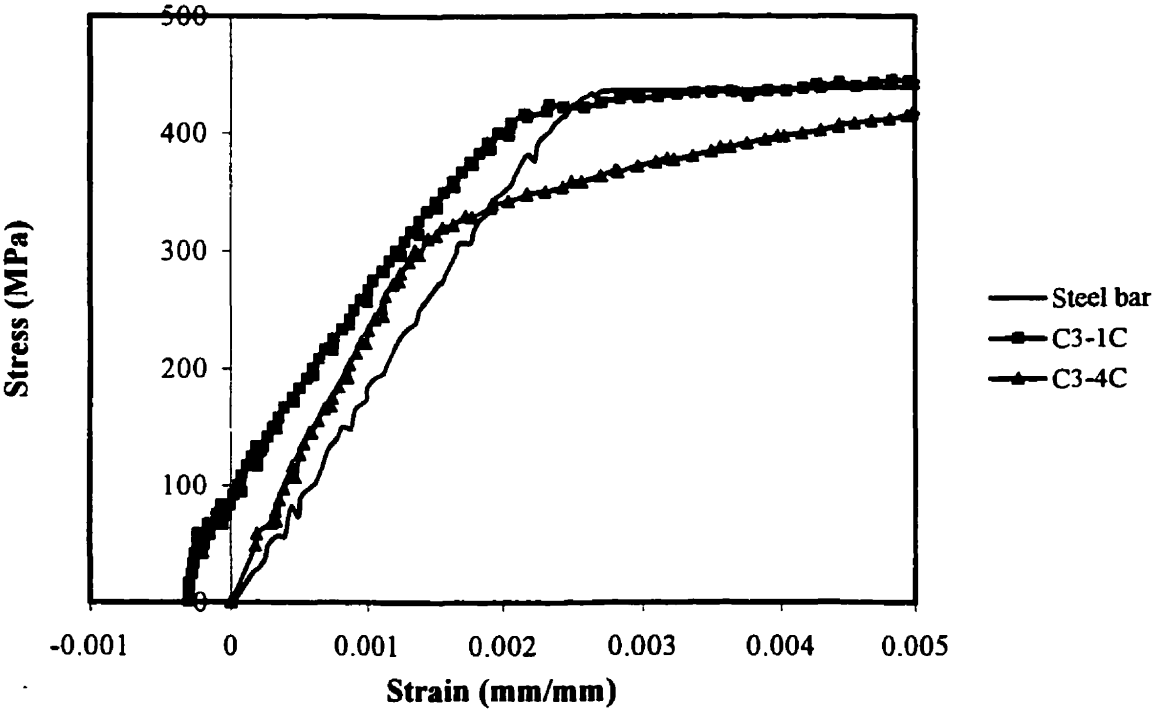

Fig. 9.18: Comparison of calculated stress-strain relationship for Specimen C3-4C (Normal Portland Cement with w/c ratio = 0.32)

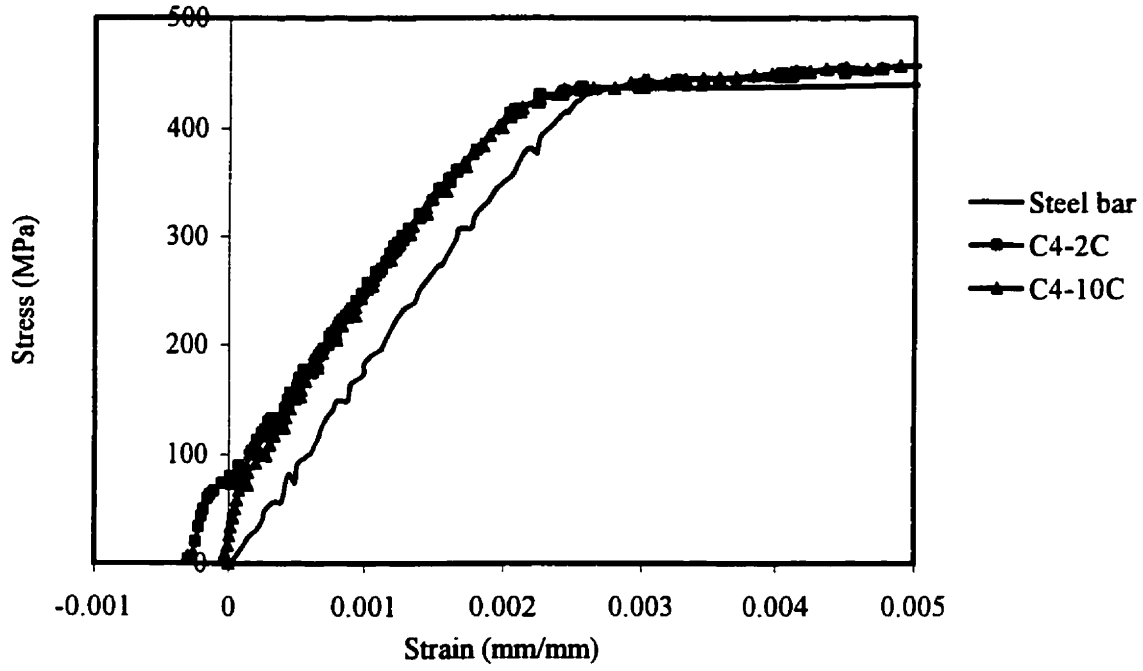

Fig. 9.19: Comparison of calculated stress-strain relationship for Specimen C4-10C (Sundance fly ash)

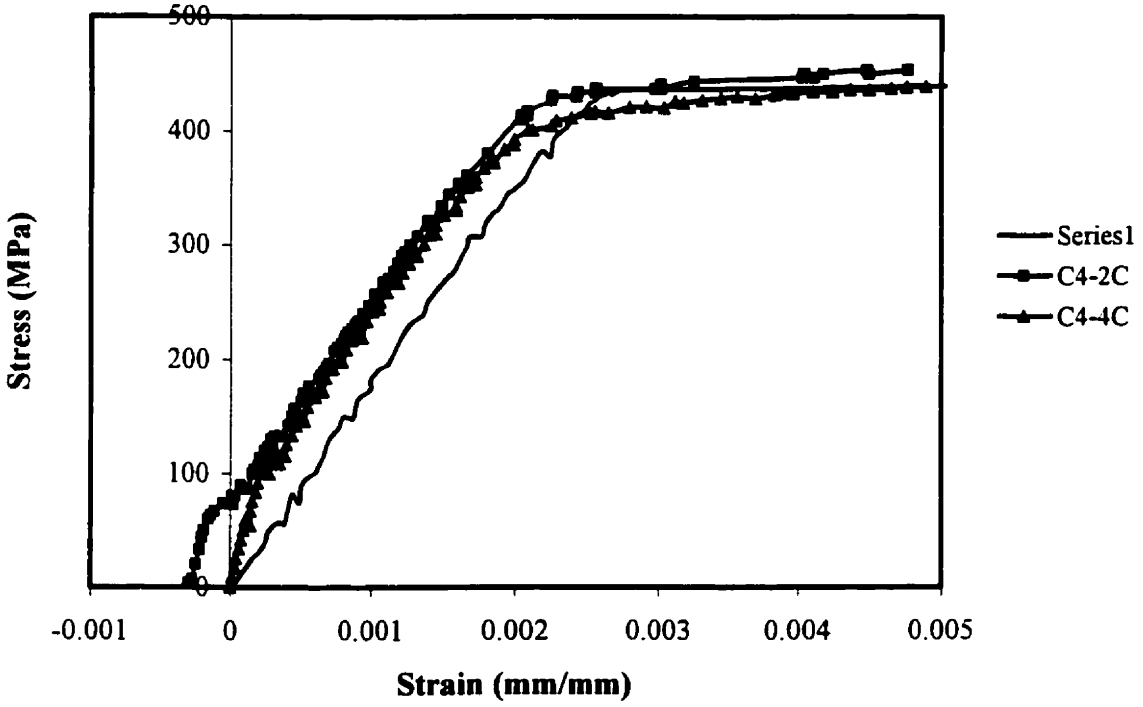

Fig. 9.20: Comparison of calculated stress-strain relationship for Specimen C4-4C (Sundance fly ash)

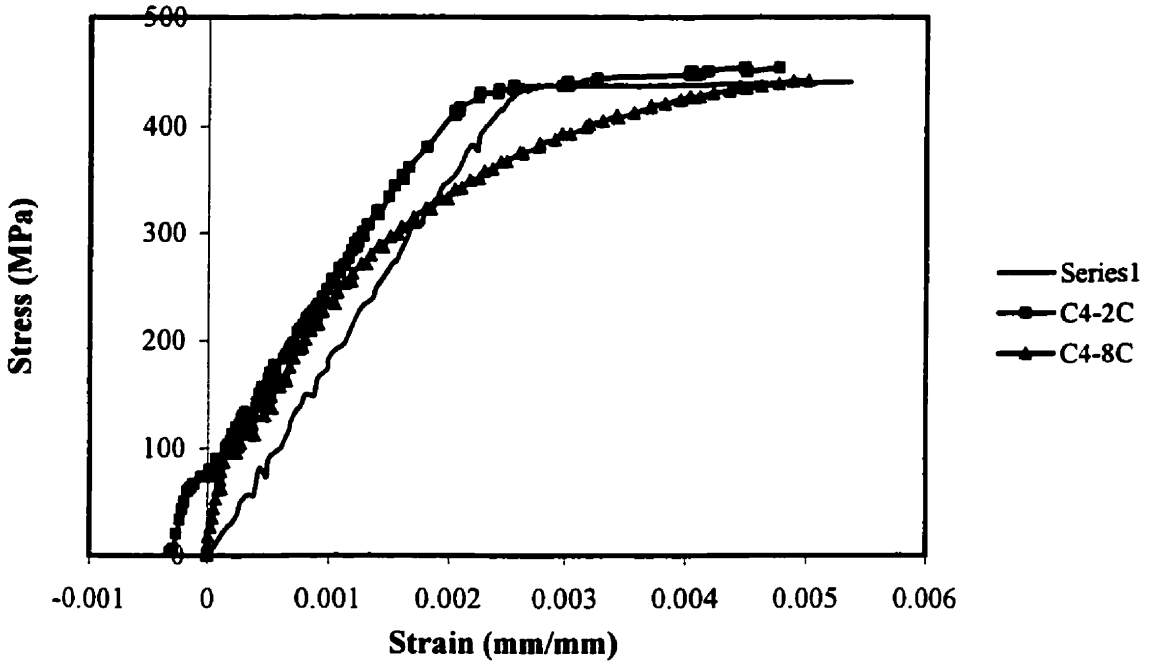

Fig. 9.21: Comparison of calculated stress-strain relationship for Specimen C4-8C (Sundance fly ash)

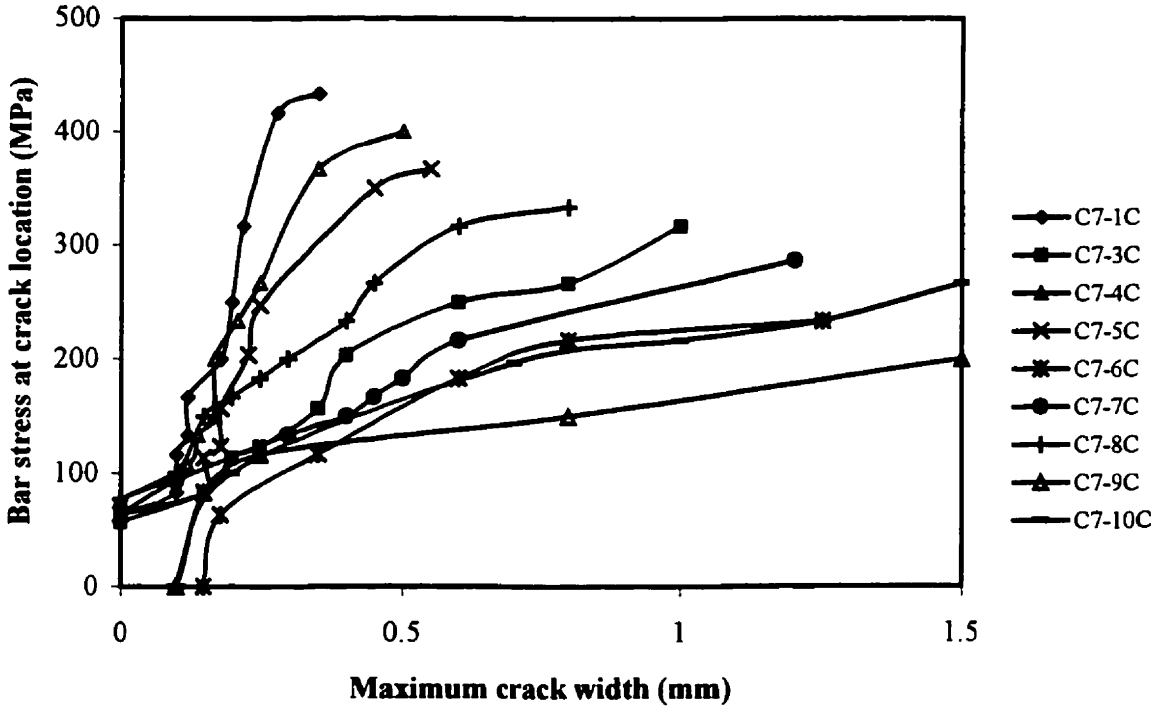

Fig. 9.22: Variation of steel bar stress at crack location with the max. crack width for all of the specimens made with Normal Portland Cement with w/c ratio = 0.52

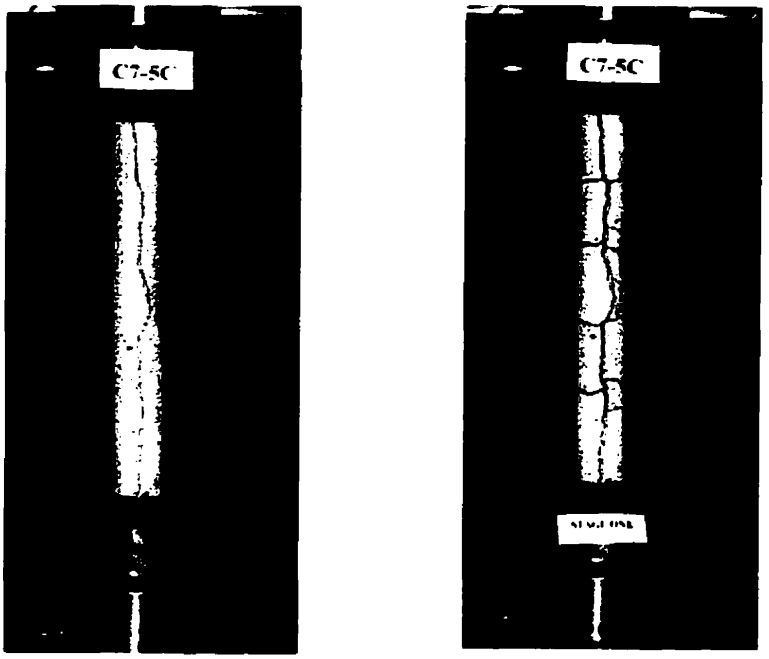

(a) C7-5C before testing (b) C7-5C end of testing

Figure 9.23: Typical cracking behaviour for a corroded Specimen C7-5C

Figure 9.24: Transverse tensile cracks for all specimens made from Normal Portland Cement with w/c ratio = 0.52 specimens (Dickson Bridge Concrete)

(a) C3-3C before testing (b) C3-3C end of testing

Figure 9.25: Typical cracking behaviour for a corroded Specimen C3-3C

Figure 9.26 : Transverse tensile cracks for specimens made from Normal Portland Cement with w/c ratio = 0.32

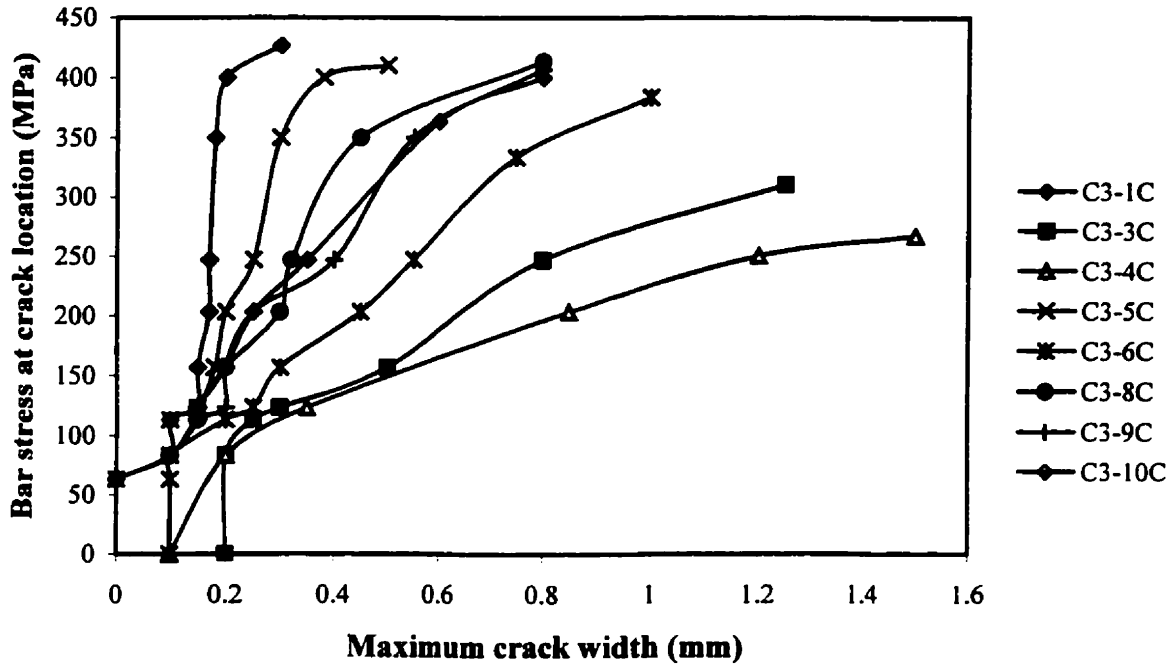

Fig. 9.27: Variation of steel bar stress at crack location with the max. crack width for all of the specimens made with NPC with w/c = 0.32

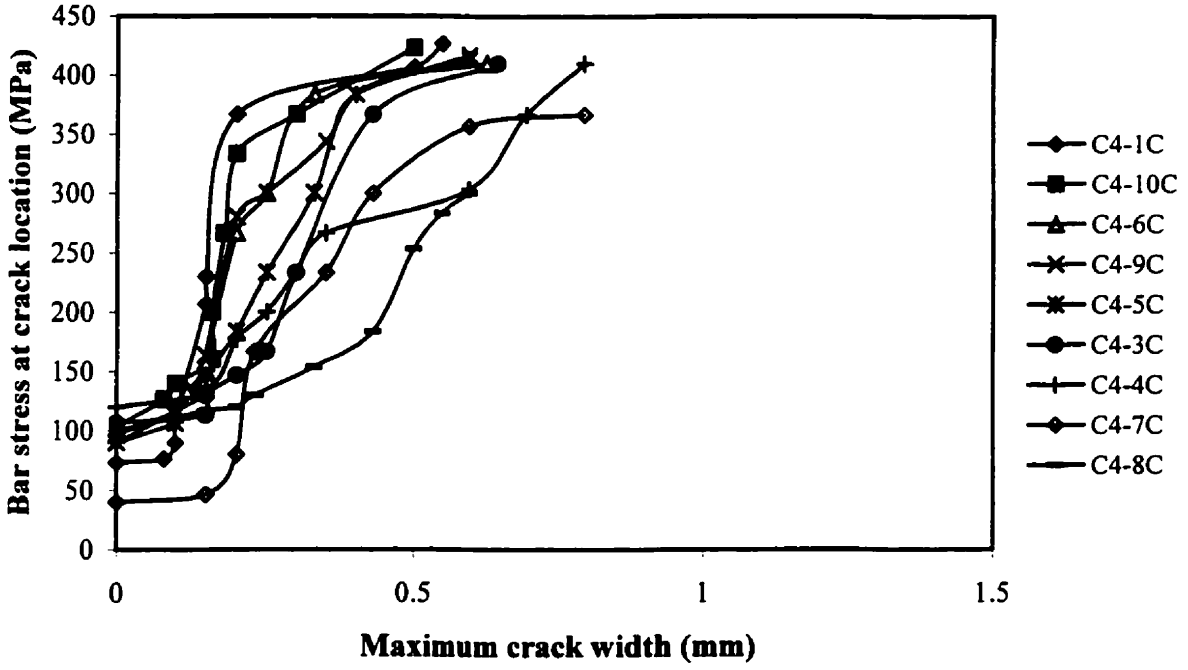

Fig. 9.28: Variation of steel bar stress at crack location with the max. crack width for all of the specimens made with Sundance fly ash

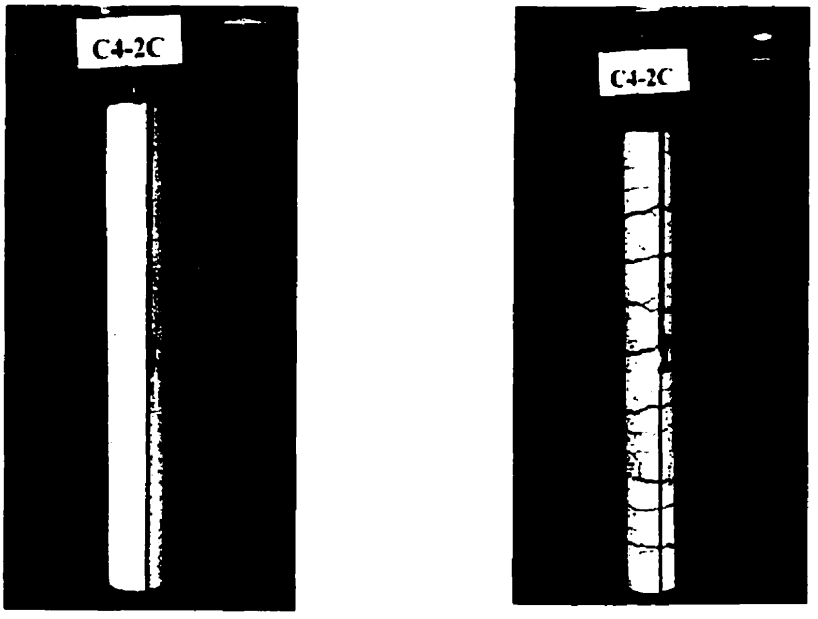

(a) C4-2C before testing (b) C4-2C end of testing

Figure 9.29: Typical cracking behaviour for the control Specimen C4-2C

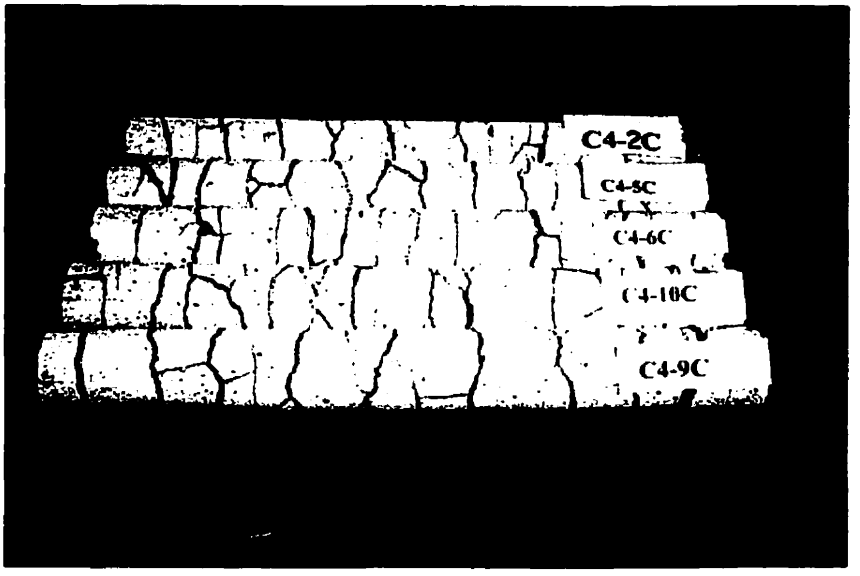

Figure 9.30: Transverse tensile cracks for specimens made from Sundance Fly Ash Concrete with w/c ratio = 0.32 specimens

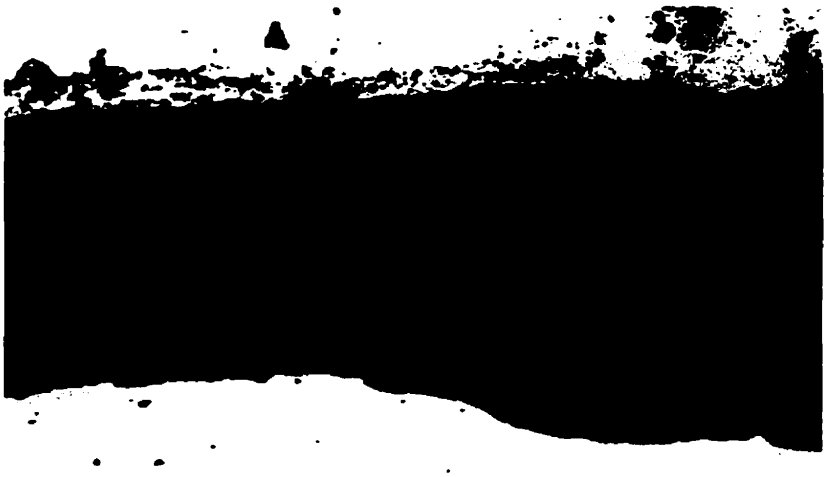

(a)

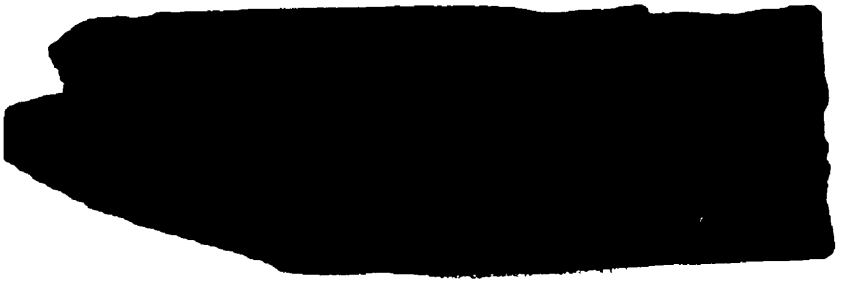

(b)

Figure 9.31: Heavy layer of the corrosion products

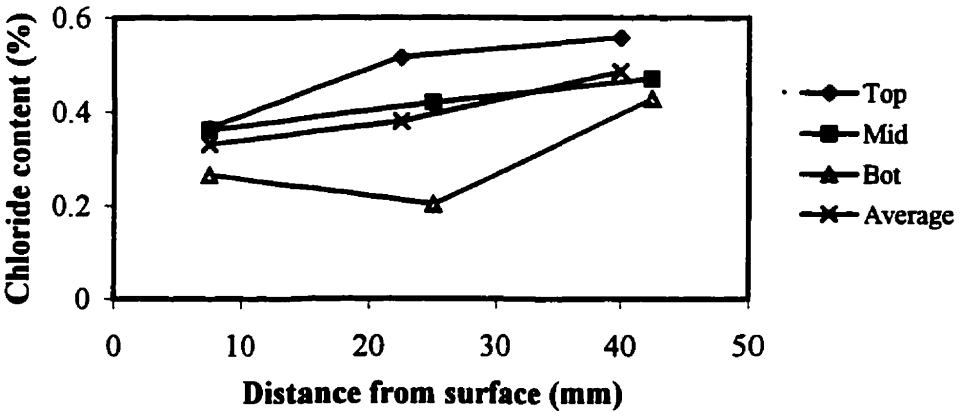

Fig. 9.32(a): Chloride ion content for Specimen C7-5C, away from crack location

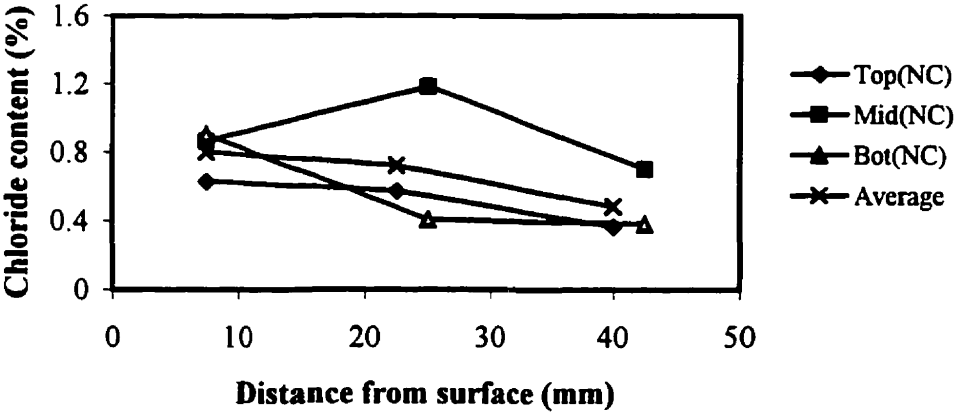

Fig. 9.32(b): Chloride ion content for Specimen C7-5C, near crack location

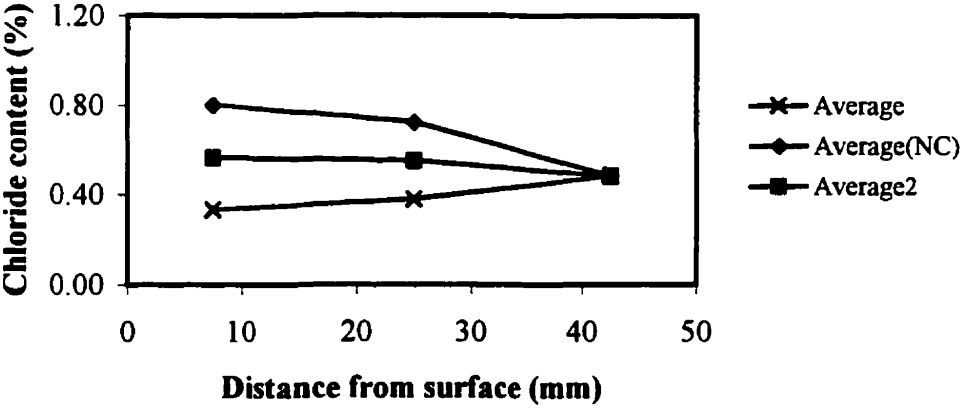

Fig. 9.32(c): Average chloride ion content for Specimen C7-5C

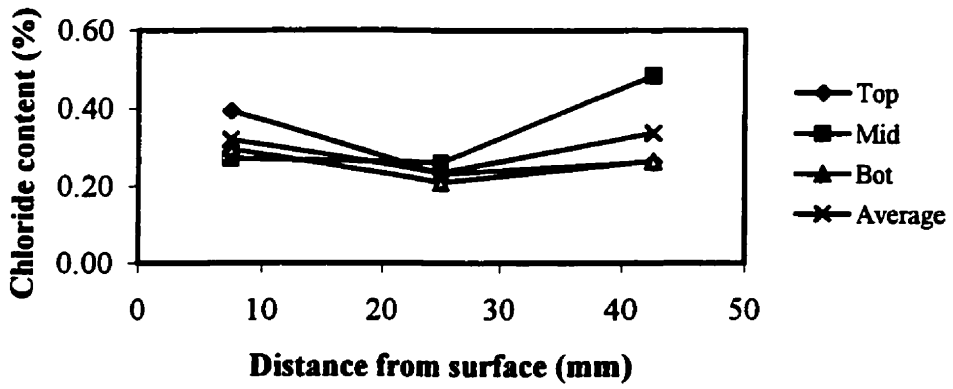

Fig. 9.33 (a): Chloride ion content for Specimen C3-3C, away from crack location

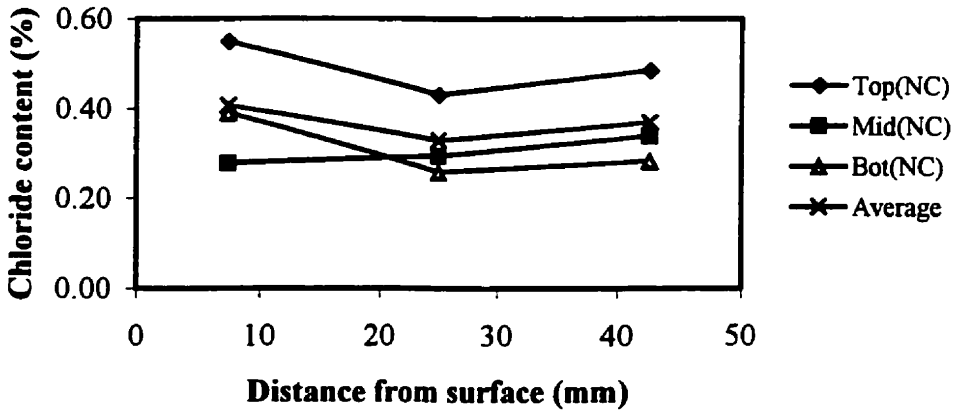

Fig. 9.33 (b): Chloride ion content for Specimen C3-3C, near crack location

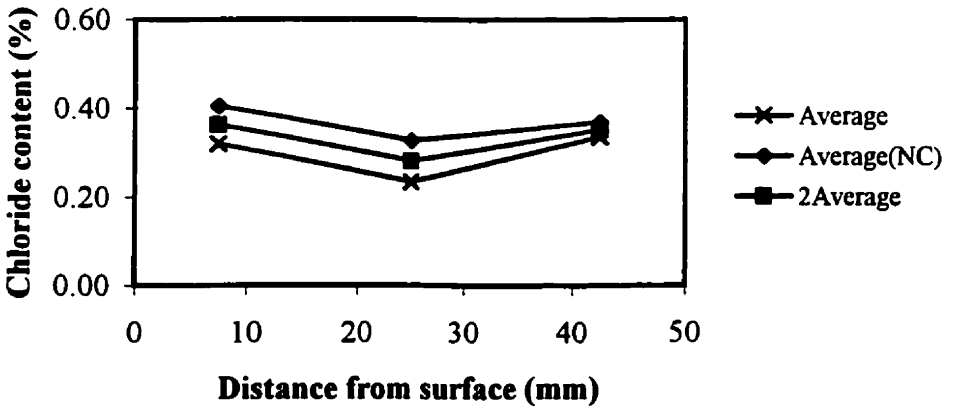

Fig. 9.33 (c): Average chloride ion content for Specimen C3-3C

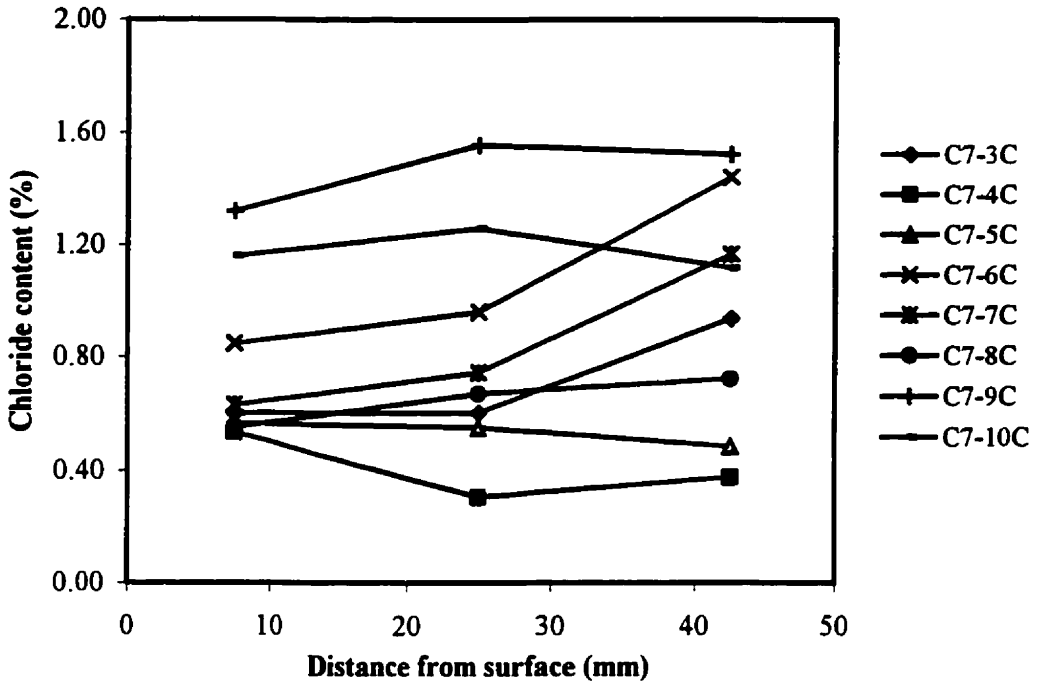

Fig. 9.34: Chloride ion profile for each specimen made with Normal Portland Cement (water/cement = 0.52)

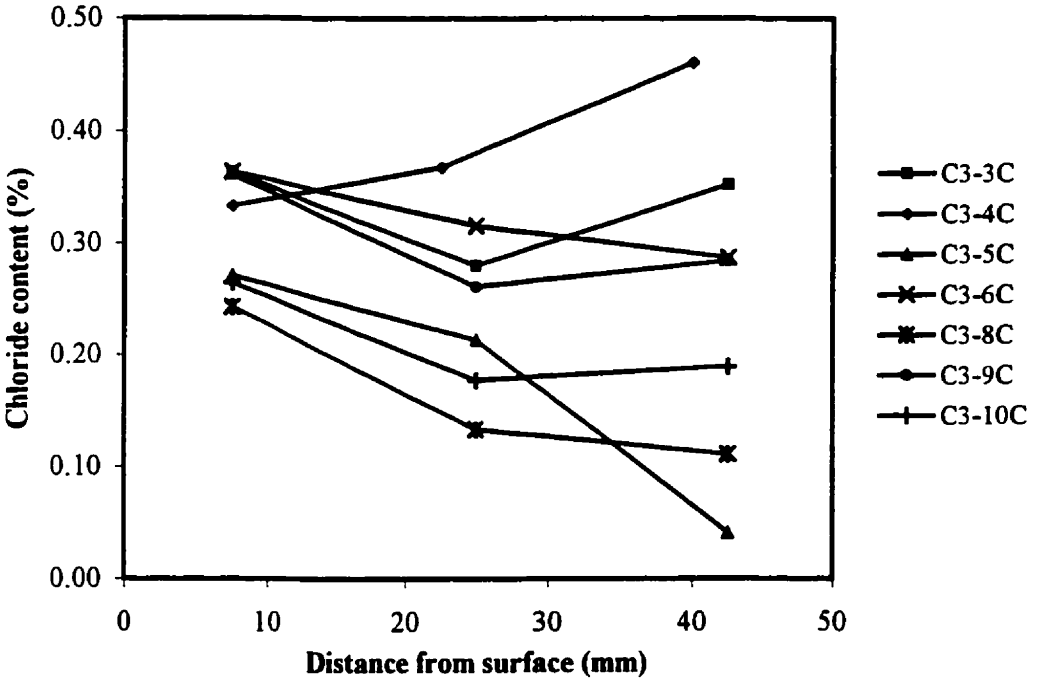

Fig. 9.35: Chloride ion profile for each specimen made with Normal Portland Cement (water/cement = 0.32)

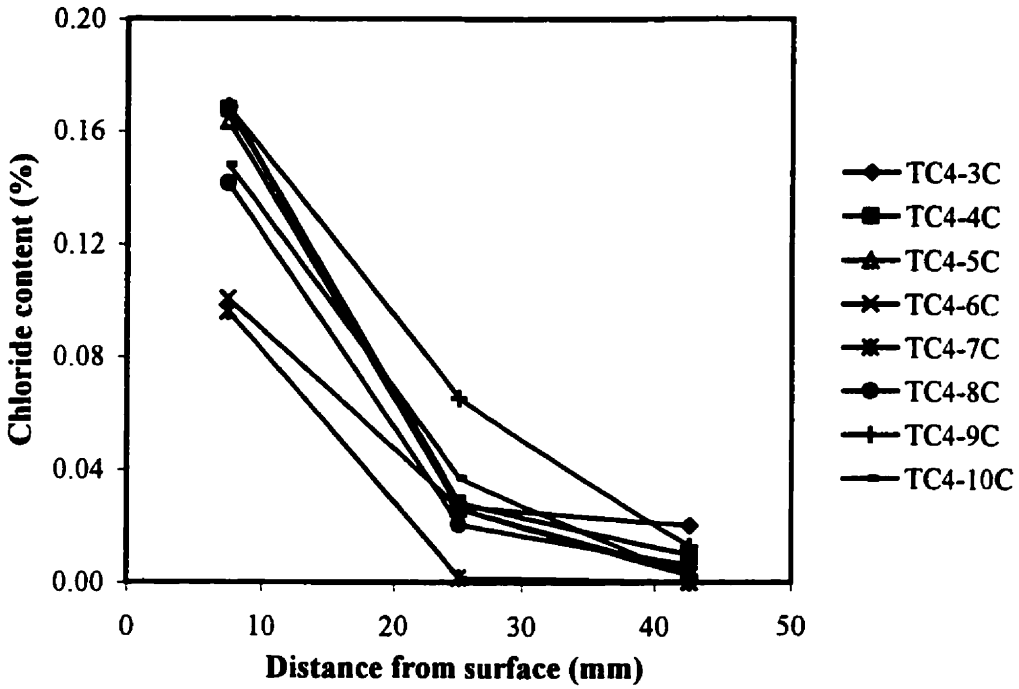

Fig. 9.36: Chloride ion profile for each specimen made with Sundance fly ash concrete

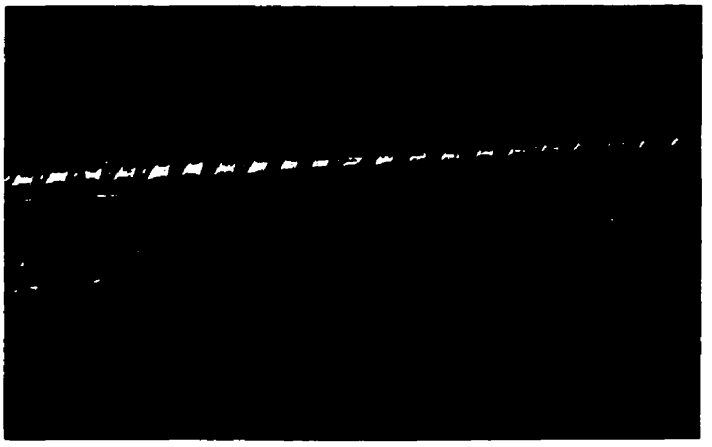

Figure 9.37: Severe localized "pitting" corrosion

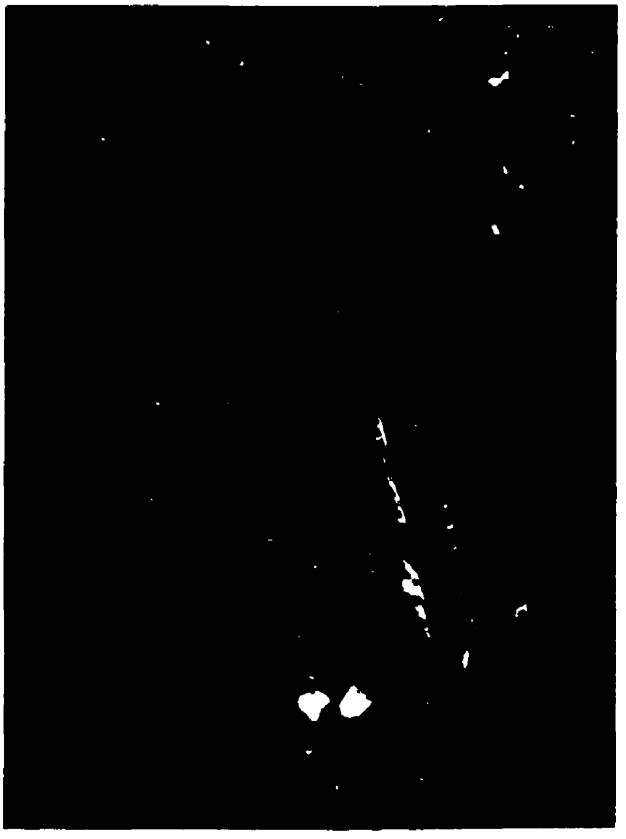

Figure 9.38: Effect of extensive loss of cross-sectional area due to "pitting" corrosion

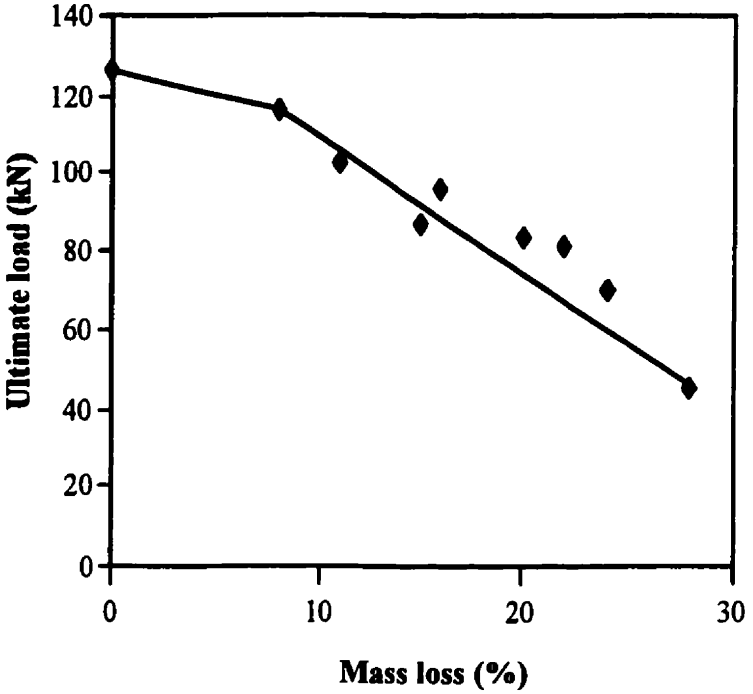

Figure 9.39: Effect of corrosion on ultimate load at bond failure for Normal Portland Cement with 0.52 w/c

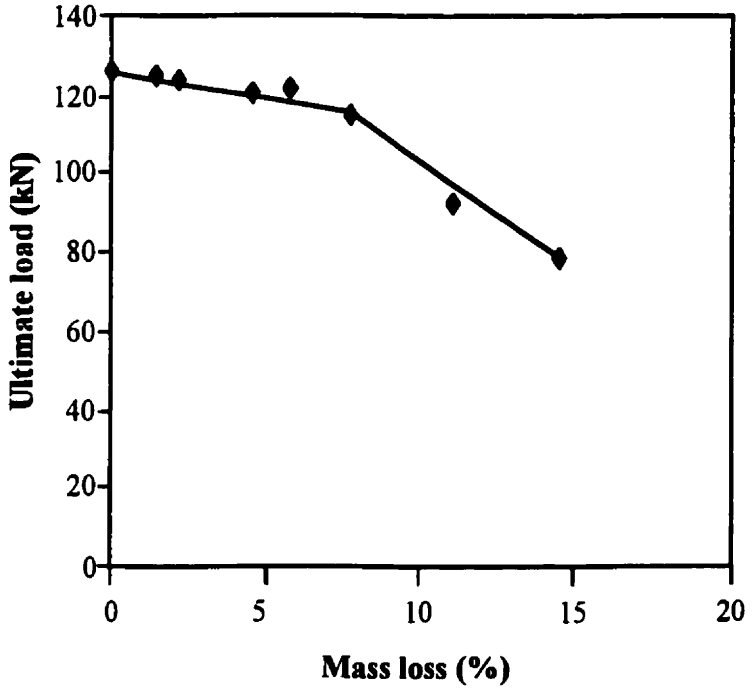

Figure 9.40: Effect of corrosion on ultimate load at bond failure for Normal Portland Cement with 0.32 w/c

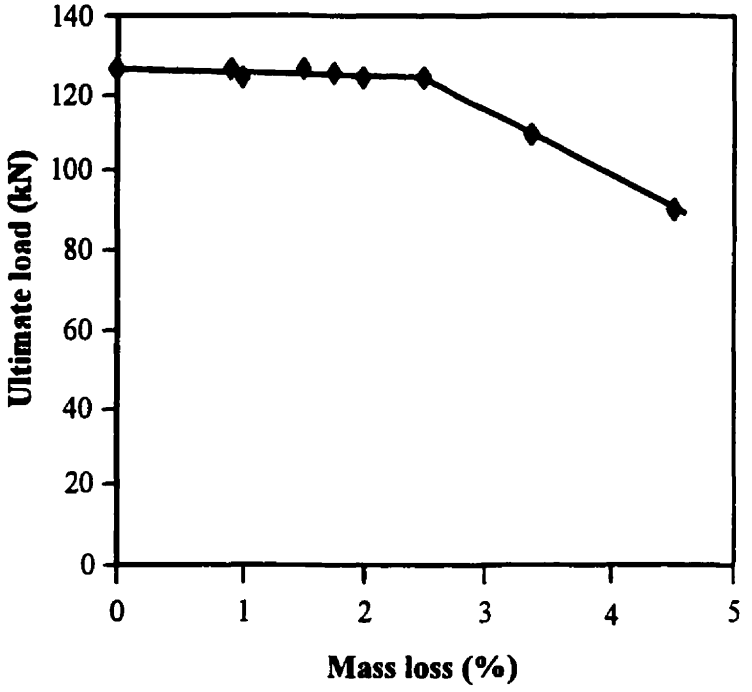

Figure 9.41: Effect of corrosion on ultimate load at bond failure for Sundance fly ash concrete

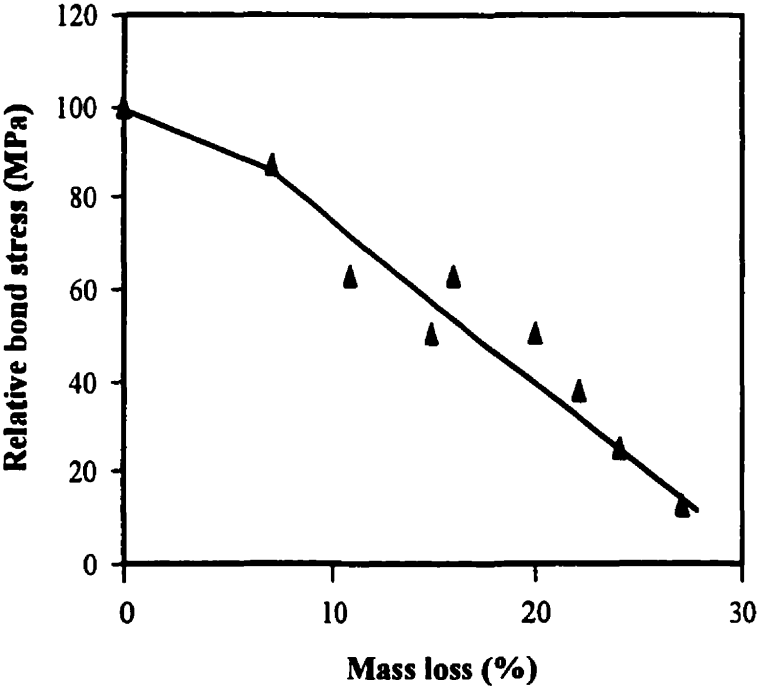

Figure 9.42: Effect of corrosion on relative bond stress for Normal Portland Cement with 0.52 w/c

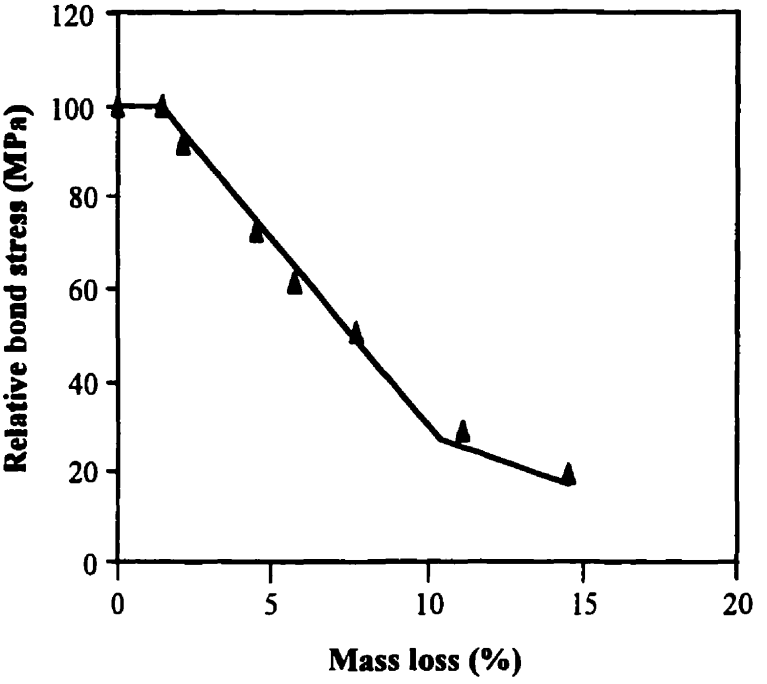

Figure 9.43: Effect of corrosion on relative bond stress for Normal Portland Cement with 0.32 w/c

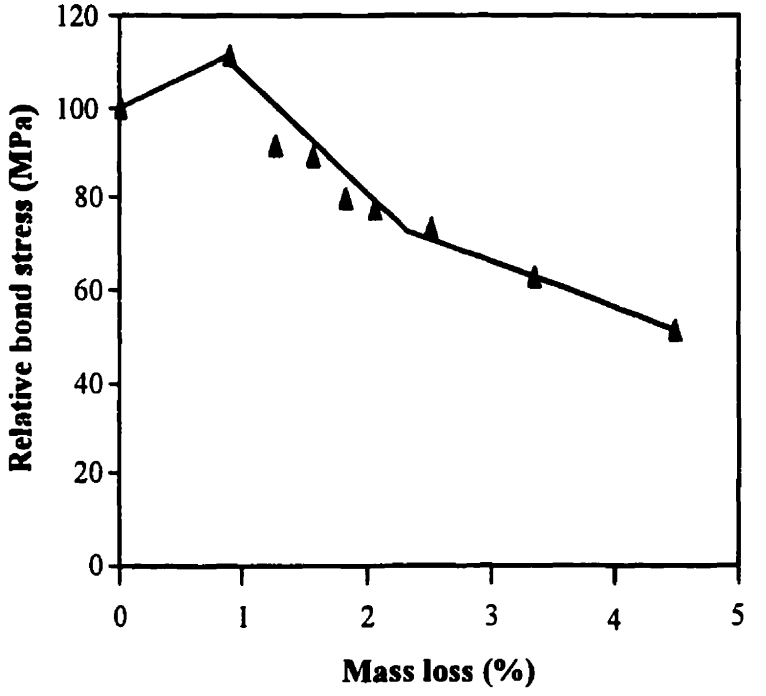

Figure 9.44: Effect of corrosion on relative bond stress for Sundance fly ash concrete

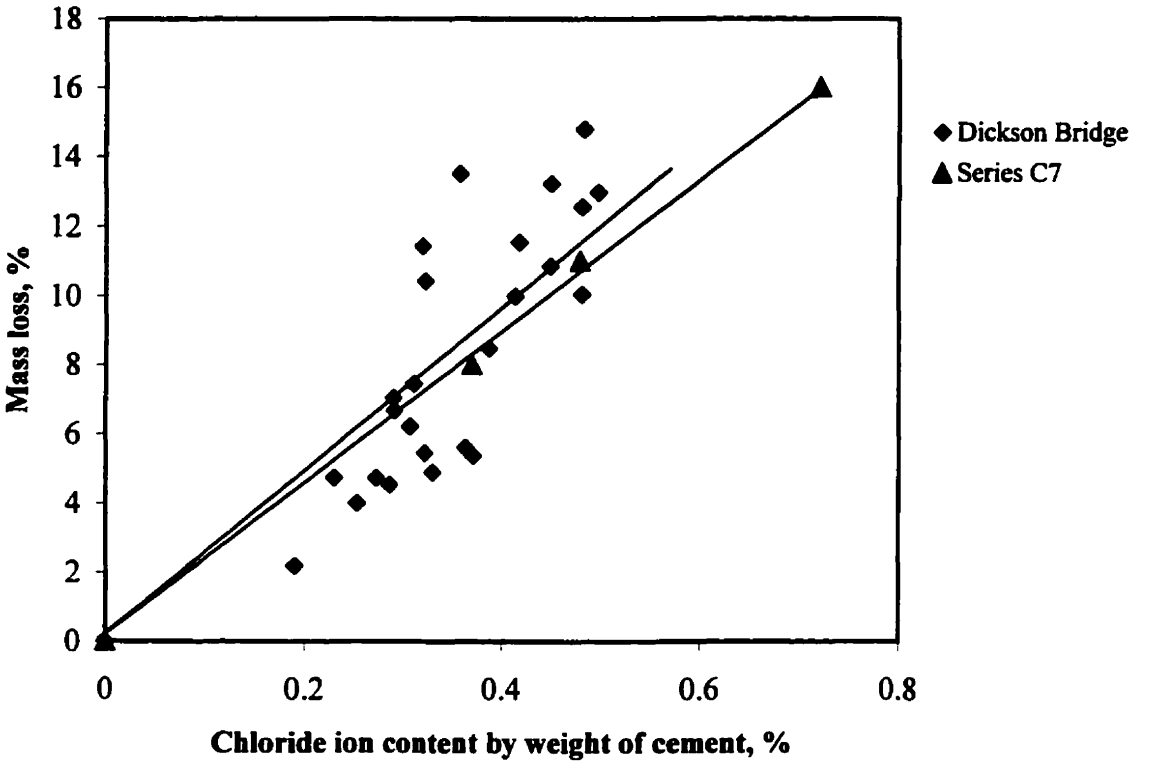

Fig. 9.45: Correlation between mass loss and chloride ion contents for Dickson Bridge and Series C7 specimens

Chapter 10

Bond Design for Deterioration

This chapter deals with the practical aspects of the effect of corrosion on bond behaviour at the reinforcing steel-concrete interface. Where possible, appropriate design equations are formulated for bond strength in structural concrete at a given stage of corrosion deterioration after being subjected to an aggressive environment for a given time. Reference is also made to the analytical formulation presented in Chapter 8.

10.1 Introduction

Analysis of the experimental response of the tension specimens and the related results was carried earlier out to evaluate the influence of the level of corrosion on bond behaviour at the steel-concrete interface in tension specimens. A formulation based on strain compatibility was used to determine the load at which the first cracking occurred, and further analytical procedures were then developed to predict the behaviour of the pullout specimens from the first cracking until final failure.

10.2 Corrosion Types

Two types of corrosion were observed in the experimental phase-uniform corrosion over the entire surface of the reinforcing steel and pitting corrosion (very concentrated corrosion over a small segment of the steel bar) in both tension and pullout specimens. The process of the breakdown of bond between the reinforcing steel and the concrete was different in each case.

Although all of the specimens developed uniform corrosion over significant parts of their lengths, these bars also developed concentrated corrosion in several localized regions. With uniform corrosion during the first few levels of corrosion (5 to 10 percent mass loss), the specimens experienced some uniform loss of bond over the entire embedded length, while at higher levels of corrosion, the bond is almost completely lost at the pitting corrosion locations. Therefore, the bar experiences partial bond loss over the entire length and almost complete local debonding at the locations of concentrated or pitting corrosion. This bond breakdown is irreversible and the calculation of the residual bond strengths can vary greatly depending on the test conditions and the many variables such as the concrete type, concrete cover thickness, and others.

The formation of a pit is similar to that of a notch in a cylindrical specimen, leading to a triaxial tensile stress condition at the pit and brittle fracture of the steel bar. With the Sundance fly ash concrete mixture, two of the corroded specimens experienced extensive pitting corrosion causing local bond breakdown and a large reduction in the local cross-section, resulting in a brittle fracture of the steel rebar without any prior warning.

As explained earlier in Chapter 8, low values of the concrete permeability would normally result in more internal cracking, causing the applied load to be resisted by the remaining undamaged surface. In practical design, this feature can be problematic, because a larger development length would be required because of the considerably reduced bond. Further detailed experimental work needs to be undertaken to quantify the development length for such corroded bars. It is therefore possible that concrete with normal portland cement, or lower volumes of fly ash could prove to be a more practical solution.

10.3 First Cracking

As expected, regardless of the type of the concrete mixture used, the behaviour up to first cracking for all of the uncorroded and precracked corroded specimens, is similar. A strain compatibility approach is used to determine the theoretical load at which first cracking occurs. In this approach, the strain is assumed to remain constant throughout any cross-section of the tension specimen (plain section remains plane), and at any given section, the concrete strain and the reinforcing steel strain are identical.

10.4 Design Procedure

It is not considered possible to formulate generalized design equations for critical free end slip solely on the basis of the current work. The results of this investigation showed that the critical free-end slip is highly dependent on the level and type of corrosion, and hence, the general value of the critical slip used in design, needs to be reviewed. To establish a design equation, it would therefore be prudent to add an additional slip to compensate for the effect of corrosion in terms of such parameters, as the mass loss and size of the cracks due to corrosion, to the anticipated original design critical free-end slip (the magnitude of this variable would be the subject of future work).

The results of this study provide information for the formulation of generalised design equations incorporating the effect of corrosion on the ultimate bond strength. The criteria, which are relevant to the design equations, have been discussed previously. Of course, the influence of harsh or aggressive microclimate at the concrete surface and at the steel-concrete interface needs to be considered separately to estimate the rebar mass loss over a given period of time.

The practical focus of this section is the formulation of design equations for the uncorroded specimens using different concrete mixtures, along with the effect of

corrosion on the bond at the steel-concrete interface in the corroded specimens. It is assumed that a constant average bond stress distribution is a reasonable representation of the "actual" bond stress along the length of the reinforcing steel (hence, Equation 8.1 is applicable).

Excellent bond at the steel-concrete interface resulted in the formation of several transverse cracks in the tension specimen with uncorroded steel reinforcing bars. Seven or eight cracks were observed in the uncorroded specimens for different types of concrete mixtures. As the level of corrosion increases, the number of these transverse cracks decreases, until finally when the bond at the steel-concrete interface is lost almost completely (more than 90 percent), not enough force is transferred from the steel to the concrete to reach a load value large enough to crack the concrete. In short, in a heavily corroded tension specimen, a minimum number of cracks or no cracks at all will form, as was observed in this investigation.

10.5 Basic Design Philosophy

The analytical relationship to calculate the reduction of bond strength caused by a given level of corrosion can be obtained by regression analysis of the experimental results which influence the relationship between the bond strength and the mass loss due to corrosion, and by disregarding the values where slight corrosion leads to an increase in bond strength. Using the test results for the uncorroded specimens, Tepfers Equation 3.1 was found to be adequate for both of the normal portland cement concretes, however, this equation did not correlate well with the other concrete types. As discussed earlier, the results of this investigation showed that the tensile strength of the high volume fly ash concrete did not relate to its compressive strength in the same numerical manner as that for the normal portland cement concrete. For design purposes, it would be useful to formulate a relationship between the bond strength at the steel-concrete interface and the compressive strength of the concrete.

10.6 Design for Bond Deterioration Based on Mass Loss

Figures 10.1 through 10.6 show the variation of bond strength with the mass loss for the six types of concrete used in this investigation. It is clear that the bond strength at the steel-concrete interface decreases linearly with the mass loss of the steel rebar. The results for all six concretes clearly show that the use of a 25 mm thick concrete cover must not be recommended with any type of concrete.

Table 10.1: Bond strength equations for pullout tests as a function of the mass loss.

Concrete mixture	Bond strength equation *(u)*	Correlation coefficient *(r^2)*
Point Tupper fly ash concrete	$u = (0.4 + 0.16\frac{c}{d_b})\sqrt{f_c'} - 0.34(ML)$	0.95
Thunder Bay fly ash concrete	$u = (0.4 + 0.21\frac{c}{d_b})\sqrt{f_c'} - 0.45(ML)$	0.93
Sundance fly ash concrete	$u = (0.4 + 0.25\frac{c}{d_b})\sqrt{f_c'} - 0.62(ML)$	0.91
NPC (w/c ratio = 0.32)	$u = (0.35 + 0.3\frac{c}{d_b})\sqrt{f_c'} - 0.42(ML)$	0.97
NPC (w/c ratio = 0.42)	$u = (0.35 + 0.3\frac{c}{d_b})\sqrt{f_c'} - 0.34(ML)$	0.90
HAC (w/c ratio = 0.37)	$u = (0.56 + 0.135\frac{c}{d_b})\sqrt{f_c'} - 0.31(ML)$	0.90

The coefficients obtained from the multiple regression analysis (c, d_b, f'_c and ML) were adapted as coefficients in the proposed design equations; these include the tensile strength parameter used traditionally in the various bond strength design equations. The equations derived for the various types of concrete are listed in Table 10.1 which also includes the values of the correlations coefficient indicating the level of confidence obtained in the derive equations. Here ML is the percentage mass loss.

10.7 Design for Bond Deterioration Based on Chloride Content

The mass loss of the steel reinforcing bar is generally related to the chloride content of the concrete. These chlorides would normally permeate or diffuse through the concrete cover, however, as cracks form and widen, much of the chlorides flow directly through the cracks to the surface of the steel bar and destroy the passive layer to initiate corrosion. However, if the cracks are fine, 1mm or less in width, this flow of chlorides to the bar surface is not as significant. A detailed analysis of the chloride content in all of the pullout specimens in the six different concretes agreed with this interpretation that up to a crack width of 1mm, the amount of chlorides present were related to the mass loss. However, for larger crack widths, this relationship, which is based on the diffusion phenomenon does not hold any more.

The results of a detailed regression analysis led to the six equations list in Table 10.2, relating the bond stress to the chloride content for transverse crack widths of less than 1mm. The correlation coefficients are listed for each case showing confidence in the equations developed.

Note that good correlations were obtained for the proposed bond strength equations for the normal portland cement and fly ash concretes, however the correlation was lower for the high alumina cement concrete. Also, the NPC concrete with the lower water-cement ratio (0.32) showed better correlation than the one with the higher water-cement ratio.

Table 10.2: Bond strength equations for pullout tests as a function of chloride content.

Concrete mixture	Bond stress equation *(u)*	Correlation coefficient *(r^2)*
Point Tupper fly ash concrete	$u=(0.4+0.16\frac{c}{d_b})\sqrt{f_c'}-10.6(Cl^-)$	0.94
Thunder Bay fly ash concrete	$u=(0.4+0.21\frac{c}{d_b})\sqrt{f_c'}-11.9(Cl^-)$	0.94
Sundance fly ash concrete	$u=(0.4+0.25\frac{c}{d_b})\sqrt{f_c'}-34.5(Cl^-)$	0.93
NPC (w/c ratio = 0.32)	$u=(0.35+0.3\frac{c}{d_b})\sqrt{f_c'}-24.5(Cl^-)$	0.94
NPC (w/c ratio = 0.42)	$u=(0.35+0.3\frac{c}{d_b})\sqrt{f_c'}-12.9(Cl^-)$	0.80
HAC (w/c ratio = 0.37)	$u=(0.56+0.135\frac{c}{d_b})\sqrt{f_c'}-6.6(Cl^-)$	0.70

10.8 Illustrative Example

The bond strength available in corroded reinforcing steel bars in normal portland cement concrete (water-cement ratio= 0.32) with concrete cover thickness of 50mm calculated to show the practical use of these equations, based on the steel rebar mass loss and the concrete chloride content.

Assume that a No. 20 bar in NPC (w/c ratio= 0.32) can suffer a mass loss of 7.3% over a given service life of the structure. Then the bond strength of the uncorroded bar with a concrete cover thickness of 50mm, from the equation in Table 10.1, is:

$$u = (0.35 + 0.3 \times 50/19.5)\,(60.2)^{1/2} - 0.42 \times 7.3$$

$$u = 5.62 \text{ MPa}$$

The same example is reattempted with NPC concrete (w/c ratio = 0.32), chloride ion content = 0.13 percent by the weight of cement, concrete cover thickness of 50mm and the bar diameter = 19.5mm. The available bond strength, from the equation in Table 10.2, is given by:

$$u = (0.35 + 0.3 \times 50/19.5)\,(60.2)^{1/2} - 24.5 \quad (0.13)$$

$$u = 5.50 \text{ MPa}$$

The design bond strength = $\phi_b\, u = 0.65\, u = 0.65 \times 5.5 = 3.58$ MPa

The experimental value of bond strength for Specimen C4-5C (corrosion stage 4, ML=7.26%, chloride content 0.13%) is 6.37 MPa.

The calculated values are conservative as compared with the experimental values and are within 16% of the experimantal values. Therefore, these values can be accepted for design purposes along with the introduction of a capacity reduction factor ϕ_b for bond which needs to be evaluated based on the statistics for the concrete cover thickness (c), bar diameter (d_b) and the concrete compressive strength (f'_c). While this factor ϕ_b can be calculated using the second order probabilistic method, a value of 0.65 is used until a better estimation of the value is available.

It is noted that the value of the coefficient of variations of bond strength (u), calculated based on the experimental data, is 46% for fly ash and high alumina cement concretes, and it is 60% and 66% for normal portland cement concretes with water-cement ratios of 0.32 and 0.42, respectively. As more data become available, more reliable values of the coefficient of variation and the other statistics will become available and these can be used for more detailed probabilistic analysis, based on the variability of the strengths, materials characteristics and loadings, and on the consequences of failure, can be undertaken to derive a value of the undercapacity factor for bond strength deterioration due to corrosion. In the mean time, it is

suggested that a value of $\phi_b = 0.65$ be used as the undercapacity factor for bond, i.e. the value of (u) calculated from the recommended equations be multiplied by 0.65 to obtain the design values.

10.9 Summary

The various aspects of the corrosion response of steel reinforcing bars in different types of concrete are rationalized and practice-oriented design equations for bond deterioration are proposed based on both the percentage steel rebar mass loss and the concrete chloride content at the steel rebar level. The application of these design equation is illustrated by an example.

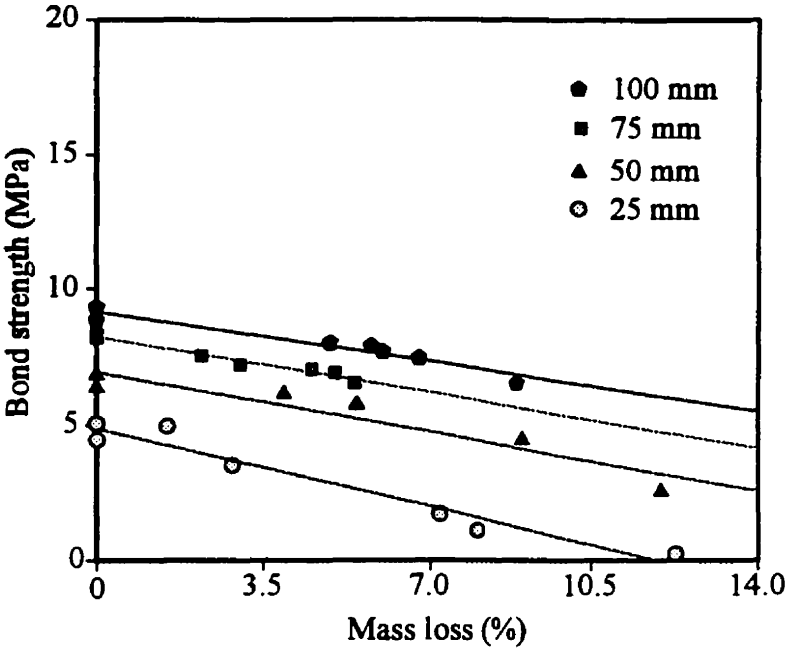

Fig. 10.1: Variation of bond strength with mass loss for the Point Tupper fly ash concrete mixture and different concrete cover thicknesses

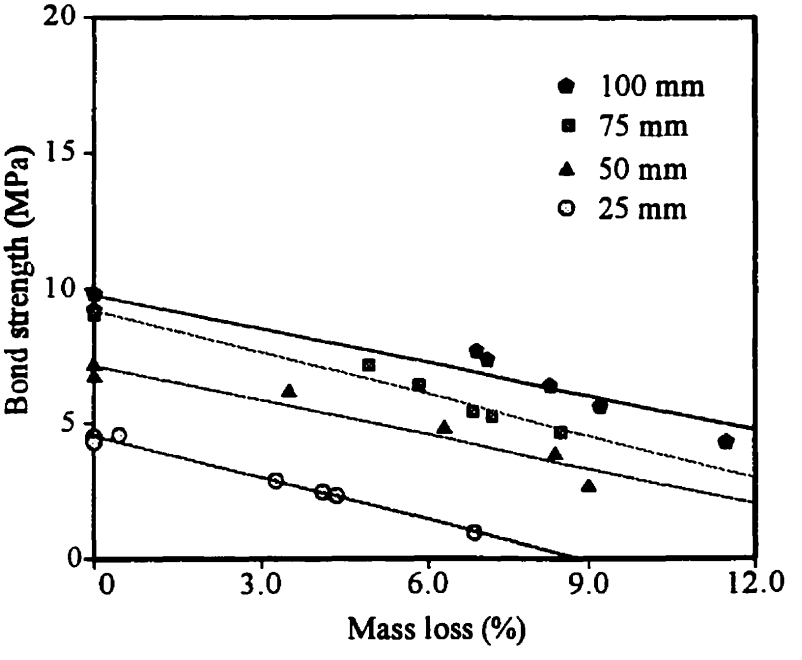

Fig. 10.2: Variation of bond strength with mass loss for the Thunder Bay fly ash concrete mixture and different concrete cover thicknesses

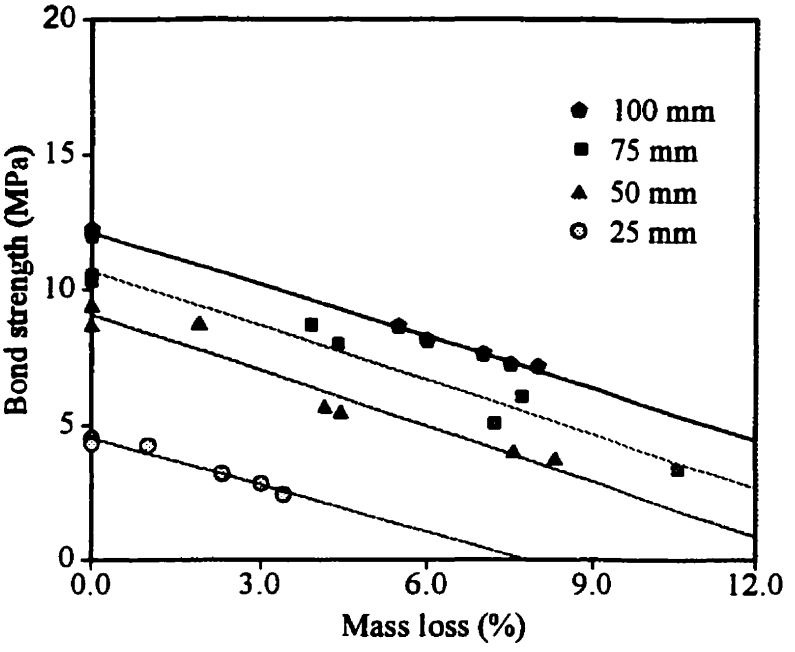

Fig. 10.3: Variation of bond strength with mass loss for the Sundance fly ash concrete mixture and different concrete cover thicknesses

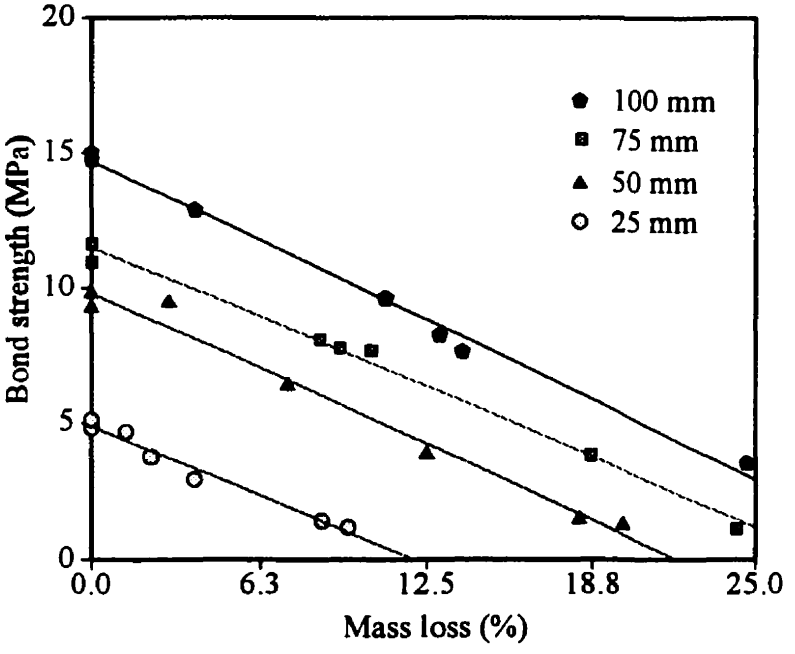

Fig. 10.4: Variation of bond strength with mass loss for the Normal Portland Cement concrete mixture with 0.32 w/c ratio and different concrete cover thicknesses

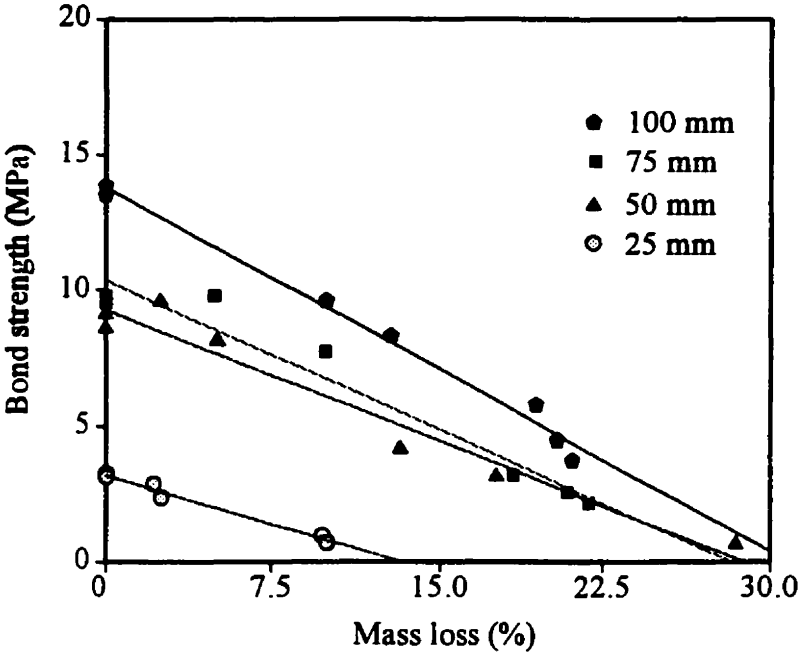

Fig. 10.5: Variation of bond strength with mass loss for the Normal Portland Cement concrete mixture with 0.42 w/c ratio and different concrete cover thicknesses

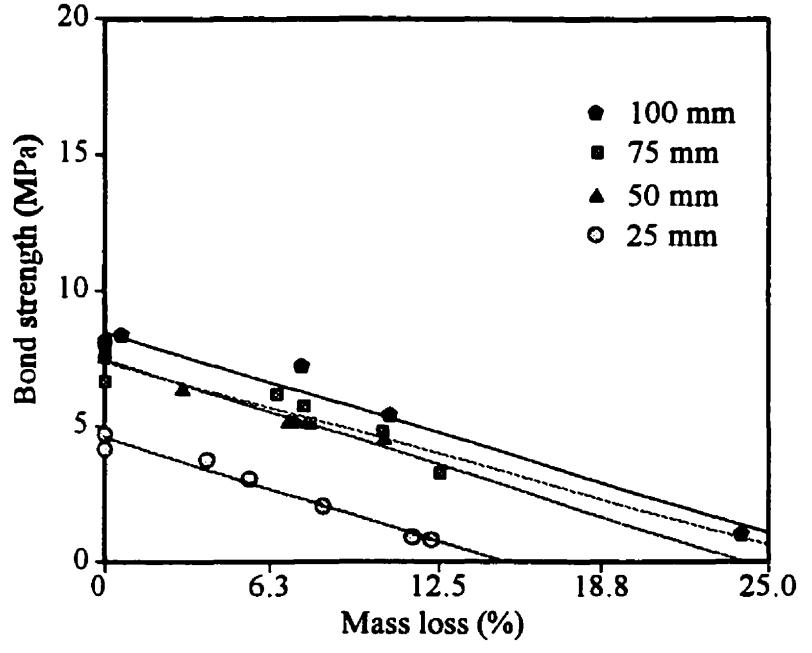

Fig. 10.6: Variation of bond strength with mass loss for the High Alumina Cement concrete mixture and different concrete cover thicknesses

Chapter 11

Conclusions and Future Direction

11.1 Summary and Conclusions

The results of this laboratory and field research program on evaluation of the structural integrity of the abandoned Dickson Bridge in Montreal and the associated problem of the influence of increasing levels of corrosion on the progressive deterioration of bond between the steel and the concrete, can be summarized and conclusions drawn as follows:

1 A practical method was developed for accelerated corrosion of steel reinforcing bars embedded in concrete by immersing the specimens in a strong (5%) solution of sodium chloride (NaCl) and applying a voltage of 5 volts. This procedure enabled achieving high levels of corrosion (20-25%) within a few months. A monitoring technique was developed involving measurement of the corrosion current and half-cell potential at 24-hour intervals. The corrosion cell was disconnected for one hour before the half-cell potentials were recorded. Every two weeks, the specimens were removed from the corrosion tanks, causing temporary cessation of the corrosion cell, and dried for four days before any half-cell potential, linear polarization resistance or other readings were taken.

This electrochemical and electrical monitoring was coupled with the visual examination of the specimen for longitudinal and transverse cracking

(measurement of crack widths) and the combined information was used to establish one of the seven or eight levels of corrosions in the various specimens. The level of corrosion was reconfirmed by removing the corroded bar from the specimen and determining its mass loss as compared with the originally measured mass of the uncorroded specimen.

2 (a) The bond characteristics of the reinforcing bars in pullout specimens made with six different concrete mixtures were first investigated using the control specimens (two per concrete mixture per cover thickness) to study the effect of the concrete cover/bar diameter (c/d_b) ratio and the concrete compressive strength.

(b) The tensile strengths of fly ash concretes did not demonstrate the same numerical relationship as for the normal portland cement concretes. Most of the control specimens with 100mm cover thickness, failed due to yielding of the steel reinforcement and its fracture subsequently without any bond distress; some fly ash concrete specimens with 100mm thick concrete cover failed due to the splitting of the concrete cover. The available bond strength increased with the increase in the thickness of the concrete cover.

3 (a) The bond stress-slip response of the embedded bar in the pullout specimen, as well as the bond stiffness, which is the slope of the bond stress-slip curve, are adversely affected by the width of the crack due to corrosion, and therefore the level of corrosion.

(b) The maximum bond strength in the pullout test is affected significantly by the number of cracks and their widths, due to corrosion.

4 For a given value of the crack width due to corrosion in a pullout specimen, or the crack width to the concrete cover thickness ratio, the available bond strength is higher for larger cover thicknesses than for the smaller cover thicknesses. This relationship was observed to hold even after some deterioration of the steel bar due to corrosion and shows the significance of larger concrete cover thicknesses for protection of reinforcing steel in structural concrete elements. Of course, the

quality of concrete in terms of its permeability is equally important for the corrosion protection phenomena. The investigation results clearly show that under no circumstances, a concrete cover thickness of 25mm should be used in aggressive microclimates acting on the surface of the element.

5 The pullout test results also show clearly that low levels of corrosion (about 1-3% mass loss) lead to the formation of a firm layer of corrosion products on the steel rebar-concrete interface, thereby improving the bond strength characteristics slightly. However, at higher levels of corrosion deterioration (more than 5% mass loss), the firm layer of corrosion products transforms into a flaky layer with the associated deterioration in both the bond strength and slip characteristics. Following this stage, the available bond strength decreases almost linearly with the increase in the mass loss. The bond strength deterioration with mass losses of 20-25% is significant and at the later stages (25-30% mass loss), about 85 to 90 percent of the bond strength is lost.

6 The bond strength in the pullout specimens is observed to decrease with an increase in the chloride ion content at the steel bar surface, which is directly related to the mass loss.

7 The tension specimens made from three different concretes-normal portland cement concretes with water-cement ratios of 0.32 and 0.52(the latter being used for the construction of the Dickson Bridge, Montreal, which was abandoned in 1993) and the Sundance fly ash concrete showed generally similar behaviour with the concrete cracking associated with the loss of stiffness (slope of the bond stress-slip curve) followed by yielding of the reinforcing steel for the larger cover thickness, or transverse and longitudinal cracking of the cover showing significant bond distress for the smaller cover thicknesses.

8 The corrosion of the reinforcing steel bar consisted of uniform corrosion over the entire length of the bar and concentrated or pitting corrosion at some locations along the bar length. This resulted in relatively small uniform reduction of bond

strength over the entire bar length, accompanied by almost a total loss of bond at the pitting locations. The location of the pit is similar to a notch in a cylindrical steel specimen and upon loading, it leads to a brittle fracture. This brittle fracture of the steel bar was noted in a few of the specimens.

9 As the level of corrosion of the steel rebar increased, the load-elongation curve showed a shift to the right, demonstrating a decrease in the tension stiffening phenomenon due to the concrete. When the corrosion level was high, the load-elongation response showed almost no concrete contribution by way of tension-stiffening and it coincided with the stress-strain curve for the bare bar.

10 As with the pullout specimens, the tension specimens also showed a gradual decrease (almost linear) with an increase in the level of corrosion. A low level of corrosion (slight corrosion associated with a 1-3 percent loss of cross-sectional area exhibited a small increase of about 10 percent in the bond strength. However, at higher levels of corrosion such as a 10-15 percent mass loss in the NPC 0.32 specimens resulted in an 85 percent loss of the bond strength. Similarly, a 4.5 percent rebar mass with the Sundance fly ash concrete showed a 55 percent bond strength loss. At higher levels of deterioration, such as 27 percent in the last stage of corrosion, the bond strength loss was 88 percent, i.e., almost all of the bond strength was lost at this stage due to the loss of the ribs and the formation of a heavy layer of the corrosion products.

11 The concrete permeability is a significant factor in the corrosion deterioration of the rebars in different concretes subjected to different microclimates. The permeability of the Sundance fly ash concrete was about two orders smaller than that of the normal portland cement concrete with a water-cement ratio of 0.32. This reflected in smaller corrosion deterioration for the same cover thickness in the NPC 0.32 specimens as compared with the Sundance fly ash concrete specimens, showing its superior low permeability, which resulted in a lower ingress of chloride ions into the specimen.

12 The reduction of bond strength caused by a given level of corrosion is quantified by regression analysis of the experimental results for the relationship between the bond strength and the mass loss due to corrosion and by disregarding the values when slight corrosion leads to an increase in the bond strength. These results are presented in Table 8.7. An analysis of these results showed clearly that the available bond strength at the steel-concrete interface decreases linearly with the mass loss of the steel bar. Mass losses up to 5 percent can cause the element to crack and spall, however, this is an early stage of deterioration with the remaining service life not as significantly influenced, provided that adequate repairs are undertaken urgently. However, a 10-25 percent mass loss in the critical zones of the structure will result in the depletion of its service life (Andrade et al. 1990). These relationships were used to derive practice-oriented equations for deterioration of bond at the steel-concrete interface due to corrosion, and are presented in Tables 10.1 and 10.2 as function of the steel bar mass loss and chloride content, respectively.

13 The field study on the abandoned Dickson Bridge provided valuable data on the effects of deicing salts on the rate of chloride ingress and the resulting distress in the bridge deck and other elements, which influenced its durability drastically. The test results showed a lack of uniformity in the mix composition, compaction and curing (reflecting a poor quality control). The variation in the concrete mix characteristics, its compaction and the variation due to local surface conditions observed in this investigation, is a dominant parameter in the vastly varying field behaviour of this bridge. Usually, this factor is not studied in research programs.

14 Data from this field investigation show that the chloride content, quality of the concrete cover to reinforcement, and the electrical resistivity of the concrete had a significant effect on the rebar corrosion severity.

15 Very severe corrosion and concrete cracking/spalling were observed in the 62 sample cores, which had more than the recommended concrete cover thickness of 25mm. It was found that in the aggressive conditions of the local region,

corrosion cannot be reduced to acceptable limits when the cover thickness is increased using low quality concrete.

16 Concrete electrical resistivity plays a key role in determining the reinforcement condition. Electrical resistivity values of about 1000 ohm-cm for moist concrete increased corrosion to a level where the loss of metal was more than 65 percent after only 35 years of exposure.

17 Several national codes emphasise specific material quality requirements such as the minimum concrete strength, minimum cement content, maximum water/cement ratio, minimum concrete cover thickness, placing, compaction and curing of the concrete, to ensure durability of the system. However, because the quality of workmanship, including placing of the concrete, its compaction and curing can vary from site to site, the use of a minimum cement content, minimum concrete strength and maximum water/cement ratio is less than adequate to assure durability and to attain the design or service life of the system (Mirza and Amleh 1995).

18 The results of the various electrochemical, electrical, chemical and physical tests show a considerably larger coefficient of variation than in the traditional strength and other values presently used in the concrete design and technology. This shows the inherent nature of the various phenomena, which must be considered in the design of both new structures for durability against corrosion of the reinforcing steel, and for the design of repair and rehabilitation of concrete structures damaged by corrosion or other similar phenomena.

The results of the laboratory and the field studies enabled a good understanding of the various phenomena, which influence the durability of similar bridges and other structures, subjected to aggressive environment. An examination of the various phenomena in the laboratory led to a better understanding and qualitative impact of the various deterioration phenomena on the bridge structures. The results were analysed to provide same practice-oriented design criteria for prediction of bond

deterioration due to the mass loss or the accumulated chlorides at the reinforcing bar-concrete interface at some stage during the life of the structure. The data from the entire bridge and the laboratory studies have been analysed and is being used presently for developing a procedure for design of new concrete structures for durability against the corrosion of the reinforcing steel and for the design of repair and rehabilitation of existing deteriorated structures. A nonlinear finite element program for analysis and design of concrete and steel structures is being performed presently for analysing the nonlinear behaviour of existing structures deteriorated due to corrosion. The details of these programs in progress at McGill University are beyond the scope of this thesis and will be presented elsewhere.

11.2 Future Research Work

The future research and development activities can focus on the effect of corrosion on the reinforcing steel and prestressing tendons in structural concrete, with emphasis on the following:

1 It would be extremely useful to the engineering practice to develop reliability-based design methods for new and deteriorated concrete infrastructure, involving the various protective measures, innovative materials, novel construction techniques, maintenance, repair and management practices.

2 Presently, there is no data available on the deterioration of bond between the concrete and the reinforcing steel with the level of corrosion of the bar using new materials and new technologies, such as high-performance and high-strength concrete. The preliminary test program clearly showed that the bond between the reinforcing steel and the concrete deteriorated with increasing levels of corrosion and it was almost completely lost at advanced stages of corrosion. Attempts must be made to adapt the results of the extensive research programs undertaken worldwide and in Canada on the corrosion phenomenon and the related areas over the past two decades.

3 A comprehensive long-term study, using reinforced concrete pullout, tension and beam specimens of the following parameters, needs to be undertaken:

(a) Effect of concrete strength and permeability (with normal portland cement, fly ash, silica fume and ground granulated blast furnace slag- all found in Canada).

(b) Effect of admixtures (such as superplasticizers, water reducing agents, etc).

(c) Effect of concrete cover thickness (ranging from 25mm to 75mm).

(d) Effect of normal reinforcing steel and reinforcements with different protective coatings (such as epoxy-coating, galvanizing and others). Bar sizes ranging from 15m to 30m bars.

(e) Effect of chloride inhibitors.

(f) Effect of surface sealants and coatings.

(g) Effectiveness of selected repair techniques to enhance the service life (cathodic protection).

4 The structural integrity of prestressing strands in a prestressed concrete member deteriorating due to corrosion of the prestressing strands needs to be studied by using tension specimens. The specimens will be examined for cracking and spalling during the process of accelerated corrosion and during the test. After evaluation of the chloride ion profile along the cover thickness, the prestressing strand will be removed from the specimen and examined for the corroded condition, and will also be tested to determine its stress-strain characteristics and to verify if there was any embrittlement during the accelerated corrosion process. The parameters, which will be studied during the first phase are:

(a) Concrete mixtures (normal portland cement concrete and high performance concrete)

(b) Different admixtures (Air entraining agents and corrosion inhibitors).

(c) Concrete cover thickness (50mm and 75mm).

(d) Evaluation of the response of galvanized steel during the first 24-30 hours after casting and at later stages using tension specimens, with the objectives as stated earlier.

Statement of Originality

The author has made the following original contributions to the broad area of corrosion of structural concrete:

1. Develop an accelerated corrosion method for completely corroding steel reinforcing bars in a period of 15-20 weeks; monitoring of the various stages of corrosion using electrochemical, electrical and mechanical tests.
2. Study of the influence of different levels of corrosion on the response of steel bars embedded in pullout and tension specimens, detailed evaluation of the various electrochemical, chemical, physical, mechanical and other tests for use in condition surveys of existing concrete structures.
3. Independently established the mechanisms of the loss of bond at the steel-rebar-concrete interface. At higher levels of corrosion, the bond between the concrete and steel can be completely lost. Showed that the loss of bond at the steel-concrete interface can be more detrimental than the loss of the cross-sectional area due to corrosion.
4. Detailed parametric studies (concrete types, water-cement ratio, fly ash, high alumina cement, concrete cover thickness) on pullout and tension specimens using the accelerated corrosion test developed by the candidate.
5. Established quantitative relationships between the loss of bond at the steel-concrete interface for different stages of corrosion during the service life of the structure represented by the percentage mass loss and the chloride ion content at the steel surface. Development of practice-oriented equations for evaluation of deterioration of bond for use in service life design of concrete structures.

6. Detailed tests on four selected sites on the Dickson Bridge and correlation with the other tests on the Bridge and the related detailed parametric studies in the laboratory.
7. Creation of a data bank from all of the tests on the Dickson Bridge; development of the basic statistics for use in the reliability based design of concrete structures for durability against corrosion, and for design of repair and rehabilitation of existing deteriorated structural concrete infrastructure.

References

Abrams, D. A. (1951), "The Readers Write Section," Civil Engineering, Vol. 21, No. 6, pp. 51-52.

Abrishami, H.H., Cook, W.D., and Mitchell, D. (1994), "Studies on Bond and Cracking Of Strucrural Concrete," Structural Engineering Series Report No. 94-5, Department of Civil Engineering and Applied Mechanics, McGill University, Montreal, Canada, 183 pp.

ACI Committee 408 (1966), "Bond Stress - The State of the Art," Journal of the American Concrete Institute, Vol. 63, No. 11, pp. 1161-1188.

ACI Committee 318 (1971), "Building Code Requirements for Reinforced Concrete," American Concrete Institute, Detroit.

ACI Committee 222R (1989), "Corrosion of Metals in Concrete," Report of the ACI Committee 222, ACI Manual of Concrete Practice 1994, Part I, Materials and General Properties of Concrete, pp. 222R-1 to 222R-30.

ACI Committee 318 (1983), "Building Code Requirements for Reinforced Concrete (ACI 318-83)," American Concrete Institute, Detroit, 111 pp.

ACI Committee 408 (1991), "Bond Under Cyclic Loading - State of the Art," ACI Materials Journal, Vol. 88, No. 6, pp. 669-673.

ACI Committee 224.2R (1994), "Cracking of Concrete in Direct tension," Report of the ACI Committee 224, ACI Manual of Concrete Practice 1994, Part 3, Use of Concrete in Buildings - design Specifications and Related Topics, pp. 224.2R-1 to 224.2R-12.

Alekseev, S. N., Ivanov, F. M., Modry, S. and Schiessel, P., (1993), "Durability of Reinforced Concrete in Aggressive Media" Oxford & IBH Publishing CO. PVT Ltd., New Delhi, India.

Al-Sulaimani, G. J., Kaleemullah, M., Basunbul A., and Rasheeduzzafar (1990), "Influence of Corrosion and Cracking on Bond Behavior and Strength of Reinforced Concrete Member," ACI Journal, pp. 220-230.

Amleh, L., (1996), "Bond Behaviour between Reinforcing Steel and Concrete," Master Thesis, Mcgill University.

Amleh, L., and Mirza, M.S. (2000), "Corrosion Deterioration of Dickson Bridge," Departmental Report, McGill University, Montreal, Canada.

Amleh, L., Mirza, M.S., and Mirza, J. (1998), "Effect of Fly Ash Concrete Mix on Corrosion of Steel Reinforcement," Proceedings of the Annual Conference of the Canadian Society for Civil Engineering, Halifax, Nova Scotia, June 10-13, pp. 783- 92.

Andrade, C., Alonso, M.C., and Gonzalez, J.A. (1990), "An Initial Effort to Use The Corrosion Rate Measurements for Estimating Rebar Durability," Corrosion Rates of Steel in Concrete, Specail Technical Publication 1065, American Society For Testing and Materials, Philadelphia, Pennsylvania, pp. 29-37.

ASTM C39 (1986), "Compressive Strength of Cylindrical Concrete Specimens," American Society for Testing and Materials, Vol. 4.02, Philadelphia, PA.

ASTM C642 (1990), "Standard Test Method for Specific Gravity, Absorption, and Voids in Hardened Concrete," American Society for Testing and Materials, Vol. 4.02, Philadelphia, PA.

ASTM C876 (1991), "Standard Test Method for Half-Cell Potentials of Uncoated Reinforcing Steel in Concrete," American Society for Testing and Materials, Philadelphia, PA.

ASTM C78-84 (1992), "Standard Test Method for Flexural Strength of Concrete (Using Simple Beam with Third Point Loading)," Section 4 - Contruction, Volume 04.02 Concrete and Aggregates, pp. 33-35.

ASTM C496-90 (1992), "Standard Test Method for Splitting Tensile Strength of Cylindrical Specimens," Section 4 - Construction, Volume 04.02 Concrete and Aggregates, pp. 269-272.

ASTM C856-83 "Standard Recommended Practice for the Petrographic Examination of Hardened Concrete."

ASTM C876-91 (1992), "Test Methods for Potentials of Uncoated Reinforcing Steel in Concrete," 1992 Annual Book of ASTM Standards, Section 4 - Construction, Volume 04.02 Concrete and Aggregates, pp. 437-442.

ASTM A615-90 (1992), "Specifications for Reformed and Plain Billet-Steel Bars for Concrete Reinforcement," 1992 Book of ASTM Standards, Section 1 - Iron and Steel Products, Volume 01.04 Steel - Structural, Reinforcing Pressure Vessel, Railway, pp. 389-392.

Atimtay, E., and Ferguson, P.M. (1974), "Early Chloride Corrosion of Reinforced Concrete-a Test Report," Mater. Perform., 13 (12), pp. 18-21.

Bamforth, P. B., (1987), "The Relationship Between Permeability Coefficients for Concrete Obtained Using Liquid and Gas," Magazine of Concrete Research, Vol. 39, No. 138, pp. 3-11.

Bamforth P.B., and Pocock, D.C., (1990), "Minimising the Risk of Chloride Induced Corrosion by Selection of Concreting Materials." Third international symposium on corrosion of reinforcement in concrete construction. UK, 21-24, pp. 119-131.

Barrer, R. N., (1967), "The Solid-Gas Interface," E. A. Flood (Ed.), Vol II, Dekker, New York, pp. 557-609.

Basheer, P. A. M., (1991), "Clam Permeability Tests for Assessing the Durability of Concrete, Ph.D. Thesis, The Queen's University of Belfast.

Basheer, P. A. M., (1991), "The Autoclam for Measuring Permeation Properties of Hardened Concrete Near the Surface." Structural Materials Research Group, U.K.

Bazant, Z.P. (1992), "Fracture Mechanics of Concrete Structures," Elsevier Applied Science, Proceedings of the First International Conference on Fracture Mechanics of Concrete Structures, Breckenridge, Colorado.

Bazant, Z. P., (1979), "Physical Model for Steel Corrosion in Concrete Sea Structures Theory, Journal of the Structural division," American Society of Civil Engineers, Vol. 105, No. 6, pp. 1137-1153.

Bazant, Z. P., (1979), "Physical Model for Steel Corrosion in Concrete Sea Structures Application, Journal of the Structural Division," American Society of Civil Engineers, Vol. 105, No. 6, pp. 1155-1167.

Beaton, J.L., Spellman, D.L., and Stratfull, R.F. (1967), "Corrosion of Steel in Continuously Submerged Reinforced Concrete Piling." Highway Res. Rec. No. 204, Highway Research Board, Washington, D.C., pp. 11-21.

Beeby, A.W. (1978), "Corrosion of Reinforcing Steel in Concrete and its relation to Cracking," The Structural Engineer, Vol. 56A, No. 3, pp. 77-81.

Beeby, A.W. (1979), "The prediction of Crack Widths in Hardened Concrete," The Structural Engineer, Vol. 57A, No. 1, pp. 9-17.

Beeby, A.W. (1983), "Cracking, Cover, and Corrosion of Reinforcement." Concrete Intternational, Vol. 5 No.(2), pp. 35-40.

Bentz, Dale P.; Edward J. Garboczi, (1991), "Simulation Studies of the Effects of Mineral Admixtures on the Cement Paste-Aggregate Interfacial Zone," ACI Materials Journal (American Concrete Institute), V. 88, No. 5, pp. 518-529.

Berkeley, K.G.C., and Pathmanaban, S. (1990), "Cathodic Protection of Reinforcement Steel in Concrete," Butterworth & Co., London, U.K, pp. 1-52.

Biczók, I. (1972), "Concrete Corrosion Concrete Protection," Eighth Edition, Akadémiai Kiadó, Budapest, Hungary, pp. 1-37.

Bisaillon, A., and Malhotra, V. M., (1988), "Permiability of Concrete Using a Uniaxial Water-Flow Method" Ed.: D. Whiting and A. Walitt, ACI, Detriot, MI, Special Publication SP-108, pp. 175-194.

Bischoff, P.H. (1995), "Influence of Shrinkage on Tension Stiffening of Concrete", Proceedings of the Annual Conference of the Canadian Society for Civil Engineering, Ottawa, Ontario, pp. 433-442.

Borgard, B., Warren, C., Somayaji, S., and Heidersbach, R. (1990), "Mechanisms of Corrosion of Steel in Concrete," Corrosion Rates of Steel in Concrete, ASTM STP 1065, N. S. Berke, V. Chaker, and D. Whiting, Eds., American Society for Testing and Materials, Philadelphia, pp 174-188.;

British Standard 1881 (1988), Part 124, "Methods for Analysis of hardened Concrete," Testing Concrete, British Standards Institution, London, U.K., pp. 1-35.

Broomfield, J.P. (1997), "Corrosion of Steel in Concrete," E & FN Spon, an imprint of Chapman & Hall, London, UK.

Broms, B., and Raab, A. (1961), "The Fundamental Concepts of the Cracking Phenomenon in Renforced Concrete Beams," Report No. 310, School of Civil Engineering, Cornell University, Ithaca, pp. 1095-1108.

Brown, R.D. (1980), "Mechanism of Corrosion of Steel in Concrete in Relation to Design, Inspection and Repair of Offshore and Coastal Structures," Performance of Concrete in Marine Environments, SP-65, ACI, Detroit, pp. 169-204.

Byfors, K., Hansson, C.M., and Tritthart, J., (1986), Cement and Concrete Research, Vol.16, pp. 760-770.

Cabrera, J.G., (1985), "The Use of Fly Ash to Produce Durable Concrete". ICE Proceedings, Institution of Civil Engineers, Thomas Telford Ltd, London, pp. 164.

Cabrera J.G., and Ghoddousi, P. (1992), "The effect of Reinforcement Corrosion on the Strength of the Steel/Concrete Bond" International Conference Bond in Concrete from Research to Practise Proceedings, pp. 11-24.

Cady, Philip D.; R.E. Weyers, (1983), "Chloride Penetration and the Deterioration of Concrete Bridge Decks," Cement, Concrete, and Aggregates, Vol. 5, No. 2, pp. 81-87.

Canadian Environmental Protection Act (CEPA) (2000), "Summary of the Draft Report of the Assessment of the Substance Road Salts Specified on the Priority Substances List" The Draft Assessment report on road salts, Environment Canada's web site at: www.ec.gc.ca/cceb1/eng/public/index_e.html

Cao, H. T., Bucea, L., Wartley, B., and Sirivivatnanon, V., (1993), "Corrosion Behaviours of Steel Embedded in Fly Ash Blended Cements" SP145-11, pp.215-226.

CEB Task Group VI (1981), "Bond Action Behaviour of Reinforcement - State of the Art Report," Comité Euro-International du Béton, 153 pp.

CEB-MC90 (1990), "CEB-FIP Model Code 1990," Thomas Telford Services Ltd., London, England.

Collins, M.P., and Mitchell, D. (1991), "Prestressed Concrete Structures," Prentice-Hall Inc. Englewood Cliffs, N.J.

Cornet, I., Ishikawa, T., and Bresler, B. (1968), Materials Protection, Vol. 7, No. 3, pp.44-47.

Craig, R. J., and Wood, L. E., (1970), "Effectiveness of Corrosion Inhibitors and Their Influence on the Physical Properties of Portland Cement Mortars." Highway Research Record, No. 328, pp. 77-88.

Crow, R. D., and Dunstan, E. R., (1981), "Properties of Fly Ash Concrete," Proceedings, Symposium on Fly Ash Incorporation in Hydrated Cement Systems; Editor, Sidney Diamond; Materials Research Society; Boston; pp. 214-225.

Crumpton, D. F., Pattengill, M. G., and Badgley, W. A., (1969), "Bridge Deck Deterioration Study-Part 8" Kansas State Highway Department, Topeka.

CSA Standard A23.2-2-13C (1994), "Splitting Tensile Strength of Cylindrical Concrete Specimens," CSA A23.2-94 Methods of Tests for Concrete, Canadian Standard Association, Rexdale, Ontario, pp. 333-338.

CSA Standard A23.3-M84 (1984), "Design of Concrete Structures for Buildings," Canadian Standard Association, Rexdale, Ontario, 281 pp.

CSA Standard A23.2-8C (1994), "Flexural Strength of Concrete (Using Simple Beam with Third Point Loading)," CSA A23.2-94 Methods of Tests for Concrete, Canadian Standard Association, Rexdale, Ontario, pp. 314-316.

CSA Standard A23.2-2A (1994), "Sieve Analysis of Fine and Coarse Aggregates," CSA A23.2-94 Methods of Tests for Concrete, Canadian Standard Association, Rexdale, Ontario, pp. 158-163.

CSA Standard G30.14-M83 (1983), "Deformed Steel Wire for Concrete Reinforcement," Rexdale, Ontario.

Cusick, R.W., and Kesler, C.E. (1976), "Interim Report-Phase 3: Behaviour of Shrinkage-Compensating Concretes Suitable for Use in Bridge Decks," T. & A.M. report No. 409, Department of theoretical and Applied Mechanics, University of Illinois, Urbana.

Dakhil, F. H., Cady, P. D., and Carrier, R. E., (1975), "Cracking of Fresh Concrete as Related to Reinforcement," Journal of the American Concrete Institute, Vol. 72, No. 8, pp. 421-428.

Davis, J. R. (2000), "Corrosion: Understanding the Basics" ASTM International, The Materials Information Society.

Davis, R.E. (1954), "Pozzolanic Materials-with Special Reference to their Use in Concrete Pipe." Tech. Memorandum, American Pipe Assoc., Arlington, Va.

Dhir, R. K., Hewlett, P. C., and Chan, Y. N., (1987), "Near-Surface characteristics of concrete: Assessment and Development of In-Situ Test Methods." Magazine of Concrete Research, Vol. 39, No. 141, pp. 183-195.

Diamond, S. (1986), "Chloride Concentrations in Concrete Pore Solutions Resulting from Calcium and Sodium Admixture" Cement Concrete Aggregates, Vol. 8, No. 2.

Elfert, R.J. (1973), "Bureau of Reclamation Experiances with Fly Ash and Other Pozzolans in Concrete." Proc., 3rd Int. Ash Utilization Symposium, Information Circular IC8640. U.S. Bureau of Mines, Washington, D.C., pp. 80-93.

Elsener, B., and Böhni, H. (1990), "Potential Mapping and Corrosion of Steel in Concrete," Corrosion Rates of Steel in Concrete, Special Technical Publication 1065, American Society For Testing and Materials, Philadelphia, Pennsylvania, pp. 143-156.

Erlin, B., and Verbeck, G.J, (1978), "Corrosion of Metals in Concrete-Needed Research, " SP-49, Corrosion of Metals in Concrete, ACI, Detroit, pp. 39-46.

Evans, U. R., (1960), "The Corrosion and Oxidation of Metals." Arnold & Co., London.

Farah, F. (1993), "Accelerated Corrosion Testing of Reinforcing Steel Embedded in Concrete," M.Eng. Thesis, Department of Civil Engineering and Applied Mechanics, McGill University, Montreal, Canada, pp 217.

Feldman, R. F., Chan, G. W., Brousseau, R. J., and Tumidajski, P. J. (1994),"Investigation of the Rapid Chloride Permeability Test," ACI Materials Journal (American Concrete Institute), Vol. 91, No. 3, pp. 246-255.

Figg, J. W., (1973), "Methods of Measuring Air and Water Permeability of Concrete." Magazine of Concrete Research, Vol. 25, No. 85, pp. 213-219.

Fontana, Mars Guy, (1986), "Corrosion Engineering," McGraw-Hill Book Company.

Franczek, J. (1987), "A Review of Electrochemical Principles as Applied to Corrosion of Steel in a Concrete or Grout Environment", in Gibson, F. W., Corrosion Concrete, and Chlorides-Steel Corrosion in Concrete: Causes and Restraints, American Concrete Institute, Detroit, SP-102-2. pp. 13-24.

French, W. J. (1991), "Concrete Petrography: A Review" Quarterly Journal of Engineering Geology, 24, pp. 17-48.

Funahashi, Miki, (1990), "Predicting Corrosion-free Service Life of a Concrete Structure in a Chloride Environment," ACI Materials Journal (American Concrete Institute), Vol. 87, No. 6, pp. 581-587.

Gambarova, P. G., Rossat, G. P., (1996), "Bond and Splitting in Reinforced Concrete: Test Results on Bar Pull-Out" Materials and Structures, Vol. 29, pp. 267-276.

Garboczi, Edward J. (1990), "Permeability, Diffusivity, and Microstructural Parameters," A Critical Review, Cement and Concrete Research, Vol. 20, No. 4, pp. 591-601.

Garboczi, E. J., Schwartz, L. M., and Bentz, D. P. (1995), "Modeling the Influence of the Interfacial Zone on the DC Electrical Conductivity of Mortar" Advance Cem. Bas. Mat. Elsevier Science Inc., pp. 169-181.

Gjorv, O. E. (1975), "Control of Steel Corrosion in Concrete Sea Structures", SP-49, Corrosion of Metals in Concrete, ACI, Detroit, pp. 1-9.

Gjorv, O. E. (1983), "Durability of Concrete containing condensed Silica Fume" Proceedings, First International Conference on the Use of Fly Ash, Silica Fume, Slag and Other Mineral By-Products in Concrete, Montebello, Canada, Editor: V.M. Malhotra, ACI special publication SP-79, pp. 695-708.

Gjorv, O. E., Monteiro, P. J. M., and Mehta, P. K. (1990), "Effect of Condensed Silica Fume on the Steel-Concrete Bond." ACI Materials Journal, pp. 573-580.

Gjorv, O. Vennesland, O., and El-Busaidy, A. (1976), "Diffusion of Dissolved Oxygen Through Concrete," Corrosion/76, Paper No. 17, National Association Of Corrosion Engineers, Houston.

Gonzalez, J. A., Algaba, S., and Andrade, C., (1980), "Corrosion of Reinforcing Bars in Carbonated Concrete," Bridge Corrosion Journal, Vol. 3, pp. 135-139.

Gonzalez, J. A., Lopez, W. and Rodriguez, P., (1993), "Effects of Moisture Availability on Corrosion Kinetics of Steel Embedded in Concrete", Corrosion, pp. 1004-10.

Gouda, V. K., (1970), "Corrosion and Corrosion Inhibition of Reinforcing Steel. I: Immersion in Alkaline Solution." British Corrosion Journal, London, England, pp. 198-203.

Goto, Y. (1971), "Cracks Formed in Concrete Around Deformed Tension Bars," ACI Journal, Proc. Vol. 68, No. 4, pp 244-251.

Goto, S., and Roy, D. M., (1981), "The Effect of W/C Ratio and Curing Temperature on the Permeability of Hardened Cement Paste." Cement and Concrete Research, Vol.11, No. 4, pp. 575-579.

Griffin, D. and Henry, R. (1963), Proceedings, American Society for Testing and Materials, Vol. 63, pp. 1046-1079.

Gu, P., Beaudoin, J. J., Zhang, M.-H. and Malhotra, V. M. (1999), "Performance of Steel Reinforcement in Portland Cement and High Volume Fly Ash Concretes Exposed to Chloride Solution." ACI Materials Journal, September-October, pp. 551-558.

Hansson, C. M., (1984), "Comments on Electrochemical Measurements of the Corrosion rate of Steel in Concrete," Cement Concrete Research, Vol. 14, pp. 574-5784.

Hausmann, D. A. (1967), " Steel Corrosion in Concrete." Material Protection, pp. 19-23.

Hobbs, D. W., (1983), "Possible Influence of Small Additions of pfa, gbfs and Limestone Flour Upon Expansion Caused by the Alkali-Silica Reaction," Magazine of Concrete Research, pp. 35-55.

Hooton, R. D., (1986), "Permeability and Pore Structure of Cement Pates Containing Fly Ash, Slag and Silica Fume," Blended Cements, ASTM STP, pp. 128-143.

Houde, J., and Mirza, M. S., (1972), "A Study of Bond Stress-Slip Relations in Reinforced Concrete." Structural Concrete Series No. 72-8, McGill University.

Hwang, S. J., Lee, Y. Y., Lee, C. S., (1994), "Effect of Silica Fume on the Splice Strength of Deformed Bars of High-Performance Concrete." ACI Structural Journal, Vol. 91, No. 3, pp. 294-302.

Iske, P. L., Sterk, N. K. J., and Oortwijn, J., (1994), Physica A, Vol. 209, pp. 96-128.

Jhonson, C. D., (1994), "Deicer Salt Scaling Resistance and Chloride Permeability", Concrete International: Design and Construction, Vol. 16, No. 8, pp. 48-55.

Jimenez, R., White, R.N., and Gergely, P., (1979), "Bond and Dowel Capacities of Reinforced Concrete." Journal ACI, Vol. 74, pp. 73-92.

Jirsa, J. O. et al., (1979), "Rationale for Suggested Development, Splice, and Standard Hook Provisions for Deformed bars in Tension." Concrete International, No. 7, pp. 47-61.

John, D.G., Eden, D.A., Dawson, J.L., and Langford, P.E. (1987), Proceedings, CORROSION/87, Paper No. 136, National Association of Corrosion Engineers, Houston.

Jones, D. A., (1992), "Principles and Prevention of Corrosion," Macmillan Publishing Company, New York, NY.

Kayyali, O.A (1989), "Strength and Porosity of Portland Cement Paste Subjected to Chloride Penetration," Journal of Materials in Civil Engineering, Vol.1 No.1, pp. 10-18.

Kemp, E.L., and Wilhelm, W.J., (1979), "Investigation of the Parameters Influencing Bond Cracking." Journal ACI, Vol. 76, pp. 47-71.

Klemm, W. A., (1989), "Cementitious Materials: Historical Notes" Materials Science of Concrete I, Editor: Jan P. Skalny, The American Ceramic Society, Inc.

Klieger, Paul, Joseph F. Lamond (Eds.), (1994), "Significance of Tests and Properties of Concrete and Concrete-Making Materials," ASTM STP 169C.

Klinkenberg, L. J., (1941), "The Permeability of Porous Media to Liquids and Gases, Drilling and Production Practice", American Petroleum Institute, New York, pp. 200-214.

Kumar, A., and Roy, D.M. (1986), "Pore Structure and Ionic Diffusion in Admixture Blended Portland Cement Systems." Proceedings, 8th International Congress on the Chemistry of Cement, Vol. V, pp. 73-79.

Kumar, A., Komarneni , S., and Roy, D.M. (1987), "Diffusion of C_s^+ and Cl^- Through Sealing Materials." Cement and Concrete Research, 17 (1), pp. 153-160.

Lamond, J. F. (1983), "Twenty-five Years' Experience Using Fly Ash in Concrete", Proceedings, First International Conference on the Use of Fly Ash, Silica Fume Slag and Other Mineral By-Products in Concrete; Montebello, Canada; Editor, V. M. Malhotra ; ACI Special Publication SP-79; pp.47-69.

Lea, F. M., (1971), "The Chemistry of Cement and Concrete", Chemical Publishing, Inc.

Leonhardt, F., (1964), "Prestressed Concrete Design and Construction, 2nd Edition, Wilhelm Ernst & Sohn.

Lewis, D.A., (1962), "Some Aspects of the Corrosion of Steel in Concrete," Proceedings, 1st International Congress on Metallic Corrosion, Butterworths, Washington, DC, pp. 547-555.

Lounis, Z. and Mirza, M.S., (2001) "Reliability Base Service Life Prediction of Durability of Concrete Structures." 3rd International Conference on Concrete under Severe Conditions, Vancouver, Canada.

Lounis, Z. and Mirza, M.S., (1999) "A Framework for Design of Concrete Structures for Durability Against Corrosion." Workshop on Corrosion in Civil Engineering, McGill University, Montreal, Canada.

Lutz, L.A., and Gergely, P. (1967), "Mechanics of Bond and Slip of Deformed Bars in Concrete," ACI Journal, pp. 711-721.

Lutz, L.A., and Gergely, P., and Einter, G. (1966), "The Mechanics of Bond and Slip of Deformed Reinforcing Bars in Concrete," Structural Engineering Report No. 324, Cornell University.

Malhotra, V. M. and Carino, N. J., (1991), "Non-Destructive Testing of Concrete." CRC press, pp. 217-225.

Malhotra, V. M., (1994), "CANMET Investigations Dealing with High Volume Fly Ash," Advances in Concrete Technology, 2nd Edition, Natural Resources Canada, Ottawa. Canada, pp. 445-482.

Manmohan, D., and Mehta, P.K. (1981), "Influence of Pozzolanic, Slag and Chemical Admixtures on Pore Size Distribution and Permeability of Hardened Cement Pastes." Cement Concrete and Aggregates, Vol. 3 No.1, pp. 63-67.

Marsh, B.K., Day, R.L., and Bonner, D.G., (1985), "Pore Structure Characteristics Affecting the Permeability of Cement Paste Containing Fly Ash." Cement and Concrete Research Magazine, Vol. 15, pp. 1927-1038.

Mather, K., (1982), "Current Research in Sulphate Resistance at the Waterways Experiment Station." Proceedings of the George Verbeck Symposium on Sulphate Resistance of Concrete, ACI Special Publication SP-77, pp.63-74.

Mathey, P., and Watstein, P. (1959), "Width of Cracks in Concrete at the Surface of Reinforcing Steel Evaluated by Means of Teansile Bond Specimens," ACI Journal, Proceedings Vol. 56, No.1, pp 47-56.

Mehta, P. K., (1984), "Mineral Admixtures," from Concrete Admixtures Handbook, Properties Science and Technology, Ed. V. S. Ramachandran.

Mehta, P. Kumar, (1993), "Concrete Structure, Properties, and Materials," Prentice-Hall, Inc., Englewood Cliffs, N.J. 07632.

Mehta, P.K., and Monteiro, P.J.M. (1992), "Concrete Strucrure - Properties and Materials," Prentice-Hall Inc. Englewood Cliffs, N.J.

Midgley, H.G., and Illston, J.M. (1984), "The Penetration of Chlorides into Hardened Cement Pastes," Cement and Concrete Research, Vol. 14 No.4, pp. 546-558.

Miller, R., Krouskop, B., Minkarah, I., Bodocsi, A., "Chloride Penetration and the Effect on Porosity in a Pavement," Paper No. 930327, Transportation Research Board, 72nd Annual Meeting.

Mirza, M. S., (1995), "Permeability of Concrete-Key to Concrete Durability." Paper Presented at the Annual Conference of the Canadian Society for Civil Engineering, Ottawa, Ontario.

Mirza, M. S., (1995), "Infrastructure Renewal" Forum on Facilities Renewal Program, Government of Canada, Department of Public Works, Ottawa, Ontario, November 1995, pp. 1-74.

Mirza, M. S., (1995), "Design Needs for Sustainable Development." Seventh International Collquiom on Structural and Geotechnical Engineering, Vol. II, Cairo, Egypt, pp 10-30 (Key-Note Presentation)

Mirza, M. S., and Amleh, L. (1995), "Recent Developments in Diagnosis and Rehabilitation of Concrete Structures," Proceedings of the Special ACI Conference, Montreal, Quebec, November 7, pp 193-235.

Mirza, M. S., and Houde, J. (1979), "Study of Bond Stress-Slip Relationships in Reinforced Concrete," ACI Journal, Vol. 76, No. 1, pp 19-46.

Mirza M.S., and Lounis, Z. (1996), "Durability Design of Concrete Structures," Seventh International Colloquim on Structural and Geotechnical Engineering, Vol. II, Cairo, Egypt, December, pp. 1-18.

Mirza M.S., Shao Y., and Collinge J.P. (1998), "Post-Mortem of the Abandoned Dickson Bridge," Proceedings of the Annual Conference of the Canadian Society for Civil Engineering, Halifax, Nova Scotia, June 10-13.

Monosi, S., Troli, R., Coppola, L., and Collepardi, M. (1996), "Water reducers for the High Alumina Cement-Silica Fume System," Materials and Structures, Vol., 29, pp. 639-644.

Naish, C. C., and Carney, R. F. A, (1988), "Variability of Potentials Measured on Reinforced Concrete Structures." Materials Performance, pp. 45- 48.

Neville, A., (1987), "Why We Have Concrete Durability Problems." Editor: J. M. Scanlan, ACI SP-100, pp. 21-30.

Nielsen, A. (1985), "Durability," Beton Bogen (The Concrete Book), Edited by Aa. D. Herholdt, Chr. F.P. Justesen, P. Nepper-Christensen, and A. Nilesen, Aalborg, Portland, pp. 200-43.

Oh, B. H., Cho, Y. G., Cha, S. W., and Jang, B. S., (1999), "Prediction of Corrosion Resistance of Concrete Structure." Durability of Building Materials and Components 8, Vol. 1, Editors: Lacasse, M. A. and Vanier, D. J. NRC Research Press, Ottawa, Canada, pp. 354- 364

Orangun, C. O., Jirsa, J. O., and Breen, J. E., (1977), "A Reevaluation of Test Data on Development Length and Splices." ACI Journal, pp. 114-122.

Ouyang, C., and Shah, S.P. (1994), "Fracture Energy Approach for Predicting Cracking of Reinforced Concrete Tensile Members," ACI Structural Journal, Vol. 91, No. 1, pp. 69-78.

Page, C., Al Khalaf, M.N., and Ritchie, A.G.B. (1978), " Steel/Mortar Interfaces: Mechanical Characteristics and Electrocapillarity," Cement and Concrete Research, Vol. 8, pp. 481-490.

Page, C. L.; Short, N. R.; El Tarras, A., (1981), "Diffusion of Chloride Ions in Hardened Cement Pastes," Cement and Concrete Research, Vol. 11, No. 3, pp. 395-406.

Palsson, R. and Mirza, M.S. (2001), "Mechanical Response of Corroded Steel Reinforcement from an Abandoned Concrete Bridge," Paper submitted for possible publication in the ACI Structural Journal.

Palumbo, N. (1991), "Accelerated Corrosion Testing of Steel Reinforcement in Concrete," M.Eng. Thesis, Department of Civil Engineering and Applied Mechanics, McGill University, Montreal, Canada.

Park, R., and Paulay, T. (1975), "Reinforced Concrete Structures," John Wiley & Sons, Inc. N.Y.

Pfeifer, D. W., Landgren, J. R. et al. (1987), "Protective Systems for New Prestressed and Substructure Concrete" Report No. FHWA/RD-86/193, Federal Highways Administration, USA.

Popovics, S., Simenov, Y., Boghinov, G., and Barovsky, N. (1983), "Durability of Reinforced Concrete in Sea Water," Corrosion of Reinforcement in Concrete Construction, A. Crane, Ed., Ellis-Hor-Wood Ltd., Chichester, U.K, Vol. 19.

Pourbaix, M. (1976), "Atlas of Electrochemical Equilibrium in Aqueous Solutions," Pergamon, London.

Power, T.O. and Hammersley, G.P. (1978), "Practical Concrete Petrography." Concrete.

Powers, T. C., Copeland, l. E., Hayes, J. C., and Mann, H. M., (1954), "Permeability of Portland Cement Paste." Journal of the American Concrete Institute; Vol. 26, No. 3, pp. 285-298.

Powers, T. C., Copeland, L. E., and Mann, H. M., (1959), "Flow of Water in Hardened Portland Cement Pastes," Special Report 40, Highway Research Board, Washington, DC, pp. 308-323.

Powers, T. C., (1960), "Physical Properties of Cement Paste, Proceedings," 4th International Symposium on the Chemistry of Cement, Washington, DC, Vol. 2, pp. 577-613.

Powers, T. C., (1958), "Structure and Physical Properties of Hardened Portland Cement Paste," American Ceramic Society Journal, Vol. 41, pp. 1-6.

Pritchard, B. (1986), "A new era in concrete bridge protection," Highways, pp. 20-21.

Raba, F. Jr., Smith, S. L., and Mearing, M., (1981), "Subbituminous Fly Ash Utilization in Concrete." Proceedings, Symposium on Fly Ash Incorporation in Hydrated Cement Systems, Editor, Sidney Diamond, Materials Research Society, Boston, pp. 47-69.

Rasheeduzzafar, Dakhil, F.H., and Al-Gahtani, A.S. (1985), "Corrosion of Reinforcement in Concrete Structures in the Middle East." Concrete International, American Concrete Institute, Vol. 7 No. 9, pp. 48-55.

Rasheeduzzafar, Al-Saadoun, S.S., and Al-Gahtani, A.S. (1992), "Corrosion Cracking in Relation to Bar Diameter, Cover, and Concrete Quality." Journal of Materials in Civil Engineering, Vol. 4, No. 4, pp. 327-342.

Ravindrarajah, R., and Ong, K. (1987), "Corrosion of Steel in Concrete in Relation to Bar Diameter and Cover Thikcness." Concrete Durability, Katherine and Bryant

Rehm, G. (1957), "The Fundamental law of Bond," Proceedings, Symposium on Bond and Crack Formation in Reinforced Concrete, Stockholm, RILEM, Paris, Pub. Tekniska Hogskolans Rotaprinttrychkeri, Stockholm.

Reynolds, G. C., (1982), "Bond Strength of Deformed Bars in Tension." Cement and Concrete Association, C & CA Technical Report 548.

Richardson, M. G., (1991), "Carbonation of Reinforced Concrete: "Its Causes and Management", Citis Ltd., Dublin

Roberts, M.H. (1981), "Carbonation of Concrete Made with Dense Natural Aggregates," IP6/81, Building Research Establishment, Garston, England.

Rosenberg, A., Grace, W.R. and Co.; Hansson, C., and Andrade, C. (1991), "Mechanism of Corrosion in Steel Concrete," Materials Science of Concrete, Westerville, OH, pp. 285-313.

Rosenberg, A., Hansson, C.M. and Andrade, C. (1989), "Mechanisms of Corrosion of Steel in Concrete," Material Science of Concrete I., The American Ceramic Society, Westerville, OH, pp. 285-313.

Sakamoto, N., and Iwasaki, N. (1995), "Influence of Sodium Chloride on the Concrete/ Steel and Galvanised Steel Bond," Bond in Concrete, Applied Science Publishers, London England.

Shalon, R., and Raphael, M. (1959), "Influence of Sea water on Corrosion of Reinforcement," ACI Journal, pp. 1251-1268.

Shane , J. D., Hwang, J-H., Sohn, D., Mason, T. O., and Jennings, H. M., (1997), "Recent Development in the Measurement of Transport Properties in Cement-Bsed Materials." Mechanics of Chemical Degradation of Cement-based Systems. Edited by K. L. Scrivener and J. F. Young, pp. 413-423.

Short, N.R., and Page, C.L. (1982), "The Diffusion of Chloride Ions Through Portland and Blended Cement Pasts." Silicates Industries, 10, pp. 237-240.

SHRP-S-328 (1993), "Method for Field Determination of Total Chloride Content," National Academy of Sciences, Washington, DC.

Slater, J.E., (1975), "Corrosion of Metals in Association with Concrete", Corrosion of Metals in Concrete," ACI SP-49, American Concrete Institute, Detroit, MI, pp. 21-38.

Stanton, T. E., (1942), "Expasion of Concrete through Reaction between Cement and Aggregate," Transactions ASCE Part 2, pp. 68-85.

Stratfull R.F (1973), "Half cell potentials and the corrosion of steel in concrete," Highway Research Record, 433, pp. 12-21.

Stratfull, R.F., Jurkovich, W.J., and Spellman, D.L (1975), "Corrosion Testing of Bridge Decks," Transportation Research Record No. 539, Transportation Research Board, pp. 50-59.

Tafel, J. (1904), Physik. Chem., 50, pp. 641.

Tepfers, R. (1973), "A Theory of Bond Applied to Overlapped Tensile Reinforcement Splices for Deformed bars," Division of Concrete Structures, Chalmers University of Technology, Goteborg, Sweden, Publication 73:2, 328p.

Tepfers, R. A., (1979), "Cracking of Concrete Cover Along Anchored Deformed Reinforcing Bars," Magazine of Concrete Research, Vol. 31, No. 106, pp. 3-12.

Treece, R.A., and Jirsa, J.O. (1989), "Bond Strength of Epoxy-Coated Reinforcing Bars," ACI Materials Journal, Vol. 86, No. 2, pp. 167-174.

Trethewey, K.R., and J. Chamberlain, (1988), "Corrosion for Students of Science and Engineering," Longman Scientific & Technical, pp.228-230.

Tyler, I.L. (1960), "Long-time Study of Cement Performance in Concrete; Chapter 12- Concrete Exposed to Sea Water and Fresh Water." Journal of the American Concrete Institute, Proceedings, Vol 57, No.9, pp. 825-836.

Uhlig, H. H., Revie, R. W., (1985), "Corrosion and Corrosion Control" John Wiley & Sons, Inc.

Vassie P.R. (1978), "Evaluation of techniques for investigating the corrosion of steel in concrete," TRRL Report SR 397 Crowthorne, (Transport and Road Research Laboratory).

Vassie, P.R. (1991), "The Half-Cell Potential Method of Locating Corroding Reinforcement in Concrete Structures," Transport Research Laboratory Application Guide AG9, Crowthorne, Berkshire, U.K.

Verbeck, G.J, (1975), "Mechanism of Corrosion of Steel in Concrete", SP-49, Corrosion of Metals in Concrete, ACI, Detroit, pp. 21-38.

Wakeman, C.M., Dockweiler, E.V., Stover, H.E., and Whiteneck, L.L. (1958), "Use of Concrete in Marine Environments," Journal of the American Concrete Institute, Proceedings, Vol. 54, No. 10, pp. 841-856.

Wenner F. (1916), "A Method of Measuring Earth Resistivity," Bulletin of the US Bureau of Standards Science Paper 12 No. 3.

Weyers, R. E., Conway, J. C., and Cady, P. D., (1982), "Photoelastic Analysis of Rigid Inclusions in Fresh Concrete," Cement and Concrete Research, Vol. 12, No. 4, pp. 475- 484.

Whiting, D., (1984), "In-Situe Measurement of the Permeability of Concrete to Chloride Ions," In-Situ Nondestructive Testing of Concrete, ACI SP-82, American Concrete Institute, Michigan, pp. 501-24.